Characterisation of the efficacy of two novel host-directed therapies, SCD-19 and 4-octyl itaconate, in the treatment of *Pseudomonas aeruginosa* infection in cystic fibrosis.

Andrew O' Neill

B.Sc. Human Health and Disease

Trinity College Dublin
Coláiste na Tríonóide, Baile Átha Cliath
The University of Dublin

A thesis submitted to

Trinity College Dublin

for the degree of

Doctor of Philosophy

Supervisor: Prof. Seamas Donnelly

School of Medicine

Trinity College Dublin

January 2021

Contents

I. Declaration of Authorship

I declare that this thesis has not been submitted as an exercise for a degree at this or any other university and it is entirely my own work. I agree to deposit this thesis in the University's open access institutional repository or allow the library to do so on my behalf, subject to Irish Copyright Legislation and Trinity College Library conditions of use and acknowledgement.

_____

Andrew O' Neill

II. Acknowledgements

Firstly, I would like to that Professor Seamas Donnelly for giving me the opportunity to join The Donnelly Lab. Throughout this Ph.D. Seamas has been a source of much guidance and has been a pleasure to work for.

I would also like to thank the many collaborators that contributed to this project. Firstly, thank you to Professor George O' Toole and his lab group for welcoming me during my stint at Dartmouth College. I learned a lot of valuable knowledge about *P. aeruginosa* during my stay which definitely increased the quality of my experimental techniques. Thank you also to Dr. Julie Renwick for providing me with the *P. aeruginosa* clinical isolates used in this study and also for all of her help and guidance with the *Galleria mellonella* infection model. Thanks also to Dr. Susan Fetics for her help with the MIF purification process, and also to Professor Padraic Fallon for generously providing tissue from Irg1 knockout mice. Finally, thank you to Professor Luke O' Neill for providing me with 4-OI and for his helpful and encouraging discussions.

The biggest thank you to the members of The Donnelly & Armstrong Labs, especially Michelle, Aoife, Mohammad, Leona, Marie Claire and Joanna, who all made completing this body of work significantly more enjoyable on a daily basis. Notable mention to Aoife for all the much-needed coffees and trips to Kennedys. A special thanks to Michelle for all her guidance and encouragement throughout my Ph.D. and in particular her tireless help in producing this thesis.

Finally, I would like to thank all my family and friends for their support throughout this process. Special mention to Mam, Nanny and Alan for all their love and endless support throughout the duration of my Ph.D. I dedicate my thesis to them.

III. Abstract

Cystic Fibrosis (CF) is a life limiting genetic disease, which is caused by genetic mutations which result in defective function of the Cystic Fibrosis Transmembrane Conductance Regulator (CFTR). In CF, patients experience frequent hospitalisations from a young age as a result of recurrent respiratory infections and inflammatory lung damage, with CF patients having a median life expectancy of only 31 years. Therefore, currently there is an urgent unmet clinical need for the development of novel anti-inflammatory and antibacterial therapies in the treatment of CF.

Within the CF lung, the build-up of thick mucus secretions provides a microenvironment which is conducive to bacterial colonisation and inflammation. *Pseudomonas aeruginosa* (*P. aeruginosa*) is the most commonly isolated pathogen from the CF lung. CF patients develop a series of recurrent, intermittent colonisations of *P. aeruginosa* before the acquisition of a biofilm-driven chronic infection. The establishment of a chronic infection drives high levels of respiratory inflammation and consequent irreversible lung damage. Furthermore, these chronic infections develop a myriad of antibiotic resistant characteristics; with multidrug-resistant infections becoming a major problem in CF. Anti-microbial resistance is one of the biggest challenges facing society as a whole, with estimations that up to 10,000,000 people a year will die due to antibiotic resistant infections. As such, there is a specific unmet clinical need for the development of novel therapies that target *P. aeruginosa*-induced inflammation, biofilm formation and infection in CF patients.

The Donnelly Lab has previously demonstrated a role for macrophage migration inhibitory factor (MIF) in the pathogenesis of CF. CF patients expressing high levels of MIF have a more rapid decline in lung function, earlier *P. aeruginosa* colonisation compared with CF patients with low MIF expression levels. Furthermore, our group has previously demonstrated that MIF promotes *P. aeruginosa* biofilm formation through upregulation of genes involved in bacterial quorum sensing, alginate expression and mucoid conversion. Previously, The Donnelly Lab have described the successful use of a novel, small molecular weight inhibitor of MIF tautomerase activity, SCD-19, both *in vitro* and *in vivo* using in a murine model of chronic *P. aeruginosa* infection. In this model, SCD-19 promoted bacterial clearance and limited respiratory inflammation.

Here, we examined the role of MIF in *P. aeruginosa* biofilm formation on airway epithelial cell monolayers. Furthermore, we investigated the efficacy of SCD-19 loaded nanoparticles in the modulation of heat killed *P. aeruginosa* (HKPA) induced macrophage responses and MIF driven *P. aeruginosa* biofilm formation. We demonstrated a role for MIF in *P. aeruginosa* biofilm formation on airway epithelial cell monolayers. We also showed that SCD-19 and SCD-19 loaded nanoparticles modulate this process. Furthermore, we also illustrated that SCD-19 and SCD-19 loaded nanoparticles modulate HKPA-induced TNF-α and RANTES protein production in macrophages. We also detailed, for the first time, the characterisation of bone marrow derived macrophages (BMDMs) from novel, humanised mice which possess a 5-CATT or 7-CATT repeat in the promoter region of their MIF gene.

In this thesis, we also examined the effects of itaconate and 4-octyl itaconate (4-OI) in the context of *P. aeruginosa* infection. Itaconate is a well-established immunomodulatory by-product of the tricarboxylic acid (TCA) cycle which displays known antibiotic properties. 4-OI is a cell permeable itaconate derivative which is used in cellular experiments as there are limited reports of an itaconate receptor or transporter. We proposed that 4-OI and itaconate treatment would be beneficial in the context of *P. aeruginosa* inflammation. Here, we demonstrated that 4-OI limited *P. aeruginosa*-mediated inflammatory responses of BMDMs, promoted the expression of protective antioxidant factors and enhanced BMDM-mediated *P. aeruginosa* killing. We also demonstrated that itaconate possesses potent antipseudomonal properties, limiting *P. aeruginosa* growth, biofilm formation and pyocyanin production. Furthermore, we demonstrated that both 4-OI and itaconate, respectively, promoted survival *in vivo* in a *Galleria mellonella* model of *P. aeruginosa* infection.

In conclusion, the results from this study suggest that SCD-19 and 4-OI, respectively, may represent two novel host-directed therapies for the treatment on *P. aeruginosa* infection in cystic fibrosis.

IV. Publications

Doroudian M, **O' Neill A**, MacLoughlin R, Prina-Mello A, Volkov Y and Donnelly S.C. Nanotechnology in pulmonary medicine. *Current Opinion in Pharmacology* **2021**;56:85-92. DOI: 10.1016/j.coph.2020.11.002

O'Neill A, Doroudian M, O'Reilly C, Tynan A, Mawhinney L, McElroy A, Webster SS, MacLoughlin R, Volkov Y, E Armstrong M, O'Toole G.A, Prina-Mello A, Donnelly S.C. Aerosolized drug-loaded nanoparticles targeting migration inhibitory factors inhibit *Pseudomonas aeruginosa*-induced inflammation and biofilm formation. *Nanomedicine (Lond)* **2020**. DOI: 10.2217/nnm-2020-0344

Rezaei M, Mostafaei S, Aghaei A, Hosseini N, Darabi H, Nouri M, Etemadi A, **O' Neill A,** Nahand JS, Mirzaei H, Donnelly SC, Doroudian M, Moghoofei M. The association between HPV gene expression, inflammatory agents and cellular genes involved in EMT in lung cancer tissue. *BMC Cancer*. **2020** Sep 24;20(1):916. DOI: 10.1186/s12885-020-07428-6.

Mostafaei S, Vahidi Manesh P, Sadri Nahand J, Nesaei A, Sorayyayi S, Abasabadi F, Mirzaei H, Etemadi A, **O' Neill A**, Donnelly S.C., Doroudian M, Armstrong M.E., Moghoofei M. The role of Epstein-Barr virus-expressed genes in breast cancer development. *Breast J*. **2020** Nov;26(11):2323-2326. DOI: 10.1111/tbj.14021.

V. Conference Proceedings

Irish Society for Immunology 2019, Dublin, Ireland.

Host Macrophage Migration Inhibitory Factor (MIF) regulates both the immune response to Pseudomonas aeruginosa infection and bacterial biofilm formation.

Host-Pathogen Communication 2018, Israel.

Host-Pathogen Interactions Host-Pathogen Interactions: Human Macrophage Migration Inhibitory Factor (MIF) Enhances Pseudomonas aeruginosa Biofilm Formation in a Human Airway Epithelial Cell Co-Culture Model.

Irish Thoracic Society Scientific Meeting 2017, Limerick, Ireland.

Macrophage Migration Inhibitory Factor enhances *Pseudomonas aeruginosa* biofilms, a potential novel therapeutic for Cystic Fibrosis Patients.

Irish Society for Immunology 2018, Dublin, Ireland.

Macrophage Migration Inhibitory Factor (MIF) and its novel tautomerase-enzymatic activity enhance Pseudomonas aeruginosa biofilm formation in a human airway epithelial cell co-culture model: a potential novel therapeutic target in the treatment of cystic fibrosis (CF).

VI. Abbreviations

4-IPP – 4-Iodo-6-phenylpyrimidine

4-OI – 4-Octyl Itaconate

ACOD1 – cis-Aconitate decarboxylase

ARDS – Acute Respiratory Distress Syndrome

BIR – Baculovirus Inhibitor of Apoptosis Protein Repeat

BMDMs – Bone Marrow Derived Macrophages

CARD – Caspase Recruitment Domain

c-di-GMP – Bis-(3'-5')-Cyclic Dimeric Guanosine Monophosphate

CF – Cystic Fibrosis

CFTR – Cystic Fibrosis Transmembrane Conductance Regulator

CFU – Colony Forming Unit

cGAMP – Cyclin GMP-AMP

cGAS – cGAMP synthase

COX-2 – Cycoloxygenase-2

DAMPs - Damage Associated Molecular Patterns

DGCs – Diguanylate Cyclases

DI – Dimethyl Itaconate

DNA – Deoxyribonucleic Acid

dsRNA – Double Stranded RNA

EPS – Extracellular Polymeric Substances

ERK – Extracellular Signal-Regulated Kinases

FDA – Food & Drug Administration

FEV1 - Forced Expiratory Volume in 1 Second

GAPDH – Glyceraldehyde 3-phosphate dehydrogenase

Gclm – Glutamate-Cysteine Ligase Modifier

Gsr – Glutathione Reductase

HIF – Hypoxia-Inducible Factors

Hmox1 – Heme Oxygenase 1

HRE – Hypoxic Response Element

IDH – Isocitrate Dehydrogenase

IFN – Interferon

IKK – Inhibitor of Nuclear Factor-κB Kinase

IRAK – IL-1R- Associated Kinase

IRF3 – Interferon regulatory transcription factor-3

Irg1 – Immune-responsive gene 1

IκB – Inhibitor of Nuclear Factor-κB

JAB – Jun activation domain –binding protein

Keap1 – Kelch-Like ECH-Associated Protein 1

LDH – Lactate Dehydrogenase

LPS – Lipopolysaccharide

M. tb – Mycobacterium tuberculosis

Mal – MyD88-Adapter Like Protein

MAPK – Mitogen-Activated Protein Kinase

MIF - Macrophage Migration Inhibitory Factor

MKP1 – MAPK Phosohatase-1

MyD88 – Myeloid Differentiating Factor 88

NF-κB – Nuclear Factor-Kappa B

NLR – NOD-like Receptor

NLRP – NOD-, LRR- and Pyrin Domain-Containing Protein

NO – Nitric Oxide

NOD – Nucleotide Oligomerisation Domain

Nqo1 – NAD(P)H Quinone Dehydrogenase 1

Nrf2 – Nuclear Factor Erythroid 2-Related Factor 2

P. aeruginosa – Pseudomonas aeruginosa

PAMPs - Pattern-Associated Molecular Patterns

PDEs – Phosphodiesterases

PFKP – Phosphofructokinase

PHDs – Prolyl Hydroxylases

PI3K – Phosphatidylinositol 3-Kinase

PLA_2 – Phospholipase A_2

PLGA – Poly(Lactic-Co-Glycolic Acid)

PRR – Pathogen Recognition Receptor

QS – Quorum Sensing

RNA – Ribonucleic Acid

ROS – Reactive Oxygen Species

S. aureus – Staphylococcus aureus

SDH – Succinate Dehydrogenase

ssRNA – Single Stranded RNA

STING – Stimulator of interferon genes

T3SS – Type 3 Secretion Systems

TAK1 – TGF-β Activated Kinase

TBK1 – TANK-Binding Kinase 1

TGF-β – Transforming Growth Factor β

TIR – Toll/IL-1R

TLRs – Toll Like Receptors

TNF-α – Tumour Necrosis Factor-α

TRAF6 – TNF-α Receptor Associated Factor 6

TRAM – TRIF-Related Adaptor Molecule

TRIF – TIR-Domain-Containing Adaptor Protein Inducing IFN-β

Chapter 1 - Introduction

1.1 Cystic Fibrosis (CF)

1.1.1 Introduction

Cystic fibrosis (CF) is the most common inherited disorder in the Caucasian population, with an estimated prevalence of 1 in 2000 births (1). The disease is caused by mutations in the Cystic Fibrosis Transmembrane Conductance Regulator (CFTR), which results in defective chloride ion transport across epithelial cell surfaces (2, 3). As a result, a build-up of thick viscous secretions occurs in the respiratory tract and other organs including the liver, pancreas and gallbladder (4, 5). This results in inflammation, obstructions and tissue damage in the affected areas.

The CF lung provides a microenvironment that promotes bacterial colonisation, with the main pathogen *Pseudomonas aeruginosa* (*P. aeruginosa*) adapting to survive and promote chronic infection (2). CF is a life limiting disease which impacts multiple organ systems, but respiratory failure as a result of inflammation and chronic bacterial infection is the leading cause of CF morbidity and mortality (6-8). Historically, the international median life expectancy of a CF patient in 1974 was 8 years old (2). The development of antibiotic regimes and CFTR modulating agents has seen this life expectancy rise to a median age of 30.8 years in 2018 (9).

1.1.2 Genetics of CF

CF is an autosomal recessive disorder that arises due to mutations in the CFTR gene, which is located on the long arm of chromosome 7 at position 7q31.2 (4, 10, 11). Individuals must inherit a mutated allele from each parent in order to have a CF phenotype. Mutations in the CFTR impacts the transport of sodium and water across epithelial cell surfaces resulting in luminal secretions that are abnormally viscous (7).

To date, over 1,800 different mutations have been described in the CFTR gene and reported on the Cystic Fibrosis Mutation Database (5). These mutations are organised into five different classes in a somewhat oversimplified classification system. Mutations resulting in defective protein synthesis are class I, defective protein processing are class II, defective regulation class III, transmembrane mutations are class IV and finally transcriptional defects are class V (12-14). While some mutations result in

no CFTR function and consequently severe disease, others are associated with residual function and less severe disease (9). Class I – III mutations are associated with severe disease as these mutations result in less than 10 % expression of functional CFTR (15). Mutations in these classes result in decreased lung function, worsened nutritional status, pancreatic insufficiency, and earlier mortality compared to Class IV and V mutations (16).

While there are over 1,800 CFTR mutations, The American College of Medical Genetics reports 23 mutations that it deems as frequent mutations; whereby the mutation is present at > 0.1 % in the general US CF population (17). The most common mutation in CF is ΔF508, accounting for over ~ 70 % of European cases (18). This mutation results in the deletion of 3 base pairs which encodes phenylalanine (F) at the 508 position which causes defective CFTR folding and reduced stability at the cell membrane. The ΔF508 mutation is therefore classified as a Class II and Class III mutation (19, 20).

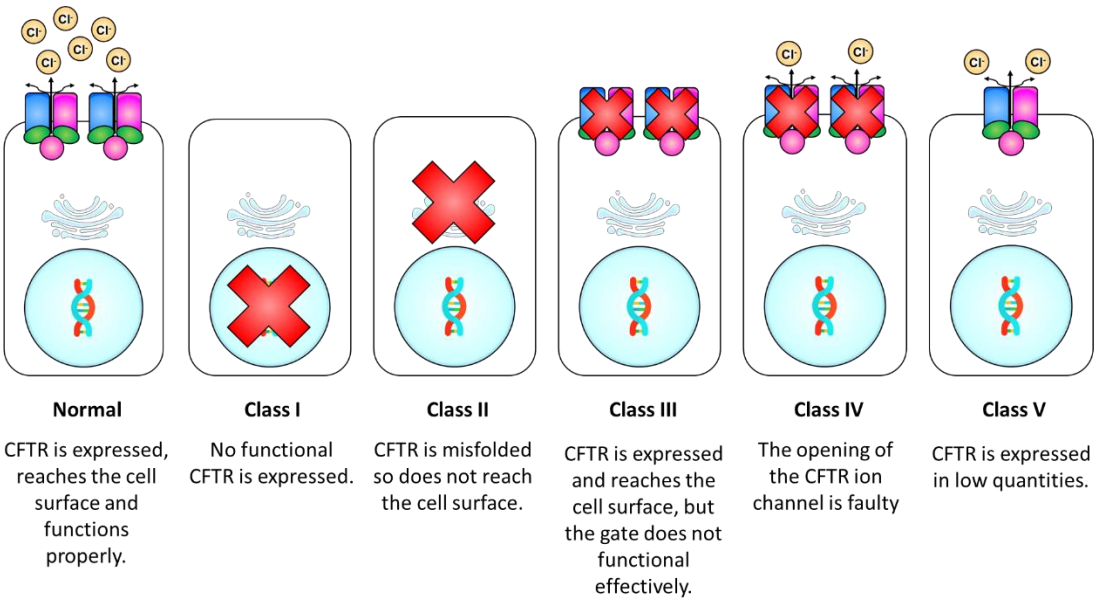

Figure 1.1 CFTR mutations by class.

CFTR mutations are divided into five sub-classes of mutations. Class I mutations result in no functional CFTR expression, class II mutations cause protein misfolding, class III mutations impair ion channel gating function, class IV impair CFTR ion channel opening and class V lead to low CFTR protein expression.

1.1.3 Pathophysiology & clinical effects of CF

Functional defects in CFTR proteins impacts ion and water transport across epithelial cell surfaces throughout the body with implications on numerous organs including the lungs, pancreas, testis, liver, intestines and sweat glands (**Figure 1.2**) (21).

Pancreatic ducts become blocked in CF resulting in chronic obstructive pancreatitis. Secondary to this the secretion of pancreatic enzymes which are required for the digestion of food becomes impaired, resulting in pancreatic insufficiency which is seen in of approximately 85 % of patients (22). This manifests as malnutrition and difficulties in weight gain in CF patients. CF associated diabetes is also an increasing problem as a result of destructive pancreatic disease which damages pancreatic islet cells which produce insulin (23). Other manifestations of CFTR dysfunction include impaired bile secretion, increased bile viscosity and bile duct obstruction (24). Reproductive issues are also almost universal in male CF patients due to the congenital bilateral absence of the vas deferens (25).

The main life-limiting effects of CF occur within the lungs. The damaging effects of CF are seen in children as young as 3 years old, with CT scans detecting mucus obstruction, bronchiectasis, and evidence of neutrophilic inflammation, neutrophil elastase activity and recurrent respiratory tract infections (26-29). Imbalances in ion transport at the level of the lung epithelium causes alterations in the airway surface liquid and results in impaired mucociliary clearance (30). Impaired mucociliary clearance promotes mucus build-up, obstruction, infection and inflammation (30).

CFTR defects have also been shown to result in reductions in the pH of airway surface liquid due to anomalies in bicarbonate transport across the epithelial surface (31). This alteration in pH impairs bacterial killing, which is pH dependent, and also reduces the function of antimicrobial peptides (32, 33). Airway mucus viscosity is also impacted by pH, with viscosity increasing and enhancing the level of mucus build-up (32). Mucus accumulation in the respiratory tract also provides an optimal breeding ground for opportunistic infections, including *P. aeruginosa* further promoting inflammation (34). Ultimately, it is cycles of immune dysfunction, recurrent infection and chronic inflammation that results in advanced CF lung disease (**Figure 1.2**) (21).

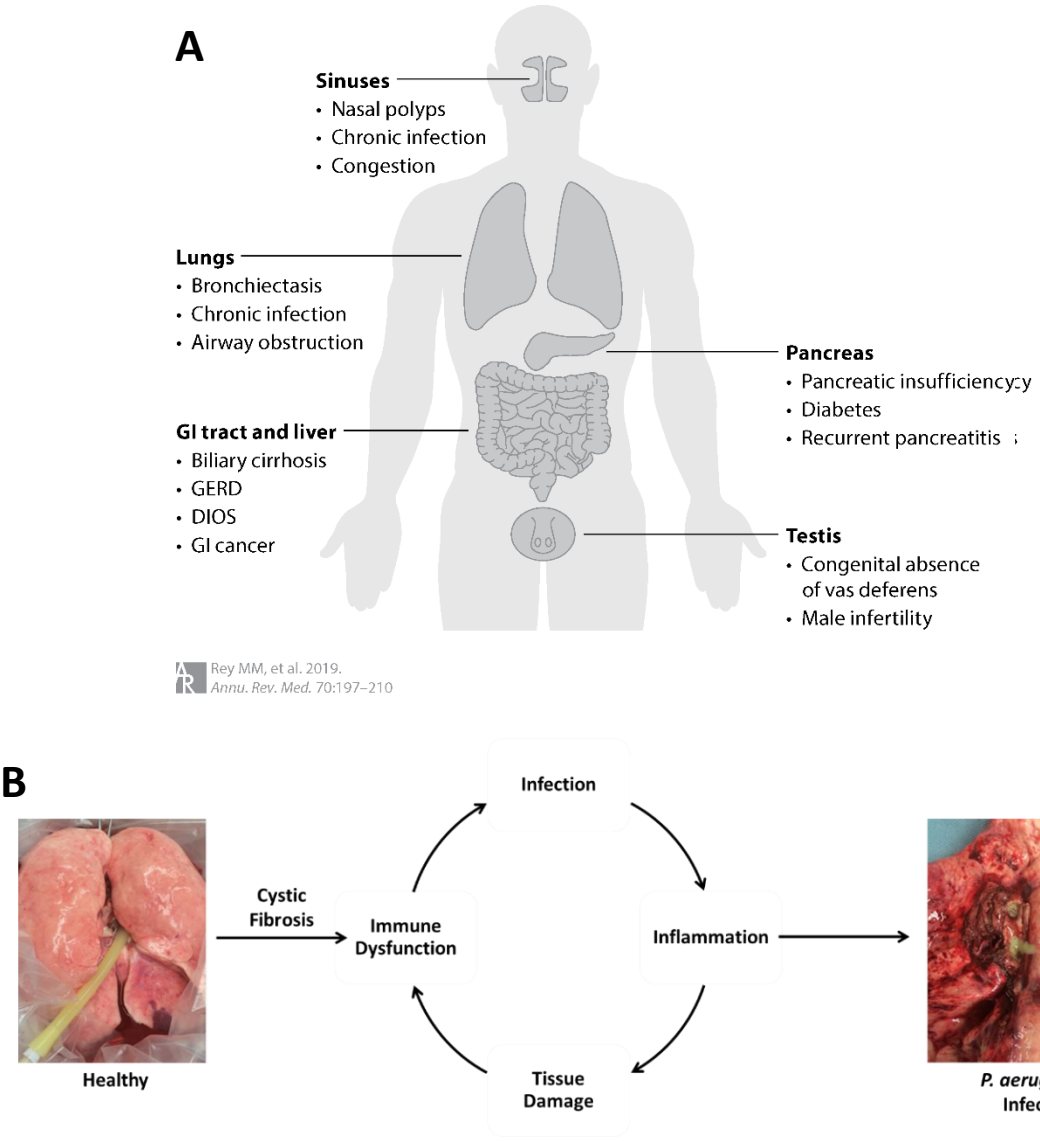

Figure 1.2 Clinical manifestations and pathophysiology of CF.

Cystic fibrosis is a multisystem disease. (**A**) It affects the lungs, sinuses, gastrointestinal tract, liver, pancreas, and other organs. Abbreviations: DIOS, distal intestinal obstruction syndrome; GERD, gastroesophageal reflux disease; GI, gastrointestinal. Adapted from (21). (**B**) CF lung disease is driven by cycles of immune dysfunction, infection, inflammation and tissue.

1.1.4 Infections in CF patients

Respiratory tract infections are extremely common in CF patients and are the cause of end stage lung disease (6-8). As a result of impaired mucociliary clearance and defective antibacterial immune responses, CF patients are predisposed to infection by several opportunistic pathogens (30, 32-34). These pathogens include *Haemophilus*

influenza, *Staphylococcus aureus* (*S. aureus*), *Stenotrophomonas maltophilia*, *Burkholderia cepacia*, *Achromobacter* and *P. aeruginosa* (35, 36).

In general, *Haemophilus influenza* and *S. aureus* are said to be the primary organisms infecting the airways of infants and children with CF. However, by the age of 25, upwards of 70 % of CF patients have had a detectable *P. aeruginosa* infection making this the most commonly isolated pathogen from the CF lung (35, 36). The textbook cycle of *P. aeruginosa* infection is a series of recurrent, intermittent colonisations before the acquisition of a chronic infection – as a result *P. aeruginosa* is regarded as one of the most important bacteria in the pathogenesis of CF (2, 37). It is the development of chronic respiratory infections that results in the onset of chronic inflammation and ultimately lung damage.

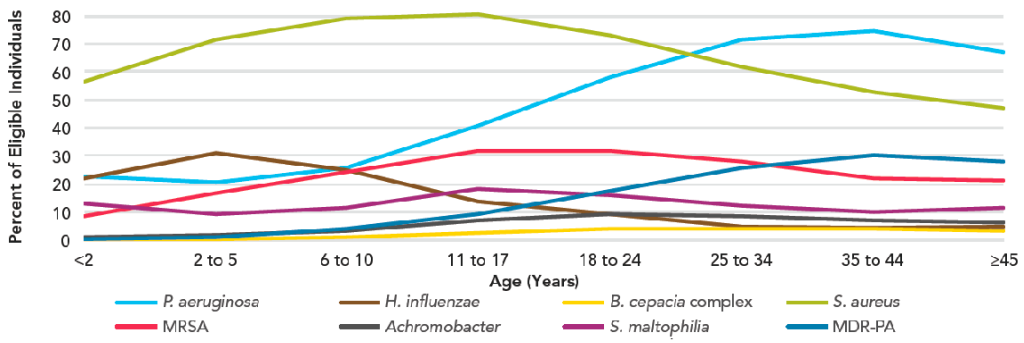

Figure 1.3 Progression of bacterial infections in patients with CF.

Prevalence of common respiratory pathogens in CF patients relative to age. *P. aeruginosa* is the most frequently found pathogen in adults. Adapted from (35). *H. influenzae*, *Haemophilus influenzae*; *B. cepacia complex*, *Burkholderia cepacia complex*; *S. aureus*, *Staphylococcus aureus*; *MRSA*, *methicillin-resistant S. aureus*; *S. maltophilia*, *Stenotrophomonas maltophilia*; *MDR-PA*, *multidrug-resistant P. aeruginosa*.

1.1.5 Treatment of CF

Historically, CF treatment has been centred around reducing airway obstructions and treating recurrent respiratory infections (38). Respiratory physiotherapy represents an effective means for clearing built up mucus from the obstructed CF airway (39). A popular method of respiratory physiotherapy is the high-frequency chest wall oscillation vest, which mechanically loosens and thins mucus enabling the user to cough and clear the airway (40). Mucolytics are also a key component of CF treatment, with dornase alfa reducing pulmonary exacerbations and improving lung function (41).

Effective antibiotic regimes are one of the key advances that have improved outcomes for CF patients, however it is clear that further therapies are necessary due to the development of antibiotic resistance (42, 43). Tobramycin and aztreonam are approved for use in the treatment of *P. aeruginosa* infection in CF patients throughout the world (44). Meropenem is a broad spectrum antibiotic from carbapenem family which is administered intravenously for the treatment of multi drug resistant gram negative bacterial infections, including *P. aeruginosa* (45, 46). These antibiotics improve lung function, quality of life and reduce exacerbations (42, 44).

The development of inhaled antibiotics has resulted in enhanced pulmonary delivery and limited the systemic side effects (47-49). Tobramycin and colistin are available as dry-powder inhaled antibiotics and act to decrease bacterial burden, improve lung function, enhance quality of life and reduce exacerbations (50, 51).

The development of CFTR modulating drugs has yielded great success in improving the treatment outcomes in CF. These drugs are designed to improve ion transport through the CFTR at the cell membrane and also to correct errors in CFTR folding to increase functionality (21). As such, these drugs are targeted towards specific classes of CFTR mutations (21).

Ivacaftor is the first commercially available CFTR modulator and works to control ion channel gating resulting in increased chloride ion movement and restoring salt and water balance in the lungs (21). Ivacaftor does not act to increase CFTR proteins at the cell surface and as such has shown limited efficacy in homozygous patients with ΔF508

mutations when administered alone. This is likely due to insufficient CFTR levels being available at the cell membrane for the drug act upon (52). However, in patients with Class III gating mutations, Ivacaftor significantly improves patients forced expiratory volume in 1 second (FEV1), increased patients weight and decreased the frequency of exacerbations (53). Ivacaftor received approval by the US Food and Drug Administration (FDA) in 2012 for class III mutations, and has since been approved for 38 new CFTR mutations (54).

Lumacaftor is a drug that helps to treat the misfolding of CFTR class II mutation and acts as a chaperone to increase the number of CFTR proteins at the cell surface (21, 55) Lumacaftor monotherapy failed to show effective results in a phase IIa clinical trial in patients homozygous for the ΔF508 mutation (56). However, dual therapy in combination with ivacaftor resulted in improved lung function and decreased exacerbations in these patients in a phase III clinical trial (57). More recent reports detail acute respiratory events in approximately 50 % of patients taking lumacaftor/ivacaftor, with high levels of treatment discontinuation (58).

Tezacaftor, another CFTR chaperone, received FDA approval in 2018 for combination use with ivacaftor in patients that are homozygous for the ΔF508 mutation or else have ΔF508 and one of 26 other mutations (21). This treatment demonstrated similar efficacy to lumacaftor/ivacaftor dual therapy with fewer side effects (59). More recently, a phase III clinical trial of a triple elexacaftor/tezacaftor/ivacaftor treatment yielded promising results. The study examined patients who have a single ΔF508 allele, a subset of patients in whom CFTR modulating therapies were ineffective, and demonstrated improved lung function, decreased rate of pulmonary exacerbations and an acceptable side effect profile (60). In 2019, triple elexacaftor/tezacaftor/ivacaftor treatment received FDA approval for CF patients with at least one ΔF508 mutation – opening up a new treatment avenue to approximately 90 % of CF patients (61).

The success of CF treatments is highlighted when one considers that forty years ago, 10 % of CF patients were over 18 years of age compared to more than 50 % today (9). Unfortunately, even with the myriad of treatment options available today, many CF patients experience respiratory failure and require lung transplantation. Without lung

transplantation, many CF patients will succumb to respiratory failure as a result of chronic infection and fulminant inflammatory responses (21).

1.1.5.1 Anti-inflammatory therapies

In CF, there has been scant use of anti-inflammatory therapies as a means of reducing the inflammatory lung damage caused by chronic infection. Currently, high-dose ibuprofen is the only anti-inflammatory treatment recommended for CF airway inflammation (62). However, long term administration may have side effects impacting the gastrointestinal and renal systems, and also worsened pulmonary inflammation (63, 64). Prolonged ibuprofen treatment also requires frequent pharmacokinetic monitoring to accurately determine an appropriate dose and as a result there has been very low uptake within the CF community (62).

Chronic use of oral corticosteroids is not recommended for CF patients. Although treatment has shown an improvement in important CF outcomes including decreased hospitalisations, significant lasting effects among cohorts were noted in growth and glucose metabolism (65, 66). As such the side effects of prolonged corticosteroid treatment outweigh the benefits and it is not recommended.

Further research is continuing to examine the effects of anti-inflammatory therapies in both animal models and CF patients. Oral treatment of CF patients with antioxidant *N*-acetylcysteine significantly decreased sputum elastase levels (67). A follow up phase II study illustrated that those treated with *N*-acetylcysteine maintained their lung function, while those receiving placebo had decreased lung function (68).

In vivo treatment with Anakinra, a recombinant IL-1 receptor antagonist, resulted in enhanced survival and *P. aeruginosa* clearance in $Cftr^{-/-}$ mice compared with untreated $Cftr^{-/-}$ mice due to dampening overexuberant inflammation mediated by the NLRP3 inflammasome (69).

It is important to note that dampening the immune response is not always of benefit, and there is a fine line between a treatment which may have beneficial versus detrimental effects. A clinical trial of a leukotriene B4 receptor antagonist in CF patients was prematurely terminated due to an association with serious adverse events in participants (70). In an animal model of chronic *P. aeruginosa* infection, the same

leukotriene B4 receptor antagonist reduced neutrophil recruitment to the lung and increased bacterial load (71).

1.2 Innate Immunity

1.2.1 Introduction

The human body is under constant threat from invading pathogens and cellular damage. The immune system has been evolutionary conserved and has developed to protect the host from such threats. The human immune system can be divided into two different arms; the innate immune response and the adaptive immune response. The innate immune system serves as the first line of the immune response to invading pathogens including bacteria, fungi and viruses (72-74).

The innate immune system is comprised of a wide variety of cell types with varying functions such as phagocytosis, antigen presentation and granulocyte release. The cells involved include phagocytes such as macrophages and neutrophils; granulocytes including mast cells, basophils and eosinophils; antigen presenting cells such as dendritic cells and also cytotoxic natural killer cells (72-75). These immune cells act to engulf and kill invading microorganisms and infected cells; by secreting antibacterial materials, or to recognise invading pathogens and subsequently recruit immune cells to the site of infection. These cells are key in the early clearance of infections and play a pivotal role in the presentation of antigens to the cells of the adaptive immune system (72-74).

The adaptive immune response occurs several days after the initial onset of the innate immune response. Antigen presenting cells, including macrophages and dendritic cells, act to present fragmented antigens to T-cells which then become activated, mature and clonally expand (76). These T cells are either cytotoxic whereby they attack infected or damaged cells, or helper T cells which coordinate an immune response by communicating with other T-cells and B-cells. This process is highly specific and results in the development of immune memory, which ensures a stronger and faster immune response if the same antigen is encountered again (76, 77). The mounting of an effective immune response relies of the detection of invading pathogens through Pattern Recognition Receptors (PRRs).

1.2.2 Pattern recognition receptors (PRRs)

PRRs are key proteins that are involved in the sensing of pathogen-associated molecular patterns (PAMPs) and damage associated molecular patterns (DAMPs). PRRs have the ability to sense both endogenous and exogenous signals as they are located at various locations on immune cells including the cell membrane, in the cytoplasm and on the endosomal membrane. Endogenous signals include DAMPs that are released from damaged and dying host cells such as ATP, uric acid, deoxyribonucleic acid (DNA) and ribonucleic acid (RNA). Exogenous signals include factors related to invading pathogens such as LPS, double stranded RNA (dsRNA) and bacterial cell wall components (72, 74).

1.2.3 Toll-like receptors (TLRs)

TLRs recognise conserved structures in pathogens and are one of the key groups of PRRs that sense invading pathogens and trigger an innate immune response (78). TLRs were originally described in the context of embryogenesis, with the Toll protein being essential for dorsoventral polarity during embryogenesis in *Drosophila melanogaster* (79). It was subsequently recognised that Toll played an essential role in the anti-fungal innate immune response (80).

1.2.3.1 TLR Structure

The structure of all TLRs consists of an extracellular domain, a single transmembrane domain and a cytoplasmic domain (81, 82). The extracellular domain comprises of leucine rich repeats which are approximately 24 amino acids in length (83). These leucine rich repeats form β-sheets and fold into a concave horseshoe structure which mediates the recognition of ligands (83). Different TLRs can recognise several structurally unrelated ligands – some of which are outlined in **Table 1.1**.

All TLRs have a conserved cytoplasmic domain, which is known as the Toll/IL-1R (TIR) domain (84). The TIR domains of TLRs is responsible for interacting with cytosolic adapter proteins which in turn interact with downstream signalling molecules to induce the production of cytokines and interferons through many inflammatory pathways.

1.2.3.2 TLR Function and Signalling

The localisation of TLRs throughout mammalian cells is indicative of the ligand which they recognise. TLR1, TLR2, TLR4, TLR5 and TLR6 are primarily located on the plasma membrane where they act to recognise various components of microbial pathogens that are extracellular in nature (78). TLR3, TLR7, TLR8 and TLR9 are primarily located intracellularly on the membranes of endosomes and lysosomes. These TLRs recognise RNA and DNA from intracellular pathogens which are detectable once the invading pathogen has been endocytosed and broken down (85).

In general, TLRs function as homodimers or heterodimers. For example, TLR3 and TLR4 act as homodimers, while TLR2 can dimerise with TLR1 or TLR6 (82). Heterodimers increase the diversity of ligands that can be recognised by TLRs. Ligand recognition and receptor dimerization results in a conformational change which brings the two C-termini into proximity and juxtaposes the intracellular TIR domains (86). This is followed by the recruitment of adapter proteins which initiate intracellular signalling cascades which culminate in the activation of transcription factors including nuclear factor-kappa B (NF-κB), mitogen-activated protein kinases (MAPKs) and members of the interferon (IFN) regulatory factor family which control the production of chemokines, cytokines and IFNs which in turn coordinate the host response to infection (**Figure 1.4**) (85).

The response that is mounted following ligand binding to TLRs is mediated by intracellular adapter proteins including Myeloid differentiating factor 88 (MyD88), MyD88-adapter like protein (Mal), TIR-domain-containing adaptor protein inducing IFN-β (TRIF) and TRIF-related adaptor molecule (TRAM). TLR signalling is divided into two key pathways; MyD88-dependent and MyD88-independent pathways (85).

MyD88 is utilised by all TLRs, except TLR3, to induce signalling cascades through IL-1R- associated kinase (IRAK) proteins. Stimulation of TLRs triggers MyD88 recruitment to the TIR domain of the TLR where it in turn recruits IRAK proteins. TLR2 and TLR4 also rely on Mal for MyD88 recruitment (87). Phosphorylation of IRAK proteins enables the recruitment of tumour necrosis factor (TNF)-α receptor – associated factor 6 (TRAF6). Phosphorylated IRAK1 and TRAF6 then dissociate from the receptor before

forming a complex with transforming-growth factor (TGF)-β activated kinase (TAK1), TAK1- binding protein 1 (TAB1) and TAB2. IRAK1 is then dissolved at the cell membrane, while the remaining complex translocates to the nucleus where it phosphorylates MAPKs or the inhibitor of nuclear factor-κB (IκB) kinase (IKK) complex. The IKK complex then phosphorylates IκB, resulting in the degradation of IκB which subsequently enables NF-κB to translocate to the nucleus and induce gene expression (73).

TLR3 and TLR4 both signal using the MyD88-independent pathway, also known as the TRIF-dependent pathway, in order to signal through interferon regulatory transcription factor-3 (IRF3) and NF-κB (88). Stimulation of TLR3 activates TRIF directly, while TLR4 activation requires TRAM to interact and activate TRIF (87). TRIF interacts with TRAF6 and activates TAK1 for NF-κB activation. TRIF also recruits TRAF3 which in turn activates TANK-binding kinase 1 (TBK1) and IKK-ε which mediates downstream IRF3 activation. Activation of TLR3 and TLR4 results in the production of IFN-β, inflammatory cytokines and other IFN inducible genes (74).

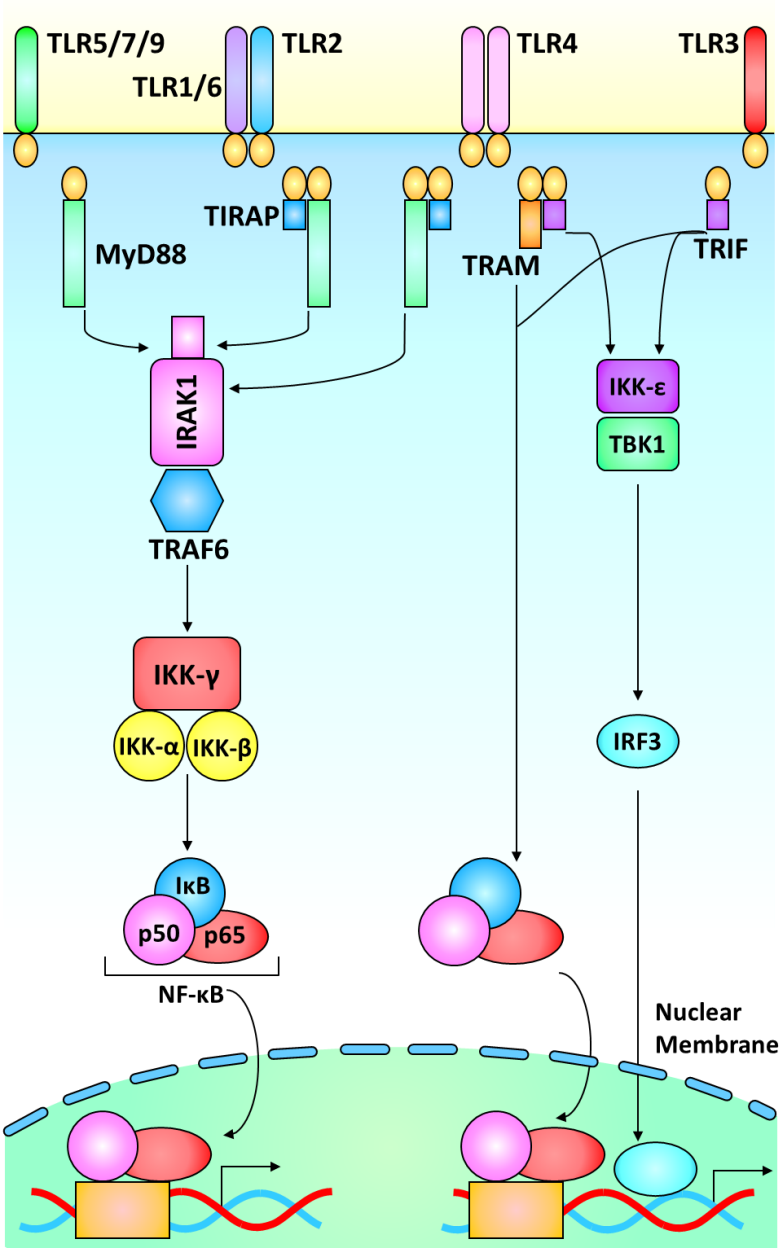

Figure 1.4 Overview of TLR mediated signalling cascades

Activation of TLRs leads to intracellular signal transduction, which is mediated by adaptor molecules MyD88, TIRAP, TRAM and TRIF resulting in downstream activation of transcription factors NF-κB and IRF3 resulting in nuclear translocation and gene transcription.

Table 1.1 Human and murine TLRs and their respective ligands

Receptor	Ligand	Location	Species
TLR1	Triacylated Lipoproteins	Cell Membrane	Human & Murine
TLR2	Di/Triacylated Lipoproteins	Cell Membrane	Human & Murine
TLR3	dsRNA	Endosomes	Human & Murine
TLR4	LPS	Cell Membrane	Human & Murine
TLR5	Flagellin	Cell Membrane	Human & Murine
TLR6	Triacylated Lipoproteins	Cell Membrane	Human & Murine
TLR7	Viral Single Stranded RNA (ssRNA)	Endosomes	Human & Murine
TLR8	Viral ssRNA	Endosomes	Human & Murine
TLR9	CpG DNA	Endosomes	Human & Murine
TLR10	Unknown		Human
TLR11	Profilin, flagellin	Endosomes	Murine
TLR12	Profilin	Endosomes	Murine
TLR13	Bacterial 23s rRNA	Endosomes	Murine

1.2.4 Nucleotide oligomerisation domain like receptors

Nucleotide oligomerisation domain (NOD) like receptors (NLRs) are a family of intracellular PRRs which are expressed in the nucleus and cytoplasm, detecting both PAMPs and DAMPs (89-91). NLRs are composed of a conserved nucleotide binding domain, a C-terminal leucine rich repeat for ligand binding and an N-terminal region for signal transduction (92). NLRs are divided into sub families depending on the structure of their N-terminal domain. There are numerous domain types including caspase recruitment domain (CARD), pyrin, and baculovirus inhibitor of apoptosis protein repeat (BIR) domains. In general, NLRs that contain a CARD domain are involved in the upregulation of proinflammatory mediators, whereas those containing pyrin or BIR domains are involved in inflammasome formation and caspase-1 activation.

NOD1 and NOD2 sense peptidoglycan motifs from invading pathogens. Activation of NOD1 and NOD2 results in NF-κB activation and the induction of proinflammatory cytokines (93). Activation of NLRs including NLRP1, NLRP3, NLRC4 and NLRP6 results in the formation of complex structures known as inflammasomes (94). Inflammasomes are high molecular weight signalling platforms that are required for the activation of caspase-1, which is required for maturation of pro-IL-1β and pro-IL-18 into their biologically active forms (95, 96).

1.2.5 Other PRR families

Retinoic acid-inducible gene I (RIG-I)- like receptors (RLRs) are a family of intracellularly expressed sensors which play a vital role in the detection of viral infections (97). This family of receptors are DExD/H box-containing helicases which function as PRRs by detecting viral RNA withing the cytosol (98). RLRs induce potent anti-viral effects through the induction of pro-inflammatory cytokine production and also the production of type I interferons as a result of NF-κB and IRF3 activation (99, 100).

C-type lectin receptors (CLRs) are a superfamily of proteins, characterised by the presence of one or more C-type lectin-like domains (CTLDs) (101). CLRs are expressed as both membrane bound and intracellular forms and play a key role in antifungal immunity (101, 102). Examples of CLRs include the mannose receptor, Dectin-1 and

Dectin-2 which detect mannose, β-glucan, α-mannans respectively (102, 103). Activation of CLR induces the production of pro-inflammatory cytokines and also mediates fungal binding, uptake and killing (101, 102).

Other cytoplasmic sensors include stimulator of interferon genes (STING), which is a key adapter protein involved in cytosolic DNA sensing (104, 105). STING can also directly recognise cyclic dinucleotides produced by bacteria (106). STING activation induces type I IFN and inflammatory cytokine production through activation of IRF3 and NF-κB (107, 108). Cyclic GMP-AMP (cGAMP) synthase (cGAS) is also a cytosolic DNA sensor which produces cGAMP which is required for STING activation. cGAMP is synthesised by cGAS from ATP and GTP before binding to STING to induce IRF3 and NF-κB mediated cytokine production (105, 107).

1.3 Macrophage Migration Inhibitory Factor (MIF)

1.3.1 Introduction

Macrophage migration inhibitory factor (MIF) is a pleiotropic pro-inflammatory protein that has been shown to possess cytokine, chemokine, enzymatic and hormonal functional characteristics (109). MIF plays a pivotal role in the regulation of the innate immune system through exerting its pro-inflammatory effects and consequently has been implicated in the pathogenesis of a number of inflammatory disorders including acute respiratory distress, rheumatoid arthritis, CF and various cancers (110-115). The involvement of MIF in the development of a myriad of diseases has led to an increase in interest with regards to the biological activity of MIF.

1.3.2 Discovery, genetics and structure of MIF

MIF is one of the first cytokines ever described and was discovered during the study of the delayed hypersensitivity reaction. These experiments demonstrated a factor secreted from antigen treated T cells could inhibit the migration of macrophages (116, 117). While this was of considerable interest to immunologists, it was not until the MIF gene was sequenced in 1989 that a further insight was gained into the biological activity of MIF (118). In 1991, research into inflammatory regulators discovered that MIF is released from cells in the anterior pituitary gland after LPS exposure *in vivo* (119).

The subsequent development of monoclonal antibodies and recombinant MIF production furthered research into the inflammatory profile of MIF (119, 120).

Although initially described in T cells, MIF has been shown to be expressed by macrophages, monocytes, B cells, neutrophils, eosinophils and epithelial cells (121-124). Interestingly, MIF is constitutively expressed and exists in pre-formed pools within the cytoplasm and as such does not require *de novo* protein synthesis so can be released rapidly (124). High concentrations of preformed MIF have been detected in macrophages, T cells and eosinophils (121, 125, 126). MIF is also expressed by a variety of tissues including the lungs, skin gastrointestinal tract and the genitourinary tract (124).

The MIF gene is exclusively located on chromosome 22 (22q11.23) and is in syntenic conservation with part of the mouse chromosome 10 which contains the *Mif* gene (127-129). This gene encodes a 12.5 kDa protein composed of 114 amino acids, who's crystal structure was solved in 1996 (130-132). MIF exists as a homotrimer which consists of three MIF monomers, with a molecular mass of 37.5 kDa (130, 133). Each monomer is composed of two anti-parallel α-helices which are packed against a four-stranded β-sheet (130). The monomers then come together to form a symmetrical trimer as three β-sheets and six α-helices form a circular protein (**Figure 1.5**) (130, 134). This protein exerts a high degree of conservation, with ~ 90 % homology across human, mouse, rat and cattle (124).

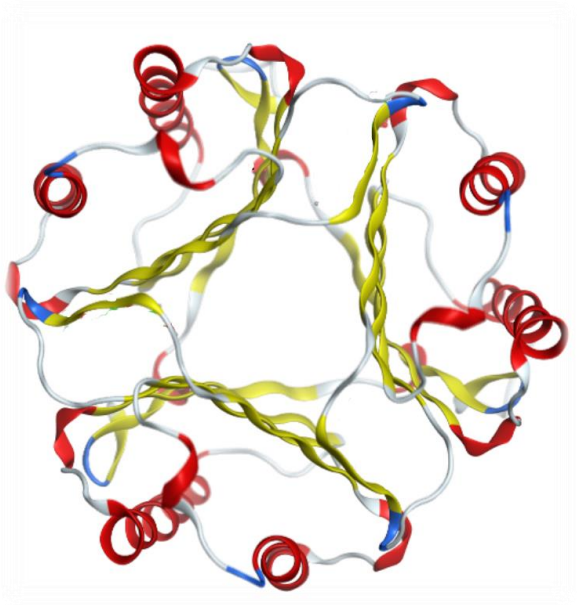

Figure 1.5 Crystal structure of MIF.

The three-dimensional crystal structure revealing the homotrimeric structure of the human MIF protein. α-helices are represented in red; β-sheets are represented in yellow.

1.3.3 Enzymatic activity of MIF

MIF is unusual in the fact that it is an enzymatically active molecule which displays specific catalytic activities. It was initially discovered that MIF can convert non-physiological 2-carboxymethylester-2,3-dihydroindole-5,6-quinone (dopachrome) to 5,6-dihydroxyindole-2-carboxymethyl ester (DHICA) through a tautomerase reaction (135). Based on the similarity of MIF to bacterial isomerase enzymes oxalocrotonate tautomerase, chorismate mutase and 5-carboxylmethyl-2-hydroxymuconate, Rosengren *et al* discovered that MIF also catalyses the keto-enol isomerations of p-hydroxyphenylpyruvate and phenylpyruvate (136-138).

The crystal structure of MIF revealed the presence of three hydrophobic active sites within the trimer which are formed at the interface between two adjacent monomers (139). Within the active site the N-terminal proline, Pro-1, is pivotal for the catalytic activity of MIF (139). Genetic mutation of the N-terminal proline to a non-nucleophilic glycine residue eliminates the tautomerase activity of MIF (139).

The importance of MIFs enzymatic activity has remained a controversial topic to date (140). The P1G mouse was developed to examine the role of MIFs enzymatic activity, whereby the N-terminal proline is mutated to a glycine resulting in the production of enzymatically inactive MIF (140). Using this mouse, the role of MIF tautomerase activity has been highlighted in numerous animal models. For example, P1G mice exhibit less lung inflammation and bacterial colonisation in a model of chronic *P. aeruginosa* infection compared to wild type mice (111). Also, P1G mice have less subcutaneous tumour development compared to wild type mice in a cancer model (112).

Early research suggests that it is not the enzymatic activity itself, but the structure of the active site that is of importance to MIFs immunological activity (140). While P1G-MIF is catalytically inactive, the protein still binds to the MIF receptor – although at a reduced rate compared to wild type MIF. The growth rate of cells derived from P1G, MIF knockout and wild type mice revealed that P1G cells were an intermediate phenotype between knockout and wild type mice. This suggests that the enzymatic activity does not fully regulate the cytokines activities, but it is likely the protein-protein interactions that control the effects (140).

To date, a physiologically relevant substrate for MIFs catalytic activity has yet to be described. As MIF is structurally similar to numerous bacterial enzymes, a popular hypothesis is that MIF my interact with bacterial products (137, 138). This is supported by research demonstrating that MIF enhances bacterial colonisation in numerous models, including chronic *P. aeruginosa* infection (111, 113). Furthermore, MIF tautomerase activity enhances biofilm formation in *P. aeruginosa* (113). However, further research is required to elucidate a physiologically relevant substrate for MIF.

1.3.4 MIF inhibitors

The active site of MIF has proven to be a popular therapeutic target for the development of small molecular weight inhibitors (112, 113, 141, 142).

ISO-1 is a commercially available MIF inhibitor and is the most frequently used reference inhibitor. ISO-1 targets the active site of MIF, where it docks to exert its inhibitory effects (143). ISO-1 inhibits the tautomerase activity of MIF, but also the

biological activity as it decreases MAPK activation, p53-dependent apoptosis, cell cycle progression and ERK phosphorylation (142, 144). ISO-1 also decreases MIF dependent arachidonic acid release and cytokine production from LPS stimulated macrophages (143). *In vivo*, ISO-1 has shown promising effects in models of asthma, chronic obstructive pulmonary disease, and various cancer models (112, 145-148). ISO-1 also demonstrated a significant effect on survival in model of induced sepsis, where ISO-1 treatment resulted in 80 % survival, compared to 20 % in untreated mice (141).

4-Iodo-6-phenylpyrimidine (4-IPP) is an irreversible inhibitor of MIFs tautomerase activity which binds to Pro-1 residue (149). 4-IPP has been shown to inhibit MIF mediated lung adenocarcinoma cell migration and anchorage dependent growth (149). 4-IPP has also been used *in vivo* where it was shown to inhibit inflammation and enhance bacterial clearance in a model of *P. aeruginosa* induced ocular keratitis (150).

SCD-19 is a small molecular weight inhibitor which targets the active site of MIF resulting in inhibition of both enzymatic and biological activity which was developed by The Donnelly Lab (112, 113). SCD-19 dose-dependently decreases LPS induced TNF-α and PGE_2 release (112). SCD-19 also inhibits MIF induced cell proliferation *in vitro* (112). *In vivo*, SCD-19 decreases subcutaneous tumour volume by 90 % compared to in a Lewis lung carcinoma mode (112). In all experiments, the effects of SCD-19 was greater than that of ISO-1 (112). In a murine model of chronic *P. aeruginosa* infection, SCD-19 significantly decreased lung inflammation, attenuated weight loss and decreased bacterial load in the lung (113).

1.3.5 MIF CATT repeat

A novel CATT tetranucleotide repeat polymorphism at position -794 in the promoter region of the MIF gene was identified, with the description of individuals with 5, 6, 7 or 8-CATT repeat alleles (**Figure 1.6**) (114, 127). It has been demonstrated that there is a direct correlation between the number of CATT repeats and MIF expression levels, with those with a 5-CATT allele having the lowest expression levels (114).

In rheumatoid arthritis, patients with a higher number of CATT repeats have higher levels of MIF transcription. These patients are also prone to more severe disease manifestations (114). In a European study, the presence of a 7-CATT repeat and

consequent high levels of MIF expression correlated with the severity of radiological joint damage (151).

Similarly, CF patients with a 5-CATT allele have reduced disease severity and reduced *P. aeruginosa* colonisation compared with CF patients that have 6,7 or 8-CATT repeats (110). Further studies demonstrated that CF patients with at least one 5-CATT allele have a significantly slower decline in lung function compared to those with no 5-CATT allele (111). Patients that were 5-CATT homozygous had significantly decreased circulating MIF than those that were 6-CATT homozygous (111). Furthermore, PBMCs from the 5-CATT homozygous patients secreted significantly more TNF-α than 6-CATT homozygous PBMCs in response to LPS stimulation (111).

These studies demonstrate that the MIF CATT microsatellite is a functional polymorphism with implications in both infections and autoimmune disease.

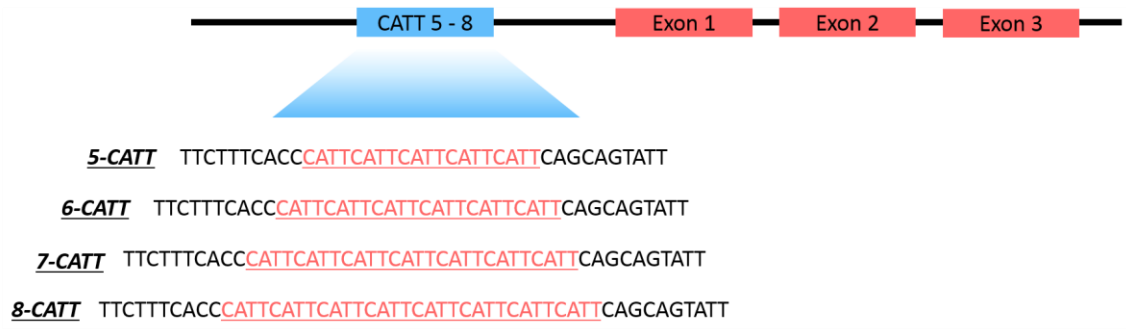

Figure 1.6 Promoter region of the human MIF gene.

Schematic image of the presence of the 5 to 8 copies of the CATT microsatellite repeat polymorphism in the promoter region of the human MIF gene. Inspired by (152).

1.3.6 MIF G/C polymorphism

The G/C single nucleotide polymorphism (rs755622) which is located at -173 in the MIF promoter sequence, is the most widely studied variant in the MIF gene (151). This polymorphism results in the generation of a glycine to cysteine transition, which generates a putative binding site for the transcription factor activating enhancer binding protein 4 (151). The presence of the MIF -173 polymorphism is associated with higher

expression levels of MIF protein production, and has been associated with increased disease susceptibility and severity in a variety of patient cohorts including rheumatoid arthritis, psoriatic arthritis and sarcoidosis patients (153-157). Although this polymorphism is more well studied than the CATT-microsatellite repeat, the latter appears to have more functionality; for this reason we will focus on the CATT-microsatellite repeat for the purposes of this project (153).

1.3.7 MIF signalling and role in immunity

MIF exerts its effects as a cytokine through both receptor mediated and receptor-independent signalling mechanisms (**Figure 1.7**). The MIF receptor is a two-component signalling complex that is composed of the ligand-binding protein CD74 and the signal transducer CD44 (153, 158, 159). CD74 is a transmembrane glycoprotein that is expressed on many cell types including B cells, monocytes and macrophages (158). CD74 has a high affinity for MIF, with ligand binding initiating horizontal membrane recruitment of CD44 (153, 160). Following CD44 recruitment, the cytosolic domains of both proteins undergo phosphorylation resulting in downstream signal transduction (153, 160). This leads to Src kinase family activation resulting in activation of the mitogen-activated protein kinase/ extracellular signal-regulated kinases (MAPK/ERK) pathway and consequently sustained phosphorylation of ERK1/2 (161). Src kinase activation also leads to activation of Akt in a phosphatidylinositol 3-kinase (PI3K) dependent manner resulting in increased glucose uptake, growth and cell survival (162, 163).

The activation of the MAPK cascade leads to the phosphorylation and activation of a variety of downstream effector molecules. Phospholipase A_2 (PLA_2), which plays an important role in the generation of a pro-inflammatory cascade, is activated via this pathway and results in the production of arachidonic acid. Cyclooxygenase-2 (COX-2) activity is also upregulated via this pathway and sequentially oxidises arachidonic acid in order to produce prostaglandins, notably PGE_2 (164). COX-2 activity also leads to the downregulation of tumour suppressor p53, inhibiting activation-induced apoptosis and prolonging cell survival and inflammatory activation (161, 165-167). Overall, MAPK

activation results in cell proliferation, inhibition of apoptosis and the production of pro-inflammatory mediators.

Furthermore, MIF binding to CD74 initiates intramembrane cleavage of CD74 (168-170). This cleaved segment then interacts with p65, where it then enters the nucleus to regulate NF-κB mediated gene transcription (170). CD44 is also engaged in this process where it acts to activate Src family kinases leading do PI3K-dependent phosphorylation of Akt (162).

MIF has also been shown to be non-cognate ligand of the chemokine receptors CXCR2 and CXCR4 , where it acts to regulate inflammatory cell recruitment (171, 172). Activation of these receptors leads to activation of ERK1/2 and Akt, again regulating chemotaxis, survival and the inflammatory profile of activated cells (171, 172). MIF can also initiate signalling in a receptor independent manner. Endocytosed MIF interacts with intracellular c-Jun activation domain-binding protein (JAB) (173). JAB is a co-activator of AP-1 which is a major regulator of pro-inflammatory cytokine production (174, 175).

MIFs inflammatory activity has been shown to override the anti-inflammatory effects of glucocorticoids (176). This effect of MIF has been demonstrated *in vitro* where MIF counteracts the glucocorticoid mediated suppression of inflammatory mediators in activated macrophages including TNF-α, IL-6 and IL-8 (177). *In vivo*, MIF completely reverses the protective effects of glucocorticoids in an LPS lethality model (177). MIF counteracts the anti-inflammatory effects of glucocorticoids in several ways. MIF supresses glucocorticoid mediated suppression of NF-κB inhibitor IκB, enhancing NF-κB activation (153, 178, 179). Glucocorticoids also upregulate levels of the MAPK inhibitor MAPK phosophatase-1 (MKP1), an effect that MIF overrides which results in increased inflammation (180). Suppression of PLA_2 and subsequent arachidonic acid production by glucocorticoids is also overruled by MIFs activation of MAPKs (161). The MIF mediated increase in arachidonic acid enhances the production of inflammatory cytokines including TNF-α and IL-6 (153, 181).

MIF also plays a key role in the response of immune cells to LPS. MIF deficient macrophages have been shown to have reduced responses to LPS due to decreased

TLR4 expression. Further investigation revealed that MIF acts to upregulate TLR4 expression by controlling levels of a crucial transcription factor, PU.1 (182). This finding highlights the importance of MIF in the innate immune system as it regulates detection of a major virulence factor and is therefore involved in the orchestration of an effective immune response.

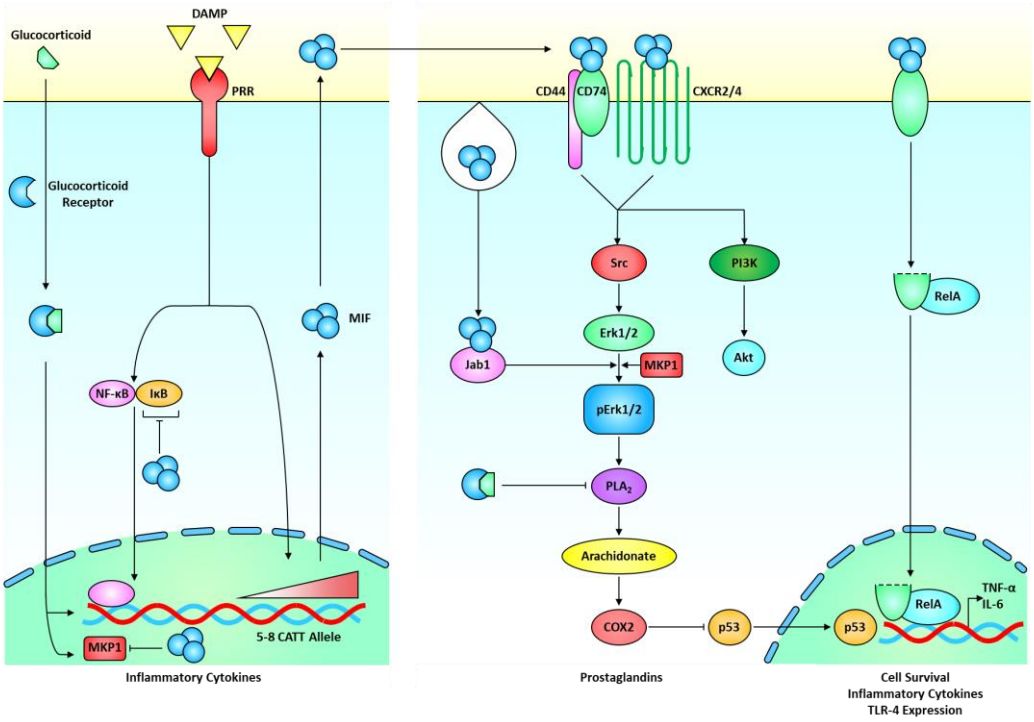

Figure 1.7 Overview of MIF signalling.

MIF induces inflammatory responses via a variety of mechanisms. Activation of PRRs by diverse stimuli activates MIF transcription and also *de novo* synthesis in an MIF allele-dependent manner (5-8 CATT). MIF induces intracellular signalling through binding with the CD74-CD44 receptor complex or CXCR2/4 resulting in downstream Erk activation and PLA2, arachidonate and COX2 production. COX2 inhibits p53 which leads to cell survival. MIF also overrides the anti-inflammatory mechanisms of glucocorticoids through inhibition of IκB, resulting in NF-κB liberation, transnuclear localisation and induction of inflammatory cytokines. Furthermore, glucocorticoids act to promote mitogen-activated protein kinase phosphatase 1 (MKP1) which inhibits MAPK phosphorylation. MIF inhibits MKP1 activities. Endocytosed MIF acts to activate JAB1, leading to MAPK activation. MIF interacting with CD74also induced cleavage which generates cleaved-CD74 which interacts with NF-κB family member RelA which enters the nucleus and regulates the transcription of NF-κB target genes. Adapted from (153).

1.3.8 MIF and hypoxia inducible factor (HIF)

The hypoxia inducible factor (HIF) pathway regulates oxygen homeostasis within cells. The HIF transcription factor family is composed of α and β subunits which form heterodimers during activation. Upon heterodimer formation, the complex translocates to the nucleus where if binds to hypoxia response elements (HRE) in the promoter regions of genes to regulate gene expression (183).

HIF-1α protein levels are regulated by the von Hippel-Lindau tumour suppressor protein (VHL)-mediated ubiquitin protease pathway which promotes continuous HIF-1α degradation. This effect is promoted by the hydroxylation of HIF-1α by prolyl hydroxylases (PHDs), which marks the protein for degradation (184-186).

HIF-1α is rapidly stabilised in response to numerous stimuli including hypoxia, high CO_2 levels, NF-κB activation and PAMPs including LPS. Activation of HIF-1α under normoxic conditions occurs upon NF-κB activation, with NF-κB binding to the NF-κB response element within the HIF-1α promoter (183, 187-189). LPS stimulation also decreases expression levels of PHDs, resulting in further HIF-1α stabilisation (190). This enables heterodimer formation with HIF-1β and subsequent alterations in gene expression involved in angiogenesis and metabolism (183, 188, 189, 191, 192). HIF-1α also drives IL-1β production in response to succinate accumulation in LPS stimulated macrophages (185).

MIF expression has previously been shown to be induced by hypoxia, with HIF binding to the HRE in the 5' untranslated region of the MIF gene (193, 194). Moreover, MIF has been shown to be essential for maximum HIF-1α expression and stabilisation through NF-κB activation in several different cell type (193, 195-197). $MIF^{-/-}$ macrophages have deficient HIF-1α stabilisation in response to hypoxia (193).

1.3.9 MIF and infection

MIF is a key regulator of innate immunity and as such plays an important role in the host response to infection. The importance of MIF in infection is likely due to the role of MIF in controlling TLR4 expression levels and also its role in the regulation of

cytokine production (182). However, it appears that MIF can have both beneficial and detrimental effects depending on the invading pathogen.

In a model of LPS induced lethality, $MIF^{-/-}$ mice had significantly increased survival compared to wild type mice (198). These mice also displayed decreased TNF-α, while there was no difference in IL-6 levels compared to wild type (198). In a separate study, LPS stimulated mice had increased levels of MIF in their blood within 2 hours; a very early release profile due to the existence of pre-formed pools (119). *In vitro*, macrophages from $MIF^{-/-}$ mice secreted significantly decreased levels of TNF-α and nitric oxide, but similar levels of IL-6 compared to wild type macrophages in response to LPS stimulation (198).

MIF is a key protein that regulates the immune response to *P. aeruginosa* infection. $MIF^{-/-}$ mice can effectively clear a pulmonary *P. aeruginosa* infection, which persists in wild type mice (198). MIF deficiency has also been shown to be beneficial in a model of *P. aeruginosa* induced ocular keratitis, with $MIF^{-/-}$ mice also demonstrating enhanced bacterial clearance and decreased corneal damage (150). In a disease context, CF patients with high expression levels of MIF have also been shown to have earlier *P. aeruginosa* infection (111). Mice expressing enzymatically inactive MIF have enhanced bacterial clearance compared to wild type mice (111). Pharmacological inhibition of MIF using small molecular weight inhibitors also enhances bacterial clearance of *P. aeruginosa* in a chronic infection model (113).

Streptococcus pneumoniae, one of the most common causative agents of bacterial meningitis, induces MIF production in whole blood. *In vivo*, neutralisation of MIF using anti-MIF antibodies resulted in decreased bacterial burden in the lungs and higher survival in a model of pneumococcal pneumonia and sepsis highlighting the potential for targeting MIF as an immune-modulating adjunctive therapy (199). In patients, the presence of a 7-CATT repeat was associated with markers of inflammation, respiratory failure and death. MIF levels in cerebrospinal fluid were significantly higher in those with unfavourable outcomes compared to those with favourable outcomes and was also significantly higher in those with systemic complications than those without (199).

In these contexts, MIF has a detrimental effect on the immune response to an invading pathogen and inflammatory stimuli. However, there are a number of infections where MIF is essential for pathogen clearance and host survival.

In a murine model of *Mycobacterium tuberculosis* (*M. tb*) infection, MIF knockout mice exhibited increased organism burden and earlier onset of death. This was associated with increased lung pathology, increased neutrophil infiltration of the lungs and a decreased innate cytokine response (200). Bone marrow derived macrophages (BMDMs) from $MIF^{-/-}$ mice demonstrated decreased cytokine production, decreased production of reactive oxygen species and overall impaired *M. tb* killing (200).

MIF has also been shown *in vivo* to be of importance in the clearance of numerous pathogens. $MIF^{-/-}$ mice fail to control infection of *Salmonella typhimurium* showing increased mortality versus control mice (201). MIF has also been shown to be necessary for host defence against *Salmonella*, *Leishmania* and *Taenia crassiceps* (202-204).

Overall the effects of MIF during infection seem to be pathogen dependent, with a fine balance between the necessity to promote clearance and the potential deleterious consequences due to overexuberant inflammation (205).

1.4 *Pseudomonas aeruginosa (P. aeruginosa)*

1.4.1 Introduction

P. aeruginosa is a rod shaped, opportunistic Gram-negative bacterial pathogen that is found in soil, abiotic surfaces, aqueous environments and mammalian tissue (206-209). As *P. aeruginosa* is an opportunistic pathogen, infection in healthy individuals is rare. Instead, the bacteria can cause both acute and chronic infections in immunocompromised and hospitalised patients with *P. aeruginosa* recognised as a major cause of nosocomial infections (210). Patient groups at risk of infection include CF patients, burns victims, those who are mechanically ventilated and individuals who are otherwise immunocompromised (211-215). Clinically, the earliest description of *P.*

aeruginosa infection dates to 1882 when Carle Gessard detailed the green and blue colour on the wounds and bandages of soldiers which he successfully extracted and identified as pyocyanin – which we now know is an important *P. aeruginosa* virulence factor (216).

The genomes of multiple *P. aeruginosa* strains have been sequenced to reveal a genome between 5.5 – 7 million base pairs with an accessory genome of 200,000 base pairs (217, 218). The adaptability of *P. aeruginosa* to survive is such polarising environments as soil, blood and lung tissue can be explained by this large genome and the ability to respond to their environment by horizontal gene transfer (219). The complex *P. aeruginosa* genome also enabled the development of multiple mechanisms of antibiotic resistance. As a result, therapeutic options are increasingly limited due to the continued emergence and dissemination of antibiotic resistant strains (220).

In 2017, the World Health Organisation named *P. aeruginosa* as one of the top three pathogens for which new antibiotics are critically needed (221). Recently, it was reported that a clinical isolate from a patient who had undergone surgery was capable of developing resistance to the last line combination treatment of Ceftolozane-tazobactam within just 3 weeks (222).

1.4.2 Pathogenesis of P. aeruginosa infection

1.4.2.1 Acute infection

P. aeruginosa is a major cause of hospital acquired infections (210). The prevalence of *P. aeruginosa* in the hospital setting is underlined by the detection of the bacteria in patient and personnel samples and also on multiple surfaces within hospital wards (223). Nosocomial *P. aeruginosa* infection is associated with previous use of broad spectrum antibiotics and a high carriage rate of multi-drug-resistant *P. aeruginosa* in hospital wards (224, 225). This is exacerbated by the nature of inpatients who likely have previous lung injury and potential immune compromise.

P. aeruginosa is a primary cause of ventilator associated pneumonia in intensive care units (226). The mechanism of infection occurs as patients often have a breached epithelium due to mechanical stress which occurs during the insertion of the endotracheal tube. While the tube itself can serve as a reservoir on which a *P.*

aeruginosa biofilm may develop, the compromised epithelial barrier facilitates bacterial entry into the respiratory tract and the onset of ventilator associated pneumonia (220, 227). Numerous studies have reported a wide range of VAP mortality rates due to *P. aeruginosa*, with estimates ranging from 13.5 % to 69 % depending on the antibiotic resistance status of the microbe (228-230).

Severe acute *P. aeruginosa* infections can occur in patients that are unable to mount an effective immune response to infection. Patients that are immunocompromised as a result of cancer treatment, burns or organ transplantation are all at risk of *P. aeruginosa* infection in both a community and a healthcare setting (230).

1.4.2.2 Chronic infection

P. aeruginosa in inextricably linked to CF, where it is the causative agent of chronic respiratory infection (219). The most common cause of CF mortality is lung disease resulting from chronic inflammation due to the development of persistent respiratory infections (6). The general cycle of *P. aeruginosa* infection is a series of recurrent, intermittent airway colonisation before the acquisition of a chronic infection (2, 37). By adulthood, *P. aeruginosa* is the most commonly detected pathogen in CF patients with approximately three quarters of adults being infected (35, 36). Post-mortem, viable *P. aeruginosa* colonies can still be isolated from within the CF lung (219).

The presence of *P. aeruginosa* has been shown to correlate to a number of prognostic factors in CF including decline in lung function, elevated C-reactive protein (CRP) levels and higher levels of neutrophil elastase in sputum samples (219, 231, 232). This, along with the high incidence of infection within the CF community highlights the importance of the development of antipseudomonal therapies.

P. aeruginosa colonies isolated from patients with chronic infection exhibit several characteristics that are indicative of an adaption of the bacteria to the lung microenvironment. Isolates from these patients exhibit loss of proteins required for motility, including flagellin, which in turn promotes biofilm formation capabilities and correlates with increased bacterial burden and disease severity (233-236).

Furthermore, alginate production and mucoid conversion is a common characteristic of isolates from chronic infections. Mucoid strains of *P. aeruginosa* have enhanced protection to host immune effectors through several mechanisms. Alginate, an exopolysaccharide produced by *P. aeruginosa,* interferes with opsonisation, compliment activation and phagocytic killing (237, 238). Mutations in several genes that regulate mucoid conversion *mucA*, *mucB* and *mucD* are common in chronic infection isolates (239, 240). Exopolysaccharides are constituents of the biofilm structural matrix and confer surface adherence and antibiotic protection (241).

The production of secreted proteases is a mechanism by which *P. aeruginosa* degrades structural components, enhances bacterial invasion and modulates the host inflammatory response. LasB, which is also known as *P. aeruginosa* elastase, degrades host elastin, and compromises the barrier function of the epithelium through disruption of epithelial tight junction proteins (242, 243). Secreted proteases also subvert the immune system through degradations of cytokines and chemokines including IL-6, IL-8 and RANTES (244, 245). Degradation of antimicrobial peptides and membrane receptors also acts to dampen the immune response (241, 246). Furthermore, proteases can also degrade bacterial flagellin which dampens the TLR5 mediated immune response and inflammasome activation (235, 247). Proteases are secreted by most isolates from acutely infected patients, while isolates from chronic infections rarely secrete proteases (248).

P. aeruginosa uses a type 3 secretion system (T3SS) in order to inject effector proteins directly the cytoplasm of host cells which results in cell death or impaired host response (249). Collectively, these injected factors act to disrupt cytoskeletal components, impair phagocytosis, cleave phospholipases and promote cytotoxicity (241, 250-252). T3SS also activate inflammasome which leads to production of mature IL-1β and the induction of pyroptotic cell death (253). In CF, patients carry antibodies against T3SS suggesting the detection of these proteins at some stage, however chronic infections appear favour and select T3SS negative bacteria (241, 254-256).

Overall, these characteristics make the infection less cytotoxic and work to promote bacterial survival by manipulating the immune response to be less inflammatory and detrimental to the bacteria (220, 254).

1.4.3 Biofilm formation

Bacteria can exist as either free floating planktonic bacteria or as a sessile biofilm community. Biofilm formation occurs in harsh conditions when planktonic bacteria encounter a surface and undergo a variety of phenotypic, physiological and metabolic changes (257). Biofilm formation is a protective mechanism employed by *P. aeruginosa* to increase tolerance to antibiotics and the host immune response (233, 258). Biofilms are surfaced attached communities of bacteria that are surrounded by a matrix which is composed of extracellular polymeric substances (EPS), extracellular DNA, proteins, lipids, pili and flagella which hold bacteria together, maintain structural integrity of the biofilm and enable surface attachment (259, 260). Host derived factors including mucus and DNA from dead cells can also become entangled in the biofilm matrix and contribute to the structure (261). Biofilms are a major threat to public health, with reports of biofilms on medical devices, wounds and also within the lung (233, 262-265). In CF, biofilm formation is said to be responsible for the difficulty in treating chronic infections (209).

Biofilm formation occurs in a cyclical manner, with five distinct steps (**Figure 1.8**). The first step is the initial reversible attachment of planktonic bacteria to a suitable surface, which then transitions to the second phase which is irreversible attachment (266). Both of these stages are mediated by flagella and pili, which are lost upon irreversible bacterial attachment and considered a hallmark of sessile cells (267). The third stage involves further growth and division within the biofilm and also further recruitment and aggregation of planktonic bacteria (266, 268). The fourth step is maturation of microcolonies, which involves significant production of the EPS which is composed of the polysaccharides psl, pel and alginate (266). The final stage of biofilm formation is dispersal, where bacteria become motile again and can travel to attach to a different surface and begin the cycle again.

Biofilm formation offers multiple layers of protection to bacteria, with physical, physiological and adaptive tolerance mechanisms enhancing resistance to antibiotics (261). Bacteria that exist within a biofilm often require up to and in excess of 1,000 times the dose of antibiotics needed to kill their planktonic counterparts (269-271).

The three dimensional structure of the biofilm, as well as the EPS and embedded products offer a physical barrier for antibiotics with limited opportunity for antibiotic diffusion through the matrix to reach the internal bacteria (261, 272).

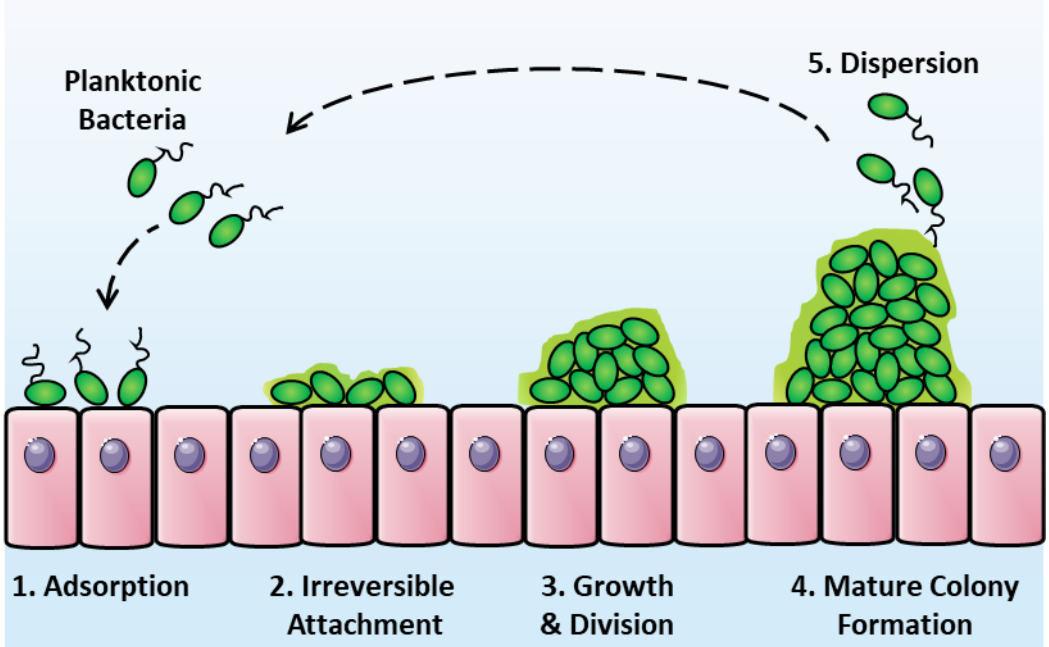

Figure 1.8 *P. aeruginosa* biofilm formation process.

P. aeruginosa biofilm formation begins with initial attachment or adsorption of bacteria to the underlying surface, which in the lungs are epithelial cells. Following this, bacteria undergo physical changes whereby they irreversibly attach before growing and dividing into a mature biofilm colony. From this, bacteria can disperse and move to other surfaces to begin the process again.

1.4.4 P. aeruginosa and MIF

MIF has been shown to have a profound effect on the pathogenesis of *P. aeruginosa* infection. Bozza *et al* were the first group to discover that $MIF^{-/-}$ mice efficiently clear intratracheally instilled *P. aeruginosa*, while the infection persists in wild type mice. These mice also displayed a significant decrease in neutrophils in the BAL compared to wild type mice (198). Numerous follow up studies have further examined the role MIF in *P. aeruginosa* infection.

In vitro, inhibition of MIF by 4-IPP significantly decreased secretion of IL-1β, IL-6 and IL-8 while also decreasing corneal epithelial cell invasion by *P. aeruginosa* (150). In

a model of ocular keratitis, $MIF^{-/-}$ mice exhibit decreased *P. aeruginosa* bacterial burden and significantly decreased corneal pathology compare to wild type mice (150). $MIF^{-/-}$ mice also have significantly decreased levels of inflammatory cytokines including TNF-α, IL-1β, IL-6 and KC (150). Consequently, these mice displayed decreased neutrophil infiltration to the cornea (150). $MIF^{-/-}$ mice that received topical corneal treatment with recombinant MIF displayed restored susceptibility to *P. aeruginosa* induced disease, with no significant difference in bacterial burden or pathological score compared to wild type mice (150). Inhibition of MIF by 4-IPP also lead to significantly decreased bacterial burden and pathological score compared to untreated mice (150).

In vivo models have also examined the role of the MIF receptor CD74 in *P. aeruginosa* infection. $CD74^{-/-}$ mice display decreased bacterial burden and decreased corneal pathology in a model of *P. aeruginosa* induced keratitis compared to wild type mice (273). However, the effect of CD74 deletion was not as striking as that seen in a previous study using $MIF^{-/-}$ mice (150). The authors hypothesise that this is due to the other mechanisms of MIF induced signalling that are independent of CD74, however it may also be related to the effects of MIF tautomerase activity. Treatment of $CD74^{-/-}$ mice with a neutralising MIF antibody significantly decreased bacterial burden and pathological scores compared to untreated $CD74^{-/-}$ mice. Furthermore, this treatment enhanced the efficacy of antibiotic treatment in the model (273).

The role of MIF in *P. aeruginosa* lung infections in CF has also been examined. The Donnelly Lab has shown that CF patients that have high MIF expression levels have decreased lung function and earlier *P. aeruginosa* colonisation (110). In a model of chronic respiratory *P. aeruginosa* infection, P1G mice expressing enzymatically null MIF displayed significantly decreased pulmonary inflammation and decreased bacterial load compared to wild type mice (111).

Most recently, The Donnelly Lab have shown that *P. aeruginosa* utilises host derived MIF in order to promote biofilm formation and enhance antibiotic resistance (113). Furthermore, inhibition of MIF with SCD-19 increased bacterial clearance, decreased lung inflammation and attenuated weight loss (113).

1.4.5 Host defence against P. aeruginosa

1.4.5.1 Mechanical barriers

Aerobic metabolism within the body requires the gaseous exchange of carbon dioxide and oxygen which occurs across the alveolar-capillary interface in the peripheral lung. Before reaching the deep lung, inhaled air must pass through the conducting airways comprising of the main bronchus, before further dividing into increasingly smaller bronchi and finally bronchioles before culminating in the alveoli. These sections of the conducting airways are comprised of type I and type II epithelial cells. It is these cells that are directly exposed to the inhaled air, pathogens and particles, and as a result they play a pivotal role in the mounting of an efficient immune response when necessary (274, 275).

The conducting airways are predominantly lined by a pseudostratified epithelium which is dominated by ciliated cells (274, 275). The function of these ciliated cells is to beat in order to push mucus and foreign bodies away from the lung. Secretory cells also sit within the epithelium and the submucosa with goblet cells secreting mucin glycolipids while club cells and type II epithelial cells secrete pulmonary surfactant (220, 276). Mucus serves to trap particles and pathogens for removal from the lung, while the surfactant functions to decrease surface tension at the air-liquid interface to prevent collapse of the alveoli at the end of exhalation. Together, the submucosal glands and conducting airways are capable of secreting a plethora of host defence proteins including lysozymes, lactoferrin, and defensins (277). Basal cells are located below the epithelial layer surface and function as progenitors for secretory and ciliated cells (275).

Another role of the respiratory epithelium is its barrier function (**Figure 1.9**). The strong cell to cell connections are mediated by junctional proteins including connexins, claudins, adhesions and zonula adherins which function to link the actin cytoskeleton of neighbouring cells to promote structural integrity and prevent the lung from being breached by invasive pathogens (275). In CF, *P. aeruginosa* biofilms form on underlying epithelial cells (206, 207, 209, 278).

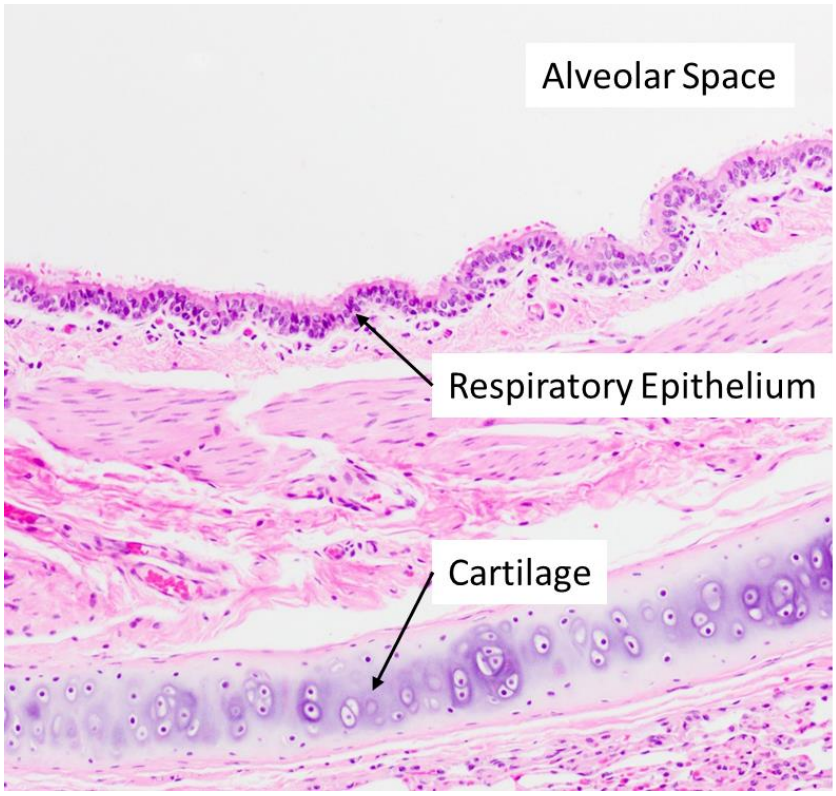

Figure 1.9 Cellular structure of the deep lung.

Bronchi are lined by pseudostratified to simple ciliated columnar epithelium. The wall is composed of an outer cartilaginous ring and moderate amounts of smooth muscle. Image adapted from (279).

1.4.5.2 Innate immune response to P. aeruginosa

P. aeruginosa expresses several PAMPs which enables the host immune system to sense the infection and in turn mount an effective immune response for bacterial clearance. Local sensors detect the invading pathogen and trigger intrinsic cell defence mechanisms to contain the microorganism and secrete chemoattractants to recruit rapid responder cells such as macrophages and neutrophils (280).

TLRs, the most well characterised group of PRRs, recognise a number of different *P. aeruginosa* related factors with TLR2, TLR4 and TLR5 recognising pilin, LPS and flagellin respectively (230). In contrast to these transmembrane receptors, TLR9 is located on the endosomal membrane where it senses bacterial CpG DNA which becomes available following phagocytosis and lysosomal degradation (281). Cytosolic NLRs NOD1 and NOD2 detect bacterial peptidoglycans and activate NF-κB mediated

proinflammatory cytokine production and also antimicrobial peptide production (93, 282).

TRIF dependent signalling plays an important role in the immune response to *P. aeruginosa* infection. *In vivo*, $TRIF^{-/-}$ mice have completely inhibited RANTES production and severely impaired TNF-α and KC production. MIP-2 and IL-1β levels were comparable to wild type. This cytokine profile was associated with impaired neutrophil recruitment to the lungs and impaired bacterial clearance (283).

Although it is usually associated with viral infections, the transcription factor IRF3 also plays an important role in modulation of an effective immune response to *P. aeruginosa* (284). IRF3 deficient macrophages display complete ablation of RANTES production and impaired TNF-α release in response to *P. aeruginosa* compared to wild type macrophages. *In vivo*, $IRF3^{-/-}$ mice have very significantly decreased RANTES in BAL fluid and lung homogenate compared to wild type mice in response to *P. aeruginosa* infection. This is accompanied with slight decreases in TNF-α and equivalent levels of KC and IL-1β in $IRF3^{-/-}$ mice compared to wild type. These IRF3 deficient mice also display decreased neutrophil and macrophage recruitment to the lung and overall impaired bacterial clearance (284).

Epithelial cells are one of the localised sensor cells which promote innate immune responses for pathogen clearance. Numerous *P. aeruginosa* PAMPs activate signalling cascades within the respiratory epithelium. Secreted *P. aeruginosa* quorum sensing molecules induce IL-8 factors from NF-κB activated epithelial cells (285). *P. aeruginosa* pyocyanin, a secreted virulence factor, also drives IL-8 production in human airway epithelial cells, while it also acts to inhibit RANTES – a key cytokine involved in the attraction of T-cell monocytes and eosinophils to sites of infection (286, 287).

Epithelial cells also respond to cytokines produced by other host cells. For example, macrophage produced IL-1β binds to the IL-1 receptor on epithelial cells and acts to promote IL-8 secretion which promotes neutrophil recruitment and also to upregulate antimicrobial ROS production (288, 289).

Isolated murine airway epithelial cells produce cytokines including KC and IL-6 in response to *P. aeruginosa* infection (290). The role of NF-κB signalling in epithelial

cells is highlighted *in vivo* whereby mice treated with an NF-κB inhibiting adenoviral construct, which specifically targets the respiratory epithelium, demonstrate impaired *P. aeruginosa* clearance, decreased cytokine production and decreased neutrophil recruitment (291). Moreover, the use of a transgenic mouse model in which MyD88 expression is limited to epithelial cells of the airways demonstrated that these mice were capable of controlling *P. aeruginosa* respiratory infection, unlike MyD88$^{-/-}$ mice (288). These studies illustrate the role of epithelial cells signalling in the innate immune response to *P. aeruginosa*.

Macrophages also play a key role in the host response to *P. aeruginosa*. Both resident macrophages and recruited monocyte-derived macrophages can carry out effector functions while also acting as local sensors (280). Recruited macrophages act as a major source of cytokines, including TNF-α and IL-6 , which enhances neutrophil recruitment to the lung (292, 293). Macrophages also carry out key effector functions including phagocytosis and production of antimicrobial products.

LPS is a major component of *P. aeruginosa* which leads to activation of TLR4 (230, 294). In macrophages, activation of TLR4 by LPS results in enhanced glycolysis, succinate accumulation, reactive oxygen species (ROS) generation and IL-1β release (185, 295).

P. aeruginosa also induces inflammasome activation through NLR mediated detection of flagellin and T3SS effector proteins which lead to NLRC4 and NLRP3 inflammasome formation. Inflammasome activation leads to maturation and processing of IL-1β and IL-18 through caspase-1 mediated cleavage (296-299). These secreted cytokines further promote inflammation on other cells, including epithelial cells, to promote cytokine production and further immune cell recruitment (300). Inflammasome activation also results in a form of cell death known as pyroptosis which results in leakage of cellular contents including metabolites and cytokines; further driving inflammation (301).

P. aeruginosa infection induces NLRP3 inflammasome activation in macrophages which results in decreased bacterial clearance as a result of macrophage autophagy, which is induced by *P. aeruginosa* as a means of evading macrophage

mediated clearance (302). Interestingly, treatment of macrophages with recombinant IL-1β resulted in enhanced autophagy and decreased bacterial clearance, highlighting an important role for IL-1β in *P. aeruginosa* infection (302). Furthermore, IL-1β levels in CF patient BAL fluid and sputum have been shown to correlate with clinical outcome (303). This is not the first time IL-1β has been implicated in *P. aeruginosa* pathogenesis. Treatment of mice with inhibitors of IL-1β converting enzyme (ICE) leads to decreased ocular inflammation and bacterial burden in a model of ocular keratitis (304). Similarly, ICE knockout mice also exhibited decreased ocular inflammation and decreased bacterial burden compared to WT mice (305). In a model of *P. aeruginosa* pneumonia, IL-1 receptor knockout mice exhibit enhanced bacterial clearance and decreased lung inflammation illustrating that IL-1 activity impedes an effective host immune response to *Pseudomonas* infection (306). *In vivo*, treatment with Anakinra, a recombinant IL-1 receptor antagonist, resulted in enhanced survival and *P. aeruginosa* clearance in *Cftr*$^{-/-}$ mice compared with untreated *Cftr*$^{-/-}$ mice due to dampening overexuberant inflammation mediated by the NLRP3 inflammasome (69). Furthermore, the use of NLRP3 inflammasome inhibitor has also been shown to reduce IL-1β production in the lung and improve *P. aeruginosa* clearance in a model of CF pulmonary infection (303).

New research suggests that the thriving of *P. aeruginosa* in environments containing high IL-1β concentrations may be due to enhanced succinate levels due to cellular pyroptosis (307). *P. aeruginosa* preferentially metabolises succinate, which is highly available in the CF lung, which leads to promotion of biofilm formation (303, 307, 308). The CF lung exhibits high succinate levels due to dysfunction of the CFTR, which acts as an anchor to the protein phosphatase and tensin homolog deleted on chromosome 10 (PTEN) – a key regulator in cellular metabolism. This results in the excessive release of succinate and ROS from CF cells (307).

Overall, different cytokines display differential effects in the context of *P. aeruginosa* infection and bacterial clearance (**Figure 1.10**).

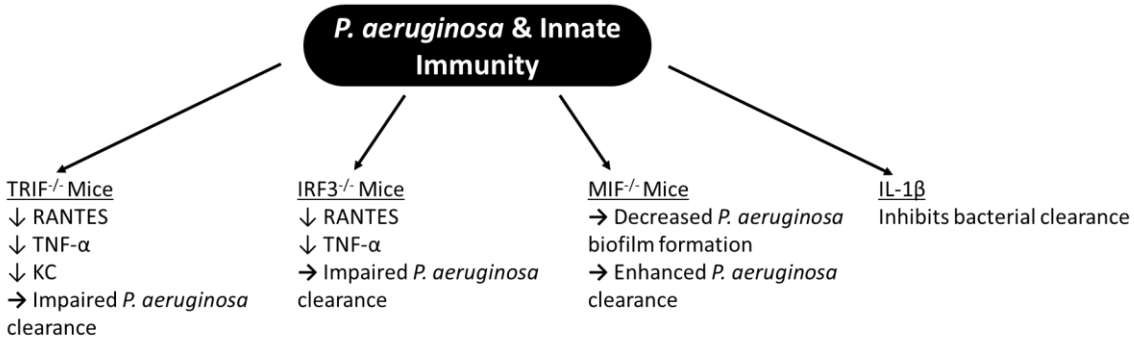

Figure 1.10. Overview of the role of cytokines in *P. aeruginosa* infection.

The role of intracellular adaptor proteins and cytokines in *P. aeruginosa* clearance. TRIF deficient mice display decreased RANTES, TNF-α and KC levels and impaired *P. aeruginosa* clearance compared with wild type mice. IRF3 deficient mice display decreased RANTES and TNF-α levels and impaired *P. aeruginosa* clearance compared with wild type mice. MIF deficient mice display decreased *P. aeruginosa* biofilm formation and enhanced bacterial clearance compared with wild type mice. IL-1β is implicated with decreased *P. aeruginosa* clearance.

1.4.6 P. aeruginosa immune evasion

P. aeruginosa has evolved mechanisms to evade the host immune system. Biofilm formation constitutes a major mode of immune evasion which is employed by *P. aeruginosa* as outlined previously. The production of elastases and alkaline proteases by *P. aeruginosa* biofilms directly inactivates complement proteins leading to reduced opsonisation (309).

P. aeruginosa has also evolved to use host derived factors in order to upregulate protective mechanisms including biofilm formation. Secretory products from primary macrophages have been shown to promote *P. aeruginosa* virulence factor production. These secreted products included a plethora of pro-inflammatory cytokines, chemokines and reactive species and resulted in increased production of alginate, siderophores, proteases and elastase alongside enhanced bacterial growth and biofilm formation (310).

More specifically, *P. aeruginosa* uses host MIF in order to promote biofilm formation and enhance antibiotic resistance (113). CF patients that have high expression levels of MIF due to the CATT microsatellite repeat exhibit decreased lung function and earlier colonisation than their low MIF expressing counterparts (110). Furthermore, both removal and inhibition of MIFs enzymatic activity resulted in

decreased lung inflammation, increased bacterial clearance in a model of chronic *P. aeruginosa* infection (111, 113)

Mucoid strains of *P. aeruginosa* have enhanced protection to host immune effectors through several mechanisms. Alginate production by *P. aeruginosa*, a key component of the biofilm ECM, interferes with opsonisation, compliment activation and phagocytic killing of bacteria (237, 238, 311). Down regulation of PAMPS including flagellin acts to decrease immune activation (267).

P. aeruginosa biofilms also induce frustrated phagocytosis which causes the release of inflammatory mediators which damage the surrounding tissue by neutrophils and macrophages (238). Rhamnolipids, which are important in the biofilm formation process, have been shown to be toxic to neutrophils and tissue surrounding sites of infection. Cellular death at this level results in the accumulation of cellular debris which provides additional substrates for the biofilm extracellular matrix (312, 313).

1.5 Immunometabolism

1.5.1 Introduction

The field of immunometabolism examines with how metabolic processes are activated in order to support host defences (314). Recent research has shown that specific metabolic processes are key regulators of immune cell activation (315). Interestingly, intermediates and by products that are produced as a result of metabolic processes can regulate the expression of inflammatory genes.

1.5.2 Overview of metabolic pathways

1.5.2.1 Glycolysis

Glycolysis a key process that utilises glucose in order to provide energy for cellular maintenance (316). Following cellular uptake by glucose transporters, metabolic processing of glucose occurs in the cytosol. Glucose is converted to pyruvate through a series of sequential enzymatic reactions yielding 2 net ATP molecules and 2

NADH molecules (317, 318). If oxygen is present, pyruvate is processed by pyruvate dehydrogenase to acetyl-CoA where it feeds into the TCA cycle (317, 318).

While glycolysis is a relatively ineffective means of generating energy, it does provide other products which are utilised in the synthesis of ribose, amino acids and fatty acids (318). Glycolysis is the predominant method of energy generation in rapidly dividing cells as it is a rapidly activated pathway, and also due to the fact that it provides key intermediates that are necessary for cell growth.

1.5.2.2 The tricarboxylic acid (TCA) cycle

The TCA cycle occurs within the inner mitochondrial matrix, where it serves to yield high energy electrons for oxidative phosphorylation for efficient ATP production.

The first step in the TCA cycle is the condensation reaction which combines acetyl-CoA with oxaloacetate to yield the six carbon molecule citrate, which is catalysed by citrate synthase (315, 319, 320). Citrate is then processed to isocitrate, in a two-step reaction requiring dehydration of citrate to cis-aconitate and subsequent rehydration to isocitrate in an aconitase mediated reaction. This process also yields the metabolic by-product itaconate (315, 321). Isocitrate is then decarboxylated by isocitrate dehydrogenase to α-ketoglutarate, generating one molecule of NADH and CO_2 (315, 322). Next, α-ketoglutarate dehydrogenase converts α-ketoglutarate to succinyl-CoA, yielding another molecule of NADH and CO_2 (323). Succinyl-CoA is next converted to succinate in a reaction catalysed by succinyl-CoA synthetase that is also coupled with the generation of GTP (319, 324).

Succinate is then oxidised to fumarate by succinate dehydrogenase (SDH) a key enzyme in the electron transport chain complex in a reaction that generates $FADH_2$ (319). Fumarate is then converted to malate by fumarate hydratase (325). Malate is then oxidised by malate dehydrogenase to oxaloacetate, yielding a further NADH molecule (326). The production of oxaloacetate enables the cycle to begin again. Following one full cycle of the TCA cycle, the outputs are 3 NADH molecules and also $FADH_2$ which feed into the electron transport chain ultimately netting 36 ATP molecules (315, 318).

The TCA cycle is generally utilised by quiescent cells, whose main requirements are energy and longevity (318). While the TCA cycle is a very efficient means of generating ATP, the process requires mitochondrial biogenesis and as such cannot be activated as rapidly as glycolysis. As a result, glycolysis is favoured by cells that need energy imminently, for example rapidly dividing cells and autoactivated immune cells (318). It is now clear that TCA cycle metabolites play a key role in regulation of the immune response, with accumulation of various intermediates within LPS activated immune cells (295, 327-330).

1.5.3 Metabolic rewiring of activated macrophages

Classically activated, also known as M1 macrophages, are activated by bacterial derived stimuli including LPS and by cytokines associated with infection including IFN-γ and TNF-α. Classical activation of macrophages leads to a highly inflammatory phenotype with high bactericidal capabilities. Alternatively activated, or M2 macrophages, are activated in response to parasitic infection and associated cytokines which gives rise to macrophages with an anti-parasitic and pro-repair phenotype (**Figure 1.11**) (331). In line with this, recent work has indicated that a general metabolic signature for immune cells stimulated with microbial antigens does not exist, with individual antigens inducing their own respective metabolic profiles (332).

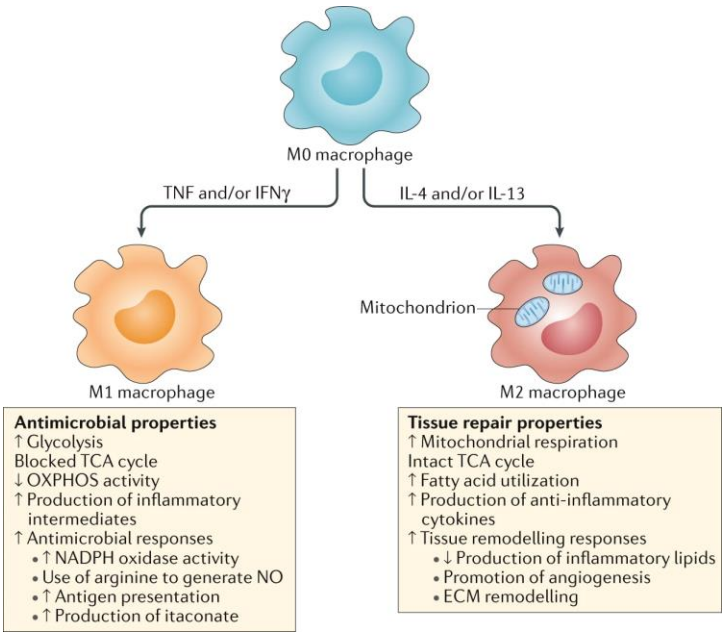

Figure 1.11 Macrophage polarisation phenotypes.

M0 macrophages are activated to an M1-like macrophage status by exposure to IFNγ and/or tumour necrosis factor (TNF), or LPS, whereas M2-like macrophages are induced through treatment with IL-4 and/or IL-13. M1-like exhibit increased glycolysis, a dysregulated TCA cycle and increased activities that are associated with anti-microbial activity. M2-like macrophages demonstrate increased mitochondrial respiration and enhanced fatty acid metabolism and upregulate activities that are associated with tissue remodelling or wound healing. ECM, extracellular matrix; NO, nitric oxide; OXPHOS, oxidative phosphorylation; TCA, tricarboxylic acid cycle. Taken from (333).

1.5.3.1 The Warburg Effect

Metabolic rewiring of macrophages plays a key role in the determination of cellular response and effector function. In LPS stimulated immune cells including macrophages, natural killer (NK) cells, T-cells and B-cells there is a shift towards aerobic glycolysis, also known as the Warburg effect (334-338). In macrophages, enhanced glycolysis supports both phagocytosis and anti-bacterial functions (339). 2-deoxyglucose (2-DG), a competitive inhibitor of glycolysis, inhibits macrophage activation and dampens inflammation *in vivo*, highlighting the role of glycolysis in macrophage activation (185, 340, 341). As such, glycolysis is considered a hallmark of immune cells undergoing rapid activation and replication (318).

The HIF pathway plays a critical role in metabolic reprogramming. HIF-1α stabilisation is promoted in response to LPS stimulation and NF-κB activation (183, 188,

189, 191). In LPS stimulated macrophages, succinate accumulation leads to inhibition of PHDs which results in HIF-1α stabilisation under both hypoxic an normoxic conditions (185, 342). HIF-1α has been shown to promote expression of proteins involved in glycolytic processing, while HIF-1$\alpha^{-/-}$ cells fail to switch to this Warburg metabolism (343-345). HIF-1α deficient macrophages exhibit decreased bactericidal capacities, including phagocytosis and bacterial killing of pathogens including *P. aeruginosa* (345, 346). HIF-1α also upregulates lactate dehydrogenase (LDH) and pyruvate dehydrogenase kinase, both of which act to decrease available levels of pyruvate to feed the tricarboxylic acid (TCA) cycle (347).

The switch to glycolysis is somewhat surprising, as this is not the most effective means of energy generation within the cell. However, glycolysis can be rapidly enzymatically activated in comparison to oxidative phosphorylation which requires mitochondrial biogenesis which may explain the shift towards glycolysis (339). There are a myriad of other benefits to activation of the glycolytic pathway including the production of numerous intermediates which serve as precursors for nucleotides, fatty acids and amino acids – all of which are necessary to enable immune cells to rapidly carry out their effector functions (318).

While the Warburg Effect is usually associated with cancer cell metabolism, there are numerous distinctions between cancer cell metabolism and LPS primed macrophages. Most notably are the increased production of nitric oxide, prostaglandins, ROS and itaconate – all of which are associated with increased antimicrobial activity (333).

1.5.3.2 TCA Cycle Rewiring

In M2 macrophages the TCA cycle is intact, whereby pyruvate is fed into the cycle and the end result is high levels of ATP generation coupled to oxidative phosphorylation (328). In classically activated M1 macrophages the TCA cycle has been shown to be dysregulated – with metabolic breaks after citrate and succinate (**Figure 1.12**) (185, 328).

1.5.3.2.1 Citrate Accumulation

Citrate accumulation within LPS activated macrophages occurs due to repression of *Idh* mRNA, the gene encoding isocitrate dehydrogenase (IDH) (185). Following on from this it was demonstrated that excess citrate is processed to *cis*-aconitate which is utilised for itaconate production; alternatively, citrate is utilised in the generation of fatty acids for membrane biogenesis (328, 348, 349). Furthermore, excess citrate is used for fatty acid production and is also utilised by pathways that generate key macrophage effector molecules including nitric oxide and prostaglandins (350).

1.5.3.2.2 Succinate Accumulation

Succinate accumulation occurs within activated macrophages as a result of a metabolic breakpoint which occurs at SDH (349). While SDH protein expression is not impacted, its enzymatic activity is impaired yielding inefficient succinate to fumarate conversion (328, 349). Inhibitors of SDH include NO and itaconate, both of which are elevated in activated macrophages (327, 328, 351).

Succinate is a pro-inflammatory metabolic by-product of the TCA cycle. Succinate has been shown to promote inflammation through HIF-1α stabilisation and subsequent upregulation of pro-inflammatory genes, including IL-1β (185). Stabilisation of HIF-1α by succinate also promotes the induction of several glycolytic enzymes as previously described (191, 352-356).

Furthermore, the activity of SDH has been shown to promote succinate driven inflammation. SDH oxidises succinate and induces mitochondrial ROS production which activates HIF-1α and suppresses production of anti-inflammatory mediators. Using BMDMs from mice that lack functional SDH, LPS stimulation resulted in reduced pro-IL-1β and HIF-1α induction compared to wild type BMDMs. *In vivo*, SDH inhibition resulted in decreased circulating IL-1β and enhanced IL-10 in a model of LPS driven sepsis (295).

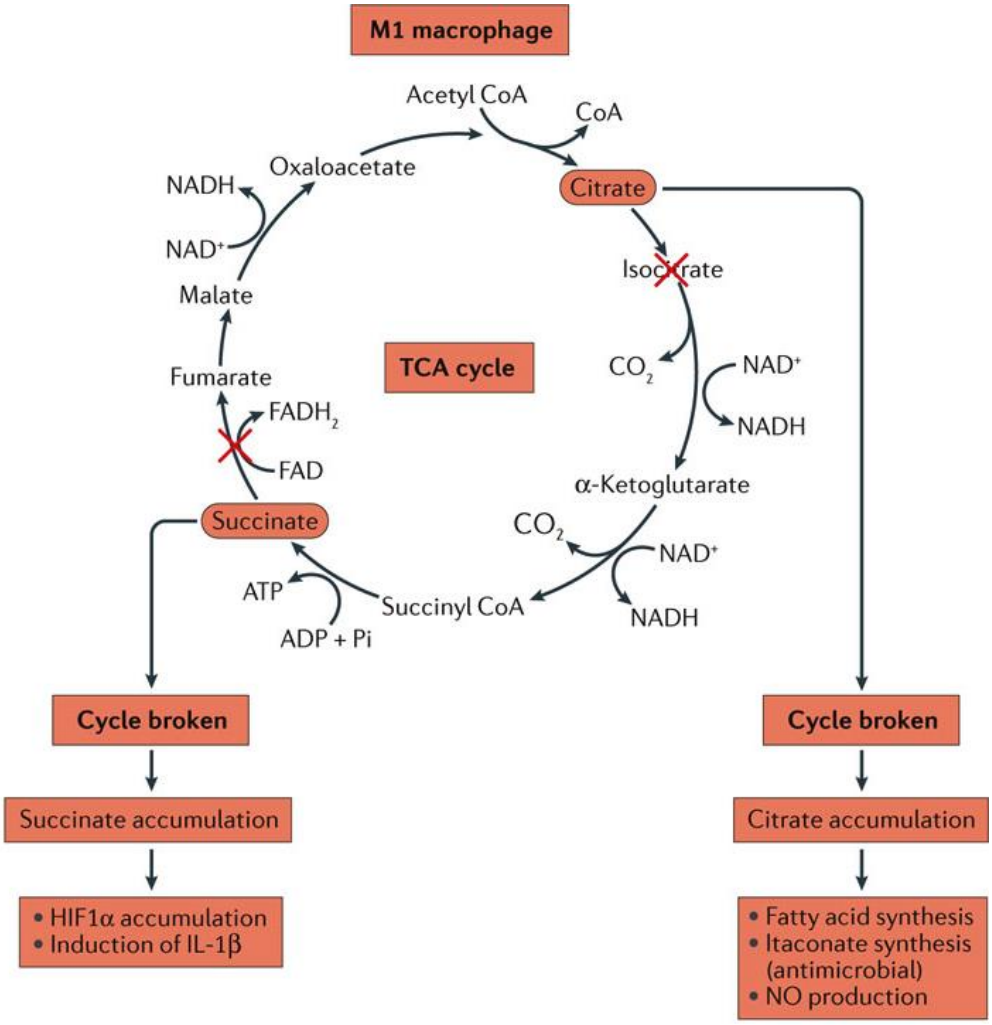

Figure 1.12 The TCA cycle in classically activated macrophages

In M1-like macrophages the TCA cycle is broken in two places — after citrate and after succinate. Citrate is used to generate fatty acids for membrane biogenesis and also itaconate production. Succinate accumulation leads to HIF1α stabilisation and IL-1β. Taken from (318).

1.5.3.3 Metabolic Response to P. aeruginosa Infection

Several studies have yielded insights into the metabolic responses of immune cells to a *P. aeruginosa*. *In vivo*, infection of mice with planktonic *P. aeruginosa* leads to HIF-1α stabilisation, IL-1β production and succinate accumulation in BAL fluid, indicative of M1 polarisation (307).

In vivo, host-adapted strains of *P. aeruginosa* generated less succinate accumulation in BAL fluid of wild type mice and exhibited less HIF-1α stabilisation compared to mice infected with lab strain PA01 (307). These mice also produce less

inflammatory cytokines including IL-1β, IL-6 and TNF-α than those infected with PA01 (307). This effect is likely due to the down regulation of virulence that is characteristic of host-adapted strains. Interestingly, these clinical isolates significantly upregulated *Irg1* expression in monocytes and itaconate levels in BAL fluid (307). In CF, patients that are chronically infected with *P. aeruginosa* display increased levels of IL-4, a key T_h2 cytokine, compared to those with only acute infections (357).

The authors hypothesise that succinate accumulation drives adaptions in *P. aeruginosa* that reduce IL-1β release and instead promote release of the anti-inflammatory metabolite itaconate (307, 327, 351).

1.5.4 Itaconate

Itaconate is a metabolic by product of the TCA cycle, which peaks in macrophages upon LPS stimulation (358). Itaconate is produced through the conversion of *cis*-aconitate by *cis*-aconitate decarboxylase (CAD), which is also known as immunoresponsive gene 1 (Irg1) (359). In general, itaconate employs several mechanisms to exerts anti-inflammatory effects making it an attractive anti-inflammatory therapeutic target. Itaconate has been shown to be protective in numerous models including *M. tb* infection and LPS lethality models (330, 360, 361). However, the anti-inflammatory properties of itaconate have been shown to be deleterious in a cancer model, with itaconate promoting tumour development (362).

1.5.4.1 Discovery

Itaconate was initially discovered by chemist Samuel Baup in 1836 and went on to have a predominantly industrial function as a component used in the synthesis of polymers (363). It is only in recent decades that the immunoregulatory functions of itaconate are being investigated.

The Immune responsive gene 1 (*Irg1)* was cloned in 1995 when it was shown to be upregulated in macrophages in response to LPS – however its function remained unclear (358). This upregulation in *Irg1* expression occurs in a TLR4-dependent but MyD88-independent manner (364). Following on from this, it was demonstrated that itaconate levels are elevated in the lungs of *M. tb* infected mice and also in LPS

stimulated murine macrophages (365-367). It was not until 2013 when it was discovered that *Irg1* was responsible for itaconate synthesis in LPS activated macrophages (359).

1.5.4.2 Itaconate mediated regulation of innate immune response

Itaconate is an immunoregulatory by-product of cellular metabolism that exerts strong anti-inflammatory activity. The anti-inflammatory activity of itaconate was first described in an LPS tolerance study that details Irg1 mediated suppression of TLR mediated production of TNF-α, IL-6 and IFN-β in LPS tolerized macrophages through inhibition of NF-κB and IRF3 activation (368). The same study also noted significantly higher levels of Irg1 mRNA in the PBMCs of sepsis patients, compared to healthy donors (368). Furthermore, primary macrophages from Irg1 knockout mice exhibit increased pro-inflammatory cytokine production following LPS stimulation (327).

To date, there have been only a limited number of reports of exogenous itaconate entering the cytoplasm of macrophages and adipocytes after 48-72 hours of exposure (369, 370). As a result, synthetic cell permeable derivatives have been developed.

Experiments using a cell-permeable methyl ester derivative of itaconate, dimethyl itaconate (DI), demonstrated inhibition of LPS induced production of IL-6 and IL-1β (327). Treatment of RAW 264.7 cells with cell permeable synthetic version of itaconate, 4-octyl itaconate (4-OI), increases intracellular levels of itaconate in a dose dependent manner (360). 4-OI treatment also significantly decreases IL-1β and inducible nitric oxide synthase (iNOS) at both mRNA and protein level in LPS stimulated macrophages (360). Furthermore, 4-OI has been shown, by two independent research groups, to be protective in an LPS lethality model while also decreasing circulating levels of IL-1β, IL-6, TNF-α and lactate (330, 360).

It remains unclear how itaconate is transported across the cell membrane, and if it can act extracellularly. Stimulation of macrophages with LPS significantly increases levels of itaconate in cell supernatant (371). To date, there has been no published description of an itaconate receptor or transporter. However, studies have revealed that itaconate can be taken up by cells; but this requires high concentrations and long incubation periods (370, 372).

In vivo, Irg1 deficient mice readily succumb to *M. tuberculosis* infection – an infectious challenge that is not lethal to wild type mice. This is accompanied with decreased bacterial clearance and increased inflammation in the lungs (361). In a model of LPS induced sepsis, Irg1 mediates the anti-inflammatory effects of heme oxygenase 1 (HO-1) protein. Treatment of mice with HO-1 activators and inducers increases *Irg1* mRNA while decreasing circulating TNF- levels. This effect was reversed with treatment of an inhibitor of HO-1 activity (373).

1.5.4.2.1 Succinate dehydrogenase (SDH) inhibition

One mechanism of itaconates anti-inflammatory effects is through inhibition of SDH. Itaconate was first established as an SDH inhibitor in 1949 (374). The inhibition of SDH has previously been shown to decrease LPS induced circulating IL-1β and enhanced IL-10 (295). The inhibitory effect of itaconate on SDH has been demonstrated using $Irg1^{-/-}$ macrophages, where decreased levels of succinate accumulation following LPS stimulation were observed compared to wild type, indicative of SDH inhibition by itaconate (327, 351).

1.5.4.2.2 Nuclear factor erythroid 2-related factor 2 (Nrf2) activation

Itaconate exerts its anti-inflammatory through modulation of nuclear factor erythroid 2-related factor 2 (Nrf2). Nrf2 is a transcription factor that is upregulated in response to oxidative stress, and acts to enhance antioxidant production and decrease inflammatory cytokine production. Primary macrophages from $Irg1^{-/-}$ mice display a complete lack of activation of Nrf2 (375). Treatment of macrophages with DI increases Nrf2 expression (375).

Under basal conditions, Nrf2 is associated with Kelch-like ECH-associated protein1 (KEAP1) which targets it for degradation (376). Upon oxidative stress, these proteins dissociate enabling Nrf2 to translocate to the nucleus and upregulate transcription of anti-oxidant genes (377). A cell permeable version of itaconate, 4-octyl itaconate (4-OI), has been shown to induce post translational modifications on cysteine residues of KEAP1 which results in the separation and release of Nrf2 which can then translocate to the nucleus and exert its anti-oxidant effects (330). These effects include enhanced antioxidant expression and reductions in ROS, HIF-1α and IL-1β (330).

1.5.4.3 Antibacterial activity

Itaconate has long been known to have antibacterial properties since it was discovered that it inhibits the enzyme isocitrate lyase - a key enzyme in the glyoxylate cycle, an anabolic process analogous to the TCA cycle in plants and microorganisms (378). This inhibitory effect of itaconate results in stunted bacterial growth of *Pseudomonas indigofera* in glucose poor conditions (378). Since then, the growth of a slew of other microorganism has been shown to be inhibited with itaconate concentrations from 10-50 mM including *M. tb*, *Salmonella enterica*, *Staphylococcus aureus* and *Legionella pneumophila* (327, 379).

The physiological relevance of itaconate's antibacterial activity has been a source of debate. Intracellular levels of itaconate have been shown to range from 40 µM to 8 mM (359, 367). Much of the work has been conducted demonstrated growth inhibition at concentrations between 5 mM and 100 mM. However, it is worth noting that a lot of bacteria studied had complete inhibition at 10 mM including *methicillin-resistant Staphylococcus aureus* - which is reasonably close to the concentration of intracellular itaconate levels in LPS stimulated RAW 264.7 macrophages (380). It is also worth noting the possibility of varying concentrations of itaconate in different cellular compartments such as lysosomes and phagosomes – an area with a lack of available information. Overexpression of *Irg1* was shown to inhibit *Legionella pneumophila* in macrophage vacuoles – suggesting elevated itaconate concentration in this compartment in response to infection (379).

Interestingly, many notable pathogenic bacteria have retained enzymes for itaconate degradation including *Yersinia pestis* and *Pseudomonas aeruginosa* (381). While this may reflect the evolutionary development of a survival mechanism to host responses – it has also been suggested that it occurred as a result of competition between bacteria and the fungus *Aspergillus* which is used to produce commercial itaconate (382). The retention of itaconate degrading enzymes by *P. aeruginosa* raises the question of is this degradation promoting a survival advantage or is it simply a protective mechanism employed by the bacteria. *P. aeruginosa* expresses three genes which encode proteins involved in itaconate processing to yield acetyl-coenzyme A (CoA) and pyruvate (**Figure 1.13**). These enzymes are itaconate-CoA transferase (Ict),

itaconyl-CoA hydratase (Ich) and (S)-citramalyl-CoA lyase (Ccl) and are encoded by *PA0882*, *PA0878* and *PA0883* respectively (381).

In vivo, *Irg1*$^{-/-}$ mice challenged with *M. tb* rapidly succumb to infection – an infection which is not lethal to wild type mice. These knockout mice also exhibited decreased bacterial clearance and increased pro-inflammatory cytokine production (361). When *Irg1*$^{-/-}$ mice were infected with a strain of *M. tb* which lacks a functional glyoxylate shunt (Δcl1), the mice still readily succumbed to infection (361). This suggests that the mechanism of itaconates antibacterial activity is not limited to its inhibition of ICL, and as such further research is needed into the mechanisms.

The role of itaconate in viral infections is less well established than its role in bacterial infections. Studies examining the role of itaconate in Zika virus infection have revealed that itaconate promotes viral clearance (383). The protein receptor-interacting protein kinase (RIPK) is required for neuronal control of Zika virus, with *Ripk3*$^{-/-}$ mice having increased mortality and viral load compared to wild type mice. In the brains of these infected mice, *Irg1* mRNA was significantly reduced in the brains of *Ripk3*$^{-/-}$ mice compared to wild type (383). The role of itaconate in Zika virus infection was followed up *in vivo*. *Irg1*$^{-/-}$ mice had significantly decreased survival and significantly increased viral loads compared to wild type mice. Mice that had concurrent administration of Zika virus and 4-OI had significantly decreased viral burden. Overall, this evidence reveals a protective role for itaconate in Zika virus infection (383).

Further studies have demonstrated that itaconate is also beneficial in West-Nile-Virus infection, with itaconate restricting viral replication within neurons (384). However, the effects of itaconate seem to vary between different viral pathogens. *In vivo*, itaconate promotes viral replication of vesicular stomatitis virus (385).

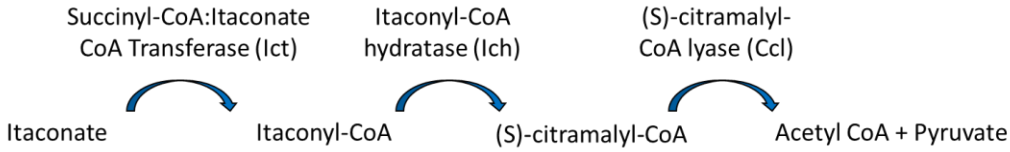

Figure 1.13 Itaconate processing in *P. aeruginosa.*

Itaconate degradation pathway in *P. aeruginosa*, processing itaconate to acetyl CoA and pyruvate.

1.6 Thesis Hypothesis and Aims

1.6.1 Hypothesis

Our central hypothesis is that SCD-19 and 4-OI, respectively, represent valid drug candidates for the treatment of *P. aeruginosa*-induced inflammation, biofilm formation and host infection.

1.6.2 Overall aim

In CF, there is an urgent unmet clinical need for the development of novel therapies that are anti-inflammatory and antibacterial. The overall aim of this Ph.D. project is to evaluate the efficacy of two potential host-directed therapies, SCD-19 and 4-OI, for the treatment of *P. aeruginosa*-induced inflammation, biofilm formation and host infection.

1.6.3 Research objectives

In this thesis we aim to investigate the role of MIF in macrophage responses to *P. aeruginosa* infection and the ability of SCD-19 to modulate these effects. We also aim to investigate the role of MIF in *P. aeruginosa* biofilm formation on airway epithelial cell monolayers and the effects of SCD-19 on this.

Furthermore, we also aim to examine the role of endogenous itaconate and 4-OI on the innate immune response to *P. aeruginosa* infection using Irg1-knockout and Irg1-wild type BMDMs. We also aim to examine the effects of itaconate treatment on *P. aeruginosa* growth, biofilm formation, virulence factor expression and antibiotic tolerance. Finally, we aim to examine the effects of itaconate and 4-OI on *P. aeruginosa* infection *in vivo*.

Chapter 2 - Materials & Methods

2.1 Materials

Item	Supplier	Catalogue Number
(6X) Gel loading dye, blue	New England BioLabs	B7021S
0.05 % Trypsin-EDTA	Gibco®, Life Technologies	25300-054
0.5ml Insulin Syringe 27G Needle	Sparks Lab Supplies	BS05M2713
10 mM dNTP Mix	Invitrogen™	18427013
100 % ethanol	Honeywell	E7023
10X Red blood cell lysis buffer	Thermo Scientific	00-4300-54
12 % Mini-PROTEAN® TGX™ precast protein gels, 10 well, 50 µl	Bio-rad	465-1044
2-Propanol	Sigma-Aldrich	I9516
4-Octyl Itaconate	Tocris	6662
4X Laemmli sample buffer	Bio-rad	161-0737
A549 cells	ATCC	CCL-185
Acrylamide 4K solution (30 %)	AppliChem	A1672,1000
Aerogen® solo nebuliser	Aerogen®	AS3100-US
Anti-goat IgG, HRP-linked antibody	Sigma-Aldrich	A4174
Anti-phospho-Erk 1/2 rabbit mAb	Merck Millipore	05-797R
Anti-rabbit IgG, HRP-linked antibody	Cell Signalling Technology®	7074
Azactam	Merck Millipore	A6848
cOmplete™ protease inhibitor cocktail tablets	Roche	11697498001
Corning® 96 Well Clear PVC Assay Microplate	Sigma-Aldrich	CLS2797
Crystal Violet	Sigma-Aldrich	C6158
Dimethyl sulfoxide (DMSO)	Sigma-Aldrich	D2650

Dulbecco's modified eagle medium (DMEM)	Gibco®, Life Technologies	4196-039
Endotoxin free water	Sigma-Aldrich	95289
Foetal bovine serum (FBS)	Gibco®, Life Technologies	10770-106
Galleria mellonella	Livefood UK Ltd	
Gentamicin	Sigma-Aldrich	G1397
Glycerol	Sigma-Aldrich	56815
Glycine	Sigma-Aldrich	G8898
Griess reagent kit	Invitrogen	G7921
Heat killed *Pseudomonas aeruginosa*	Invivogen	Tlrl-hkpa
HiLoad® 16/600 Superdex® 200 pg	GE Healthcare	GE28989335
HiPrep™ Q Fast Flow 16/10	GE Healthcare	GE28936543
Immobilon® western chemiluminescent HRP substrate	Merck Millipore	WBKLS0500
Immobilon®-FL transfer membrane pore size = 0.45µM	Merck Millipore	IPFL00010
ISO-1	Tocris	42881
Isopropyl β-D-thiogalactopyranoside solution	Sigma-Aldrich	I1284
Itaconate	Sigma-Aldrich	I29204
L-3,4-dihydroxyphenylalanine methyl ester	Sigma-Aldrich	D1507
L929 cells	ECACC	85011425
LB broth (Miller)	Sigma-Aldrich	L3522
LB broth with agar (Miller)	Sigma-Aldrich	L3147
L-Glutamine (200 mM)	Gibco®, Life Technologies	25030081
Lysozyme from chicken egg white	Sigma-Aldrich	L6876
Meropenem	Merck Millipore	PHR1772
Minimum essential medium	Gibco®, Life Technologies	11090-081
Monoclonal Anti-β-Actin−Peroxidase antibody	Sigma-Aldrich	A3854

Monoclonal Anti-β-Actin−Peroxidase antibody produced in mouse	Sigma-Aldrich	A3854
Mouse KC DuoSet ELISA	R&D Systems	DY453
Mouse MIF DuoSet ELISA	R&D Systems	DY1978
Mouse MIF DuoSet ELISA	R&D Systems	DY289
Mouse RANTES DuoSet ELISA	R&D Systems	DY478
Mouse TNF-α DuoSet ELISA	R&D Systems	DY410
MyTaq™ Red Mix	Bioline	BIO-25043
N,N,N′,N′-Tetramethylethylenediamine (TEMED)	Sigma-Aldrich	T7024
Nrf2 (D1Z9C) XP® rabbit mAb	Cell Signalling Technology®	12721
Nuclease free water	Qiagen	1039598
Oligo (dt) 20	Invitrogen™	18418012
p44/42 MAPK (Erk1/2) rabbit Ab	Cell Signalling Technology®	9102
Penicillin/Streptomycin (10,000 U/mL)	Gibco®, Life Technologies	15140-122
Pierce™ BCA protein assay kit	Thermo Scientific	23225
Pierce™ BCA Protein Assay Kit	Thermo Scientific	23225
Pierce™ High Capacity Endotoxin Removal Spin Columns	Thermo Scientific	88274
Platimnum® SYBR® Green qPCR SuperMix-UDG	Invitrogen™	11733046
PLGA-SCD-19 Nanoparticles	The Donnelly Lab	
Precision plus protein™ dual colour standards	Bio-rad	161-0374
Pro-IL-1β/IL1F2 goat mAb	R&D Systems	AF-401-NA
Quick-Load® 100 bp DNA Ladder	New England BioLabs	N0467S
Random Hexamers	Thermo Scientific	N8080127
RAW 264.7 ells	ECACC	85062803

RIPA lysis buffer, 10X	Merck Millipore	20-188
RNase Out™	Invitrogen™	70777019
SCD-19	Specs	Custom Order
SIGMA*FAST*™ OPD Tablets	Thermo Scientific	P9187
Sodium Dodecyl Sulfate (SDS)	Thermo Scientific	S-5200-53
Sodium periodate	Sigma-Aldrich	71859
Sterile phosphate buffered saline (PBS)	Gibco®, Life Technologies	14190-0940
Superscript II™	Invitrogen™	18064014
Thermo Scientific	Thermo Scientific	28314
Tobramycin	Sigma-Aldrich	T4014
Tri-reagent®	Sigma-Aldrich	T9424
Trizma base	Sigma-Aldrich	93362
TWEEN® 20	Sigma-Aldrich	P1379
β-mercaptoethanol	Bio-rad	161-0710

2.2 Methods for bacterial experiments

2.2.1 Routine bacterial culture

Bacterial cultures were grown in LB broth at 37 °C with shaking for 16 hours. Lab strain *P. aeruginosa* PA01 was purchased from ATCC. Clinical isolates were provided by Dr. Julie Renwick (Dept of Clinical Microbiology, Trinity College Dublin). In order to generate a standard curve of OD_{600} vs CFU/ml, serial dilutions of overnight cultures of PA01 were prepared, the OD_{600} measured and samples subsequently plated on LB agar plates. A standard curve was generated that yielded the following formula which was then used to calculate respective MOI of experiments:

$$CFU/ml = (2x10^9)(x)-(5x10^7), \text{ where } x = OD_{600}$$

Equation 1 *P. aeruginosa* CFU/ml equation

2.2.2 P. aeruginosa growth curve

200 µl of LB broth containing respective treatments was inoculated with 2 µl of overnight *P. aeruginosa* culture in the wells of a 96 well plate. The plate was then added to the SpectraMax i3x microplate reader, with the temperature of the instrument maintained at 37 °C throughout. A kinetic protocol was set up on SoftMax Pro software to measure the OD_{600} was every 30 minutes for 18 hours, with the plate was shaking during the kinetic interval times.

2.2.3 Checkerboard assays

Checkerboard assays are an established method that are used to investigate the effect of interactions between two individual compounds on their antibiotic properties (386, 387). We used checkerboard assays to examine the effects of the interactions between itaconate and a panel of commonly used antipseudomonal antibiotics on *P. aeruginosa* tolerance. Using a 96-well round-bottom microtiter plate, 100 µl two-fold serial dilutions of itaconate were added to the wells, with the same concentration in each column. Following this, 100 µl of two-fold serial dilutions of respective antibiotic

was then added to the wells, with the same concentration in each row. Following this, 2 µl of overnight bacterial culture were added to each well before incubating at 37 °C for 24 hours.

The resulting checkerboard contains each combination of two antibiotics (**Figure 2.1**). One row contains a serial dilution of compound A, while one column contains a serial dilution of compound B which enables the minimum inhibitory concentrations (MIC) of the individual compounds to be calculated. The MIC is defined as the minimum concentration of an agent required to completely inhibit bacterial growth. In order to quantify interactions between two compounds, the Fractional Inhibitory Concentration Index (FICI) is calculated. The FICI is calculated by comparing the MIC of each compound alone with the MIC of the compounds in combination (386). The FICI is calculated as per the following equation.

$$\text{FICI} = \frac{\text{Concentration of A in combination}}{\text{MIC of A alone}} + \frac{\text{Concentration of B in combination}}{\text{MIC of B}}$$

Compounds can act synergistically, whereby the presence of agent A lowers the concentration of agent B needed to inhibit bacterial growth to a concentration lower than that required when agent B is used alone. For example, agent A has an MIC of 32 µg/ml when used against *P. aeruginosa* alone, but in the presence of agent B the MIC of agent A becomes 8 µg/ml. Combinations of agents which result in a 4-fold decrease (FICI ≤ 0.5) in the MIC compared with the MIC of agents alone are said to act synergistically (**Figure 2.1**) (386, 387).

Compounds can also act antagonistically whereby the presence of agent A increases the concentration of agent B needed to inhibit bacterial growth to a concentration higher than that required when agent B is used alone. For example, agent A has an MIC of 32 µg/ml when used against *P. aeruginosa* alone, but in the presence of agent B the MIC of agent A becomes 128 µg/ml. Combinations of agents which result in a 4-fold increase (FICI ≥ 4) in the MIC compared with the MIC of agents alone are said to act antagonistically (**Figure 2.1**) (386, 387). Alternatively, a FICI of between 0.5 and 4 indicates that the two compounds have no interactions.

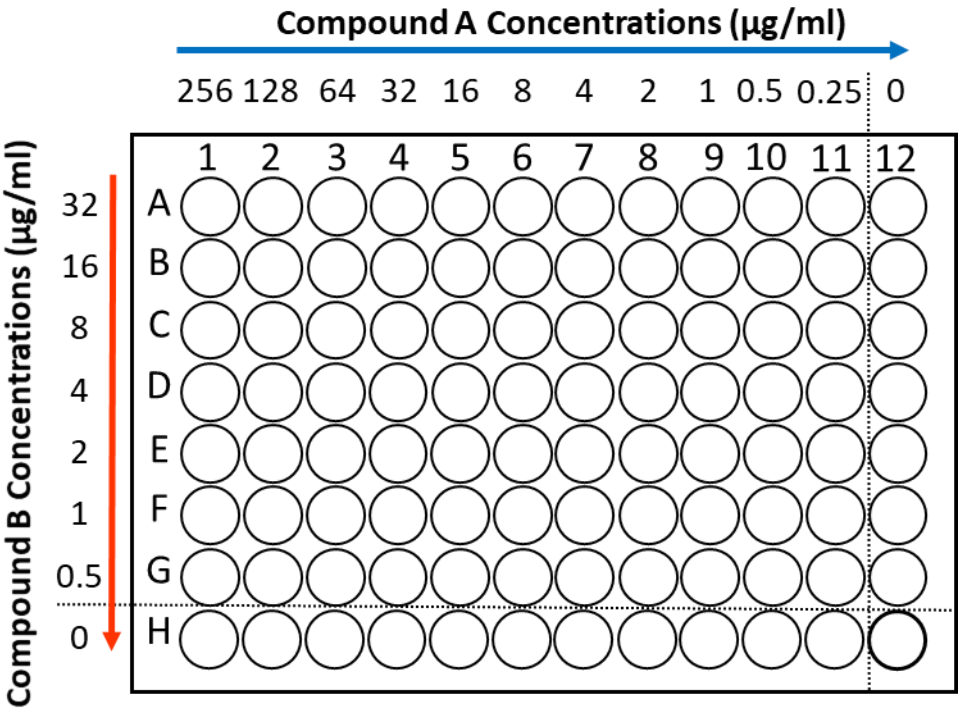

Figure 2.1. Layout for checkerboard assay.

Serial dilutions of compound A are added to each column, while serial dilutions of compound B are added to each column. This results in a checkerboard which contains each combination of two antibiotics. One row contains a serial dilution of compound A, while one column contains a serial dilution of compound B which enables the minimum inhibitory concentrations of the individual compounds to be calculated.

2.2.4 Assessment of P. aeruginosa mRNA expression by Quantitative Real Time Polymerase Chain Reaction (qPCR) using SYBR® Green.

2.2.4.1 Total RNA extraction

Overnight cultures were centrifuged at 4,500 RPM for 5 minutes at 4 °C to collect the bacterial pellet. After removing the supernatant, the bacterial pellet was snap frozen using liquid nitrogen and the allowed to thaw at room temperature. The pellet was then resuspended in 200 µl of lysozyme at a final concentration of 3 mg/ml using TE Buffer for 3 minutes. Following this, 800 µl of Trizol and 200 µl of chloroform were added to each sample before mixing vigorously. The samples were then left to sit at room temperature for 15 minutes before being centrifuged at 13,000 RPM for 15 minutes at 4 °C to allow phase separation to occur. Once separated into the three layers (RNA, DNA and protein), 400 µl the top clear layer containing RNA was removed into

new sterile 1.5 ml microcentrifuge tubes and 500 µl of 2-propanol was added. The samples were vortexed and left at room temperature for 10 minutes. The samples were again centrifuged at 13,000 RPM for 15 minutes at 4^{o}C. The supernatant was then carefully removed, leaving only the RNA pellet in the tube. 1 ml of ice cold 75 % ethanol was added to each RNA pellet. The RNA was stored in 75 % ethanol at -80 °C for later use.

2.2.4.2 First strand cDNA synthesis

First strand cDNA synthesis was carried out on previously isolated RNA. RNA thawed on ice before centrifuging at 13,000 RPM for 15 minutes at 4 ^{o}C. The ethanol was carefully removed, and pellets air dried under a laminar flow hood. RNA pellets were then resuspended in 15 µl of nuclease free water. Once resuspended, 2 µl of RNA from each sample was added to a PCR tube. To this, 2 µl of mastermix #1 (**Table 2.1**) was added to before placing the tubes in the thermocycler for 5 minutes at 65 °C with the lid heated to 95 °C to prevent evaporation. Samples were then placed on ice for 1 minute.

Table 2.1 Mastermix #1 for bacterial first strand cDNA synthesis.

Mastermix # 1	
Component	Volume
Random Hexamers	1 µl
dNTP mix (10 mM)	1 µl
DEPC-Treated Water	6 µl

9 µl of mastermix #2 (**Table 2.2**) was then added to each tube before placing the tubes in the thermocycler for 2 minutes at 25 °C with the lid heated to 95 °C to prevent evaporation. Following this, 1 µl of Superscript II Reverse Transcriptase^{TM} was added to each tube before placing the tubes in the thermocycler at an initial temperature of 42 °C for 50 minutes followed by 15 minutes at 70 °C; the lid was heated to 95 °C to prevent evaporation. cDNA was then stored at -20 °C for qPCR analysis.

Table 2.2 Mastermix #2 for bacterial first strand cDNA synthesis.

Mastermix #2	
Component	Volume
5X First Strand Buffer	4 µl
DTT 0.1 M	2 µl
RNase Out (40 U/µl)	1 µl
Nuclease Free H_2O	2 µl

2.2.4.3 qPCR analysis

qPCR was performed using Platinum® SYBR® Green qPCR SuperMix-UDG along with *P. aeruginosa* gene-specific forward and reverse primers. A qPCR mastermix was prepared as per (**Table 2.3**) and 18 µl of this was added to of 2 µl cDNA. All primers were used at a concentration of 10 µM; primer sequences and annealing temperatures are detailed in (**Table 2.4**). PCR tubes were then inserted into the QuantStudio 5 qPCR machine and run according to the thermal profile detailed in (**Table 2.5**).

qPCR data was analysed using the ΔΔ Cycle Threshold (ΔΔCt) value method. The Ct values for the target genes were normalised to the housekeeping gene *ropD*, yielding the ΔCt value. The ΔCt value of the control sample was then subtracted from the ΔCt value of the other samples, giving the ΔΔCt value. This value was normalised by the formula $2^{-(\Delta\Delta Ct)}$ to generate the fold change in expression of the target gene per unit of rpoD.

Table 2.3 PCR Mastermix for *P. aeruginosa* qPCR.

qPCR Mastermix	
Component	Volume
SYBR® Green	10 µl
Forward Primer (10 µM)	0.2 µl
Reverse Primer (10 µM)	0.2 µl
Nuclease Free Water	7.6 µl

Table 2.4 *P. aeruginosa* specific primers for qPCR.

Gene	5' Forward 3'	5' Reverse 3'	Annealing Temperature (°C)
PA_0882	GGG AGT CCG ACA TAT GAC ACA ATC	CGG TTC ATG TAA GCT TCC TCA TAC C	63
PA_0883	TGA GGA GGC GCA TAT GAA CCG AC	ATT GCT CAA GCT TGC GTT CGC GTC TG	65
AceA	CAA GAA GCA CCT GAA GAC CAC C	GCG GCT TCT CGG TTT CGA TCC A	63

Table 2.5 qPCR thermal cycling profile for *P. aeruginosa* genes.

PCR Profile				
Step		Temperature	Time	# of Cycles
1		50 °C	2 Minutes	X 1
2	Initial Denaturation	95 °C	2 Minutes	X 1
3	Denaturation	95 °C	15 Seconds	X 40
	Annealing	*x* °C	30 Seconds	
	Extension	72 °C	30 Seconds	
4		95 °C	15 Seconds	X 1
		50 °C	30 Seconds	X 1
		95 °C	30 Seconds	X 1

2.2.5 Crystal violet assay

Static biofilm formation was measured as previously described (208). Briefly, 2 µl of overnight *P. aeruginosa* culture was added to each well of a 96 well clear PVC assay microplate containing 100 µl of LB broth with the respective treatments. Plates were incubated at 37 °C for 24 hours. Plates were washed with deionised water and blotted dry. Biofilms were stained using 125 µl of 1 % crystal violet solution per well. Plates were stained for 20 minutes before being washed with deionised water three times. Once dry, 125 µl of 30 % acetic acid was added to each well for 20 minutes. 100 µl of this solution was added to a 96 well plate and the absorbance was measured at 550 nm using a spectrophotometer.

2.2.6 Preparation of planktonic P. aeruginosa filtrate

Planktonic *P. aeruginosa* filtrate (PPF) was prepared as previously described (388). Briefly, liquid cultures of PA01 were incubated for 16 hours at 37 °C with shaking. The cultures were then centrifuged at 5,000 g for 10 minutes to pellet bacteria. The supernatant was then filter sterilised using a low protein binding 0.22 µm filter. Following this, the supernatant was heat inactivated at 95 °C for 10 minutes. Sterility was confirmed by plating a sample on LB agar. PPF was then stored at -20 °C.

2.3 Methods for human experiments

2.3.1 Cell culture

2.3.1.1 16HBE14o- and CFBE41o- cell culture

16HBE14o- and CFBE41o- cells were kindly donated by Dr Catherine Greene (RCSI, Clinical Microbiology, Beaumont Hospital, Dublin, Ireland). 16HBE14o- cells are an SV40-transformed human bronchial epithelial cell line and CFBE41o- cells are human ΔF508 homozygote bronchial epithelial cells. Cells were maintained in a humidified atmosphere containing 5 % CO_2 at 37 °C. 16HBE14o- and CFBE41o- cells were maintained in minimal essential medium (MEM) supplemented with 10 % foetal bovine serum (FBS), 1 % L-glutamine, 100 U/ml penicillin and streptomycin (pen/strep). Cells were passaged every 2-3 days by removing medium and adding 5 ml of 0.05 % Trypsin-EDTA for 5 minutes at 37 °C. Trypsin was neutralised by adding medium before cells were collected and spun for 5 minutes in at 1200 RPM.

2.3.1.2 A549 cell culture

A549 cells, a lung epithelial cell line, were obtained from ATCC®. A549 cells were maintained in DMEM supplemented with 10 % FBS and 100U/ml pen/strep. Cells were maintained in a humidified atmosphere containing 5 % CO_2 at 37 °C. Cells were passaged every 2-3 days by removing medium and adding 5ml of 0.05 % Trypsin-EDTA for 5 minutes at 37 °C. Trypsin was neutralised by adding medium before cells were collected and spun for 5 minutes in at 1200 RPM.

2.3.1.3 Preparation of nanoparticles

Poly(lactic-co-glycolic acid) (PLGA) and PLGA-SCD-19 nanoparticles were provided for this project by Dr. Mohammad Doroudian (Donnelly Lab). Briefly, 100 mg of PLGA and 10 mg of SCD-19 were combined in a beaker. Following this, 8 ml of 2% (w/v) polyvinyl alcohol was added drop by drop with constant stirring. The emulsion formed was homogenised using a probe sonicator at 70 % amplitude for 30 seconds before being added to 50 ml of 0.2 % polyvinyl alcohol. The resulting emulsion was stirred with an overhead stirrer for 16 hours to allow the organic solvents to evaporate. Nanoparticles were recovered via centrifugation (21,000 × g, 10 minutes, 4°C) and washed three times in 50 ml of endotoxin free water before being resuspended in saline and stored at 4°C until use. For cellular experiments, nanoparticle solutions were passed through an Aerogen® solo nebuliser and the resulting mist collected in a 50 ml falcon tube. This work was all conducted by Dr. Mohammad Doroudian.

2.3.2 Biofilm formation on airway epithelial cells

2.3.2.1 Preparation of P. aeruginosa

P. aeruginosa liquid cultures were incubated for 16 hours at 37 °C with shaking. Cultures were then centrifuged at 4500 RPM for 15 minutes to pellet bacteria. The bacterial pellet was then resuspended in PBS and centrifuged at 4,500 RPM for 15 minutes. The pellet was then resuspended in antibiotic free DMEM. The OD_{600} was recorded and the number of CFU/ml calculated as per **Equation 1** and samples diluted to the required number of CFU/ml.

2.3.2.2 Infection of epithelial cells

Methods adapted from Anderson *et al*. (207). A549/16HBE14o-/CFBE41o- cells were plated at 2 x 10^5/ml in 500 µl of medium in a 24 well plate. Cells were cultured under normal conditions for 5 days to enable monolayer formation, with media changes every 2 days. On day 5, media was removed and cells were washed twice with warm PBS. Cells were inoculated with PA01 at an MOI of 30:1 (PA01:epithelial cell) for 1 hour using antibiotic free DMEM. Inoculum was removed and cells were washed with warm PBS. 500 µl of antibiotic free DMEM was added to each well and cells were incubated

for a further 3 hours under normal conditions. Supernatants were collected and stored, while cells were washed twice with warm PBS. Cells were lysed with 500 µl of 0.1 % Triton X-100 for 10 minutes. Cell lysates were collected and serially diluted using PBS before plating on agar plates for CFU/ml enumeration.

2.4 Methods for murine experiments

2.4.1 Animals

The generation of humanised CATT mice was carried out by Taconic Biosciences on a C57BL/6 background. Briefly, the murine *MIF* gene was deleted, and replaced with the human MIF gene containing a microsatellite repeat of 5 or 7 CATTs; enabling the production of human MIF. $MIF^{-/-}$ and wild type mice were both on a C57BL/6 background. Hind legs from $Irg1^{-/-}$ and wild type mice, both on a C57BL/6 background, were donated by Professor Padraic Fallon (Trinity College Dublin). All animals were housed in pathogen free environments at the comparative medicine unit at Trinity College Dublin. All animal experiments were conducted in accordance with the recommendations and guidelines of the Health Products Regulatory Authority (HPRA), the competent authority in Ireland, and in accordance with protocols approved by Trinity College Animal Research Ethics Committee.

2.4.2 Cell culture

2.4.2.1 RAW 264.7 cell culture

RAW 264.7 cells, a murine macrophage cell line, were maintained in DMEM medium supplemented with 10 % FBS and 100U/ml pen/strep. Cells were maintained in a humidified atmosphere containing 5 % CO_2 at 37 °C. Cells were passaged every 2-3 days when they reached 80-90 % confluence. Cells were scraped from the bottom on the wells or flasks using cell scrapers and centrifuged for 5 minutes at room temperature at 400 g. Medium was discarded, and cells were resuspended in fresh DMEM medium.

2.4.2.2 L929 cell culture

The L929 cell line is a murine connective tissue cell line. L929 supernatants are routinely used in bone marrow derived macrophage (BMDM) cell culture as L929 cells secrete M-CSF and GM-CSF to promote differentiation of BMDMs. Cells were seeded into a T175 flask at a density of $20x10^6$ cells per flask. Cells were maintained in DMEM supplemented with 10 % FBS and 100 U/ml pen/strep. Cells were maintained in a humidified environment (95 % relative humidity) containing 5 % CO_2 at 37 °C. After 10 days, supernatant was removed and filter-sterilised. Aliquots of L929 media were stored at -20 °C for use in BMDM cell culture.

2.4.2.3 Primary bone marrow derived macrophage culture

Post-mortem, the hind legs of mice were removed using a scissors on the bench top. Skin and muscle were stripped from the legs until only bones remained. The bones were sprayed in 70 % ethanol and placed in a 50 ml falcon tube with 10 ml of complete DMEM before being brought into the sterile laminar flow hood. The leg bones were separated at the hinge joint and a scalpel used to snip the ends to give access to the bone marrow. A syringe filled with complete DMEM fitted with a 25-gauge needle was inserted into the top of the bone. The media was flushed through the bone and the flow through collected in a cell strainer placed over a sterile 50 ml Falcon tube. The flow through was then centrifuged at 1,200 RPM for 5 minutes to pellet the bone marrow. The supernatant was discarded before the pellet was re-suspended in 5 ml of 1X red blood cell lysis buffer and left for 4 minutes on ice, shaking every 30 seconds. 15 ml complete DMEM was added to the 50 ml falcon to neutralise the lysis buffer before centrifuging at 1200 RPM for 5 minutes. The pellet was re-suspended in 10 ml of complete DMEM and transferred to a sterile T175 cell culture flask. The bone marrow from both legs of one mouse was added to 1 sterile T175 cell culture flask. A further 14 ml of complete DMEM was added, followed by 6 ml of L929 supernatant, with a final concentration of 20 % L929 supernatant. BMDMs were incubated for 3 days in a humidified atmosphere containing 5 % CO_2 at 37 °C to allow the cells to adhere. Following this, the supernatant containing cells that have not adhered was removed from the flask and placed directly into a new T175 flask and supplemented with L929 supernatant to a final concentration of 20 %. The original flask was given 30 ml of

complete DMEM supplemented with 20 % L929 media. Both flasks were incubated for until confluent. The original flask was confluent at ~ day 7 while the second flask was confluent at ~ day 14. Cells were harvested for plating by removing medium and adding 5 ml of 0.05 % Trypsin-EDTA for 5 minutes at 37 °C. Trypsin was neutralised by adding medium before cells were collected and spun for 5 minutes in at 1,200 RPM. Cells were counted and plated for experiments at a density of 12.5 x 10^5 /ml in a 24 well plate. Once plated, cells were placed back into the incubator overnight. Cells were stimulated with the respective stimulants and treatments for the indicated times.

2.4.2.4 Primary murine lung fibroblast culture

The lungs were removed from individual mice post-mortem. The set of lungs were then sprayed with 70 % ethanol and added into 10 ml of sterile DMEM and dissected into small fragments in a sterile petri dish in the laminar flow hood. The fragments were then transferred to a T75 flask containing 10 ml of complete DMEM before being placed into the incubator. Cells were maintained in a humidified atmosphere containing 5 % CO_2 at 37 °C. Lung fragments were left for 48 hours to allow them to adhere to the flask, before replacing the DMEM every 48 hours. After 7-8 days, the fibroblasts began to grow out of the lung fragments and began forming a monolayer on the flask. Upon the formation of these foci, the lung fragments were removed and discarded. Once the cells had reached ~ 80 % confluency, cells were trypsinised and added to a T175 with fresh DMEM. Again, once the cells had reached ~ 80 % confluency, they were trypsinised and split into two T175 flasks. Once confluent, cells were then used for experiments.

2.4.3 Live PA01 infection of macrophages

Macrophages (RAW 267.4 or BMDMs) were seeded at a density of 12 x 10^5 cells per well in a 24 well plate. Bacterial density was quantitated by reading the OD_{600} and CFU/ml calculated using a standard curve (**Equation 1**). Macrophages were infected with live PA01 at an MOI of 30 (PA01:macrophage) for 1 hour at 37 °C in a humidified environment with 5 % CO_2. Following this, all medium was removed and fresh medium was added containing 300 μg/ml gentamicin for a further 1 hour in a humidified

environment with 5 % CO_2. Following this, all medium was removed and replaced with fresh antibiotic free medium for a further 6 hours at 37 °C in a humidified environment with 5 % CO_2. Supernatants were then removed and stored at -80 °C and cells were harvested for Western blot or stored in Trizol.

2.4.4 Quantification of cytokine production by ELISA

96 well Nunc MaxiSorp™ plates were coated with 50 µl of capture antibody diluted in PBS and incubated overnight at 4 °C. Plates were then washed three times in 0.05 % PBS Tween and blotted dry. Plates were blocked by adding 150 µl of 1 % BSA in PBS to each well and incubated at room temperature for 2 hours. Plates were washed again as previously described. 50 µl of sample or standard was added to each well and incubated for overnight at 4 °C. Plates were then washed again as described. 50 µl of the detection antibody in 1 % BSA in PBS was added to each well and incubated for 2 hours at room temperature. Plates were then washed again as described. 50 µl of working concentration of Streptavidin–HRP was added to each well and plates were covered and incubated for 20 minutes at room temperature.

ELISA substrate solution was prepared by dissolving one o-Phenylenediamine dihydrochloride (OPD) tablet and one urea hydrogen peroxide/buffer tablet were 20 ml of water. 50 µl of substrate solution was added to each well and incubated for 20 minutes at room temperature. 25 µl of 2N H_2SO_4 was added to each well to stop the reaction. The optical density of each well was then measured with a spectrophotometer at 490 nm. The respective concentrations of capture antibody, detection antibody and standards are detailed in **Table 2.6.**

Table 2.6 ELISA reagent concentrations.

Murine ELISA Kits			
	Capture Antibody	Detection Antibody	Standard Curve Range
KC (Murine IL-8)	2 µg/ml	200 ng/ml	4,000 ng/ml – 62.5 ng/ml
MIF	0.4 µg/ml	200 ng/ml	16,000 ng/ml -250 ng/ml
RANTES	2 µg/ml	12.5 ng/ml	4,000 ng/ml – 62.5 ng/ml
TNF-α	0.8 µg/ml	75 ng/ml	4,000 ng/ml – 62.5 ng/ml
Human ELISA Kits (For CATT Mice)			
	Capture Antibody	Detection Antibody	Standard Curve Range
MIF	2 µg/ml	100 ng/ml	31.2 ng/ml – 2,000 ng/ml

2.4.5 Assessment of mRNA by Quantitative Real Time Polymerase Chain Reaction (qPCR) using SYBR® Green.

2.4.5.1 Total RNA extraction

Total RNA was isolated using Tri Reagent© RNA isolation reagent. Cells were stimulated with the respective stimuli for the required times before supernatants were removed. 1 ml of Trizol was added to the remaining cell monolayer in each well. The monolayer was disrupted using a pipette tip and transferred to a sterile 1.5 ml microcentrifuge tube. Following this, 200 µl of chloroform was added to each sample before mixing vigorously. The samples were then left to sit at room temperature for 15 minutes before being centrifuged at 13,000 RPM for 15 minutes at 4 °C to allow phase separation to occur. Once separated into the three layers (RNA, DNA and protein), 400 µl of the top clear layer containing RNA was removed into new sterile 1.5 ml microcentrifuge tubes and 500 µl of 2-propanol was added. The samples were vortexed and left at room temperature for 10 minutes. The samples were again centrifuged at 13,000 RPM for 15 minutes at 4 °C. The supernatant was then carefully removed, leaving only the RNA pellet in the tube. 1 ml of ice cold 75 % ethanol was added to each RNA pellet. The RNA was stored in 75 % ethanol at -80 °C for later use.

2.4.5.2 First strand cDNA synthesis

First strand cDNA synthesis was carried out on previously isolated RNA. RNA was thawed on ice before centrifuging at 13,000 RPM for 15 minutes at 4 °C. The ethanol was carefully removed before pellets were air dried in a laminar flow hood. RNA pellets were resuspended in 15 µl of nuclease free water. Once resuspended, 8 µl of RNA from each sample was added to a PCR tube. To this, 2 µl of mastermix #1 (**Table 2.7**) was added to before placing the tubes in the thermocycler for 5 minutes at 65 °C with the lid heated to 95 °C to prevent evaporation. Samples were then placed on ice for 1 minute.

Table 2.7 Mastermix #1 for mammalian first strand cDNA synthesis.

Mastermix #1	
Component	Volume
Oligo (dT) 20 (200 µg/ml)	1 µl
dNTP Mix (10 mM)	1 µl

9 µl of mastermix #2 (**Table 2.8**) was then added to each tube before placing the tubes in the thermocycler for 2 minutes at 25 °C with the lid heated to 95 °C to prevent evaporation. Following this, 1 µl of Superscript II Reverse Transcriptase^{TM} was added to each tube before placing the tubes in the thermocycler at an initial temperature of 42 °C for 50 minutes followed by 15 minutes at 70 °C; the lid was heated to 95 °C to prevent evaporation. cDNA was then stored at -20 °C for qPCR analysis.

Table 2.8 Mastermix #2 for mammalian first strand cDNA synthesis.

Mastermix #2	
Component	Volume
5X First Strand Buffer	4 µl
DTT 0.1M	2 µl
RNase Out (40 U/µl)	1 µl
Nuclease Free H_2O	2 µl

2.4.5.3 qPCR analysis

qPCR was performed using Platinum® SYBR® Green qPCR SuperMix-UDG along with murine gene-specific forward and reverse primers. A qPCR mastermix was prepared as per (**Table 2.9**) and 18 µl of this was added to of 2 µl cDNA. All primers were used at a concentration of 10 µM; primer sequences and annealing temperatures are detailed in (**Table 2.10**). PCR tubes were then inserted into the QuantStudio 5 qPCR machine and run according to the thermal profile detailed in (**Table 2.11**).

qPCR data was analysed using the ΔΔ Cycle Threshold (ΔΔCt) value method. The Ct values for the target genes were normalised to the housekeeping gene β-*actin*, yielding the ΔCt value. The ΔCt value of the control sample was then subtracted from the ΔCt value of the other samples, giving the ΔΔCt value. This value was normalised by the formula $2^{-(\Delta\Delta Ct)}$ to generate the fold change in expression of the target gene per unit of β-actin.

Table 2.9 PCR Mastermix for mammalian qPCR.

qPCR Mastermix	
Component	Volume
SYBR® Green	10 µl
Forward Primer (10 µM)	0.2 µl
Reverse Primer (10 µM)	0.2 µl
Nuclease Free Water	7.6 µl

Table 2.10 Murine specific primers for qPCR.

Gene	5' Forward 3'	5' Reverse 3'	Annealing Temperature (°C)
β-*Actin*	AAG AGC TAT GAG CTG CCT GA	TAC GGA TGT CAA CGT CAC AC	57
Hmox1	TCA GGC AGA GGG TGA TAG AA	GCT CCT GCA ACT CCT CAA A	57
Gsr	CGG TGC CAG CTT AGG AAT AA	GCC ATC TCC ACA GCA ATG TA	57
Gclm	GAC AAA ACA CAG TTG GAA CAG C	CAG TCA AAT CTG GTG GCA TC	57
Nqo1	GCT GCA GAC CTG GTG ATA TT	ACT CTC TCA AAC CAG CCT TT	57
PHD3	TGC TGA AGA AAG GGC AGA AG	GCA CAC CAC AGT CAG TCT TTA	57
TNF-α	GAT CTC AAA GAC AAC CAA CAT GTG	CTC CAG CTG GAA GAC TCC TCC CAG	63
IL-1β	AAC CTG CTG GTG TGT GAC GTT C	CAG CAC GAG GCT TTT TTG TTG T	60
Irg1	GCG AAC GCT GCC ACT CA	ATC CCA GGC TTG GAA GGT C	58
RANTES	CAA TCT TGC AGT CGT GTT TG	GGA GTG GGA GTA GGG GAT TA	57
IL-10	TTC TGC CTC ATC CTG CTG	AGA CAT CTC TGC TCA TCA TTC	56
iNOS	AGC CCT CAC CTA CTT CCT G	CAA TCT CTG CCT ATC CGT CTC	59
Caspase-1	AGG AAT TCT GGA GCT TCA ATC AG	TGG AAA TGT GCC ATC TTC TTT	59

Table 2.11 qPCR thermal cycling profile for murine genes.

PCR Profile				
Step		Temperature	Time	# of Cycles
1		50 °C	2 Minutes	X 1
2	Initial Denaturation	95 °C	2 Minutes	X 1
3	Denaturation	95 °C	15 Seconds	X 40
	Annealing	*x* °C	30 Seconds	
	Extension	72 °C	30 Seconds	
4		95 °C	15 Seconds	X 1
		50 °C	30 Seconds	X 1
		95 °C	30 Seconds	X 1

2.4.6 Assessment of protein expression by Western blot analysis

2.4.6.1 Cell harvesting

Macrophages were seeded at a density 12.5 x 10^5 cells per well in a 24 well plate. Following the respective treatment, intracellular proteins were harvested in RIPA buffer containing protease inhibitor cocktail tablets. Cell supernatant was removed before placing the cells on ice and gently washing with 1 ml of ice-cold PBS. Following this, all PBS was carefully removed before adding 25-50 µl of 1X RIPA buffer in PBS to each well. The plates were left on ice for 30 minutes before scratching each well with a p200 tip to remove the cells from the plate. Samples were then transferred to Eppendorf tubes and stored at -80 °C.

2.4.6.2 Bicinchoninic Acid (BCA) assay & sample preparation

Samples were defrosted on ice before centrifuging for 30 minutes at 15,000 RPM to pellet the cell debris. Samples were transferred to new Eppendorf tubes and the pellet discarded. For the BCA assay, standard solutions were prepared by diluting bovine serum albumin (BSA) solution to a series of know concentrations. After the samples and standard were vortexed, 10 µl of each was added to the wells of a 96 well plate. The BCA reagent was prepared by mixing reagent A with reagent B at a respective ratio of 50:1. 200 µl of the BCA reagent was then added to each well before placing the plate in a 37 °C incubator for 30 minutes. The absorbance was then recorded at 562 nm and protein levels calculated accordingly.

Following the BCA assay, samples were equilibrated to the desired concentration using loading buffer. The loading buffer consisted of 900 µl of 4X Laemmli buffer and 100 µl of β-mercaptoethanol. Samples were then boiled at 95 °C for 5 minutes and stored at -20 ^{o}C.

2.4.6.3 Western blotting

Protein samples were loaded to 10 % sodium dodecyl sulphate-polyacrylamide gel electrophoresis (SDS-PAGE) gels (**Table 2.12**). A molecular weight reference ladder was also run on each gel. The gel was run at 90 V for 90 minutes in 1X running buffer (**Table 2.13**). The wet transfer method was used using 1X transfer buffer (**Table 2.13**) to transfer proteins to a PVDF membrane which was activated in methanol before use. The

transfer tank was surrounded by ice in a Styrofoam box to prevent overheating and was run at 200 mA for 90 minutes.

Following the transfer, membranes were blocked for 1 hour at room temperature using 5 % non-fat dried milk in Tris buffered saline with 0.1 % Tween 20 (TBS-T). Membranes were then incubated with primary antibody overnight at 4 °C. Primary antibodies were diluted according to (**Table 2.14**) using 5 % BSA in TBS-T (0.1 % Tween 20).

After incubating with primary antibody, membranes were washed in 1X TBS-T (0.1 % Tween 20) for 10 minutes 3 times. Membranes were then incubated with secondary antibody for 2 hours at room temperature. Secondary antibodies were diluted according to (**Table 2.14**) using 5 % non-fat dried milk in TBS-T (0.1 % Tween 20). Membranes were again washed for 10 minutes 3 times before visualising using chemiluminescent HRP substrate on the Gel-Doc system.

Table 2.12 Western blot gel compositions.

10 % Separating Gel Composition	
dH_20	4.02 ml
Bis Acrylamide	3.33 ml
Tris-Hcl (pH 8.8)	2.5 ml
10 % SDS	100 µl
10 % APS	50 µl
TEMED	10 µl

4 % Stacking Gel Composition	
dH_20	3.05 ml
Bis Acrylamide	650 µl
Tris-Hcl (pH 6.8)	1.25 ml
10 % SDS	50 µl
10 % APS	25 µl
TEMED	8 µl

Table 2.13 Western blot buffers.

10X Running Buffer	
Trizma Base	60.4 g
Glycine	288 g
SDS	20 g
Dissolve in 2 L dH_2O, pH8.3	
1X Running Buffer	
10X Running Buffer	100 ml
dH_2O	900 ml

10X Transfer Buffer	
Trizma Base	60.4 g
Glycine	288 g
Dissolve in 2 L dH_2O, pH 8.3	
1X Transfer Buffer	
10X Transfer Buffer	100 ml
Methanol	100 ml
dH_2O	800 ml

Table 2.14 Antibody dilutions for western blot.

Primary Antibodies	Dilution Factor	Required Secondary Antibody
Nrf2	1:1000	Rabbit
Pro IL-1β	1:800	Goat
β-Actin-Peroxidase	1:50000	

Secondary Antibodies	Dilution Factor
Rabbit	1:5000
Goat	1:5000

2.4.7 Lactate dehydrogenase assay

Cellular death was assessed by measuring levels of lactate dehydrogenase (LDH) in cellular supernatant as per kit instructions. LDH is a cytosolic enzyme that is released into the supernatant upon cell death due to damage of the cell membrane. Levels of LDH in supernatant increase in proportion with the number of lysed cells. 100 µl of supernatant was added to the wells of a 96 well plate. 100 µl of the freshly prepared reaction mixture was also added to each well and the plate incubated at room temperature protected from the light for 30 minutes. The absorbance was measured with a spectrophotometer at 490 nm.

2.4.8 Analysis of P. aeruginosa phagocytosis by macrophages

Bacterial phagocytosis was performed as previously described with modifications (389). Briefly, macrophages were seeded at a density of 1 x 10^5 cells per well in a 96 well plate for 16 hours incubation. Cells were infected with PA01 (MOI 10) for 1 hour. Cells were washed with warm PBS followed by the addition of 300 µg/ml gentamycin for 1 hour to kill extracellular bacteria. Cells were then washed and lysed in DMEM containing 0.1 % Triton X-100 before plating on agar plates for CFU/ml enumeration. Where treatments were added, cells were pre-treated for 30 minutes and treatments were maintained for the duration of the experiment.

2.4.9 Analysis of P. aeruginosa killing by macrophages

Cells were seeded at a density of 1 x 10^5 cells per well in a 96 well plate before infection the next day. Overnight cultures of PA01 were centrifuged at 4500 RPM for 5 minutes at room temperature to collect the bacterial pellet. The pellet was resuspended in antibiotic free DMEM and the OD_{600} measured, using medium only as a blank. The number of CFU/ml was calculated as per the standard curve (**Equation 1**).

Macrophages were infected at a multiplicity if infection (MOI) of 10 CFU: 1 macrophage for 4 hours. In experiments involving 4-OI, this was added at the time of inoculation. Following this, supernatant was removed and placed into a fresh 96 well plate. Macrophages were then lysed using 20 µl of 0.1 % Triton X for 15 minutes. The supernatant was then added back to the corresponding well and mixed with the cell lysate. This was then serially diluted between 10^{-3} - 10^{-5} and subsequently plated on LB agar plates for CFU/ml analysis.

2.4.10 Griess assay (nitrite quantification)

Nitrite concentrations were measured using the Griess assay. Briefly, 150 µl of cell free supernatant was added to the wells of a 96 well plate with 130 µl of water and of 20 µl Griess reagent. The plate was then incubated for 30 minutes at room

temperature in the dark before reading the absorbance at 540 nm. Nitrite concentrations were calculated from the standard curve which had a range from 100 µM to 1.5 µM.

2.5 *Methods for Galleria mellonella experiments*

2.5.1 G. mellonella larvae

G. mellonella larvae were purchased from Livefood UK Ltd (Somerset, UK). Larvae were housed at 14 °C in the dark to prevent pupa formation and transformation into the greater wax moth. Prior to experiments, larvae were weighed and those between 0.2 – 0.3 grams were selected for studies.

2.5.2 G. mellonella model of P. aeruginosa infection

G. mellonella larvae were inoculated with 20 µl of a phosphate-buffered saline (PBS) solution containing 5 x 10^2 CFU/ml to 2.5 x 10^3 CFU/ml thorough injection with a 27-gauge needle via the last left pro-leg (**Figure 2.2**). For studies involving itaconate or 4-OI, a single solution containing PA01 and the respective treatment was administered at time zero. Following inoculation, larvae were housed at 37 °C in the dark until the end of the experiment. The end point of the experiment was death, at which point the *G. mellonella* appear black in colour.

Figure 2.2. Inoculation site of *G. mellonella*.

G. mellonella are inoculated via injection through the last left pro-leg, highlighted in this image.

2.6 Expression and purification of recombinant human MIF

2.6.1 Bacterial culture

Transformed *E. coli* containing the rMIF-pET11b vector were obtained from Prof. Richard Bucala (Yale University, United States of America) and was maintained on LB agar plates (120). The pET11b vector confers resistance to ampicillin, which is then used to positively select colonies containing the pET11b vector. Prior to beginning protein expression, the bacteria were cultured in LB broth containing 50 µg/ml of ampicillin at 37 °C for 16 hours. Following this, individual colonies were streaked on an LB agar plate containing 50 µg/ml of ampicillin at 37 °C for 16 hours (**Figure 2.3A**).

2.6.2 Colony PCR

Colony PCR was carried out to verify the presence of the rMIF-pET11b vector in our colonies. A mastermix was prepared as per **Table 2.15** in a PCR tube before the addition of a single bacterial colony. The PCR programme was subsequently run on the thermocycler as per **Table 2.17**. The resulting PCR product was then examined using agarose gel electrophoresis.

2.6.3 Gel electrophoresis

1X TBE buffer was prepared using 5X TBE (**Table 2.18**) and deionised water. A 1 % agarose gel was prepared as per **Table 2.18.** Once the agarose has melted and cooled, the gel was poured into the gel electrophoresis cassette, the comb was inserted and the gel was left to set. Once set, 1X TBE buffer was poured into the horizontal gel electrophoresis tank. 1 µl of 6X gel loading dye was mixed with 5 µl of PCR product and then loaded into the gel along with a Quick-Load® 100 bp DNA ladder. Gel electrophoresis was run at 120 V. The resulting gel was then visualised using a using a gel-dock and associated software. As expected, the presence of the pET11b-MIF vector was confirmed in all nine colonies as indicated by the presence of bands of approximately 345 base pairs in size, with no band present in the negative control (**Figure 2.3B**).

Table 2.15. Mastermix for colony PCR.

Colony PCR Mastermix	
Component	Volume
MyTaq™ Red Mix	25 µl
Forward Primer (5 µM)	1 µl
Reverse Primer (5 µM)	1 µl
Nuclease Free Water	23 µl

Table 2.16. Primer sequences for human MIF insert for colony PCR.

Colony PCR Primers			
Gene	5' Forward 3'	5' Reverse 3'	Annealing Temperature (°C)
MIF	ATA TGC CGA TGT TCA TCG TAA ACA C	CGG ATC CTG CGG CTC TTA GGC GAA GG	55

Table 2.17. qPCR thermal cycling profile for colony PCR.

PCR Profile				
Step		Temperature	Time	# of Cycles
1		94 °C	10 Minutes	X 1
2	Denaturation	94 °C	1 Minute	X 32
	Annealing	55 °C	1 Minute	
	Extension	72 °C	1 Minute	
3	Final Extension	72 °C	5 Minutes	X 1

Table 2.18. Reagents for colony PCR.

5X TBE Buffer	
Trizma Base	32.4 g
Boric acid	16.5 g
EDTA	2.7g
Dissolve in 1 L dH_2O, pH8.3	

1 % Agarose Gel	
SYBR™ Safe DNA Gel Stain (10,000X)	3 µl
Agarose	0.3 g
Dissolve in 30 ml of 1X TBE buffer	

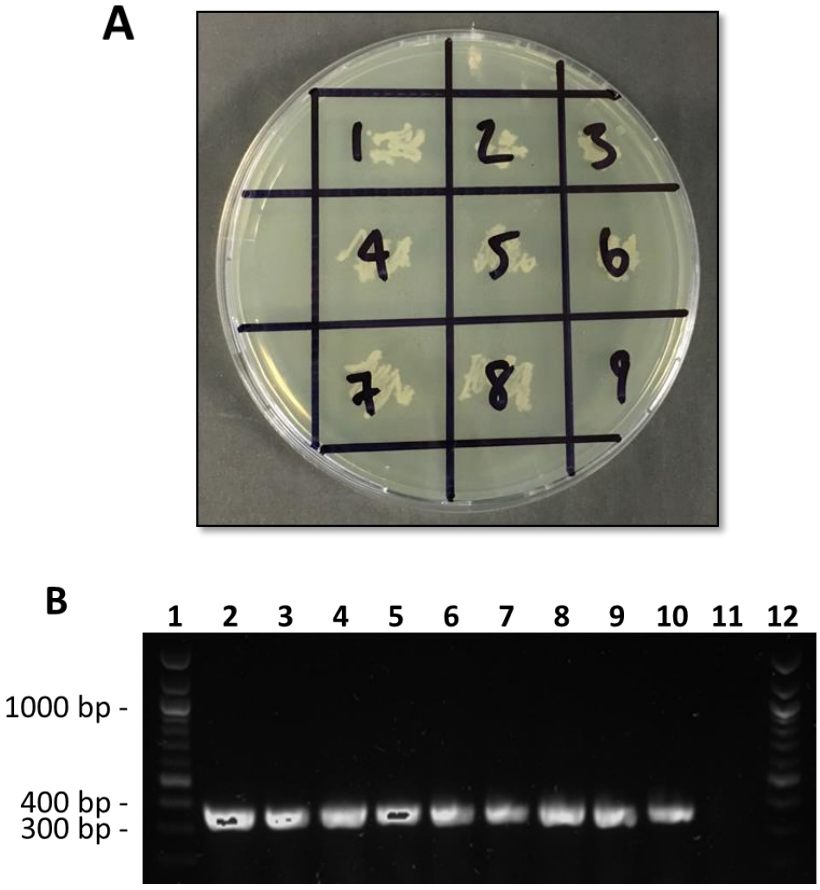

Figure 2.3. Colony PCR analysis to verify the presence of the MIF gene in transformed *E. coli* containing the pET11b vector.

Colony PCR was used to verify the presence of the rMIF-pET11b plasmid in transformed *E. coli*. (**A**) Image of 9 independent transformed E. coli stocks cultured on LB agar containing 50 µg/ml of ampicillin to select colonies containing the rMIF-pET11b plasmid. (**B**) Agarose gel images of PCR amplification products from 9 *E.coli* colonies containing the rMIF-pET11b vector cultures in LB broth with 50 µg/ml of ampicillin. Lanes 1 and 12 contain Quick-Load® 100 bp DNA Ladder, lanes 2 – 10 contain PCR products from the nine independent E. coli samples while lane 11 contains a negative control. The presence of bands in lane 2-10 at the 345 bp weight indicates the presence of the rMIF-pET11b plasmid in all *E. coli* samples examined.

2.6.4 Induction of protein expression

Following verification of the presence of the rMIF-pET11b vector, a single colony was selected and cultured in 200 ml of LB broth containing 50 µg/mL of ampicillin overnight at 37 °C with shaking. Add 30 ml of the overnight culture to 1 L of fresh LB broth containing 50 µg/mL of ampicillin and incubate until the OD_{600} reached 0.8. Once the appropriate OD_{600} had been reached, isopropyl β-D-1-thiogalactopyranoside was added at a final concentration of 1 mM to induce the expression of recombinant MIF (rMIF). The culture was then incubated for a further 5 hours. Bacteria were harvested by centrifugation and the cell pellets were stored at -80 °C until use.

2.6.5 Protein harvesting

Prior to protein purification, the bacterial pellet was resuspended 50 ml of Buffer A () and stirred overnight at 4 °C. To release the protein from the bacterial cells, they were sonicated five times at 48 % power for 30 seconds with 30 second intervals. The solution was then centrifuged at 20,000 RPM for 20 minutes. The liquid, which contains the protein, was then poured into a volumetric flask sitting on ice, stirring with a stir bar. Nucleic acids were precipitated out by adding 10 µl of benzonase nuclease drop by drop and subsequently stirred for 45 minutes at 4 °C. The solution was then centrifuged at 20,000 RPM for 20 minutes and subsequently filter sterilised using a 0.2 µm filter. The sample from this process were analysed to verify that the protein was successfully expressed using SDS-PAGE.

2.6.6 SDS-PAGE

Samples were mixed in a 1:1 ratio with 2X SDS-PAGE sample buffer (**Table 2.19. Buffers for protein purification**). Samples were then denatured by heating them to 95 °C for 15 minutes. Samples were then loaded into a 12 % Mini-PROTEAN® TGX™ precast gel before being run at 100V for 1 hour. Following this, the gel was submerged in fixing solution (**Table 2.19**) and then placed on a shaker for 15 minutes at room temperature.

The gel was then washed three times with dH_2O. The gel was then stained using Comassie blue and subsequently de-stained using de-staining solution (Table 2.19).

MIF has a molecular weight of 37.5 kDa and is composed of three monomeric subunits, each of 12.5 kDa in size. In the lanes containing supernatant and bacterial debris samples that had IPGT added, lanes 2 and 5, thick bands are visible at 12.5 kDa which are indicative of the presence of MIF monomers (**Figure 2.4**). In the lanes containing supernatant and bacterial debris that did not have IPTG added, lanes 3 and 4, these bands are much smaller – most notably in lane 3.

Buffer A	
Tris-HCl	7.88 g
NaCl	8.76 g
Adjust volume to 1 L with dH_20, pH 7.5	
10 X SDS-PAGE Sample Buffer	
SDS	10 g
Tris-base	30.30 g
Glycine	144 g
Adjust volume to 1 L with dH_20	

Fixing Solution	
Glacial acetic acid	100 ml
Methanol	500 ml
dH_20	400 ml
De-staining Solution	
Glacial acetic acid	100 ml
Methanol	150 ml
dH_20	750 ml

Table 2.19. Buffers for protein purification

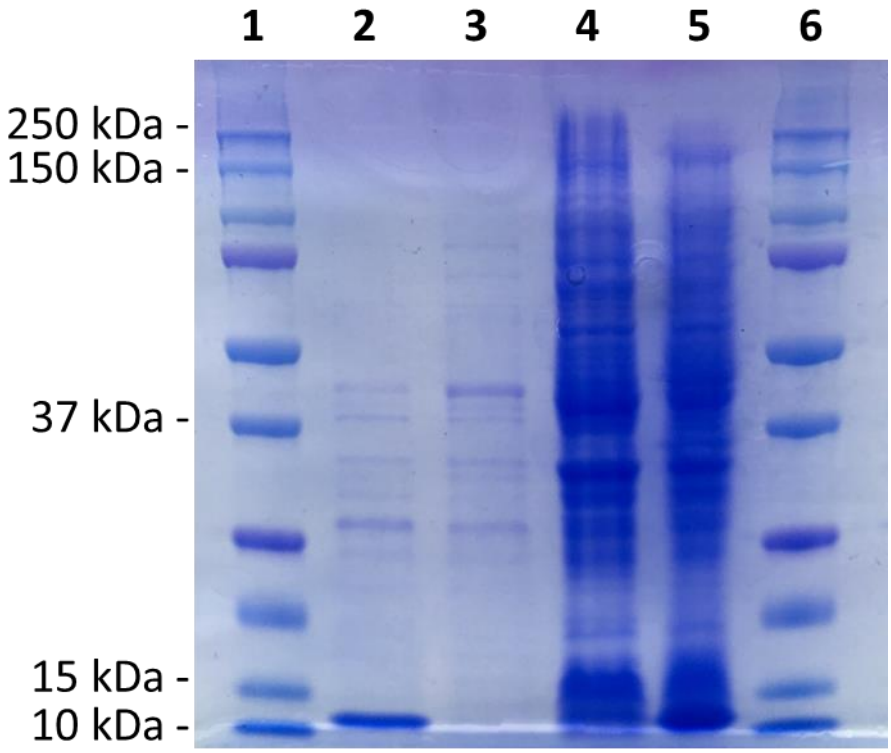

Figure 2.4. SDS-PAGE analysis of supernatant and cell debris from transformed *E. coli* liquid cultures.

SDS-PAGE was used to analyse samples of supernatant and cell debris from liquid cultures of *E. coli* containing the pET11b vector. Isopropyl β- d-1-thiogalactopyranoside (IPTG) was used as an inducer of rMIF expression. Lane 1 and lane 6 contain precision plus protein dual colour standard, lane 1 contains induced supernatant, lane 2 contains uninduced supernatant, lane 3 contains uninduced cell debris and lane 4 contains induced cell debris.

2.6.7 Purification of rMIF – Anion exchange & Gel filtration chromatography

The protein samples was loaded onto a pre-equilibrated HiPrep™ Q Fast Flow 16/10 anion exchange column which was eluted with TBS (**Table 2.19**). Recombinant MIF is eluted with the flow through fractions as it does not stick to the column, so the flow through fractions collected straight away in 5 ml volumes. The flow through fraction was then concentrated using a 10,000 molecular weight cut off filter before being added to a HiLoad 16/600 superdex 200pg gel filtration column and eluted with Tris-buffered saline in numerous fractions. The purity of the fractions was verified using SDS-PAGE as described in S*ection 2.6.6*. **Figure 2.5** shows the SDS-PAGE analysis of the fractions eluted from the gel filtration column. Larger proteins, up to approximately 37 kDa, are eluted from the column early and are shown in lanes 2-5. In the later fractions, lanes 6 to 9, a high concentration of smaller protein is eluted, most notably in the 10-15 kDa region which corresponded to the size of MIF monomers. The fractions corresponding to lanes 6 to 9 were then pooled before being concentrated to 15 mg/ml and stored in TBS buffer at -80 °C.

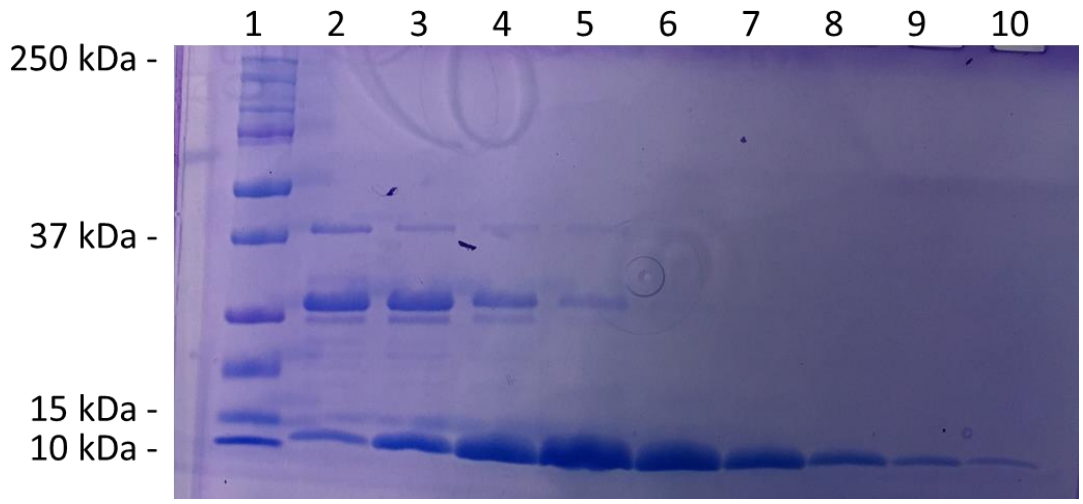

Figure 2.5. SDS-PAGE analysis of fractions following gel filtration chromatography.

Following gel filtration chromatography, a number of sample fractions were analysed using SDS-PAGE to identify pure fractions. Fractionation following gel filtration chromatography. Lane 1 contains precision plus protein dual colour standard, while lanes 2-10 contain individual sample fractions.

2.6.8 Endotoxin removal

As the recombinant protein has been expressed using a gram-negative bacteria, it was necessary to remove any residual LPS which may be contaminating the recombinant MIF stock. LPS removal was achieved by passing the protein through a Pierce™ high capacity endotoxin removal spin column. First the spin column was equilibrated by loading it with 0.2N NaOH (**Table 2.20**) and placing it on a rotator overnight at room temperature. The column was then centrifuged at 500 g for 1 minute at 4 °C and the flow through discarded. 2M NaCl (**Table 2.20**) was then flushed through the column three times by centrifuging at 500 g for 1 minute at 4 °C, and the waste discarded. The column was then flushed with endotoxin free water. Endotoxin free buffer (**Table 2.20**) was then flushed through the column three times by centrifuging at 500 g for 1 minute at 4 °C, and the waste discarded. The sample was then added to the column which was placed on a rotator overnight at 4 °C. The sample was retrieved by centrifuging at 500 g for 1 minute at 4 °C. LPS contamination levels were assessed using a limulus amebocyte lysate (LAL) assay.

0.2 N NaOH	
NaOH	8 g
Make to 1 L with endotoxin free water	

2 M NaCl	
NaCl	116.88 g
Make to 1 L with endotoxin free water	

Endotoxin free buffer	
NaCl	5.84 g
Make to 1 L with Tris-HCl buffer, pH 7	

Table 2.20. Buffers for endotoxin removal from recombinant protein.

2.6.9 Limulus amebocyte lysate (LAL) Assay

An LAL assay was carried out as per the kit instructions. A standard curve was prepared by diluting the standard provided in the kit. 50 µl of standard or sample was added to the wells of a 96 well plate. 50 µl of LAL solution was added to the wells before incubating at room temperature for 10 minutes. 100 µl of substrate solution was added

to the wells and incubated for 6 minutes at 37 °C. 50 µl of stop solution was added and the absorbance read at 405 nm.

LPS levels were measured at 0.66 EU/ml of endotoxin in samples before endotoxin removal and 0.06 EU/ml post endotoxin removal (**Figure 2.6A**). The US Food and Drug Administration state that a level of up to 0.5 EU/ml is permissible in sterile water for human consumption. One EU is equivalent to approximately 100 picograms of *E. coli* LPS. The MIF stock was prepared at 10 mg/ml prior to LAL assay analysis, in which there was 0.06 EU/ml of LPS. For future experiments, the highest concentration of recombinant MIF used is 100 ng/ml. This is a 100,000-fold dilution meaning a negligible level of LPS would be present in these experiments.

2.6.10 Tautomerase assay

Briefly, L-dopachrome methyl ester was prepared with 500 µl of 40 mM L-3,4-dihydroxyphenylalanine methyl ester and 500 µl of 80 mM sodium periodate in 4 ml of dH_2O. The solution was placed at room temperature for 5 minutes before being placed on ice in the dark. MIF was added at a final concentration of 100 ng/ml. Absorbance was measured using a spectrophotometer at 475 nm every 23 seconds for 10 minutes. The recombinant protein was found to be enzymatically active (**Figure 2.6B, C**).

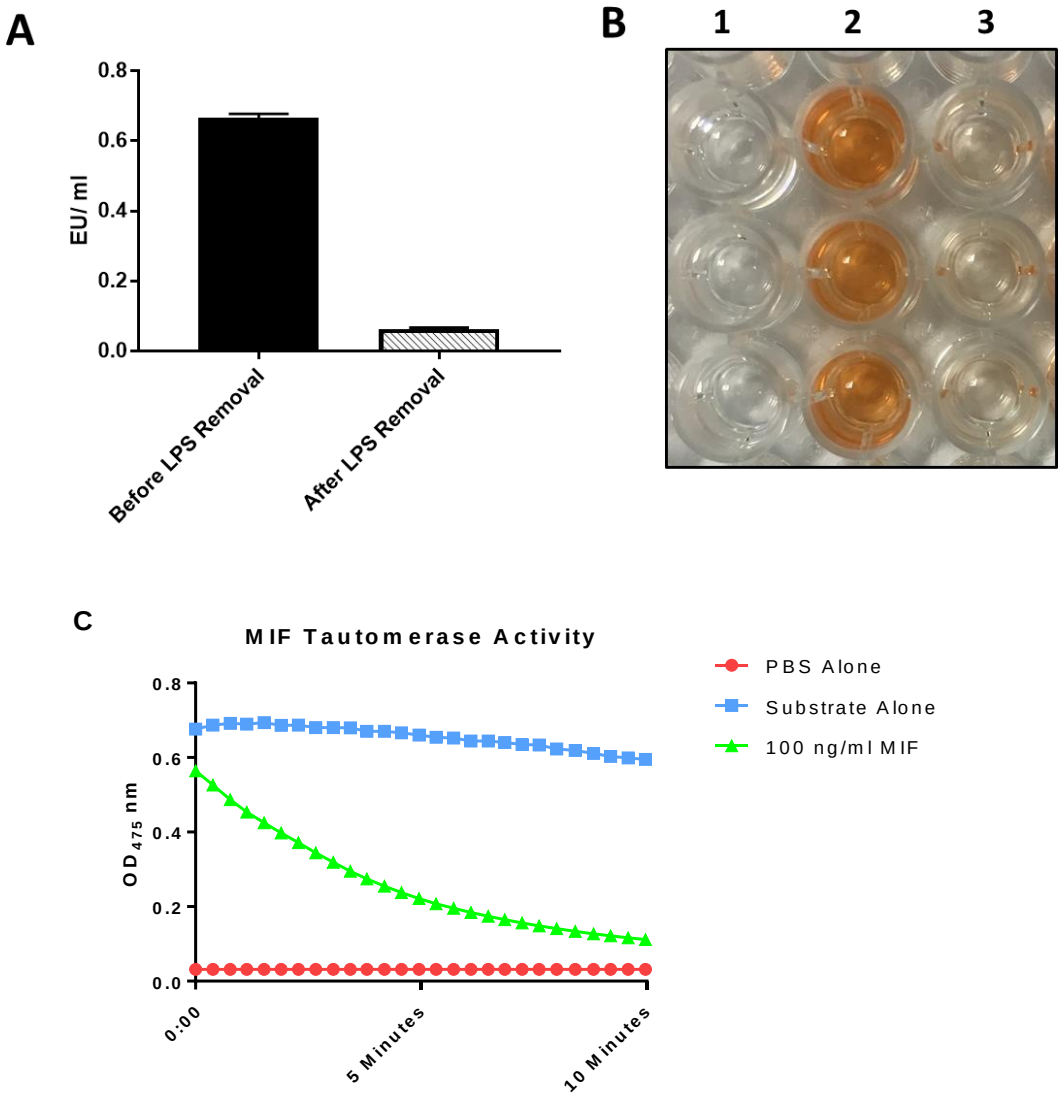

Figure 2.6. Characterisation of purified recombinant MIF.

Purified recombinant MIF has acceptably low levels of LPS contamination and exerts tautomerase activity against its substrate L-dopachrome. (**A**) Purified recombinant MIF has low levels of LPS contamination following purification, with decreased LPS levels observed upon filtration through a Pierce™ high capacity endotoxin removal spin column. Limulus amebocyte lysate assay was used to quantify LPS levels. (**B**) Lane 1 contains PBS alone, lane 2 contains 2.4 mM L-dopachrome methyl ester while lane 3 contains 100 ng/ml recombinant MIF + 2.4 mM L-dopachrome methyl ester. Tautomerase activity is evident through the colour change from orange to colourless. (**C**) PBS alone (red), 2.4 mM L-dopachrome methyl ester alone (blue), 100 ng/ml recombinant MIF + 2.4 mM L-dopachrome methyl ester (green). The kinetic tautomerase activity was measured using a spectrophotometer at 475nm every 20 seconds for 10 minutes. Figures are representative of 3 independent experiments with similar results.

2.7 Statistical analysis

All statistical analyses were carried out using GraphPad Instat Software (GraphPad Software Inc. CA, USA). For data sets with only two experimental groups with equal standard deviations, unpaired T tests were used to compare data sets. Statistical significance was recorded at $p<0.05$. One-way analysis of variance (ANOVA) was used to test for statistical significance between experimental groups of three or more where there is only one independent variable. Two-way ANOVA was used was used to test for statistical significance (two tailed analysis) between experimental groups of three or more where there are two independent variables. Multiple comparisons between groups were then assessed using the Tukey-Kramer *post-hoc* test (for parametric analysis) or Dunn's *post-hoc* test (for non-parametric analysis).

Chapter 3 - Investigation of the effects of SCD-19 on macrophage responses to *Pseudomonas aeruginosa* related stimuli and *P. aeruginosa* biofilm formation on airway epithelial cells.

3.1 Introduction

MIF is a proinflammatory cytokine that has been shown to drive of a number of inflammatory diseases including cystic fibrosis (CF), asthma, rheumatoid arthritis and acute respiratory distress syndrome (ARDS) (111, 114, 115, 390). MIF has also been implicated in the pathogenesis of several viral and bacterial infections including Dengue virus, *P. aeruginosa* and *Streptococcus pneumoniae* (111, 113, 150, 198, 199, 273, 391). Notably, $MIF^{-/-}$ mice exhibit enhanced clearance of intratracheally instilled *P. aeruginosa* and have significantly enhanced survival in an LPS-induced endotoxic shock model, while neutralising MIF antibodies protect from septic shock in a cecal ligation and puncture mouse model (198, 392). MIF exerts its pro-inflammatory effects through a variety of mechanisms including activation of the MAPK pathway, NF-κB activation, increasing TLR4 expression and overriding the anti-inflammatory effects of glucocorticoids, all of which promote pro-inflammatory cytokine expression (161, 167, 170-172, 176, 177).

The Donnelly Lab have developed SCD-19 which is a small molecular weight inhibitor which targets the active site of MIF (112, 113). SCD-19 has been shown to inhibit LPS-induced TNF-α production, which is regulated by MIF via upregulation of TLR4 expression (112, 124, 182, 393). SCD-19 was also shown to inhibit MIF-induced cancer cell proliferation and tumour development *in vivo* (112). As previously mentioned, MIF has been shown to play a role in the pathogenesis of *P. aeruginosa* infection in numerous *in vitro*, *in vivo* and patient centred studies (110, 111, 113, 150, 198). The Donnelly Lab have demonstrated that MIF tautomerase activity promotes inflammatory damage in a model of chronic respiratory *P. aeruginosa* infection (111). Most recently, we reported that MIF promotes *P. aeruginosa* antibiotic resistance and biofilm formation (113). Furthermore, we demonstrated that SCD-19 represents a valid therapeutic agent in a murine model of chronic respiratory *P. aeruginosa* infection (113).

In this chapter, we aimed to investigate the inflammatory responses of macrophages to two *P. aeruginosa* related antigens, heat killed *P. aeruginosa* (HKPA) and planktonic *P. aeruginosa* filtrate (PPF). Furthermore, we aimed to examine the effects of targeting the MIF tautomerase active site with the novel MIF inhibitor, SCD-

19, in the context of the inflammatory response to HKPA and PPF. The Donnelly Lab have previously developed and characterised poly(lactic-co-glycolic acid) (PLGA) nanoparticles which contain the MIF inhibitor SCD-19 (394). Here, we examined the efficacy of SCD-19 loaded PLGA nanoparticles to inhibit HKPA and PPF-induced pro-inflammatory cytokine production.

In CF, *P. aeruginosa* biofilm formation confers antibiotic resistance and the development of chronic infection which results in inflammatory lung damage (233, 265). Biofilm formation is a cyclical process which begins with the attachment of planktonic bacteria to a surface which, in the context of CF, is the underlying lung epithelium. Numerous studies have demonstrated *P. aeruginosa* attachment and biofilm formation on airway epithelial cells (207, 278, 395, 396). As a result, we hypothesised that MIF promotes *P. aeruginosa* attachment of epithelial cell monolayers. In this chapter, we aimed to investigate the effect of MIF on *P. aeruginosa* attachment of epithelial cell monolayers. We also examined the effect of SCD-19 on bacterial attachment to epithelial cells. Furthermore, we investigated the effect of SCD-19 loaded PLGA nanoparticles on *P. aeruginosa* attachment to airway epithelial cells.

The MIF CATT repeat polymorphism, at position -794 in the promoter region of the MIF gene, has been implicated in a wide range of inflammatory diseases. The Donnelly Lab has previously published studies examining the role of MIF and the CATT repeat polymorphism in ARDS, asthma, breast cancer, CF, and rheumatoid arthritis (110-115, 125, 390, 397). *In vivo*, the number of CATT repeats correlates with MIF expression levels, with higher numbers of repeats (> 5) conferring higher expression levels (111, 114). At present, there remains no effective murine model to investigate the effects of the MIF CATT repeat in infection and disease *in vivo*. In order to address this, we report for the first time, the generation of a humanised mouse model which involves the replacement of the murine *Mif* gene with the human *Mif* gene. Moreover, two distinct genotypes were developed – mice that contain 5-CATT repeats in the MIF promoter region, and mice that contain 7-CATT repeats in the MIF promoter region. We hypothesised that BMDMs generated from 7-CATT mice will have a more potent inflammatory cytokine response to stimuli than 5-CATT mice. In this chapter, we

characterised the cytokine response of 5-CATT and 7-CATT BMDMs to LPS and poly(I:C) stimulation *in vitro*.

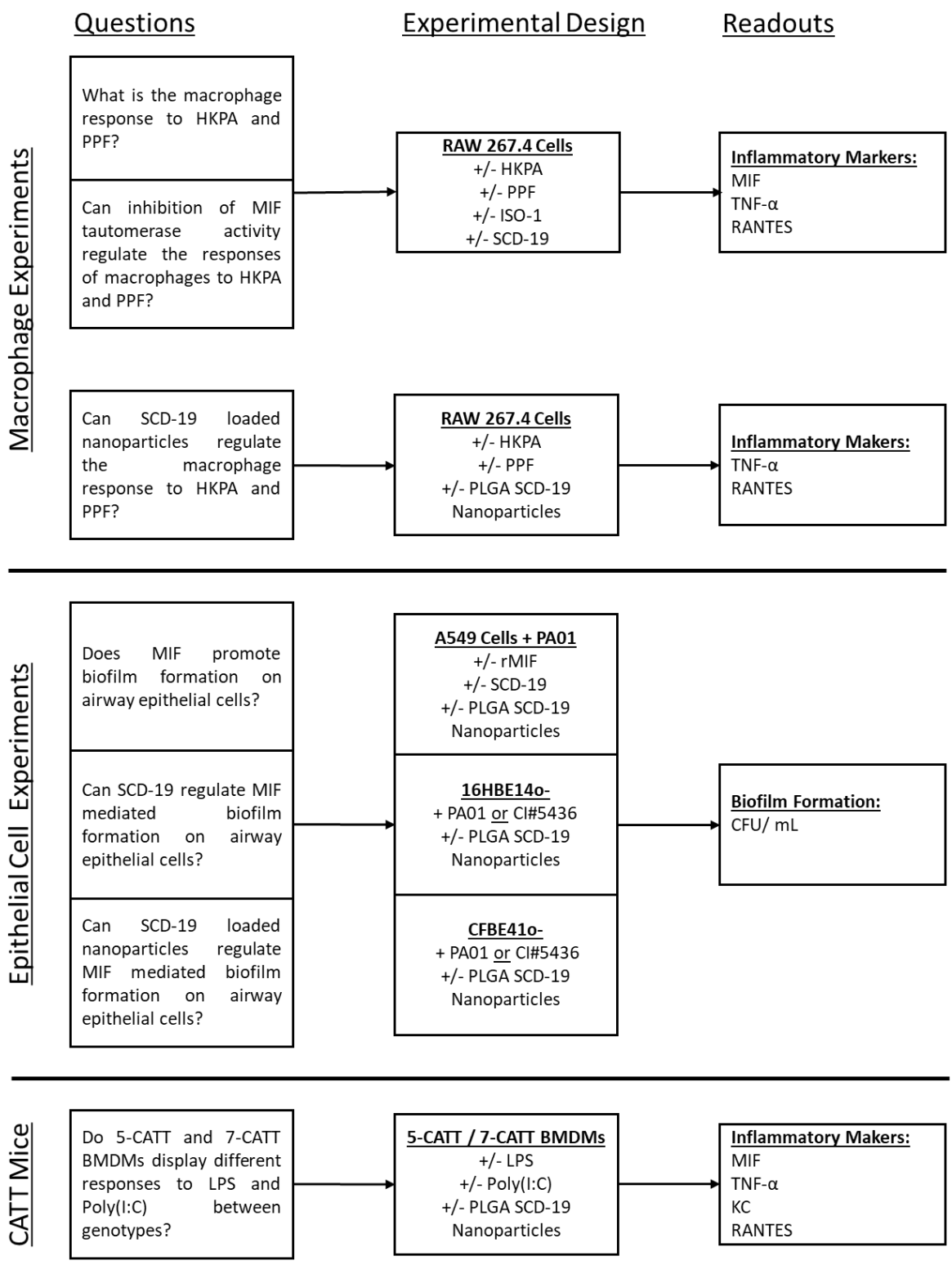

Figure 3.1. Overview of the experimental design for Chapter 3.

3.2 Regulation of heat killed *P. aeruginosa* (HKPA) mediated MIF, TNF-α and RANTES production by SCD-19, ISO-1 and SCD-19 nanoparticles in RAW 264.7 cells.

Here, we investigated the cytokine response of RAW 264.7 macrophages to HKPA stimulation, a TLR2 and TLR5 agonist. As MIF has been shown to be required for optimal TNF-α release, TNF-α was used as a readout for NF-κB activation (198, 398). MIF has been shown to modulate RANTES production through activation of CD74 and subsequent c-Jun N-terminal kinase activation (399). RANTES is a chemokine that plays a key role in pathogen clearance through the recruitment of immune cells to the site of infection (284). RANTES production is induced following activation of numerous transcription factors including both NF-κB and IRF3 activation (400). High levels of RANTES has also been associated with inflammatory disorders including rheumatoid arthritis and asthma, through the promotion of leukocyte recruitment (401).

3.2.1 HKPA stimulates TNF-α and RANTES protein production in RAW 264.7 cells.

MIF, TNF-α and RANTES protein levels were analysed by ELISA at 6 and 24 hours following stimulation with a gradient of HKPA (MOI 1, 10, 100). High levels of basal MIF expression were observed at each time point (**Figure 3.2A**). Stimulation with a HKPA gradient induced MIF expression at 6 hours, but not at 24 hours. Stimulation with a HKPA gradient resulted in a dose-dependent increase in TNF-α protein at 6 and 24 hours, with a notable increase in TNF-α protein production at 24 hours (**Figure 3.2B**). Similarly, stimulation with a HKPA gradient resulted in a dose-dependent increase in RANTES protein at 6 and 24 hours, with a notable increase in RANTES protein production at 24 hours (**Figure 3.2C**).

At 24 hours, HKPA (MOI 1, 10, 100) did not induce MIF protein production (**Figure 3.3A)**. Stimulation with HKPA at an MOI of 10 significantly increased TNF-α protein (** $p< 0.01$**, Figure 3.3B**), as did stimulation with HKPA at an MOI of 100 (*** $p< 0.001$**, Figure 3.3B)** compared with medium cells. RANTES protein production was

also significantly increased following 24 hour simulation with HKPA at an MOI of 10 (*** p< 0.001, **Figure 3.3C**) and MOI of 100 (*** p< 0.001, **Figure 3.3C**) compared with medium.

3.2.2 SCD-19, but not ISO-1, modulates TNF-α and RANTES protein production in in HKPA stimulated RAW 264.7 cells.

As we have established that effects of HKPA on the production of MIF, TNF-α and RANTES production, we next examined the effects of small molecular weight inhibitors of MIFs tautomerase activity on HKPA induced cytokine production. ISO-1 is a commercially available MIF inhibitor that has been shown to inhibit the pro-inflammatory activity of MIF and enhance survival in a murine model of sepsis (141). SCD-19 is a novel small molecular weight inhibitor of MIFs tautomerase activity (112). Previously, we described the inhibition of LPS driven cytokine release and inflammation by SCD-19 (112). Furthermore, SCD-19 has been shown limit inflammatory damage in a model of chronic respiratory *P. aeruginosa* infection (113). Here, we investigated the ability of SCD-19 and ISO-1 to inhibit HKPA mediated MIF, TNF-α and RANTES protein production in RAW 264.7 cells.

MIF, TNF-α and RANTES protein levels were analysed by ELISA at 6 and 24 hours following stimulation with a HKPA (MOI 100) and treatment with SCD-19 (100 μM). High levels of basal MIF expression were observed at each time point (**Figure 3.4A**). Stimulation with a HKPA increased MIF protein production at 6 hours only, while with SCD-19 gradient had no effect on HKPA mediated MIF protein production at any time point. Treatment with SCD-19 induced MIF expression at 6 hours and 24 hours compared with untreated cells. Stimulation with HKPA resulted in increased TNF-α protein production at 6 and 24 hours compared with medium alone, which was attenuated with SCD-19 treatment (**Figure 3.4B**). Similarly, stimulation with HKPA resulted in increased RANTES protein production at 6 and 24 hours compared with medium alone, which was attenuated with SCD-19 treatment (**Figure 3.4C**).

MIF, TNF-α and RANTES protein levels were also analysed by ELISA at 6 and 24 hours following stimulation with a HKPA (MOI 100) and treatment with ISO-1 (100 μM). ISO-1 treatment resulted in decreased expression of MIF protein in unstimulated cells at all timepoints examined (**Figure 3.5A**). Furthermore, ISO-1 inhibited MIF expression in HKPA stimulated cells to levels lower than that observed in unstimulated cells. ISO-1 failed to attenuate the induction of HKPA mediated TNF-α protein across all time points (**Figure 3.5B**), while HKPA mediated RANTES protein production levels also remained unchanged with ISO-1 treatment (**Figure 3.5C**).

At 24 hours, we demonstrated that treatment with SCD-19 significantly inhibits HKPA mediated TNF-α protein production compared with HKPA stimulation alone (** p< 0.01**, Figure 3.6A**), while ISO-1 fails to modulate HKPA induced TNF-α protein (**Figure 3.6B**). We also demonstrated that at 24 hours, SCD-19 treatment significantly inhibits HKPA mediated RANTES protein production compared with HKPA stimulation alone (*** p< 0.001**, Figure 3.6C**), while ISO-1 fails to modulate HKPA induced RANTES protein (**Figure 3.6D**).

3.2.3 Nebulised PLGA-SCD-19 nanoparticles modulate HKPA mediated TNF-α and RANTES protein production.

SCD-19 is a nonpolar compound and as such, must be dissolved in a solvent such as dimethyl sulfoxide (DMSO). While this is routinely used for *in vitro* experiments, there are a number of caveats associated with the use of DMSO as a vehicle. Nanoparticles represent a modern mode of drug delivery with numerous benefits including improved drug solubility, improved bioavailability and high biocompatibility (47). Inhalation therapy is associated with increased pulmonary drug delivery, with numerous clinical trials under way examining the effects of inhaled nanoparticles in a myriad of diseases (47, 402).

The Donnelly Lab has developed and characterised the size, charge, drug release profile, toxicity and cellular uptake of aerosolised PLGA nanoparticles containing SCD-19 (394). These nebulised nanoparticles provide drug delivery to cells with high cellular

uptake and limited cellular toxicity. Here, we examined the ability of SCD-19 loaded PLGA nanoparticles to inhibit HKPA mediated TNF-α and RANTES protein production (**Figure 3.7**). In order to allow time for drug release from the PLGA, nanoparticles cells were pre-treated with a concentration gradient of drug loaded nanoparticles (50, 100, 200 μM) for 24 hours, as per the drug release profiles of these nanoparticles (394). Treatment with PLGA nanoparticles or SCD-19 loaded PLGA nanoparticles had no impact on basal TNF-α (**Figure 3.7A**) or RANTES (**Figure 3.7B**) levels. Treatment of cells with SCD-19 loaded PLGA nanoparticles significantly inhibited HKPA (MOI 100) mediated TNF-α release compared with cells treated with empty PLGA nanoparticles and HKPA (**Figure 3.7C**). Furthermore, treatment of cells with SCD-19 loaded PLGA nanoparticles significantly inhibited HKPA mediated RANTES release compared with cells treated with empty PLGA nanoparticles and HKPA (**Figure 3.7D**).

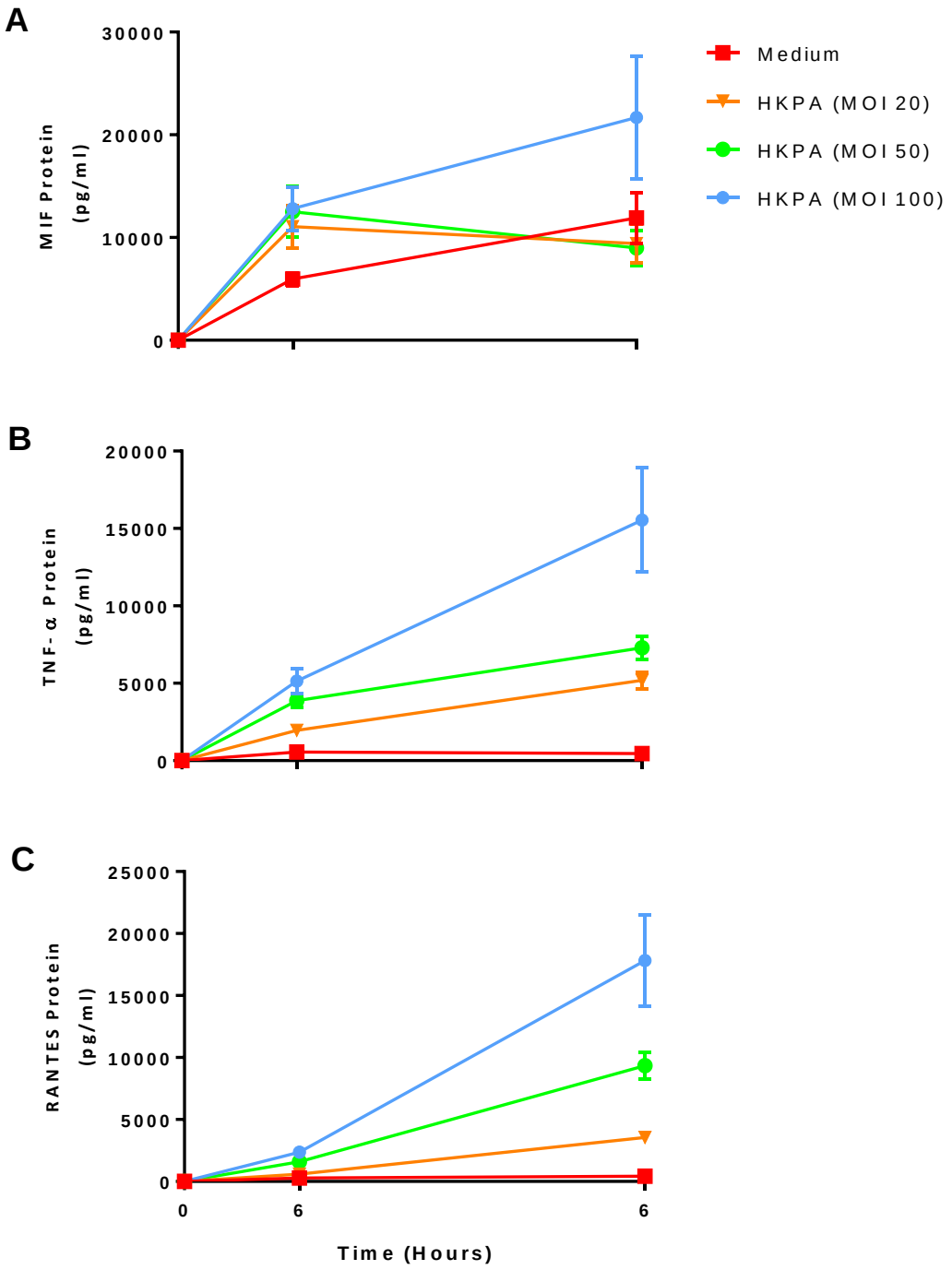

Figure 3.2. Time-course of MIF, TNF-α and RANTES protein production by RAW 264.7 macrophages following HKPA stimulation.

Levels of (**A**) MIF, (**B**) TNF-α and (**C**) RANTES from RAW 264.7 macrophages were assessed at 6 and 24 hours. Protein production was quantified by ELISA. Data is presented as mean ± SEM of 3 independent experiments with 3 technical replicates. [Medium (red), HKPA MOI 20 (orange), HKPA MOI 50 (green) and HKPA MOI 100 (blue)].

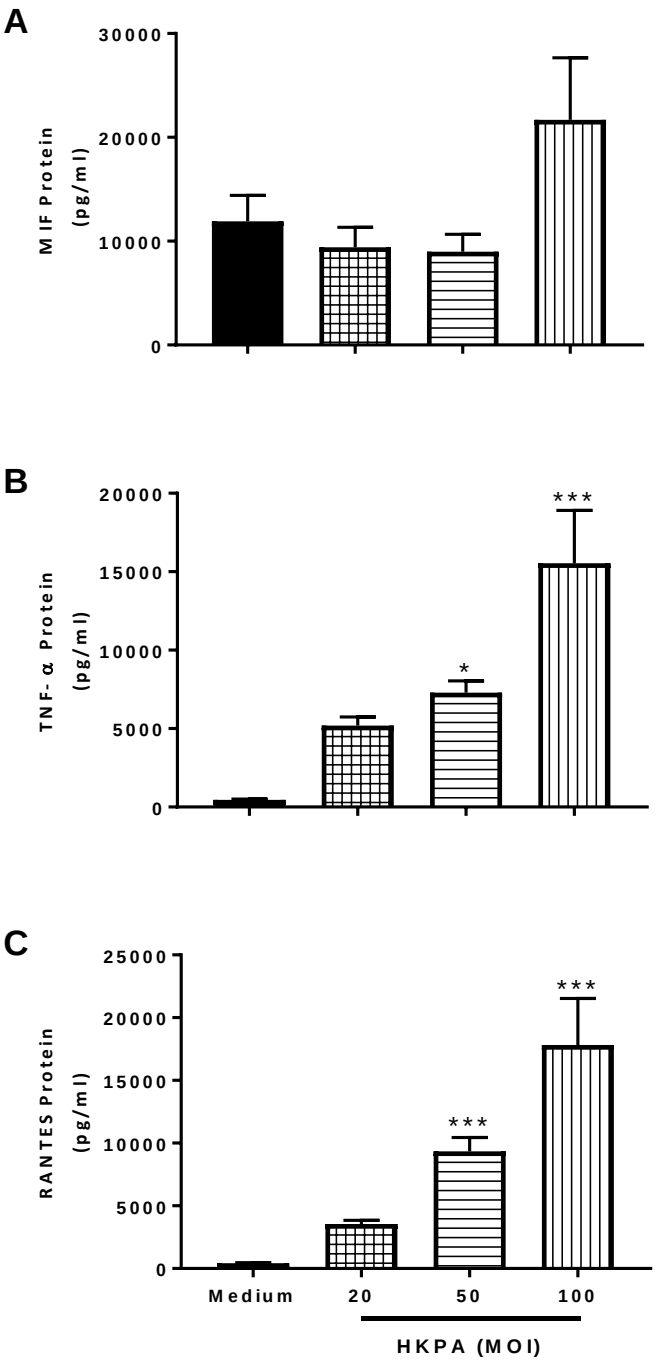

Figure 3.3. HKPA stimulates MIF, TNF-α and RANTES protein production in RAW 264.7 cells at 24 hours.

RAW 264.7 murine macrophages were stimulated with HKPA at MOI 20, 50 and 100 for 24 hours. HKPA stimulates (**A**) MIF, (**B**) TNF-α and (**C**) RANTES protein production. Protein production was measured by ELISA. Data is presented as mean ± SEM of 3 independent experiments with 3 technical replicates. (A) A Kruskal-Wallis Test with a Dunn's multiple comparison post-hoc test was used to test for statistical differences. (**B, C**) A One-way ANOVA with a Tukey's multiple comparison post-hoc test was used to test for statistical differences. *p<0.05, **p<0.01, ***p<0.001; respective treatment compared with medium.

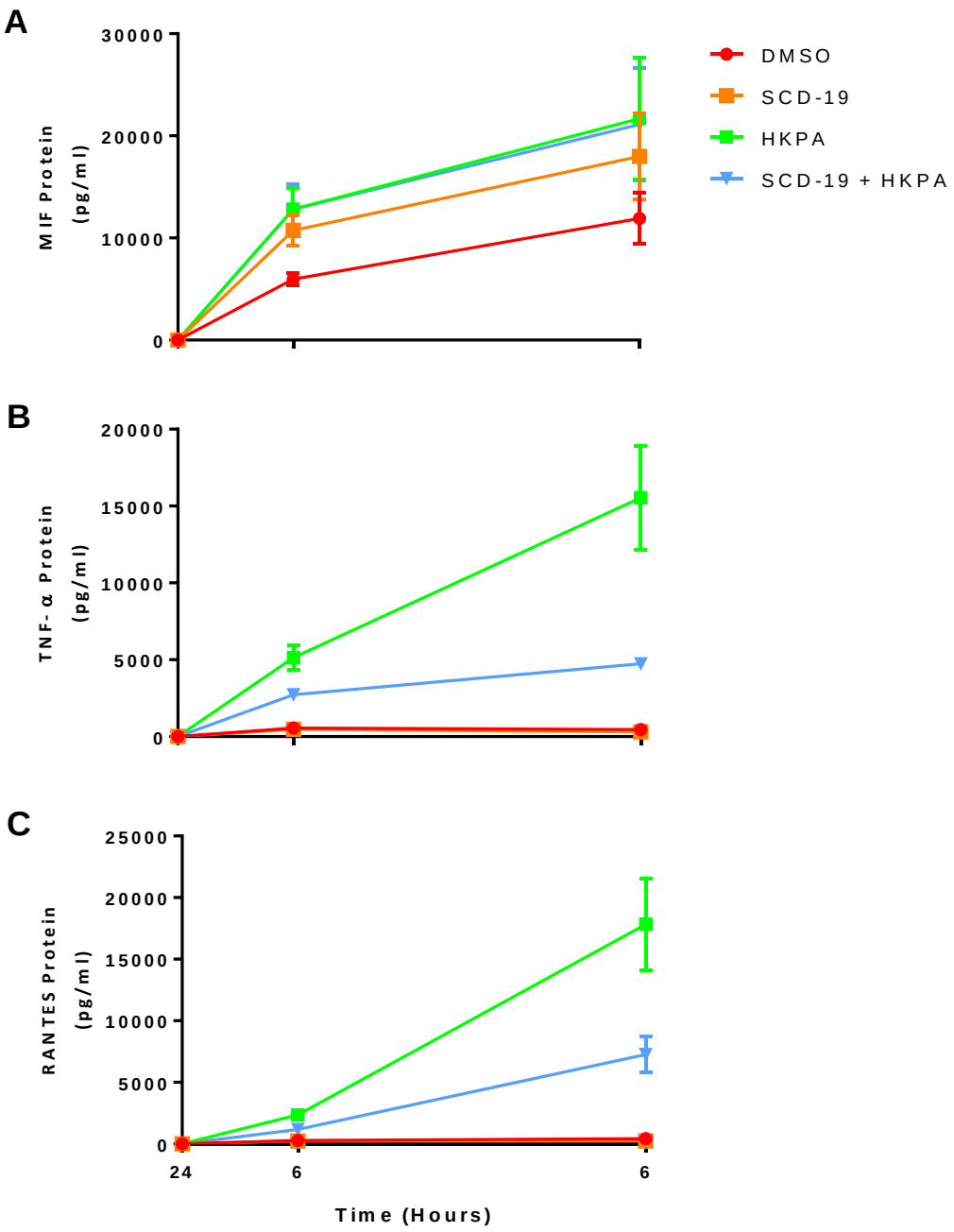

Figure 3.4. Time-course of MIF, TNF-α and RANTES protein production by RAW 264.7 macrophages following HKPA and SCD-19 treatment.

Levels of (**A**) MIF, (**B**) TNF-α and (**C**) RANTES protein from RAW 264.7 macrophages were assessed at 6 and 24 hours. Protein production was quantified by ELISA. Data is presented as mean ± SEM of 3 independent experiments with 3 technical replicates. [DMSO (red), 100 µM SCD-19 (orange), HKPA (green) and SCD-19 + HKPA (blue)].

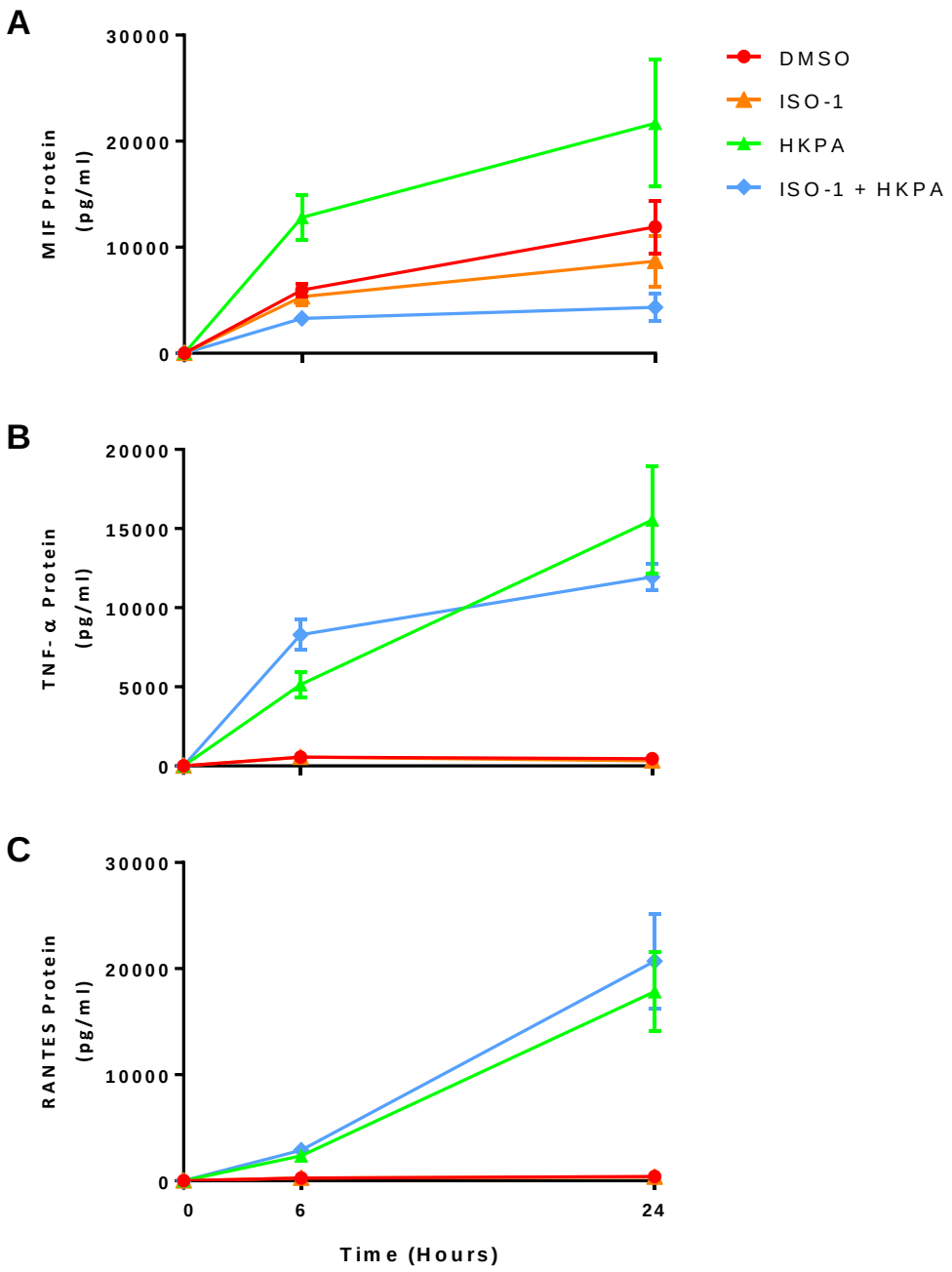

Figure 3.5. Time-course of MIF, TNF-α and RANTES protein production by RAW 264.7 macrophages following HKPA and ISO-1 treatment.

Levels of (**A**) MIF, (**B**) TNF-α and (**C**) RANTES protein from RAW 264.7 macrophages were assessed at 6 and 24 hours. Protein production was quantified by ELISA. Data is presented as mean ± SEM of 3 independent experiments with 3 technical replicates. [DMSO (red), 100 µM ISO-1 (orange), HKPA (green) and ISO-1 + HKPA (blue)].

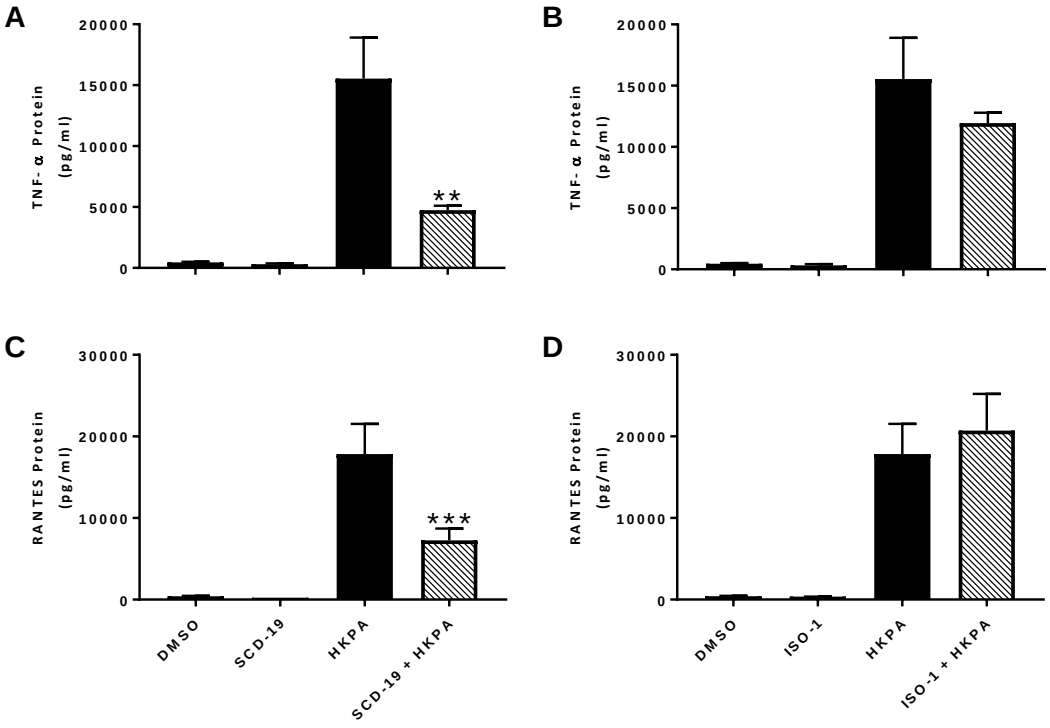

Figure 3.6. SCD-19, but not ISO-1, modulates TNF-α and RANTES protein production in response to HKPA stimulation at 24 hours.

RAW 264.7 murine macrophages were stimulated with HKPA at MOI 100 and treated with SCD-19 (100 µM) or ISO-1 (100 µM) for 24 hours. SCD-19 inhibits HKPA mediated (**A**) TNF-α and (**C**) RANTES protein production. ISO-1 does not modulate HKPA mediated (**B**) TNF-α or (**D**) RANTES protein production. Protein production was measured by ELISA. Data is presented as mean ± SEM of 3 independent experiments with 3 technical replicates. A One-way ANOVA with a Tukey's multiple comparison post-hoc test was used to test for statistical differences. **p<0.01, ***p<0.001; respective treatment compared with HKPA.

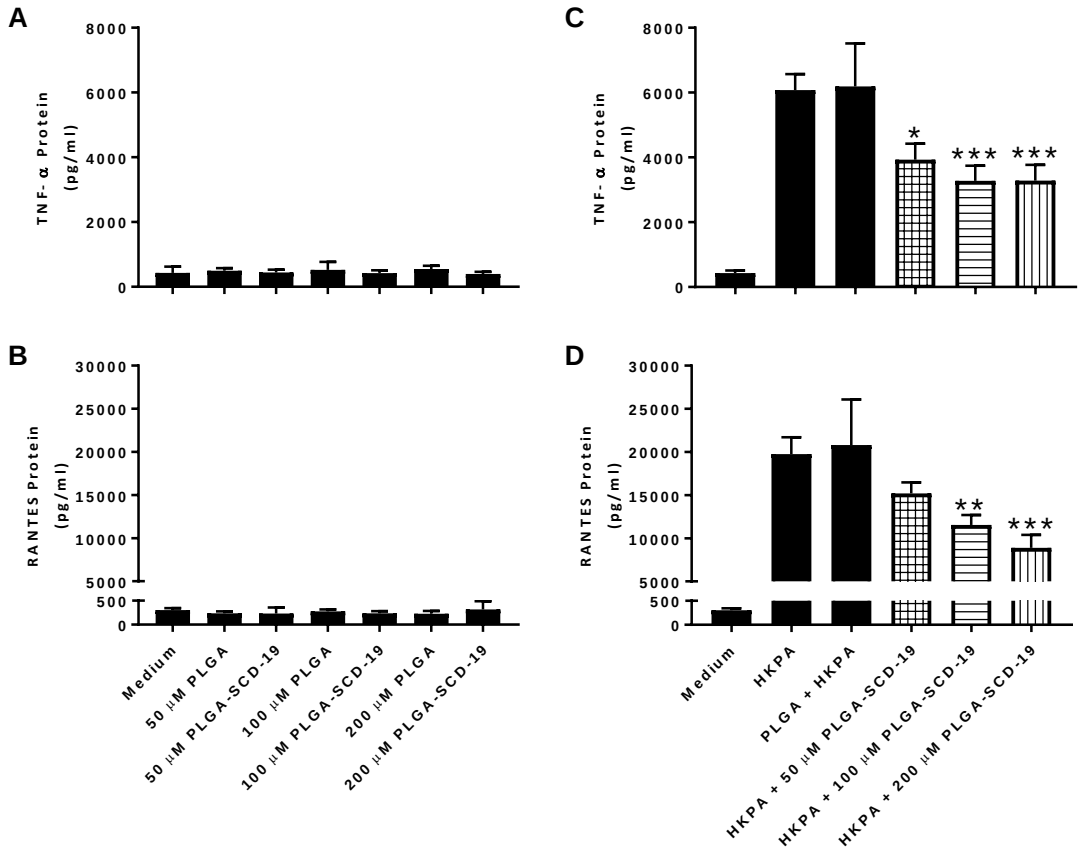

Figure 3.7. Nebulised PLGA-SCD-19 nanoparticles modulate the production of TNF-α and RANTES protein at 24 hours.

RAW 264.7 murine macrophages were pre-treated with a dose response (50, 100, 200 μM) of nebulised PLGA or PLGA-SCD-19 nanoparticles for 24 hours. Following this, cells were treated with fresh nanoparticles ± HKPA (MOI 100) for a further 24 hours. Treatment with PLGA or PLGA-SCD-19 nanoparticles alone did not impact (**A**) TNF-α or (**B**) RANTES protein levels. Nanopackaged SCD-19 inhibits HKPA mediated (**C**) TNF-α and (**D**) RANTES release. Protein production was measured by ELISA. Data is presented as mean ± SEM of 3 biological replicates with 3 technical replicates. (**C**) A One-way ANOVA with a Tukey's multiple comparison post-hoc test was used to test for statistical differences. (**D**) A Kruskal-Wallis Test with a Dunn's multiple comparison post-hoc test was used to test for statistical differences. *p<0.05, **p<0.01, ***p<0.001; respective treatment compared to PLGA + HKPA.

3.3 Regulation of planktonic *P. aeruginosa* filtrate (PPF) mediated MIF, TNF-α and RANTES production by SCD-19, ISO-1 and SCD-19 Nanoparticles in RAW 264.7 cells.

Planktonic *P. aeruginosa* filtrate (PPF) contains a variety of diffusible products including, but not limited to, LPS, quorum sensing molecules and bacterial DNA (388). As such, PPF represents a crude cocktail of *P. aeruginosa* secreted factors that activates a myriad of PRRs (388).

3.3.1 PPF promotes MIF, TNF-α and RANTES protein production in RAW 264.7 cells.

Here, we investigate the effect of a concentration gradient of PPF (2.5%, 5%, 10%) on MIF, TNF-α and RANTES protein production from RAW 264.7 macrophages (**Figure 3.8**) (388). MIF, TNF-α and RANTES protein levels were analysed by ELISA at 6 and 24 hours following stimulation PPF. High levels of constitutive MIF production were observed at each time point (**Figure 3.8A**). Stimulation with all concentrations of PPF increased MIF protein production at 6 hours only, while there was no difference in MIF protein levels on PPF stimulated cells at 3 or 24 hours compared with unstimulated cells. Stimulation with a PPF gradient resulted in a dose-dependent increase in TNF-α protein at 6 and 24 hours, with a notable increase in TNF-α protein production at 24 hours (**Figure 3.8B**). Similarly, stimulation with a PPF gradient resulted in a dose-dependent increase in RANTES protein at 6 and 24 hours, with a notable increase in RANTES protein production at 24 hours (**Figure 3.8C**).

At 24 hours, we demonstrate that PPF (2.5%, 5%, 10%) did not significantly induce MIF protein production (**Figure 3.9B**). Stimulation with 2.5% PPF for 24 hours significantly increased TNF-α release (** $p<0.01$, **Figure 3.9B**) compared with unstimulated cells; as did 5% PPF (*** $p<0.001$, **Figure 3.9B**) and 10% PPF (** $p<0.01$, **Figure 3.9B**). RANTES protein production was also significantly increased following 24 hour simulation with 5% PPF (* $p<0.05$, **Figure 3.9C**) and 10% PPF (* $p<0.05$, **Figure 3.9C**) compared with unstimulated cells.

3.3.2 SCD-19 and ISO-1 modulate PPF-induced TNF-α protein production in RAW 264.7 cells.

Having established the pattern of MIF, TNF-α and RANTES protein production in response to PPF, we subsequently examined the effects of SCD-19 and ISO-1 of PPF-induced cytokine production. As previously described, MIF drives the expression of both TNF-α and RANTES (198, 399). Here, we investigated the ability of SCD-19 and ISO-1 to inhibit PPF-induced MIF, TNF-α and RANTES protein production in RAW 264.7 cells. Furthermore, we examined the effects of SCD-19 loaded PLGA nanoparticles on the cytokine response to PPF stimulated RAW 264.7 cells.

MIF, TNF-α and RANTES protein levels were analysed by ELISA at 6 and 24 hours following stimulation with PPF (2.5%) and treatment with SCD-19 (100 μM) (**Figure 3.10**). Stimulation of cells with PPF did not induce MIF protein production at any time point (**Figure 3.10A**). Treatment with PPF and SCD-19 enhanced MIF protein production at 6 hours compared with PPF stimulated cells alone. SCD-19 treatment led to a striking decrease in PPF-induced TNF-α at both 6 and 24 hours compared with PPF treated cells (**Figure 3.10B**). SCD-19 also decreased RANTES protein production in PPF stimulated cells compared PPF stimulated cells alone at 6 and 24 hours (**Figure 3.10C**).

MIF, TNF-α and RANTES protein levels were also analysed by ELISA at 6 and 24 hours following stimulation with a PPF (2.5%) and treatment with ISO-1 (100 μM) (**Figure 3.11**). Although PPF did not induce MIF expression at any timepoint examined, cells stimulated with ISO-1 and PPF displayed less MIF protein production than both unstimulated and ISO-1 stimulated cells (**Figure 3.11A**). Furthermore, ISO-1 inhibited the increase in PPF-induced TNF-α protein production observed between 6 and 24 hours (**Figure 3.11B**), but did not impact upon PPF-induced RANTES release at any timepoint examined (**Figure 3.11C**).

At 24 hours, we demonstrated that treatment with SCD-19 significantly inhibited PPF-induced TNF-α protein production compared with PPF stimulation alone (** **p< 0.01, Figure 3.12A**). ISO-1 also significantly inhibited PPF-induced TNF-α protein production compared with PPF stimulation alone (* p< 0.05**, Figure 3.12B**). Both SCD-

19 and ISO-1 failed to significantly decrease PPF-induced RANTES release (**Figure 3.12C, D**).

3.3.3 Nebulised PLGA-SCD-19 nanoparticles modulate PPF-induced TNF-α protein production.

We also examined the ability of SCD-19 loaded PLGA nanoparticles to inhibit PPF-induced TNF-α and RANTES protein production (**Figure 3.13**). As before, cells were pre-treated for 24 hours with a concentration gradient of drug loaded nanoparticles (50, 100, 200 μM) to allow for drug release from the PLGA nanoparticles.

Treatment of cells with SCD-19 loaded PLGA nanoparticles significantly inhibited PPF (2.5%) mediated TNF-α release compared with cells treated with empty PLGA nanoparticles and PPF (* $p<0.05$, **Figure 3.13A**). Similarly, treatment of cells with SCD-19 loaded PLGA nanoparticles reduced PPF-induced RANTES release compared with cells treated with empty PLGA nanoparticles and PPF; however, this was not significant (**Figure 3.13B**).

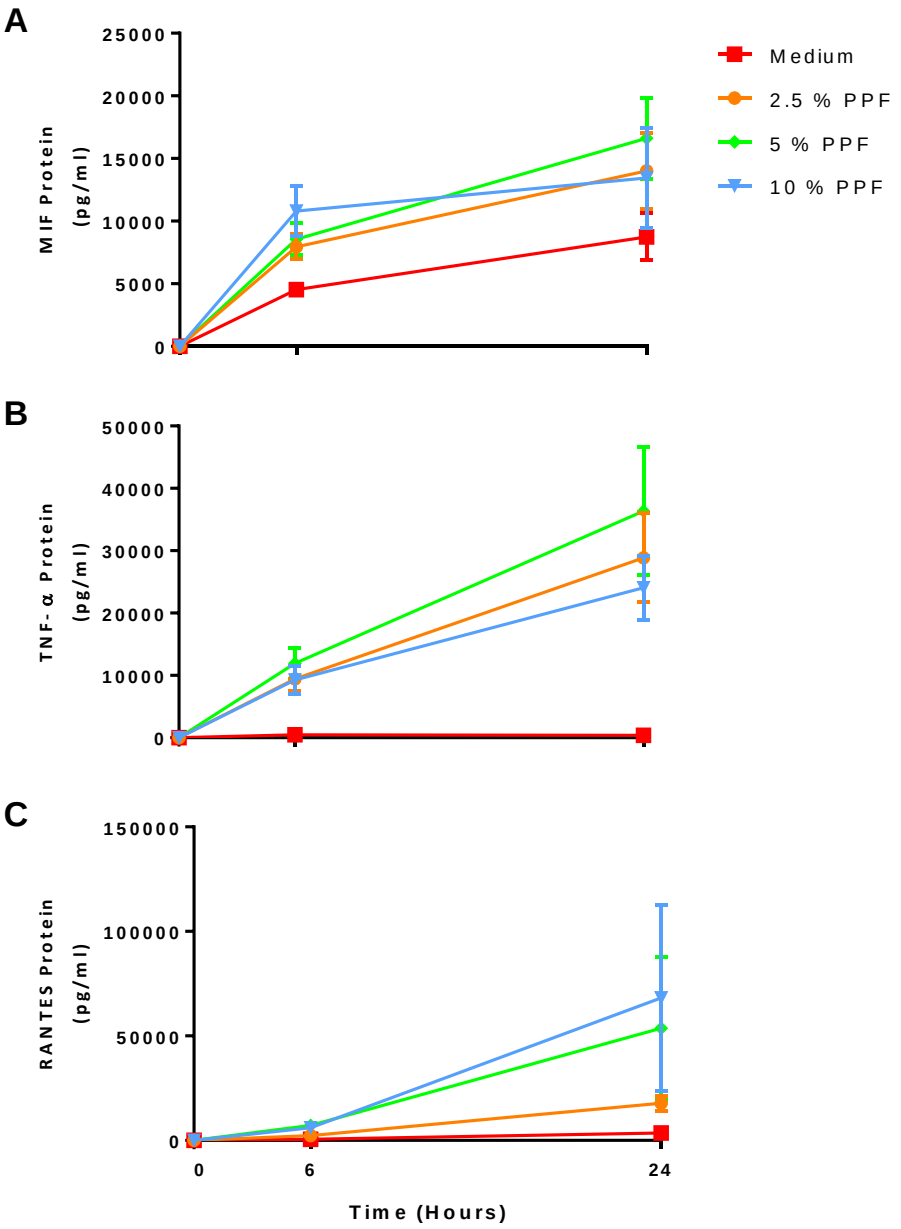

Figure 3.8. Time-course of MIF, TNF-α and RANTES production by RAW 264.7 macrophages following PPF stimulation.

Levels of (**A**) MIF, (**B**) TNF-α and (**C**) RANTES from RAW 264.7 macrophages were assessed at 6 and 24 hours. Protein production was quantified by ELISA. Data is presented as mean ± SEM of 3 independent experiments with 3 technical replicates. [Medium (red), 2.5% PPF (orange), 5% PPF (green) and 10% PPF (blue)].

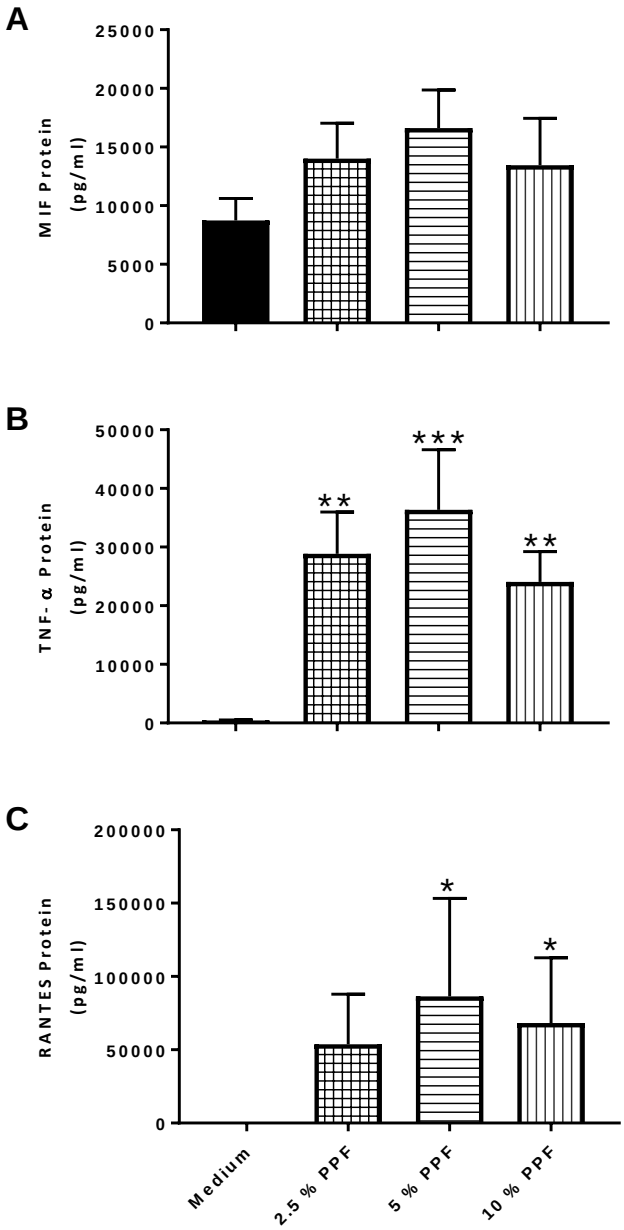

Figure 3.9. PPF stimulates TNF-α and RANTES protein production at 24 hours.

RAW 264.7 murine macrophages were stimulated with PPF (2.5%, 5%, 10%) for 24 hours. (**A**) PPF stimulates MIF protein production. PPF stimulates significant (**B**) TNF-α and (**C**) RANTES production at 24 hours. Protein production was measured by ELISA. Data is presented as mean ± SEM of 3 independent experiments with 3 technical replicates. (**B, C**) A Kruskal-Wallis Test with a Dunn's multiple comparison post-hoc test was used to test for statistical differences. *p<0.05, **p<0.01; respective treatments compared with medium.

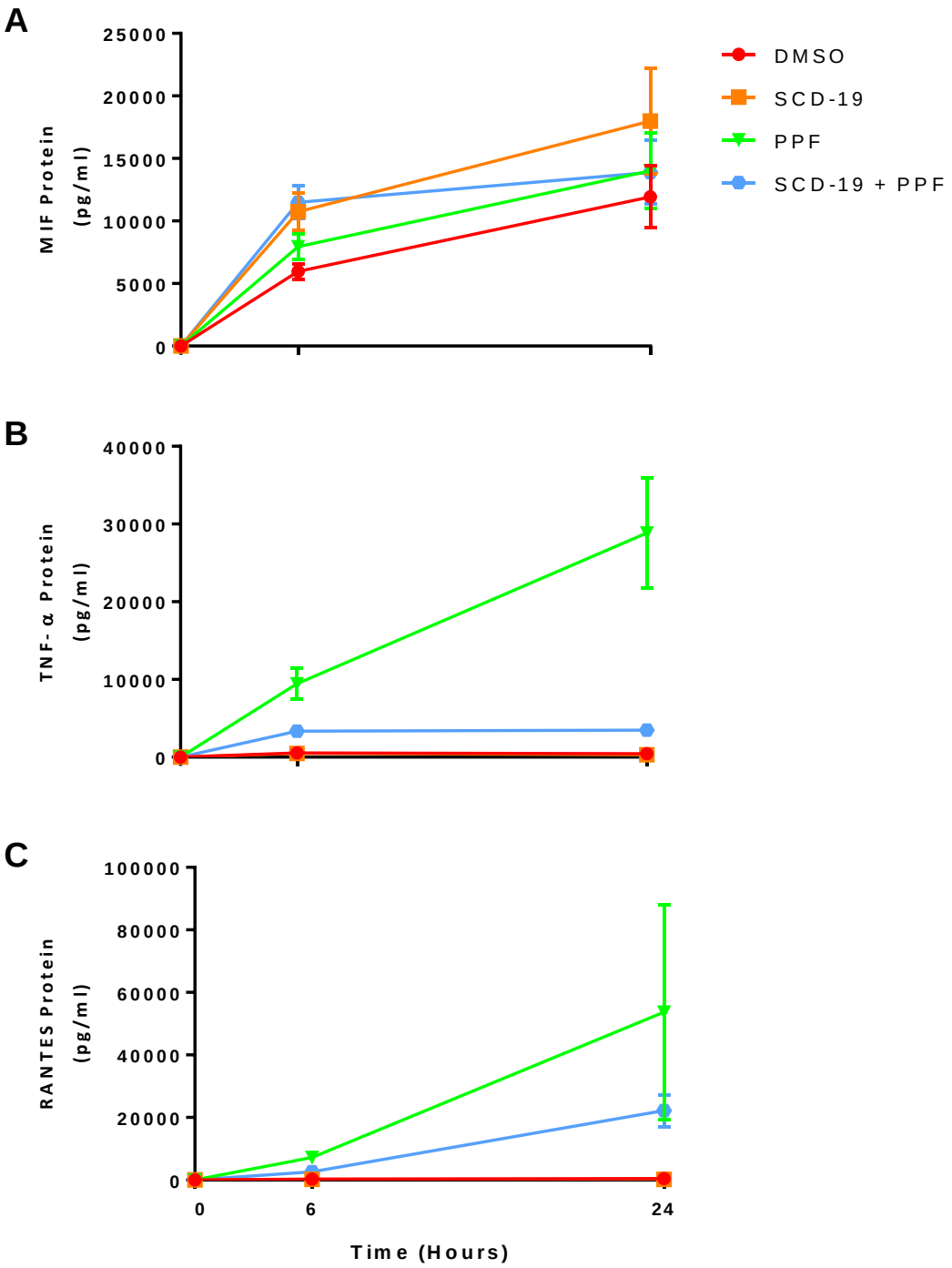

Figure 3.10. Time-course of MIF, TNF-α and RANTES protein production by RAW 264.7 macrophages following PPF and SCD-19 treatment.

Levels of (**A**) MIF, (**B**) TNF-α and (**C**) RANTES protein from RAW 264.7 macrophages were assessed at 6 and 24 hours. Protein production was quantified by ELISA. Data is presented as mean ± SEM of 3 independent experiments with 3 technical replicates. [DMSO (red), 100 µM SCD-19 (orange), 2.5% PPF (green) and SCD-19 + PPF (blue)].

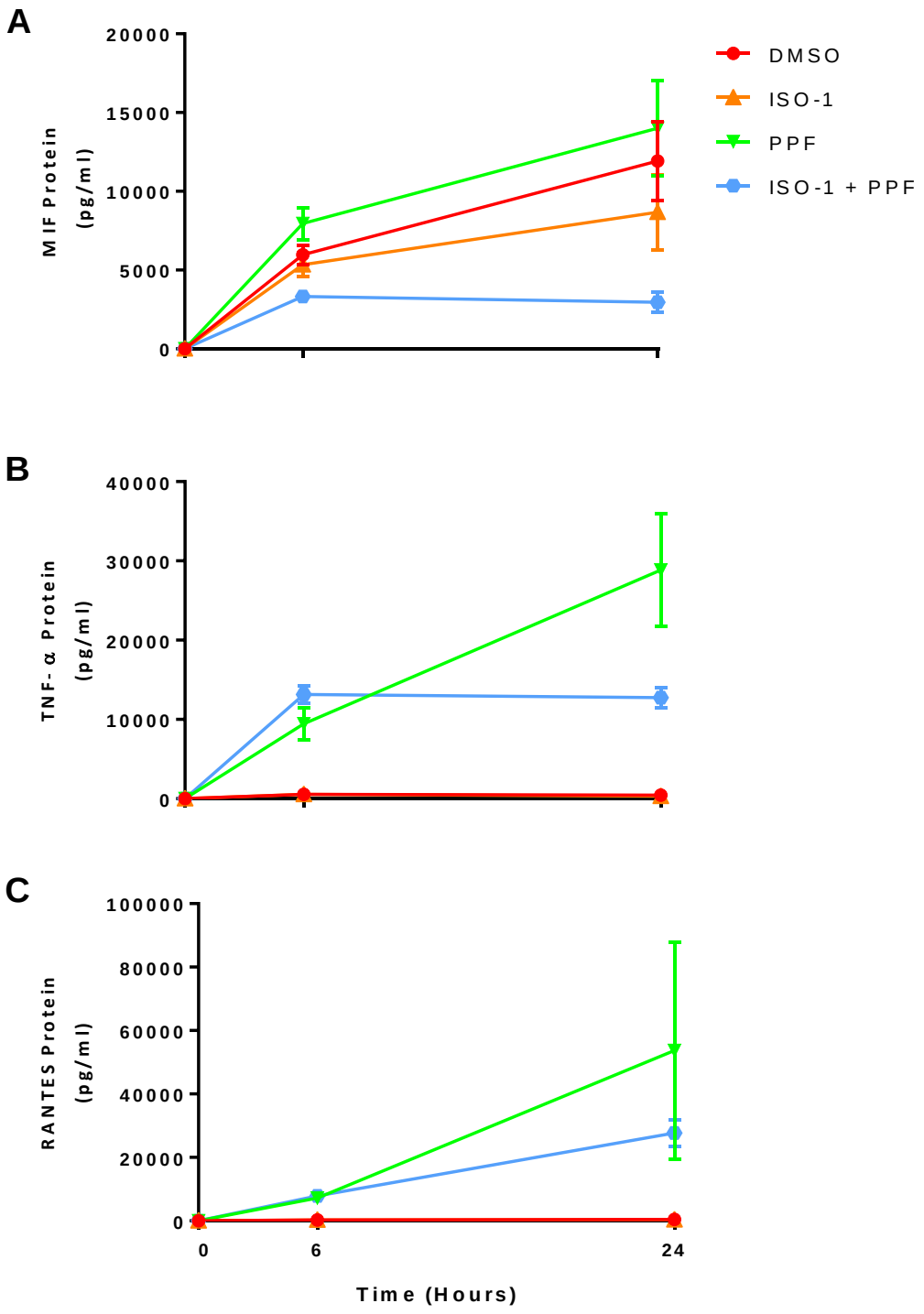

Figure 3.11. Time-course of MIF, TNF-α and RANTES production by RAW 264.7 macrophages following PPF and ISO-1 treatment.

Levels of (**A**) MIF, (**B**) TNF-α and (**C**) RANTES protein from RAW 264.7 macrophages were assessed at 6 and 24 hours. Protein production was quantified by ELISA. Data is presented as mean ± SEM of 3 independent experiments with 3 technical replicates. [DMSO (red), 100 µM ISO-1 (orange), 2.5% PPF (green) and ISO-1 + PPF (blue)].

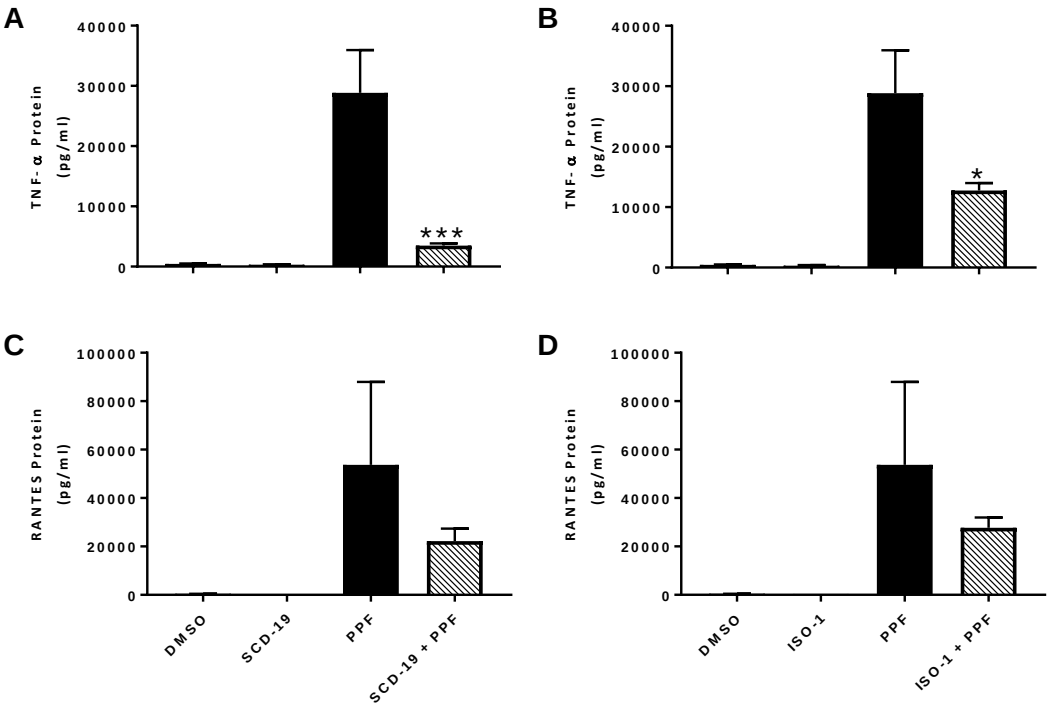

Figure 3.12. SCD-19 and ISO-1 modulate PPF-induced TNF-α but not RANTES production.

RAW 264.7 murine macrophages were stimulated with 2.5% PPF and treated with SCD-19 (100 µM) or ISO-1 (100 µM) for 24 hours. SCD-19 inhibits PPF-induced (**A**) TNF-α, but not (**C**) RANTES protein production. ISO-1 inhibits PPF-induced (**B**) TNF-α, but not (**D**) RANTES protein production. Protein production was measured by ELISA. Data is presented as mean ± SEM of 3 independent experiments with 3 technical replicates. A One-way ANOVA with a Tukey's multiple comparison post-hoc test was used to test for statistical differences. * $p<0.05$, ***$p<0.001$; respective treatment compared with PPF.

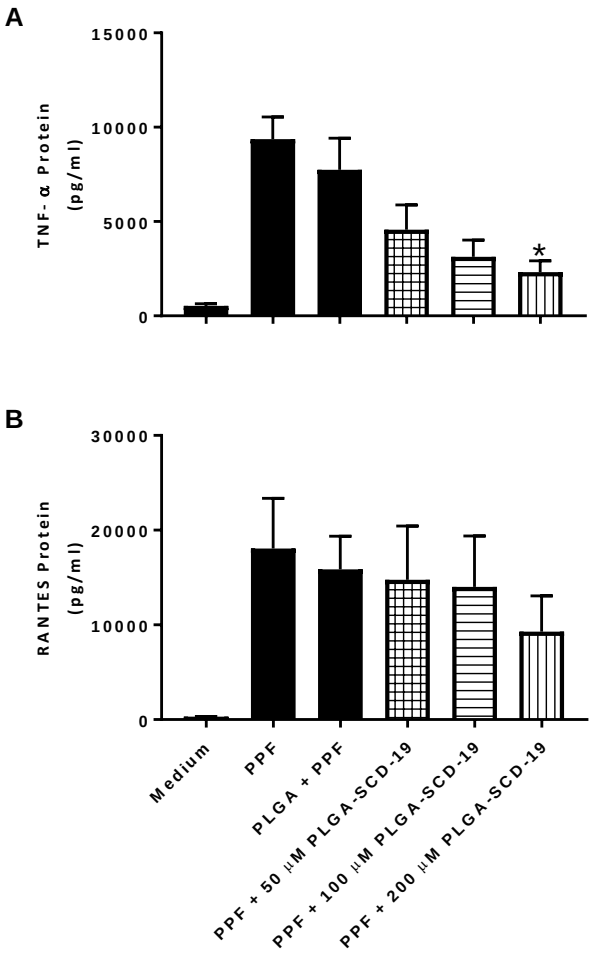

Figure 3.13. Nebulised PLGA-SCD-19 nanoparticles can modulate PPF-induced TNF-α and RANTES production.

RAW 264.7 murine macrophages were pre-treated with a dose response (50, 100, 200 μM) of nebulised PLGA or PLGA-SCD-19 nanoparticles for 24 hours. Following this, cells were treated with fresh nanoparticles ± 2.5% PPF for a further 24 hours. PLGA-SCD-19 nanoparticles inhibit PPF-induced (**A**) TNF-α and (**B**) RANTES release. Protein production was measured by ELISA. Data is presented as mean ± SEM of 3 biological replicates with 3 technical replicates. A One-way ANOVA with a Tukey's multiple comparison post-hoc test was used to test for statistical differences. *$p<0.05$; respective treatment compared with PLGA + PPF.

3.4 MIF regulates *P. aeruginosa* biofilm formation on airway epithelial cells.

Biofilm formation is employed by bacteria as a protective mechanism that has been shown to enhance bacterial survival and antibiotic resistance, which is of particular importance in CF (233, 258, 278). Biofilm formation is a cyclical process which begins with initial attachment, followed by growth and maturation of microcolonies and finally biofilm dispersion (266). Previously, we have shown that MIF promotes inflammation in a model of chronic respiratory *P. aeruginosa* infection (111). We have also shown that MIF drives *P. aeruginosa* biofilm formation and enhances antibiotic resistance; with SCD-19 representing a valid therapeutic agent in a model of chronic respiratory *P. aeruginosa* infection (113). *P. aeruginosa* biofilm formation on live airway epithelial cells has been well documented (206, 207, 278, 396). Here, we investigated the ability of MIF to modulate *P. aeruginosa* attachment to healthy and CF epithelial cells. Additionally, we investigated the effect of targeting MIF's tautomerase activity with SCD-19 and SCD-19 loaded PLGA nanoparticles.

3.4.1 MIF promotes P. aeruginosa (PA01) attachment to A549 epithelial cells, while SCD-19 and PLGA-SCD-19 nanoparticles inhibit PA01 attachment to A549 epithelial cells.

Initially, we examined the effects of recombinant MIF on the attachment of the lab strain, PA01, to A549 cells, a lung adenocarcinoma cell line (Figure 3.14). A549 cells were infected with PA01 at MOI 30 for 1 hour before washing with PBS to remove unadhered bacteria. Fresh antibiotic free DMEM was then added for a further 3 hours incubation. Following this, the supernatant was removed, monolayers were gently washed with PBS before being lysed and serially diluted and plated on LB agar plates for CFU/ml analysis. Recombinant MIF (100 ng/ml) significantly enhanced PA01 attachment to A549 monolayers compared with medium alone following 4 hours of culture (** $p<0.01$, **Figure 3.14A**). Treatment with SCD-19 (100 μM) for the duration of the

experiment significantly decreased PA01 attachment to A549 monolayers compared with medium alone following 4 hours of culture (*** p<0.001, **Figure 3.14B**). Next, we investigated the effects of SCD-19 loaded PLGA nanoparticles (100 µM) on PA01 attachment to A549 cell monolayers. Cells were pre-treated for 24 hours with SCD-19 loaded PLGA nanoparticles or empty PLGA nanoparticles to allow for drug release. Treatment of cells with SCD-19 loaded PLGA nanoparticles (100 µM) significantly inhibited PA01 attachment to A549 monolayers following 4 hours of culture compared with cells treated with empty PLGA nanoparticles (vehicle) (** p<0.01, **Figure 3.14C**).

3.4.2 Nanopackaged SCD-19 inhibits P. aeruginosa (PA01) attachment to healthy and CF airway epithelial cells.

We next examined the ability of SCD-19 loaded PLGA nanoparticles to inhibit PA01 attachment to 16HBE14o- human bronchial epithelial cell monolayers and CFBE41o- human CF bronchial epithelial cell monolayers (**Figure 3.15**). Treatment of 16HBE14o- cell monolayers with SCD-19 loaded PLGA nanoparticles (100 µM) significantly inhibited PA01 attachment following 4 hours of culture compared with cells treated with empty PLGA nanoparticles (vehicle) (* p<0.05, **Figure 3.15A**). Similarly, treatment of CFBE41o- cell monolayers with SCD-19 loaded PLGA nanoparticles (100 µM) significantly inhibited PA01 attachment to following 4 hours of culture compared with cells treated with empty PLGA nanoparticles (vehicle) (** p<0.01, **Figure 3.15B**).

3.4.3 Nanopackaged SCD-19 inhibits clinically isolated P. aeruginosa (CI#5436) attachment CF airway epithelial cells.

Finally, we examined the ability of SCD-19 loaded PLGA nanoparticles to inhibit the attachment of a *P. aeruginosa* clinical isolate, CI#5436, which was isolated from the airway of a CF patient, to 16HBE14o- human bronchial epithelial cell monolayers and CFBE41o- human CF bronchial epithelial cell monolayers. These experiments were conducted as *P. aeruginosa* isolates from patients have often adopted numerous mechanisms of host adaption compared with lab strains including downregulation of

virulence factors and increased biofilm formation (220, 254). Here, we demonstrated that treatment of 16HBE14o- cell monolayers with SCD-19 loaded PLGA nanoparticles (100 µM) inhibited CI#5436 attachment following 4 hours of culture compared with cells treated with empty PLGA nanoparticles (vehicle) (**Figure 3.16A**). We also demonstrated that treatment of CFBE41o- cell monolayers with SCD-19 loaded PLGA nanoparticles (100 µM) significantly inhibited CI#5436 attachment following 4 hours of culture compared with cells treated with empty PLGA nanoparticles (vehicle) (**, $p<0.01$, **Figure 3.16B**).

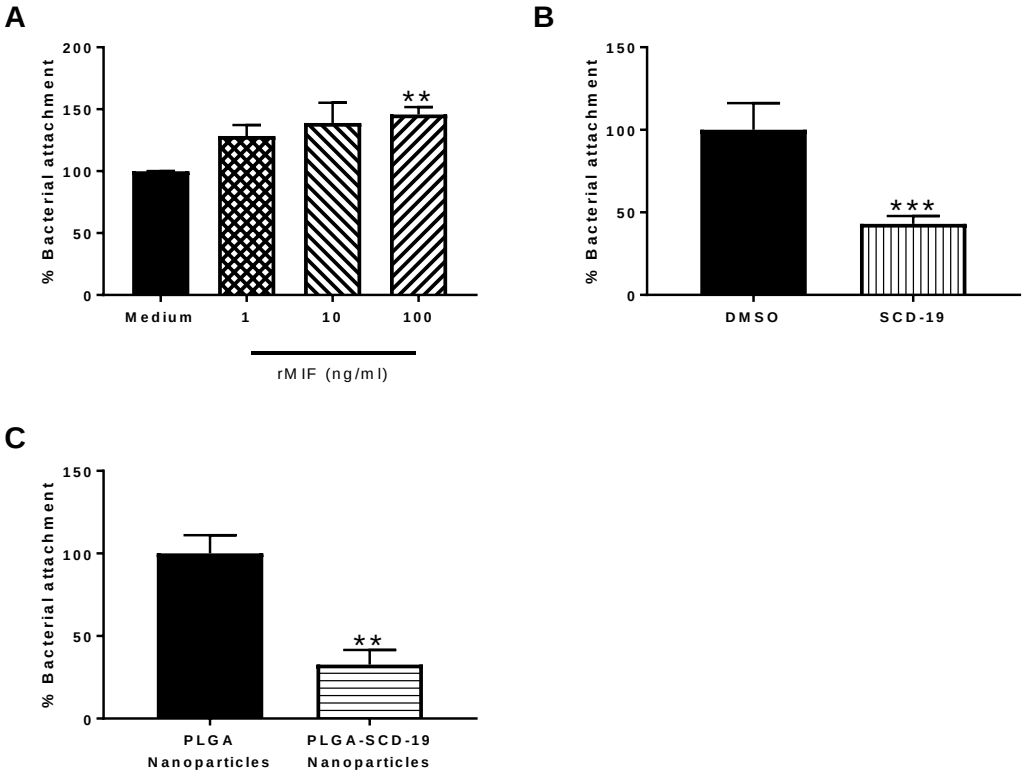

Figure 3.14. MIF promotes *P. aeruginosa* (PA01) attachment to A549 epithelial cells.

(**A**) Recombinant MIF enhances attachment of *P. aeruginosa* (PA01) to A549 epithelial cells. (**B**) SCD-19 (100 µM) significantly decreases attachment of PA01 to A549 epithelial cells. (**C**) SCD-19 loaded PLGA nanoparticles decreases attachment of PA01 to A549 epithelial cells. A549 airway epithelial cell monolayers were infected with PA01 (MOI 30) in the presence or absence of MIF (1-100 ng/ml), SCD-19, empty PLGA nanoparticles (vehicle) or SCD-19-PLGA nanoparticles (100 µM) for 4 hours. Bacterial attachment was quantified by cell lysis and spot plating for CFU/ml analysis. Data is presented as mean ± SEM of 3 biological replicates with 4 technical replicates. (A) A One-way ANOVA with a Tukey's multiple comparison post-hoc test was used to test for statistical differences. (**B, C**) A two-tailed unpaired t test was used to test for statistical significance of differences. **p<0.01, ***p<0.001; (**A**) respective treatment compared with medium.

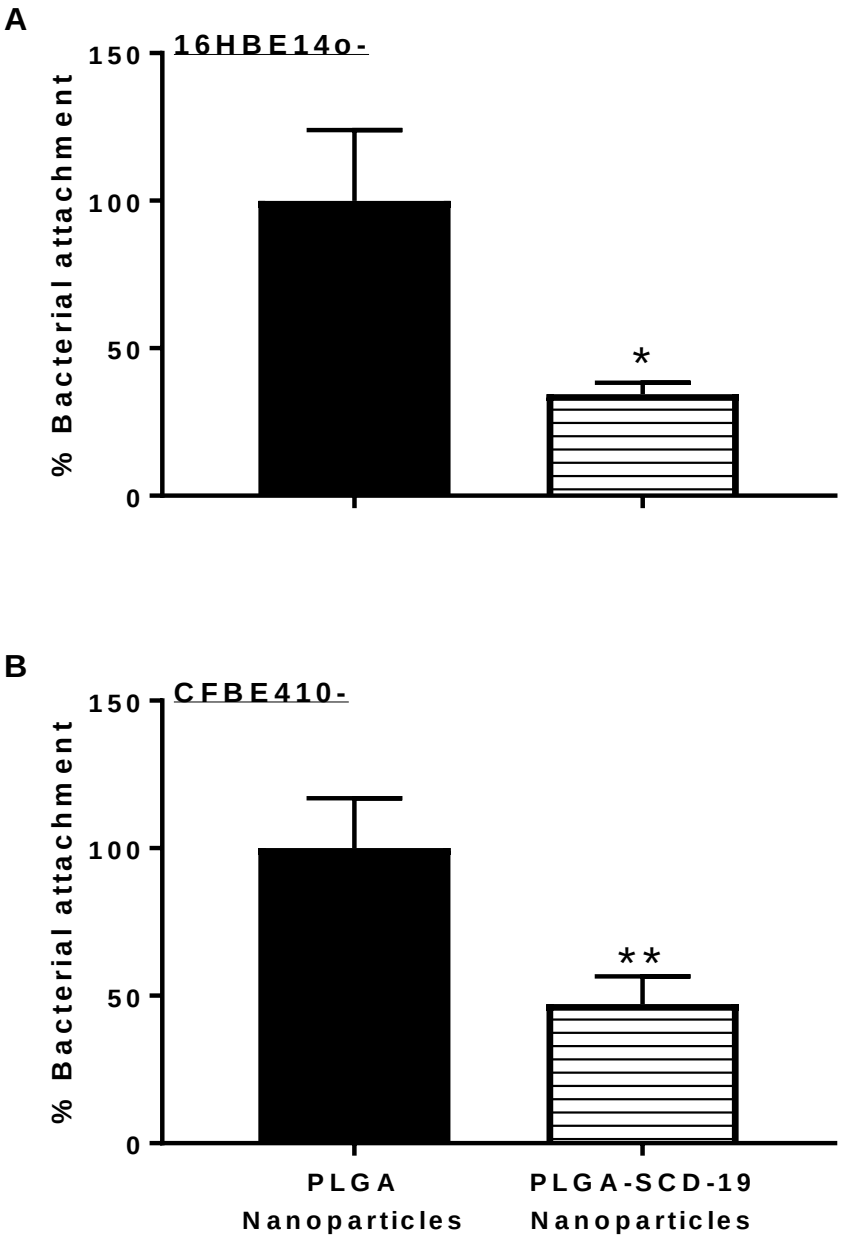

Figure 3.15. Nanopackaged SCD-19 inhibits *P. aeruginosa* (PA01) attachment to healthy and CF airway epithelial cells.

16HBE14o- **(A)** and CFBE410- **(B)** epithelial cell monolayers were pre-treated with nanopackaged PLGA-SCD-19 or PLGA alone (vehicle) for 24 hours. Cells were infected with PA01 (MOI 30) in the presence of nanopackaged PLGA-SCD-19 (100 µM) or empty PLGA nanoparticles (vehicle) for 4 hours. Bacterial attachment was quantified by cell lysis and spot plating for CFU/ml analysis. Data is presented as mean ± SEM of 3 replicates from 3 independent experiments. A two-tailed unpaired t test was used to test for statistical significance of differences. *$p < 0.05$, **$p < 0.01$.

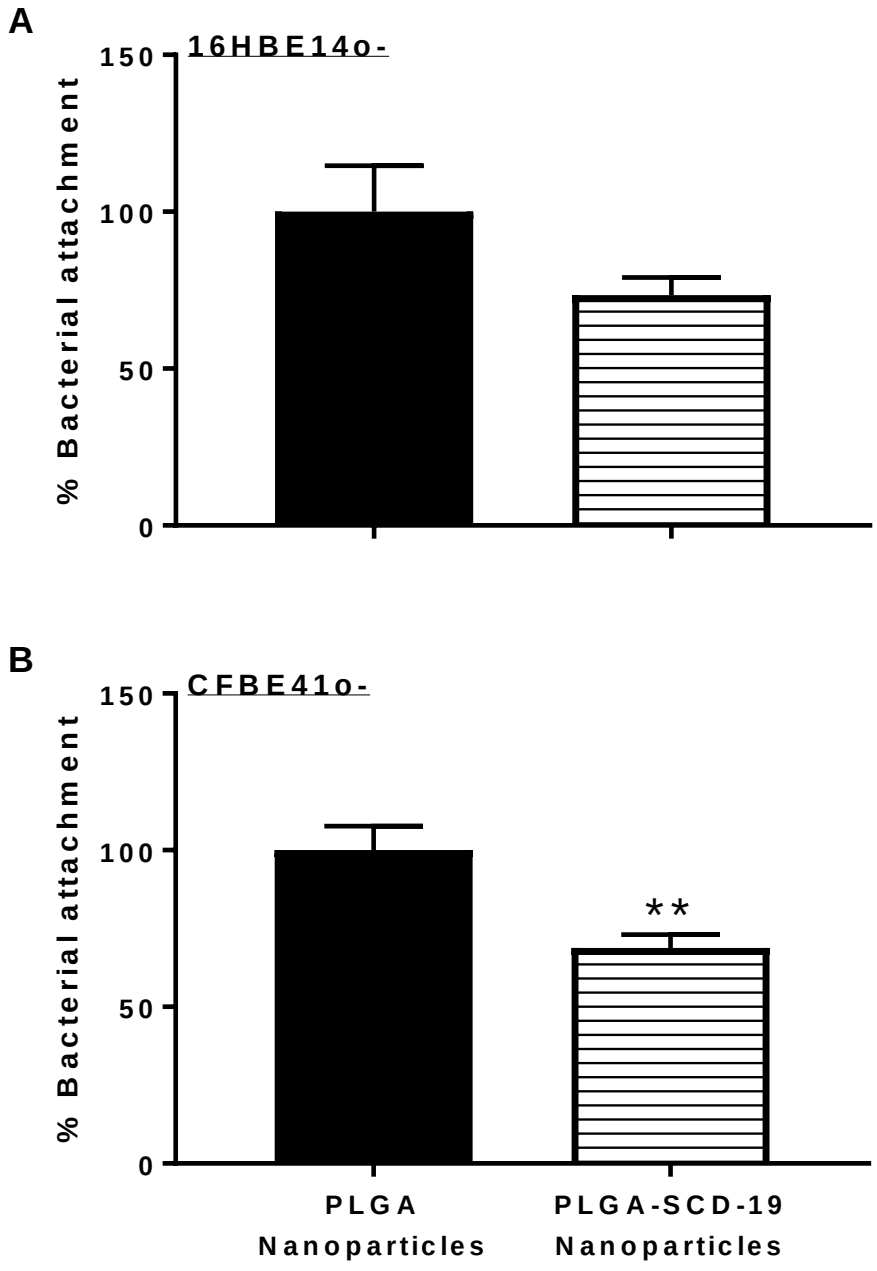

Figure 3.16. Nanopackaged SCD-19 inhibits clinically isolated *P. aeruginosa* (CI#5436) attachment CF airway epithelial cells.

(A) 16HBE14o- and **(B)** CFBE410- epithelial cell monolayers were pre-treated with nanopackaged PLGA-SCD-19 or PLGA alone (vehicle) for 24 hours. Cells were infected with CI#5436 (MOI 30) in the presence of nanopackaged PLGA-SCD-19 (100 µM) or PLGA alone (vehicle) for 4 hours. Bacterial attachment was quantified by cell lysis and spot plating for CFU/ml analysis. Data is presented as mean ± SEM of 3 replicates from 2 independent experiments. **p< 0.01; PLGA nanoparticles compared with PLGA-SCD-19 nanoparticles.

3.5 Role of MIF in *P. aeruginosa* phagocytosis and macrophage mediated killing.

Macrophages are innate immune cells which play a key role in the killing and removal of pathogens (72, 74). Macrophages employ a myriad of effector mechanisms including phagocytic killing, ROS generation and the release of antimicrobial peptides (200, 302, 403). Here, we aimed to investigated the effect of MIF on phagocytosis and killing of *P. aeruginosa*. We also sought to investigate the effect of SCD-19 on bacterial phagocytosis and killing.

3.5.1 MIF does not impact on phagocytic uptake of P. aeruginosa, while SCD-19 decreases phagocytic uptake.

Here, we demonstrated that a gradient of recombinant MIF (1, 10 100 ng/ml) had no effect of PA01 (MOI 10) phagocytosis by RAW 264.7 macrophages compared with medium (**Figure 3.17A**). We also demonstrated that SCD-19 (100 µM) significantly decreased phagocytic uptake of PA01 compared with medium alone (vehicle) (*** $p<0.001$, **Figure 3.17B**).

3.5.2 MIF regulates macrophage mediated killing of P. aeruginosa.

Next, we conducted experiments to examine the effect of MIF and SCD-19 on BMDM mediated PA01 killing. Here we demonstrated that BMDMs from $MIF^{-/-}$ mice have significantly enhanced PA01 killing compared with BMDMs from wild type mice (** $p<0.01$, **Figure 3.18A**). In this instance, higher numbers of CFUs are indicative of decreased bacterial killing. We also showed that SCD-19 (100 µM) significantly enhanced bacterial killing of PA01 by wild type BMDMs compared with medium alone (vehicle) (* $p<0.05$, **Figure 3.18B**).

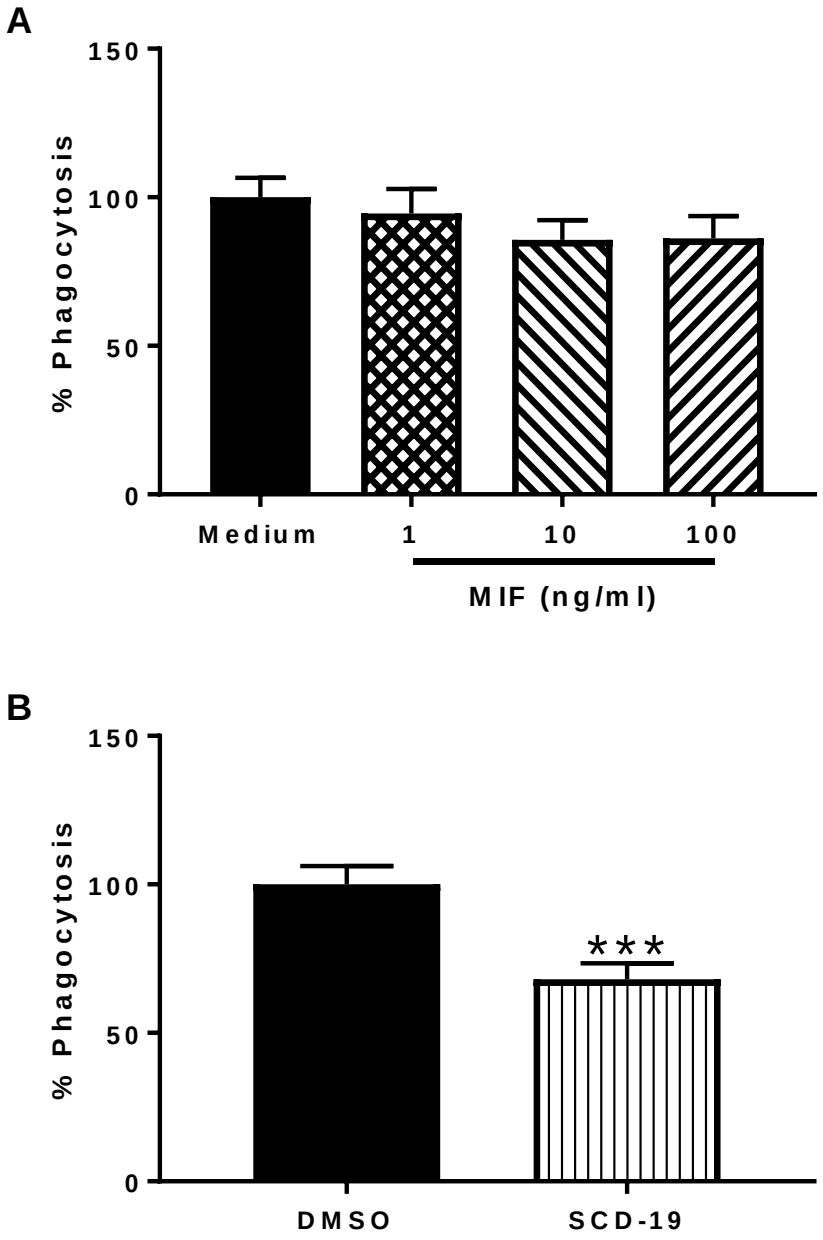

Figure 3.17. MIF does not impact on phagocytic uptake of *P. aeruginosa*, while SCD-19 decreases phagocytic uptake.

(**A**) MIF (1, 10, 100 ng/ml) had no effect on the phagocytosis of PA01 by RAW 264.7 macrophages. (**B**) SCD-19 (100 µM) decreases PA01 phagocytosis by RAW 264.7 macrophages. Data is presented as mean ± SEM of 3 independent experiments with 3 technical replicates. (**B**) An unpaired T-test was used to test for statistical significance of differences. *** $p<0.001$; SCD-19 compared to DMSO.

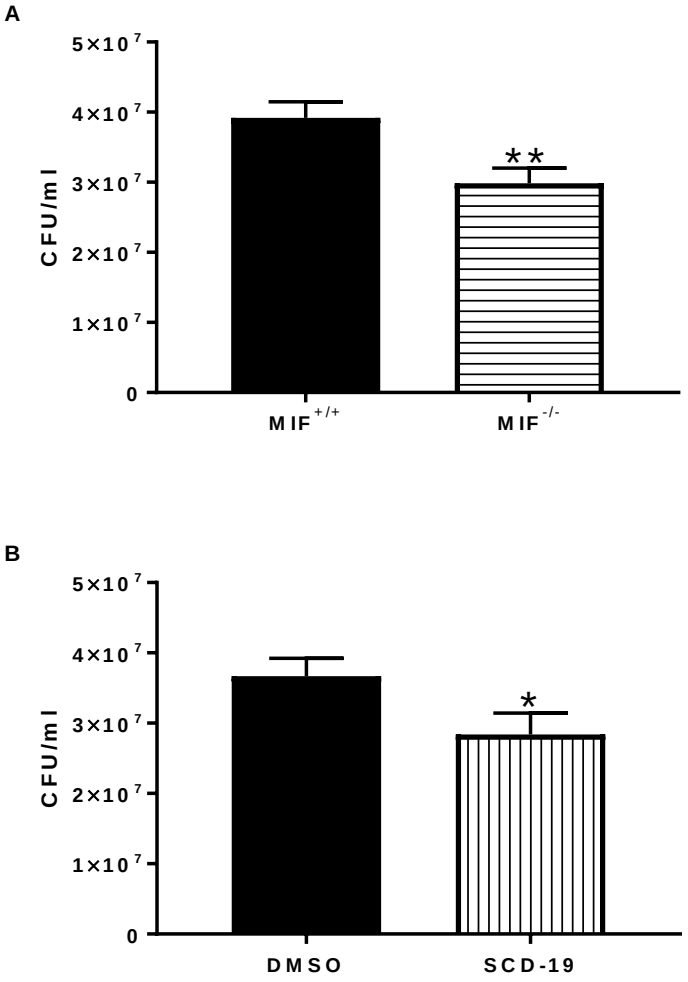

Figure 3.18. MIF regulates macrophage mediated killing of *P. aeruginosa*.

(**A**) MIF$^{+/+}$ BMDMs exhibit decreased bactericidal capacity against *P. aeruginosa* infection compared with BMDMs derived from MIF$^{-/-}$ mice. (**B**) Treatment of MIF$^{+/+}$ BMDMs with SCD-19 (100 µM) enhanced *P. aeruginosa* killing. BMDMs were infected with PA01 (MOI 10) for 4 hours. Macrophages were then lysed and combined with the respective supernatant before spot plating for CFU/ml analysis. Data is presented as mean ± SEM of 3 biological replicates with 3 technical replicates. A two-tailed unpaired t-test was used to test for statistical significance of differences. **p<0.01; MIF$^{+/+}$ compared with MIF$^{-/-}$. *p<0.05; SCD-19 compared with DMSO.

3.6 Characterisation of novel humanised 5-CATT and 7-CATT murine BMDMs.

The Donnelly Lab has previously described a role for the MIF CATT microsatellite repeat in numerous diseases including CF and rheumatoid arthritis (110, 111, 114). The number of CATT repeats has been shown to correlate with MIF expression levels, with individuals possessing 5, 6, 7 or 8-CATT repeats at position -794 in the promoter region of the MIF gene (114). To date, no murine model has been developed to examine the effects of the CATT microsatellite repeat in the promoter region of the MIF gene *in vivo*. The Donnelly Lab previously commissioned the generation of 2 distinct humanised mice, in which the murine *Mif* gene was replaced with the human *Mif* gene with either 5- or 7-CATT repeats in their promoter region. As the 5-CATT and 7-CATT mice have had the human *Mif* gene inserted, they both produce human MIF protein. This has been verified by the Donnelly Lab by using a human MIF specific ELISA kit, which facilitated the detection of human MIF in samples from the 5- and 7-CATT mice and no detection of MIF in samples from wild type mice (*data unpublished*). Here, we describe the *in vitro* characterisation of BMDMs generated from 5-CATT and 7-CATT mice.

3.6.1 Examination of the production of MIF, TNF-α, KC and RANTES protein in LPS stimulated 5-CATT and 7-CATT BMDMs.

In this study, we examined the production of MIF, TNF-α, RANTES and the murine IL-8 homolog, KC, by BMDMs from 5-CATT and 7-CATT humanised MIF mice. MIF has been shown to promote expression of TNF-α , RANTES and the murine IL-8 homolog, KC (198, 399, 404, 405). Here, we isolated and cultured primary BMDMs *in vitro* and subsequently stimulated these cells with increasing doses of LPS (1, 10 100 ng/ml) for 24 hours. LPS (1 ng/ml) significantly decreased human MIF protein production in 5-CATT BMDMs (* $p<0.05$, **Figure 3.19A**) compared with medium, while LPS (1, 10, 100 ng/ml) significantly decreased human MIF protein production in 7-CATT BMDMs (*** $p<0.001$, **Figure 3.19B**) compared with medium. Notably, 7-CATT BMDMs

had higher levels of MIF protein production than 5-CATT BMDMs under all conditions (**Figure 3.19A-B**).

TNF-α protein was significantly increased in 5-CATT BMDMs stimulated with 1 ng/ml of LPS (** p<0.01, **Figure 3.19C**), 10 ng/ml of LPS (*** p<0.001, **Figure 3.19C**) and 100 ng/ml of LPS (*** p<0.001, **Figure 3.19C**) compared with medium. Similarly, LPS (10, 100 ng/ml) stimulated 7-CATT BMDMs exhibit significantly increased TNF-α protein production compared with unstimulated cells (*** p<0.001, **Figure 3.19D)**. TNF-α protein production was higher in unstimulated and LPS stimulated (10, 100 ng/ml) 7-CATT BMDMs compared with 5-CATT BMDMs under equivalent conditions (**Figure 3.19C-D**).

Similarly, KC protein was significantly increased in 5-CATT BMDMs stimulated with LPS (1, 10, 100 ng/ml) compared with medium (*** p<0.001, **Figure 3.19E**). KC protein production was significantly increased in 7-CATT BMDMs stimulated with 1 ng/ml of LPS (* p<0.05, **Figure 3.19F**), 10 ng/ml of LPS (*** p<0.001, **Figure 3.19F**) and 100 ng/ml of LPS (*** p<0.001, **Figure 3.19F**) compared with medium. As with TNF-α, KC protein production was higher in unstimulated and LPS stimulated (10, 100 ng/ml) 7-CATT BMDMs compared with 5-CATT BMDMs under equivalent conditions (**Figure 3.19E-F**).

Similarly, RANTES protein was significantly increased in 5-CATT BMDMs stimulated with LPS (1, 10, 100 ng/ml) compared with medium (*** p<0.001, **Figure 3.19G**). RANTES protein production was significantly increased in 7-CATT BMDMs stimulated with 10 ng/ml of LPS (* p<0.05, **Figure 3.19H**) and 100 ng/ml of LPS (*** p<0.001, **Figure 3.19H**) compared with medium. As with TNF-α and KC, RANTES protein production was higher in unstimulated and LPS stimulated (1, 10, 100 ng/ml) 7-CATT BMDMs compared with 5-CATT BMDMs under equivalent conditions (**Figure 3.19G-H**).

3.6.2 Examination of the production of MIF, TNF-α and RANTES protein in poly(I:C) stimulated 5-CATT and 7-CATT BMDMs.

We also examined the cytokine responses of 5-CATT and 7-CATT BMDMs to stimulation with poly(I:C) (0.1, 1, 10 μg/ml) for 24 hours (**Figure 3.20**). Stimulation with poly(I:C) (0.1, 1, 10 μg/ml) had no effect on human MIF protein production in 5-CATT BMDMs compared with unstimulated cells (**Figure 3.20A**). In 7-CATT BMDMs, 24 hour stimulation with 10 μg/ml of poly(I:C) significantly decreased human MIF protein levels compared with unstimulated cells (*** $p<0.001$, **Figure 3.20B**). 7-CATT BMDMs had higher levels of MIF protein production compared with 5-CATT BMDMs under equivalent conditions (unstimulated; 0.1, 1, 10 μg/ml of poly(I:C)) (**Figure 3.20A-B**).

TNF-α protein was significantly increased in 5-CATT BMDMs stimulated with 10 μg/ml of poly(I:C) (* $p<0.05$, **Figure 3.20C**) compared with medium. Similarly, 10 μg/ml of poly(I:C) induced significant TNF-α protein production in 7-CATT BMDMs compared with unstimulated cells (*** $p<0.001$, **Figure 3.20D**). TNF- α protein production levels were higher in 7-CATT BMDMs compared with 5-CATT BMDMs under equivalent conditions (unstimulated; 0.1, 1, 10 μg/ml of poly(I:C)) **Figure 3.20C-D**).

RANTES protein was significantly increased in 5-CATT BMDMs following stimulation with 1 μg/ml of poly(I:C) (*** $p<0.001$, **Figure 3.20E**) and 10 μg/ml of poly(I:C) (*** $p<0.001$, **Figure 3.20E**) compared with medium. RANTES protein production was significantly increased in 7-CATT BMDMs stimulated with 10 μg/ml of poly(I:C) (*** $p<0.001$, **Figure 3.20F**) compared with medium. As with MIF and TNF-α, RANTES protein production levels were higher in 7-CATT BMDMs compared with 5-CATT BMDMs under equivalent conditions (unstimulated; 0.1, 1, 10 μg/ml of poly(I:C)) (**Figure 3.20E-F**).

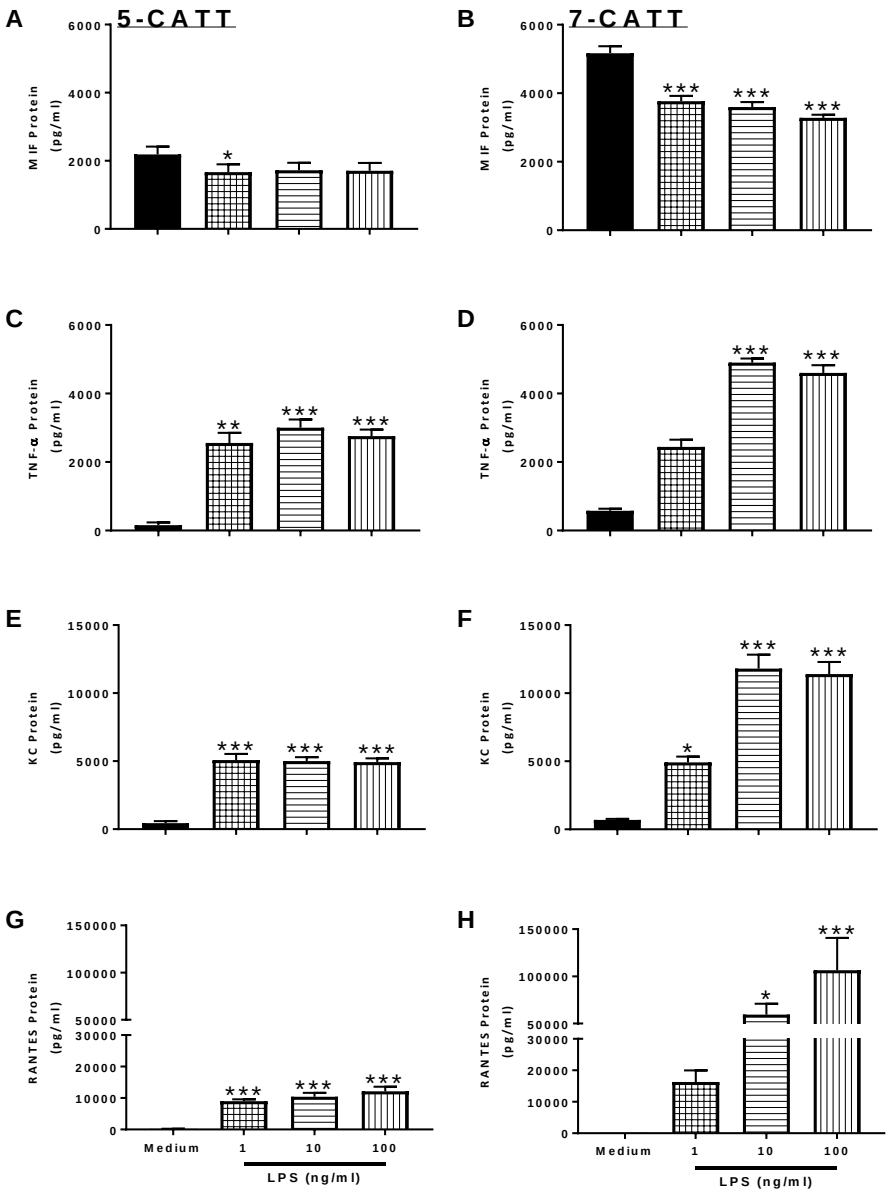

Figure 3.19. Characterisation of the effect of the 5-CATT and 7-CATT micro-satellite repeat on LPS induced MIF, TNF-α, KC and RANTES protein production in BMDMs from 5-CATT and 7-CATT mice.

Basal levels of MIF protein production levels were lower in (**A**) 5-CATT BMDMs than (**B**) 7-CATT BMDMs. 5-CATT BMDMs stimulated with LPS (1, 10,100 ng/ml) for 24 hours produced lower levels of MIF protein that 7-CATT BMDMs. Basal levels of TNF- α protein production levels were lower in (**C**) 5-CATT BMDMs than (**D**) 7-CATT BMDMs. LPS stimulation for 24 hours increased TNF-α, KC and RANTES protein production levels in 5-CATT BMDMs (**C,E,G**) and also in 7-CATT BMDMs, to a greater extent (**D,F,H**). Protein production was measured by ELISA. Data is presented as mean ± SEM of 3 biological replicates with 3 technical replicates. (**A, C, D, F**) A Kruskal-Wallis Test with a Dunn's multiple comparison post-hoc test was used to test for statistical differences. (**B, E, G, H**) A One-way ANOVA with a Tukey's multiple comparison post-hoc test was used to test for statistical differences. *p<0.05, **p<0.01, ***p<0.001; respective treatment compared with medium.

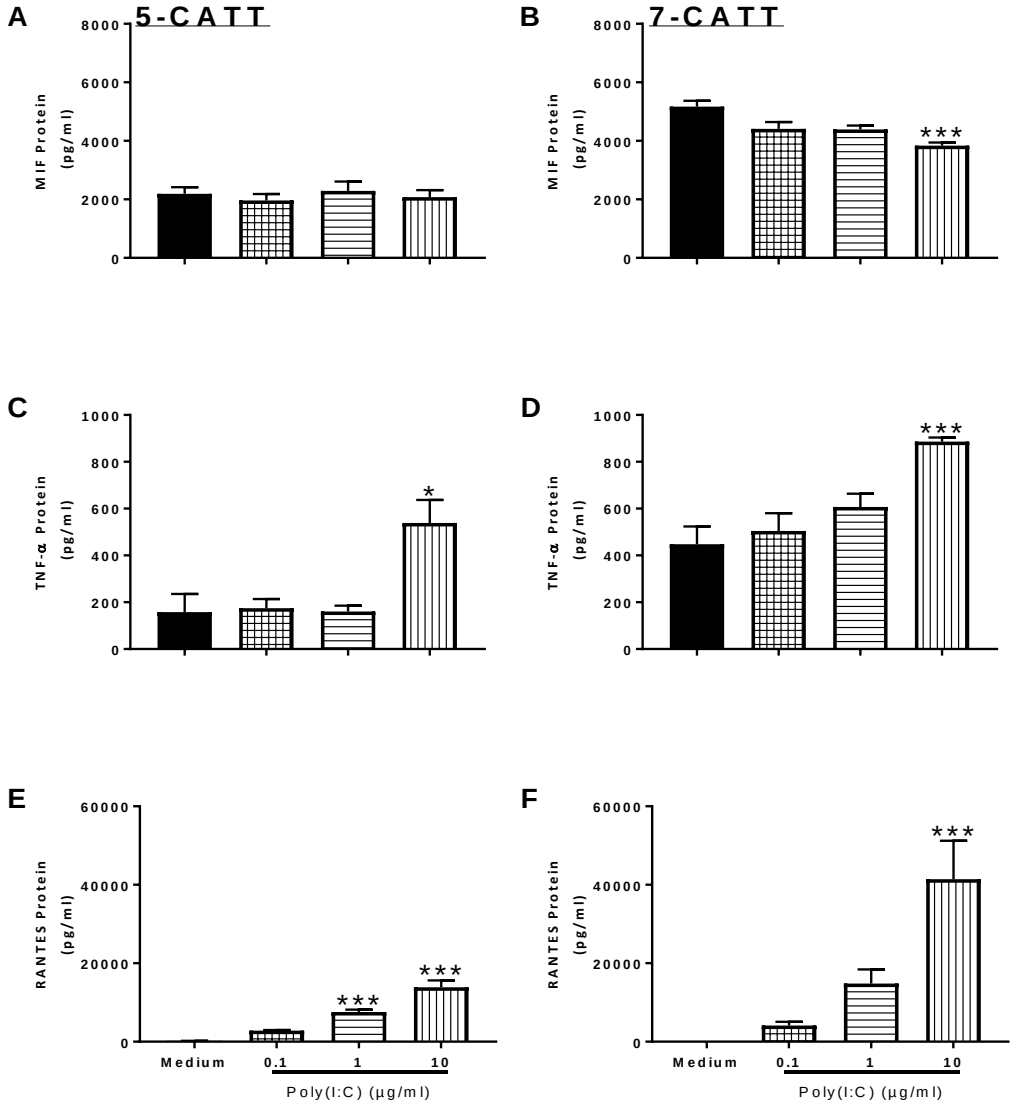

Figure 3.20.Characterisation of the effect of the 5-CATT and 7-CATT micro-satellite repeat on poly(I:C)-induced MIF, TNF-α and RANTES protein production in BMDMs from 5-CATT and 7-CATT mice.

5-CATT BMDMs stimulated with poly(I:C) (0.1, 1, 10 µg/ml) for 24 hours produced lower levels of MIF protein that 7-CATT BMDMs. poly(I:C) stimulation for 24 hours increased TNF-α and RANTES protein production levels in 5-CATT BMDMs (**C, E**) and also in 7-CATT BMDMs, to a greater extent (**D,F**). Protein production was measured by ELISA. Data is presented as mean ± SEM of 3 biological replicates with 3 technical replicates. (**B, C, D**) A Kruskal-Wallis Test with a Dunn's multiple comparison post-hoc test was used to test for statistical differences. (**E, F**) A One-way ANOVA with a Tukey's multiple comparison post-hoc test was used to test for statistical differences. *p<0.05, **p<0.01, ***p<0.001; respective treatment compared with medium.

3.7 Discussion

In this chapter, we investigated the relationship between MIF and two key facets of CF disease; *P. aeruginosa* induced inflammation and *P. aeruginosa* biofilm formation. CF is a multisystemic disease caused by defects in the CFTR with implications for the gastrointestinal, reproductive and respiratory systems (2-5). Most notably, CF patients develop a series of intermittent respiratory infections before the development of chronic infection, with *P. aeruginosa* being the most commonly isolated pathogen (2, 35, 37). Ultimately, CF patients progress to end-stage lung disease as a result of over exuberant inflammation and chronic infection, resulting in the need for a lung transplant (219). As such, new therapies directed at decreasing inflammation and preventing the establishment of chronic infection represent an unmet clinical need.

A plethora of research exists which implicates MIF as a driver of the pathogenesis of *P. aeruginosa* infection, highlighting the potential of MIF as a valid therapeutic target. $MIF^{-/-}$ mice effectively clear intratracheally instilled *P. aeruginosa* and exhibit decreased pulmonary neutrophil recruitment compared with $MIF^{+/+-}$ mice (198). In a model of ocular keratitis, $MIF^{-/-}$ mice exhibit improved *P. aeruginosa* clearance, decreased neutrophil infiltration, and decreased inflammatory responses compared with wild type mice; an effect which was reversed upon topical application of recombinant MIF to infected corneas (150). Pharmacological inhibition of MIF with the small molecular weight inhibitor, 4-IPP, inhibited *P. aeruginosa* cellular invasion and *P. aeruginosa* induced cytokine expression compared with infected mice treated with vehicle only (150). The Donnelly Lab previously demonstrated that MIF tautomerase activity promotes *P. aeruginosa* induced inflammatory damage in a model of chronic respiratory infection (111). Furthermore, we previously demonstrated that MIF also promotes *P. aeruginosa* biofilm formation (113). Finally, our lab has demonstrated that CF patients with high levels of MIF expression exhibit earlier *P. aeruginosa* colonisation and a more rapid decline in lung function compared with those with low MIF expression levels (110, 111).

In this chapter, we aimed to examine the induction of pro-inflammatory responses in HKPA and PPF stimulated macrophages, and the regulation of this response by inhibitors of MIF. We demonstrated that both HKPA and PPF stimulation

induced significant production of TNF-α and RANTES. TNF-α production was induced upon NF-κB activation, while RANTES production was upregulated upon NF-κB and IRF3 activation (398, 400). HKPA activates both TLR2 and TLR5, both of which converge upon NF-κB activation (73). PPF contains a myriad of secreted products including, but not limited to, LPS, quorum sensing molecules and bacterial DNA (388). Thus, PPF is capable of activating a myriad of PRRs including both TLRs and cytosolic sensors. Notably, MIF regulates the production of both TNF-α and RANTES (198, 399).

We hypothesised that SCD-19 would limit the induction HKPA and PPF-induced pro-inflammatory responses. SCD-19 is a small molecular weight inhibitor of MIF's tautomerase activity that has been shown to limit LPS-induced inflammation *in vitro* and *P. aeruginosa* induced inflammation *in vivo* (112, 113). Here, we report for the first time that SCD-19 significantly decreased HKPA mediated TNF-α and RANTES production. Furthermore, SCD-19 also significantly decreased PPF-induced TNF-α production. In CF, irreversible lung damage occurs as a result of excessive inflammation which is contributed to by *P. aeruginosa* associated PAMPs. The ability of SCD-19 to inhibit the induction of pro-inflammatory cytokines by both HKPA and PPF adds weight to previous studies from our laboratory that established that SCD-19 represented a candidate therapeutic agent for the treatment of *P. aeruginosa* induced inflammation (**Figure 3.21**) (113).

The use of nanotechnology in medicine is a rapidly evolving field, with a large increase in the development of nanoparticles as a vehicle for drug delivery to the lung (47, 406). Nanoparticles offer numerous benefits including targeted drug delivery, improved drug stability and limitations in systemic toxicity (47). To date, an estimated 40% of commercially available drugs and 90% of drugs in development are poorly water-soluble (47, 407). Solubility of therapeutic agents is a key factor which is required to achieve desired concentrations of drug in systemic circulation necessary for optimal pharmacological response. Drugs which are poorly water-soluble require higher doses in order to reach therapeutic plasma concentrations after oral administration compared with water soluble compounds (408). As with most drugs in development, SCD-19 is poorly water miscible. As a result, the Donnelly Lab have recently synthesised and characterised SCD-19 loaded PLGA nanoparticles (394). The use of PLGA nanoparticles

is an attractive option as they have high levels of biodegradability and biocompatibility, low levels of toxicity and enable targeted drug delivery (409). PLGA is also approved by the FDA and European Medicine Agency (EMA) for the use in drug delivery systems for parenteral administration (409). The packaging of SCD-19 in PLGA nanoparticles overcomes the issue of poor water-solubility and enables the therapy to be delivered using water or saline as a vehicle (394). These nanoparticles have been optimised for nebulisation using the Aerogen® Solo nebuliser (394). The Aerogen® Solo nebuliser utilises a vibrating mesh in order to nebulise produce a low velocity aerosol optimised for targeted drug delivery to the lungs (410). Furthermore, they exhibit limited toxicity, high levels of cellular uptake and high levels of stability. They also are the optimal size for deep lung deposition, with the majority of nebulised nanoparticles reaching the deep lung in experiments utilising a human breathing simulator (394).

In this chapter, we detail for the first time the effective application of nebulised SCD-19 loaded PLGA nanoparticles in decreasing pro-inflammatory cytokine production induced by *P. aeruginosa* related antigens. SCD-19 loaded PLGA nanoparticles effectively inhibit the induction of TNF-α by PPF, and both TNF-α and RANTES by HKPA in macrophages. These results are extremely promising when coupled with the low toxicity, high stability and high levels of cellular uptake of SCD-19 loaded PLGA nanoparticles (394). Furthermore, these nebulised nanoparticles are suitable for delivery via inhalation with the majority of nanoparticles depositing within the area of deep lung (394).

We believe that these nanoparticles represent a potential anti-inflammatory therapy for the treatment of *P. aeruginosa* induced inflammation (**Figure 3.21**). However, it is important to note that complete ablation of an inflammatory response is not the ultimate goal, as a fine balance exists between lowering the levels of cytokines to a level that does not result in inflammatory damage, and that which results in immunocompromised phenotype. For example, there is an increased risk of viral, bacterial and fungal infection in patients receiving anti-TNF therapy for the treatment of chronic inflammatory diseases (411). As such, further *in vivo* studies need to be conducted to verify these nanoparticles would not tip the delicate balance towards an immunocompromised phenotype. In future studies, we would like to examine the effect

of these nebulised nanoparticles in a model of chronic respiratory *P. aeruginosa* infection.

As previously mentioned, the Donnelly Lab has demonstrated that MIF promotes *P. aeruginosa* biofilm formation (113). This finding was significant as biofilm formation is one of the main mechanisms which facilitates antibiotic resistance and chronic infection in CF (21, 23, 37). However, these experiments examined *P. aeruginosa* biofilm formation on non-living surfaces (113). To date, it has remained unclear if the observed effect would remain the same in the context of biofilm formation on airway epithelial cells; the surface on which biofilms develop within the lung (412). In order to address this, we utilised a system whereby we examined the development of *P. aeruginosa* on airway epithelial cell monolayers. This system takes into account the crosstalk that occurs between the bacterial and host cells (209). Our experiments revealed, for the first time, that recombinant human MIF significantly enhances biofilm formation of PA01 on airway epithelial cell monolayers. Following on from this, we hypothesised that SCD-19 may be able to inhibit the increase in MIF mediated biofilm formation. We demonstrated that SCD-19 significantly inhibited PA01 biofilm formation on airway epithelial cell monolayers compared with those treated with the vehicle control. This is the first description of an inhibitor of MIF being used to inhibit *P. aeruginosa* biofilm formation.

One of the difficulties associated with the treatment of infections in CF is resistance which develops as a result of poor biofilm penetration of antibiotics (413). Nanoparticles have been shown to enhance the efficacy of antibiotics against biofilm infections (414). Nanoparticles have the advantage of being small enough to penetrate and diffuse through thick biofilm ECM, enabling the antibiotics to come into contact with the underlying bacteria (47, 415). In a phase II clinical trial, CF patients with chronic *P. aeruginosa* infection received treatment with inhaled amikacin sulfate encapsulated in a liposomal nanoparticle, or placebo (415). The authors concluded that packaging amikacin sulfate in liposomal nanoparticles maximises the delivery of the antibiotic agent to the lung via nebulisation, enhances biofilm penetration and improves the bioavailability of the drug at the site of infection (415). These benefits were achieved all

while increasing the half-life of the compound within the lungs and limiting systemic toxicity, due to the inhaled route of delivery (415).

With the benefits of inhaled nanoparticles in mind, we examined the ability of SCD-19 loaded PLGA nanoparticles to inhibit *P. aeruginosa* attachment to airway epithelial cells. We demonstrated for the first time the SCD-19 loaded PLGA nanoparticles inhibited the attachment of both lab strain and a clinically isolated *P. aeruginosa* to healthy and CF bronchial epithelial cell monolayers. This result is important, as in this chapter we have demonstrated both anti-inflammatory and anti-biofilm formation characteristics of these nanoparticles; two key characteristics which are of interest in the treatment of infections in CF. Furthermore, the SCD-19 loaded PLGA nanoparticles are optimised for nebulised delivery and deep lung deposition. Overall, we believe that these nanoparticles represent a potential adjunctive therapy in combination with conventional antibiotic therapies to decrease *P. aeruginosa* biofilm formation and limit *P. aeruginosa* induced inflammatory damage (**Figure 3.21**).

As previously described, MIF promotes *P. aeruginosa* colonisation, decreases bacterial clearance and promotes an aggressive disease phenotype in CF patients (110, 111, 198). In this chapter, we examined the effect of MIF on macrophage mediated bacterial killing. Macrophages play a key role in the innate immune response to infection and act to kill and remove pathogens. Macrophages utilise a number of effector mechanisms to clear infections including phagocytic killing, ROS generation and the release of antimicrobial peptides (42-44). We hypothesised that MIF would inhibit macrophage mediated killing, and that SCD-19 would enhance the bactericidal capacity of macrophages against *P. aeruginosa*. We have shown that recombinant MIF recombinant MIF had no effect of PA01 phagocytosis by macrophages. However, using MIF deficient macrophages we demonstrated that MIF inhibits macrophage mediated *P. aeruginosa* killing. SCD-19 was also shown to decrease phagocytic uptake of PA01 and enhance macrophage mediated bacterial killing. In this instance, decreased phagocytosis may occur due to enhanced bacterial killing and thus lower bacterial numbers.

While these experiments give an insight into the effect of MIF and its targeting using SCD-19 on macrophage phagocytosis and bacterial killing, it is important to note

that it does not offer an explanation on the mechanism of bacterial killing. Further research is necessary to ascertain the mechanism of killing, for example, increased ROS production or enhanced antimicrobial peptide production. It may also be the case that the antibacterial phenotype of the macrophage itself remains unchanged upon MIF or SCD-19 treatment, while the phenotype of the bacteria adapts to impact macrophage mediated killing.

Finally, in this chapter we detailed for the first time the characterisation of BMDMs from humanised mice in which the murine Mif gene was removed and replaced with the human Mif gene with either 5 or 7-CATT repeats in the promoter region. A large body of work has implicated the MIF CATT microsatellite repeat in numerous diseases including CF, rheumatoid arthritis and cancer, with the number of CATT repeats correlating with MIF expression levels and consequently disease development and severity (110, 111, 114, 416). To date, there has been no description of the generation of a humanised murine model to examine the effects of the CATT microsatellite repeat. In order to address this, the Donnelly Lab previously commissioned the generation of two distinct humanised mice, described as 5-CATT and 7-CATT mice.

In this chapter, we detailed the cytokine response of BMDMs generated from 5-CATT and 7-CATT mice and stimulated with LPS and poly(I:C). Poly(I:C) is a double stranded RNA analogue, which activates TLR3 on the cell surface and endosomal membrane, while LPS initiates an immune response by binding to TLR4 located extracellularly on the cell membrane (417, 418). Both TLR3 and TLR4 activation results in the activation of NF-κB and IRF3, with subsequent induction of pro-inflammatory cytokine production (418, 419). We analysed protein levels of TNF-α, RANTES and the murine IL-8 homolog, KC; all of which are regulated by MIF (198, 399, 404, 405). We hypothesised that the level of pro-inflammatory cytokine production would be higher in BMDMs from 7-CATT mice than 5-CATT mice following stimulation.

The first key observation in these experiments was that constitutive levels of MIF, and also MIF levels in LPS stimulated and poly(I:C) stimulated 7-CATT BMDMs were higher than those observed in 5-CATT BMDMs. This is important, as the functionality of the mice relies on the fact that the 7-CATT mice express higher levels of MIF compared

with the 5-CATT mice. It is important to note that as this a humanised mouse, these mice produced human MIF and not murine MIF, as previously verified by the Donnelly Lab (*data unpublished*). In LPS stimulated cells, we observed the induction of TNF-α, RANTES and KC, as expected. The concentration of all three cytokines under these conditions was higher in 7-CATT BMDMs, as hypothesised. We also observed the induction of TNF-α and RANTES in poly(I:C) stimulated cells. The induction of these cytokines was higher in 7-CATT BMDMs compared with 5-CATT BMDMs. These results demonstrated for the first time the cytokine responses of BMDMs from the CATT mice to LPS and poly(I:C). These results are promising as the cytokine responses are in agreement with those observed in human patients, with 7-CATT mice having increased MIF levels and subsequent higher TNF-α, RANTES and KC protein levels other pro-inflammatory cytokines compared with 5-CATT mice (110, 114, 198, 399, 404, 405). These results suggested that the humanised mice are functional, although further characterisation is required. MIF has been shown to regulate TLR4 expression, counter regulate the anti-inflammatory effects of glucocorticoids and promote HIF-1α stabilisation among a myriad of other effects (176, 182, 193, 194). Investigating differences in these characteristics in the 5-CATT and 7-CATT mice would shed further light on the functionality of the CATT mice. Should these experiments also indicate functionality, these mice are a valuable tool for investigating the effects of the CATT microsatellite repeat in numerous diseases *in vitro* and *in vivo*.

Overall, in this chapter we have demonstrated that inhibition of MIF, using SCD-19 loaded PLGA nanoparticles, effectively decreased *P. aeruginosa*-induced inflammatory cytokine production and early *P. aeruginosa* biofilm formation on epithelial cell monolayers. Furthermore, we demonstrated that MIF inhibited macrophage-mediated *P. aeruginosa* killing, while SCD-19 promoted bacterial killing. These results illustrated the validity of SCD-19 as a therapeutic agent in CF. Furthermore, we detailed the characterisation of macrophages from the novel humanised 5-CATT and 7-CATT mice, which may be used in future studied to examine the effects of the CATT microsatellite repeat.

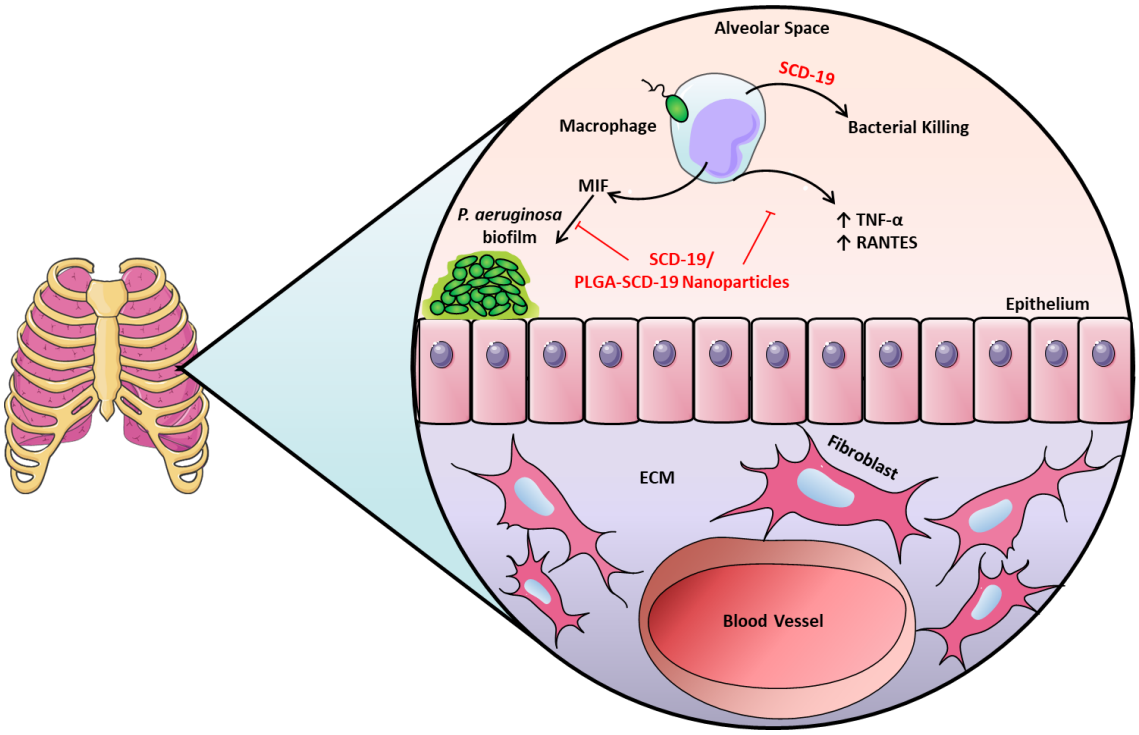

Figure 3.21. Proposed benefits of SCD-19/ SCD-19 nanoparticles in CF.

HKPA and PPF induce the production of TNF-α, MIF and RANTES protein. MIF promotes *P. aeruginosa* biofilm formation of airway epithelial cells. SCD-19 and SCD-19 nanoparticles inhibit HKPA and PPF-induced TNF-α and RANTES production and *P. aeruginosa* biofilm formation of airway epithelial cells. SCD-19 also promotes macrophage mediated *P. aeruginosa* killing.

Chapter 4 - Investigation of the effects of 4-octyl itaconate and endogenous itaconate on the cellular response to lipopolysaccharide and heat killed *P. aeruginosa*.

4.1 Introduction

Itaconate is an anti-bacterial and immunomodulatory metabolic by-product of the citric acid (TCA) cycle. Production of itaconate is mediated by cis-aconitate decarboxylase (Acod1), also known as immunoresponsive gene 1 (Irg1), which converts cis-aconitate to itaconate (359). The most prominent examples of the upregulation of itaconate are in LPS stimulated and *Mycobacterium tuberculosis* (*M. tb)* infected murine macrophages (365, 367). More recently, upregulation of Irg1 mRNA expression has been described in response to a variety of stimuli including poly(I:C) and TNF-α and also in response to live infection with *Staphylococcus aureus*, *Escherichia coli* and Zika virus (330, 383, 420-423).

The immunomodulatory effects of itaconate has been the subject of much ongoing research. Interestingly, there has been no description of an itaconate transporter or receptor. To date, there have been only a limited number of reports of exogenous itaconate entering the cytoplasm of macrophages and adipocytes after 48-72 hours of exposure (369, 370). As a result, synthetic cell permeable derivatives have been developed. Experiments conducted using the cell permeable itaconate derivative, dimethyl itaconate (DI), demonstrated the inhibition of reactive oxygen species (ROS), nitric oxide (NO), IL-6 and IL-1β production in LPS stimulated macrophages (327). DI exhibits electrophilic properties due to the nature of the structure of the compound which enhances the likelihood that observed effects are independent of itaconate (424). Consequently, 4-octyl itaconate (4-OI) was developed as a compound which is cell permeable, less electrophilic than DI and more akin to itaconate. 4-OI has been shown to inhibit IL-1β and iNOS mRNA and protein in LPS stimulated macrophages (330, 360). Furthermore, 4-OI also inhibits nitrite, IL-1β ,TNF-α, IL-6 production in an LPS lethality model (330, 360).

The development of $Irg1^{-/-}$ mice has enabled researchers to examine the effects of endogenous itaconate in innate immunity (351, 425). Stimulation of $Irg1^{-/-}$ BMDMs with LPS and IFN-γ results in significantly higher levels of IL-12p70 and NO compared with $Irg1^{+/+}$ cells (327). $Irg1^{-/-}$ BMDMs stimulated with LPS results in significantly higher levels of IL-6, IL-1β and HIF-1α protein compared with $Irg1^{+/+}$ cells, while TNF-α protein

levels do not differ, demonstrating that itaconate does not simply promote a uniform shutdown of the inflammatory response (327).

Itaconate exerts anti-inflammatory effects through a number of mechanisms of action. Firstly, itaconate has been shown to inhibit succinate dehydrogenase (SDH) (374). SDH oxidises succinate and also part on the electron transport chain, both of which promote the generation of reactive species and inflammation (295). Inhibition of SDH has been demonstrated in LPS stimulated $Irg1^{-/-}$ BMDMs, which have significantly lower levels of succinate accumulation compared with $Irg1^{+/+}$ cells, indicating that itaconate promotes SDH inhibition (327, 351). A second mechanism of itaconates anti-inflammatory effects is through nuclear factor erythroid 2-related factor 2 (Nrf2) induction (375, 426). Irg1 deficient macrophages display impaired activation of Nrf2 (426). 4-OI induces production of the master antioxidant transcription factor Nrf2 which initiates transcription of downstream antioxidant genes including NAD(P)H Quinone Dehydrogenase 1 (Nqo1), Glutamate-Cysteine Ligase Modifier (Gclm), Glutathione Reductase (Gsr) and Heme Oxygenase 1 (Hmox1) (424, 427). Promotion of antioxidant effectors reduces levels of ROS, which results in less HIF-1α stabilisation and decreased HIF-1α dependant inflammatory cytokine expression (424).

As previously mentioned, MIF is a pro-inflammatory cytokine that has been shown to promote the pathogenesis of a number of inflammatory diseases including cystic fibrosis (CF), asthma, rheumatoid arthritis and acute respiratory distress syndrome (111, 114, 115, 390). MIF promotes inflammation through activation of the MAPK pathway, NF-κB activation, increasing TLR4 expression and overriding the anti-inflammatory effects of glucocorticoids all of which promote pro-inflammatory cytokine expression (161, 167, 170-172, 176, 177, 182). Furthermore, MIF has been shown to be required for optimal HIF-1α stabilisation (193, 194). Activation of HIF-1α mediated signalling has been shown to result in alterations in gene expression involved in pro-inflammatory cytokine production and cellular metabolism (183, 188, 189, 191, 192).

In LPS stimulated macrophages, the metabolism of activated cells shifts towards aerobic glycolysis, also known as the Warburg effect (334-338). Glycolysis is essential for activated immune cells to enable replication and serves to support phagocytosis and

anti-bacterial functions (318, 339). HIF-1α has been shown to promote expression of proteins involved in glycolytic processing, while HIF-1α$^{-/-}$ cells fail to switch to this Warburg metabolism (343-345). Pharmacological inhibition of glycolysis with 2-deoxyglucose (2-DG) has been shown to limit macrophage activation and inflammation *in vivo* (185, 333, 340, 341). Furthermore, in LPS stimulated macrophages there is dysregulation of the TCA cycle whereby there is accumulation of succinate and citrate as a result of decreased activity of their respective processing enzymes (185, 328). Excess citrate is then processed for fatty acid synthesis and itaconate production (327, 328, 348, 349).

There are several overlapping effects of MIF and itaconate, respectively. MIF has been shown to regulate TLR4 expression, which induces Irg1 expression when stimulated with LPS (182, 351). Furthermore, MIF is required for HIF-1α stabilisation which is essential for Warburg metabolism and mediates the anti-inflammatory effects of itaconate (193, 194, 318, 339). As such, we hypothesised that MIF may play a mechanistic role in the immunomodulatory effects of itaconate and 4-OI (**Figure 4.1**). We proposed that MIF drives HIF-1α and TLR4 expression. In MIF deficient cells, we hypothesised that levels of Irg1 mRNA will be lower following LPS stimulation compared with wild type cells, due to lower levels of TLR4 expression (182). Furthermore, we believed that the effects of 4-OI would be limited in MIF deficient cells as one of the main mechanisms of 4-OI is inhibition of HIF-1α stabilisation, which has been shown to be reduced in MIF deficient cells (193).

In CF, irreparable damage to the lungs occurs as a result of chronic infection and consequent chronic inflammation (21, 233, 265). The most commonly isolated pathogen from the CF lung is *Pseudomonas aeruginosa* (*P. aeruginosa)* (35). Our lab has previously demonstrated a key role for MIF in the promotion of inflammation and disease severity in CF (110, 111). In CF, chronic lung inflammation results in irreversible tissue destruction and as such there is a major unmet clinic need for the development of anti-inflammatory therapies (6, 219). We hypothesised that 4-OI may modulate cellular responses to LPS and heat killed *P. aeruginosa* (HKPA), which may be of benefit in the development of a novel anti-inflammatory therapy for the treatment of CF.

In this chapter, we examined the effects of MIF on the immunoregulatory activity of the exogenous itaconate analogue, 4-OI. Furthermore, we examined the effects of both 4-OI and endogenous itaconate on the macrophage response to LPS and HKPA stimulation. Finally, we investigated the effects of 4-OI on HKPA and LPS stimulated primary murine lung fibroblasts, key structural cells within the lung.

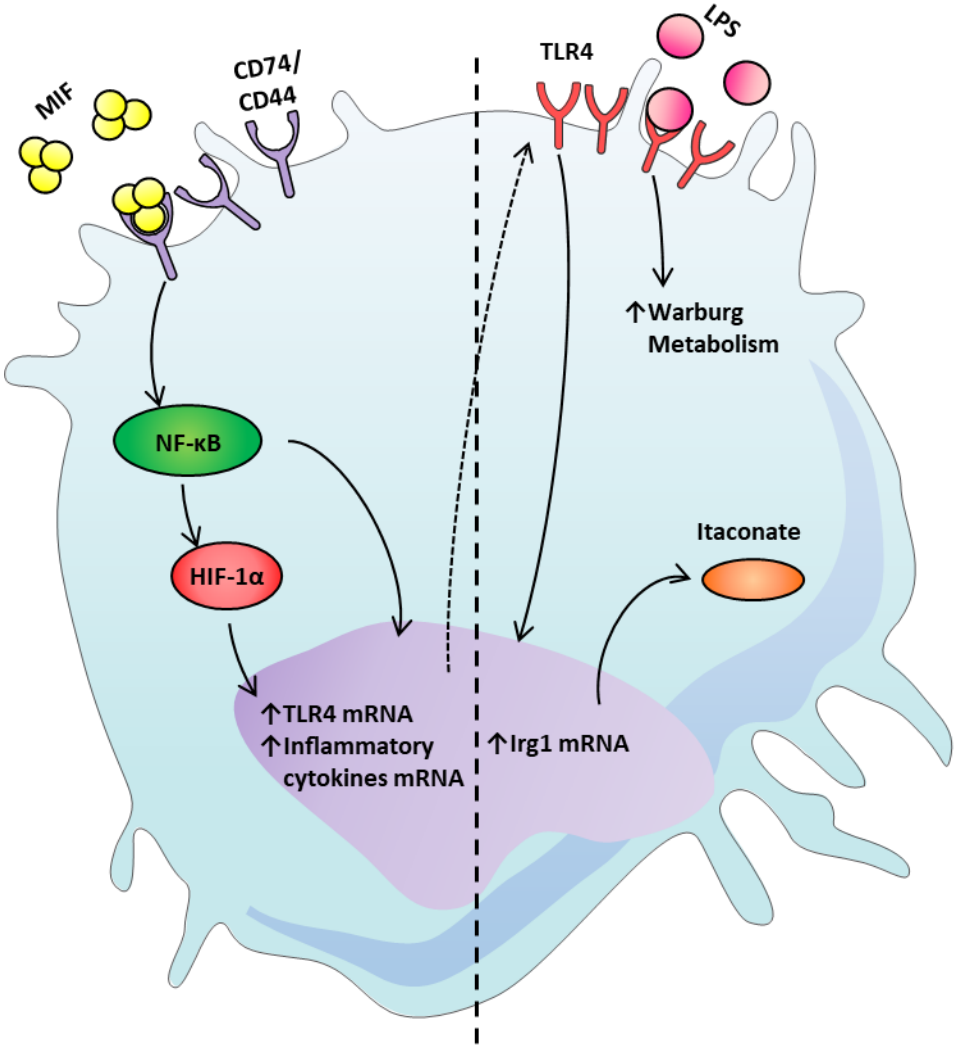

Figure 4.1. Hypothesised effects of MIF on itaconate and 4-OI.

MIF binds to its receptor complex CD74/CD44 which promotes NF-κB activation, HIF-1α stabilisation and increased TLR4 expression. Enhanced TLR4 expression promotes increased Irg1 expression and itaconate production following LPS stimulation.

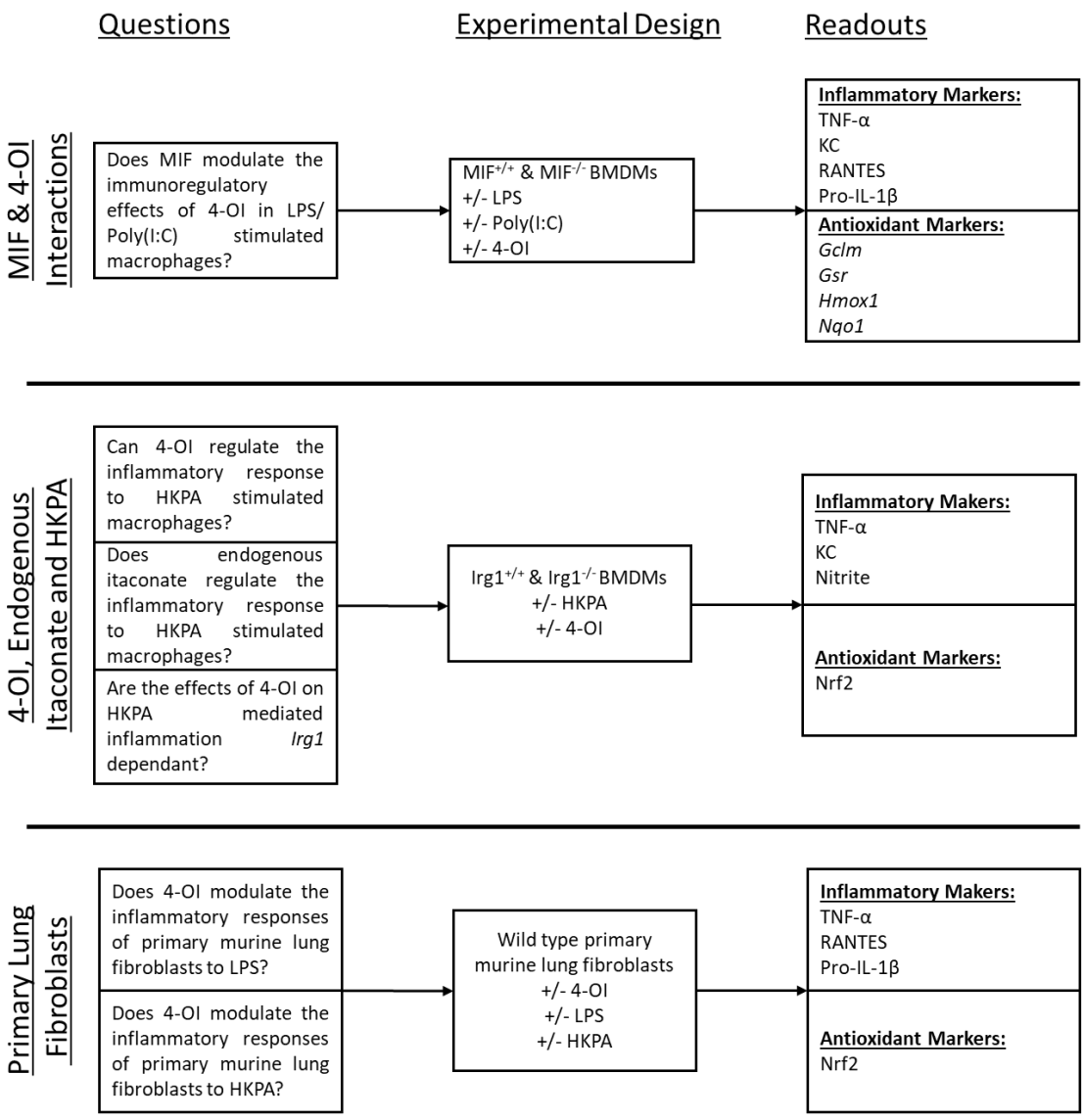

Figure 4.2. Overview of the experimental design for Chapter 4.

4.2 MIF does not regulate the effects of 4-OI on LPS stimulated bone marrow derived macrophages.

Here, we investigated the effect of MIF on the immunoregulatory effects of itaconate. MIF is a key regulator of innate immunity, while Irg1 mRNA expression and itaconate production are significantly upregulated in both human and murine activated macrophages (124, 180, 182, 330, 351, 358, 359, 364-367). MIF has been shown to regulate TLR4 expression, which induces Irg1 expression when stimulated with LPS (182, 351). Furthermore, MIF is required for HIF-1α stabilisation, a key protein involved in the immunoregulatory effects of 4-OI (193, 194, 330, 339). LPS stimulation of macrophages results in enhanced glycolysis and the induction a pro-inflammatory phenotype, with concurrent *Irg1* expression and itaconate expression, in a HIF-1α dependant manner (185, 330, 428). As such, we hypothesised that MIF may play a mechanistic role in the immunomodulatory effects of itaconate and 4-OI.

4.2.1 4-OI modulates LPS induced TNF-α and KC protein production in BMDMs from MIF$^{+/+}$ and MIF$^{-/-}$ mice.

Here, we examined the effects of 4-OI on LPS induced TNF-α and KC protein production in MIF$^{+/+}$ and MIF$^{-/-}$ BMDMs. 4-OI is cell permeable derivative of itaconate and has been shown to limit LPS induced IL-1β , while having no effect on TNF-α protein expression in MIF$^{+/+}$ BMDMs (330).

Here, we demonstrated that LPS (100 ng/ml) stimulation for 24 hours significantly increased TNF-α protein production in both MIF$^{+/+}$ and MIF$^{-/-}$ BMDMs compared with DMSO treatment (*** p<0.001, **Figure 4.3A, B**). Furthermore, treatment with 4-OI (125 μM) had no effect on LPS mediated TNF-α protein production in both MIF$^{+/+}$ and MIF$^{-/-}$ BMDMs compared with LPS treatment (**Figure 4.3A, B**). LPS stimulation for 24 hours also significantly increased KC protein production in both MIF$^{+/+}$ (*** p<0.001, **Figure 4.3C**) and MIF$^{-/-}$ BMDMs (** p<0.01, **Figure 4.3D**) compared with DMSO treatment. 4-OI treatment significantly increased LPS mediated KC protein production

compared with LPS in $MIF^{+/+}$ (+ p<0.05, **Figure 4.3C**) and $MIF^{-/-}$ BMDMs (++ p<0.01, **Figure 4.3D**) compared with LPS treatment.

4.2.2 LPS stimulation induces Irg1 mRNA expression, while 4-OI regulates LPS induced RANTES and IL-1β mRNA expression in BMDMs from $MIF^{+/+}$ and $MIF^{-/-}$ mice.

Here, we demonstrated that LPS (100 ng/ml) stimulation induced significant RANTES mRNA expression in $MIF^{+/+}$ (*** p<0.001, **Figure 4.4A**) and $MIF^{-/-}$ BMDMS (*** p<0.001, **Figure 4.4B**) compared with DMSO treatment after 24 hours of stimulation. 4-OI (125 µM) treatment significantly inhibited LPS induced RANTES compared with LPS in $MIF^{+/+}$ BMDMs (+ p<0.05, **Figure 4.4A**) and $MIF^{-/-}$ cells (+ p<0.05, **Figure 4.4B**) compared with LPS treatment.

LPS stimulation for 24 hours significantly increased IL-1β mRNA expression in both $MIF^{+/+}$ (*** p<0.001, **Figure 4.4C**) and $MIF^{-/-}$ BMDMs (***** p<0.05, **Figure 4.4D**) compared with DMSO. Treatment with LPS and 4-OI significantly decreased LPS induced IL-1β mRNA expression compared with LPS in $MIF^{+/+}$ (+ p<0.05, **Figure 4.4C**) and $MIF^{-/-}$ BMDMs (+ p<0.05, **Figure 4.4D**).

We also demonstrated that LPS stimulation significantly increased expression of Irg1 mRNA in $MIF^{+/+}$ BMDMs after 24 hours (*** p<0.001, **Figure 4.4E**). Furthermore, we demonstrated that LPS stimulation significantly increased expression of Irg1 mRNA in $MIF^{-/-}$ BMDMs after 24 hours (*** p<0.001, **Figure 4.4F**).

4.2.3 Regulation of Gclm, Gsr, Hmox1 and Nqo1 mRNA expression by 4-OI in LPS stimulated BMDMs from $MIF^{+/+}$ and $MIF^{-/-}$ mice.

Previously, 4-OI has been shown to promote Nrf2 expression levels and subsequently induce expression of antioxidant genes including Gclm, Gsr, Hmox1 and Nqo1 which are downstream of Nrf2 (330, 429).

Here, we demonstrated that treatment of $MIF^{+/+}$ BMDMs with 4-OI (125 μM) for 24 hours increased the expression of Gclm mRNA (**Figure 4.5A**), Gsr mRNA (**Figure 4.5C**), Hmox1 mRNA (**Figure 4.5E**) and Nqo1 mRNA (**Figure 4.5G**) compared with DMSO treatment, although this increase was not significant. A similar trend was observed in $MIF^{-/-}$ BMDMs whereby 4-OI increased expression of Gclm mRNA (**Figure 4.5B**), Hmox1 mRNA (**Figure 4.5F**) and Nqo1 mRNA (**Figure 4.5H**), although this was not significant compared with DMSO treatment. Gsr mRNA expression was significantly increased in 4-OI treated $MIF^{-/-}$ BMDMs compared with DMSO (* $p<0.05$, **Figure 4.5D**). Co-stimulation with LPS (100 ng/ml) and 4-OI significantly increased expression of Gclm (+ $p<0.05$, **Figure 4.5A**) and Nqo1 (+ $p<0.05$, **Figure 4.5G**) mRNA in $MIF^{+/+}$ BMDMs compared with LPS. Nqo1 mRNA expression was also significantly increased in $MIF^{-/-}$ BMDMs treated with 4-OI and LPS compared with LPS (+ $p<0.05$, **Figure 4.5H**).

These results demonstrated that MIF does not regulate Irg1 mRNA expression or play a role in 4-OI mediated responses to LPS.

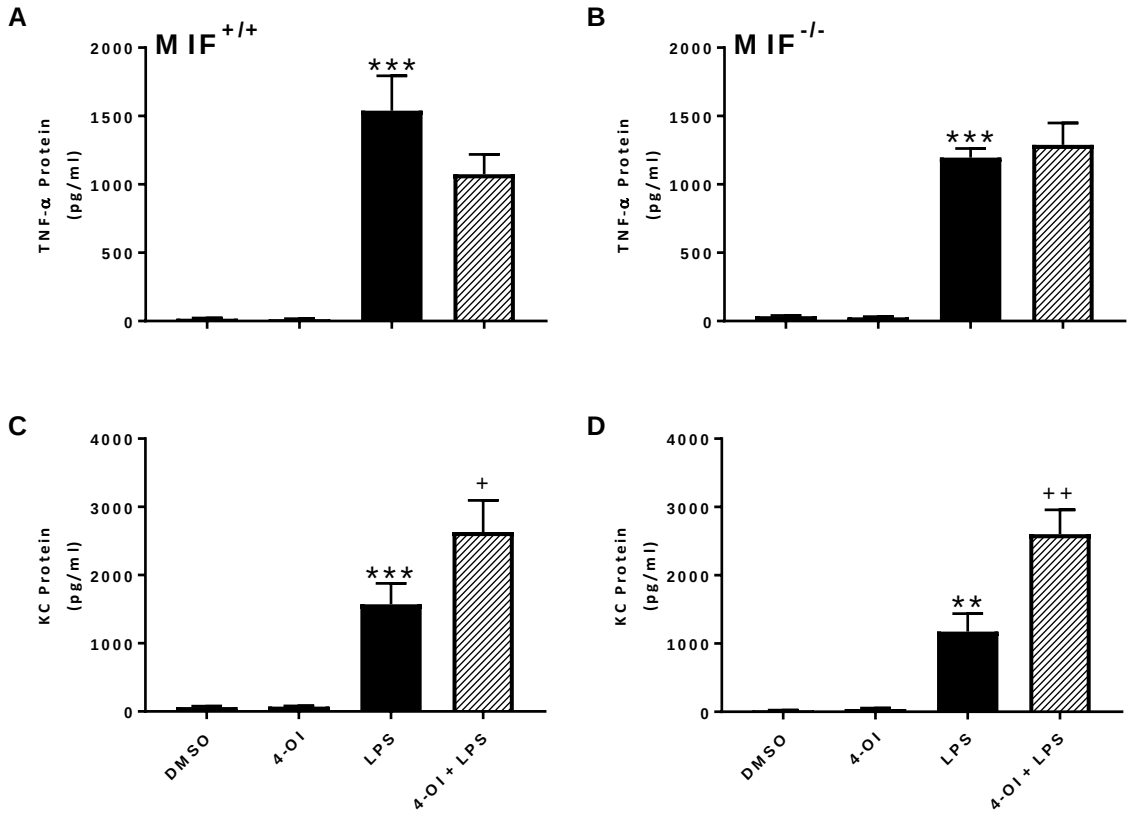

Figure 4.3. Effect of 4-OI on LPS induced TNF-α and KC protein production in BMDMs from MIF$^{+/+}$ and MIF$^{-/-}$ mice.

BMDMs from MIF$^{+/+}$ and MIF$^{-/-}$ mice were stimulated with LPS (100 ng/ml) in the presence or absence of 4-OI (125 µM) for 24 hours. Protein production was measured by ELISA. TNF-α protein was measured in supernatant from (**A**) MIF$^{+/+}$ and (**B**) MIF$^{-/-}$ BMDMs. KC protein was measured in supernatant from (**C**) MIF$^{+/+}$ and (**D**) MIF$^{-/-}$ BMDMs. Data is presented as mean ± SEM of 3 independent experiments with 3 technical replicates. A One-way ANOVA with a Tukey's multiple comparison post-hoc test was used to test for statistical differences. ** p< 0.01, *** p<0.001; respective treatment compared with DMSO. + p<0.05, ++ p<0.01; respective treatment compared with LPS.

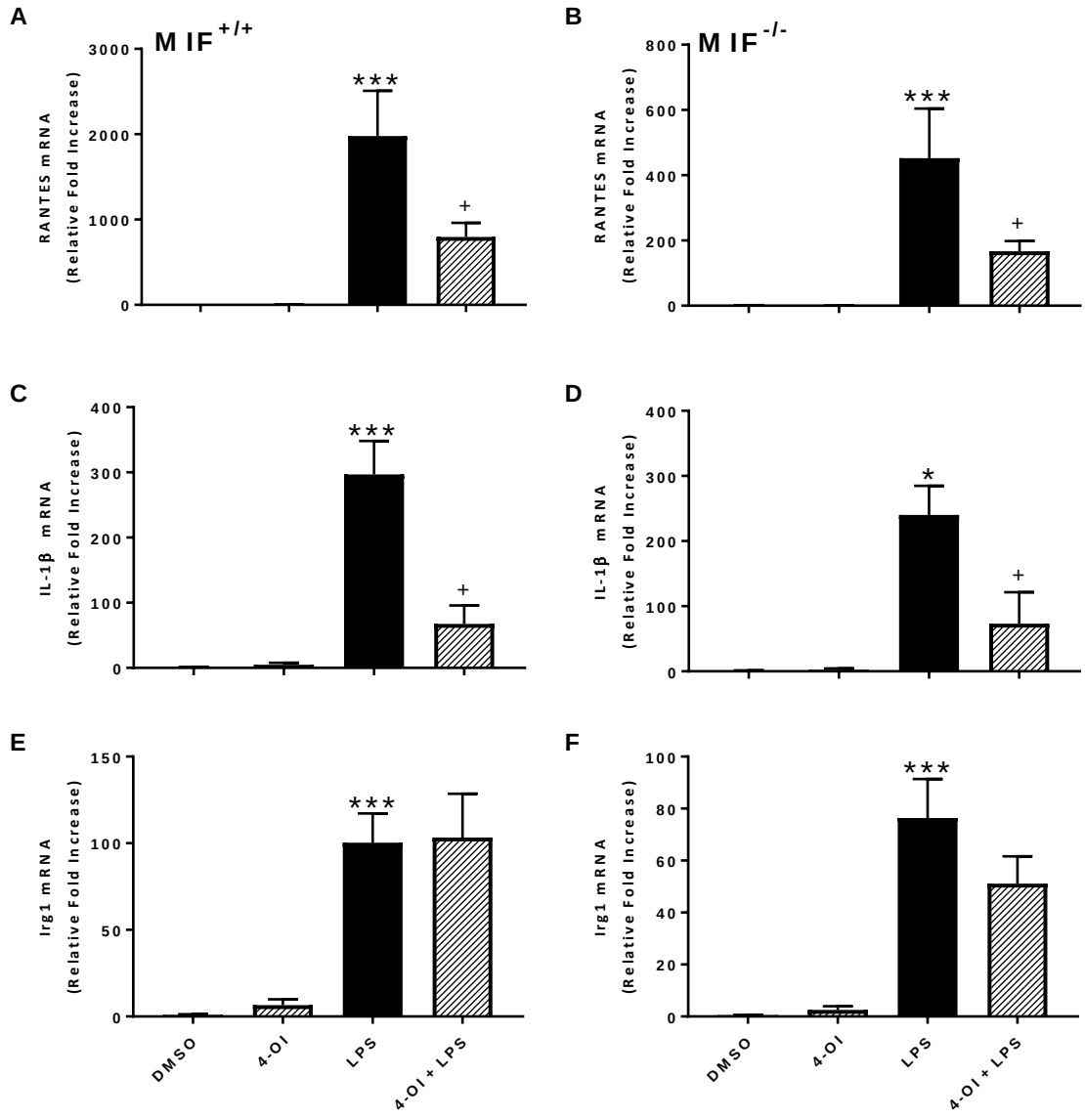

Figure 4.4. Effect of 4-OI on LPS induced RANTES, IL-1β and Irg1 mRNA expression in BMDMs from MIF$^{+/+}$ and MIF$^{-/-}$ mice.

BMDMs from MIF$^{+/+}$ and MIF$^{-/-}$ mice were stimulated with LPS (100 ng/ml) in the presence or absence of 4-OI (125 µM) for 24 hours. mRNA levels were quantified using qPCR analysis. RANTES mRNA levels were measured in (**A**) MIF$^{+/+}$ and (**B**) MIF$^{-/-}$ BMDMs. IL-1β mRNA was measured in (**C**) MIF$^{+/+}$ and (**D**) MIF$^{-/-}$ BMDMs. Irg1 mRNA was measured in (**E**) MIF$^{+/+}$ and (**F**) MIF$^{-/-}$ BMDMs. mRNA levels were standardised per unit of β-actin. Results are expressed as a relative fold increase compared with DMSO. Data is presented as mean ± SEM of 3 independent experiments with 3 technical replicates. (**A, B, E, F**) A One-way ANOVA with a Tukey's multiple comparison post-hoc test was used to test for statistical differences (**C, D**) A Kruskal-Wallis test with Dunn's multiple comparison post-hoc test was used to test for statistical differences. * $p<0.05$, *** $p<0.001$; respective treatment compared with DMSO. + $p<0.05$; respective treatment compared with LPS.

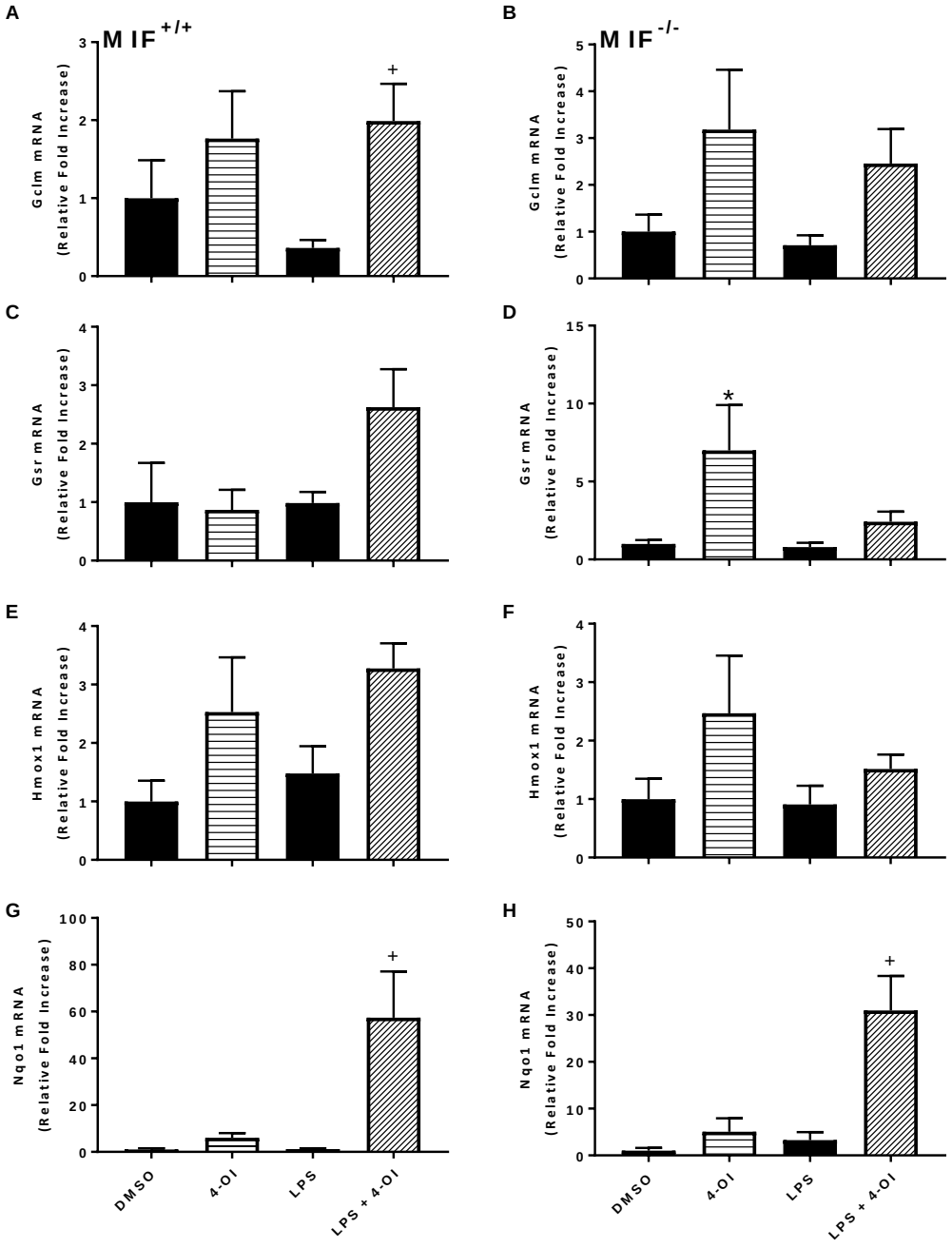

Figure 4.5. Effect of 4-OI on Gclm, Gsr, Hmox1 and Nqo1 mRNA expression in LPS stimulated BMDMs from MIF$^{+/+}$ and MIF$^{-/-}$ mice.

BMDMs from MIF$^{+/+}$ and MIF$^{-/-}$ mice were stimulated with LPS (100 ng/ml) in the presence or absence of 4-OI (125 µM) for 24 hours. mRNA levels were quantified using qPCR analysis. mRNA levels of (**A, B**) *Gclm*, (**C, D**) *Gsr*, (**E, F**) *Hmox1* and (**G, H**) *Nqo1* in MIF$^{+/+}$ and MIF$^{-/-}$ BMDMs. mRNA levels were standardised per unit of β-actin. Results are expressed as a relative fold increase compared with DMSO. Data is presented as mean ± SEM of 3 independent experiments with 3 technical replicates. (**A, E, F**) A Kruskal-Wallis test with Dunn's multiple comparison post-hoc test was used to test for statistical differences. (**D**) A One-way ANOVA with a Tukey's multiple comparison post-hoc test was used to test for statistical differences. * $p<0.05$: respective treatment compared with DMSO. + $p<0.05$: respective treatment compared with LPS.

4.3 MIF does not regulate the effects of 4-OI on poly(I:C) stimulated BMDMs.

Here, we investigated the effect of MIF on the immunoregulatory effects of itaconate in poly(I:C) stimulated macrophages. MIF is a key regulator of the inflammatory response, while Irg1 mRNA expression and itaconate production are significantly upregulated in poly(I:C) stimulated macrophages (124, 180, 182, 330, 358). We hypothesised that MIF may play a role in the immunoregulatory effects of itaconate in poly(I:C) stimulated macrophages.

4.3.1 Poly(I:C) stimulation induces Irg1 mRNA expression, while 4-OI regulates poly(I:C) induced RANTES and IL-1β mRNA expression in BMDMs from $MIF^{+/+}$ and $MIF^{-/-}$ mice.

We examined the effects of 4-OI on poly(I:C) induced RANTES and IL-1β mRNA expression. Here, we demonstrated that poly(I:C) (10 μg/ml) stimulation for 24 hours significantly increased RANTES mRNA expression in $MIF^{+/+}$ (*** p<0.001, **Figure 4.6A**) and $MIF^{-/-}$ BMDMS (** p<0.01, **Figure 4.6B**) compared with DMSO treatment. 4-OI (125 μM) significantly inhibited poly(I:C) induced RANTES in $MIF^{+/+}$ BMDMs (+++ p<0.001, **Figure 4.6A**) compared with poly(I:C), but not in $MIF^{-/-}$ BMDMs (**Figure 4.6B**).

Poly(I:C) stimulation also significantly increased IL-1β mRNA expression in both $MIF^{+/+}$ (** p<0.01, **Figure 4.6C**) and $MIF^{-/-}$ BMDMs (** p<0.01, **Figure 4.6D**) compared with DMSO treatment. 4-OI significantly decreased poly(I:C) mediated IL-1β mRNA expression compared with poly(I:C) in $MIF^{+/+}$ (+ p<0.05, **Figure 4.6C**) and $MIF^{-/-}$ BMDMs (+ p<0.05, **Figure 4.6D**).

We also demonstrated that poly(I:C) stimulation significantly increased expression of Irg1 mRNA in $MIF^{+/+}$ BMDMs after 24 hours (*** p<0.001, **Figure 4.6E**) compared with medium. Furthermore, poly(I:C) stimulation significantly increased expression of Irg1 mRNA in $MIF^{-/-}$ BMDMs after 24 hours (** p<0.01, **Figure 4.6F**).

4.3.2 Regulation of Gclm, Gsr, Hmox1 and Nqo1 mRNA expression by 4-OI in poly(I:C) stimulated BMDMs from MIF$^{+/+}$ and MIF$^{-/-}$ mice

As previously mentioned, 4-OI has been shown to promote Nrf2 expression levels and subsequently induce expression of antioxidant genes including Gclm, Gsr, Hmox1 and Nqo1 which are downstream of Nrf2 (330, 429).

We examined the ability of 4-OI to upregulate the expression antioxidant genes which are downstream of Nrf2 in poly(I:C) stimulated macrophages. Stimulation of BMDMs with poly(I:C) and 4-OI significantly increased expression of Gclm mRNA compared with poly(I:C) alone in MIF$^{+/+}$ (+ $p<0.05$, **Figure 4.7A**) and MIF$^{-/-}$ cells (+ $p<0.05$, **Figure 4.7B**). Similarly, stimulation of MIF$^{+/+}$ and MIF$^{-/-}$ BMDMs with poly(I:C) and 4-OI increased expression of Gsr mRNA(**Figure 4.7C, D**) , Hmox1 mRNA(**Figure 4.7E, F**) and Nqo1 mRNA (**Figure 4.7G, H**) compared with poly(I:C) treatment, although this was not significant.

These results demonstrated that MIF does regulate Irg1 mRNA expression or play a role 4-OI mediated response to poly(I:C).

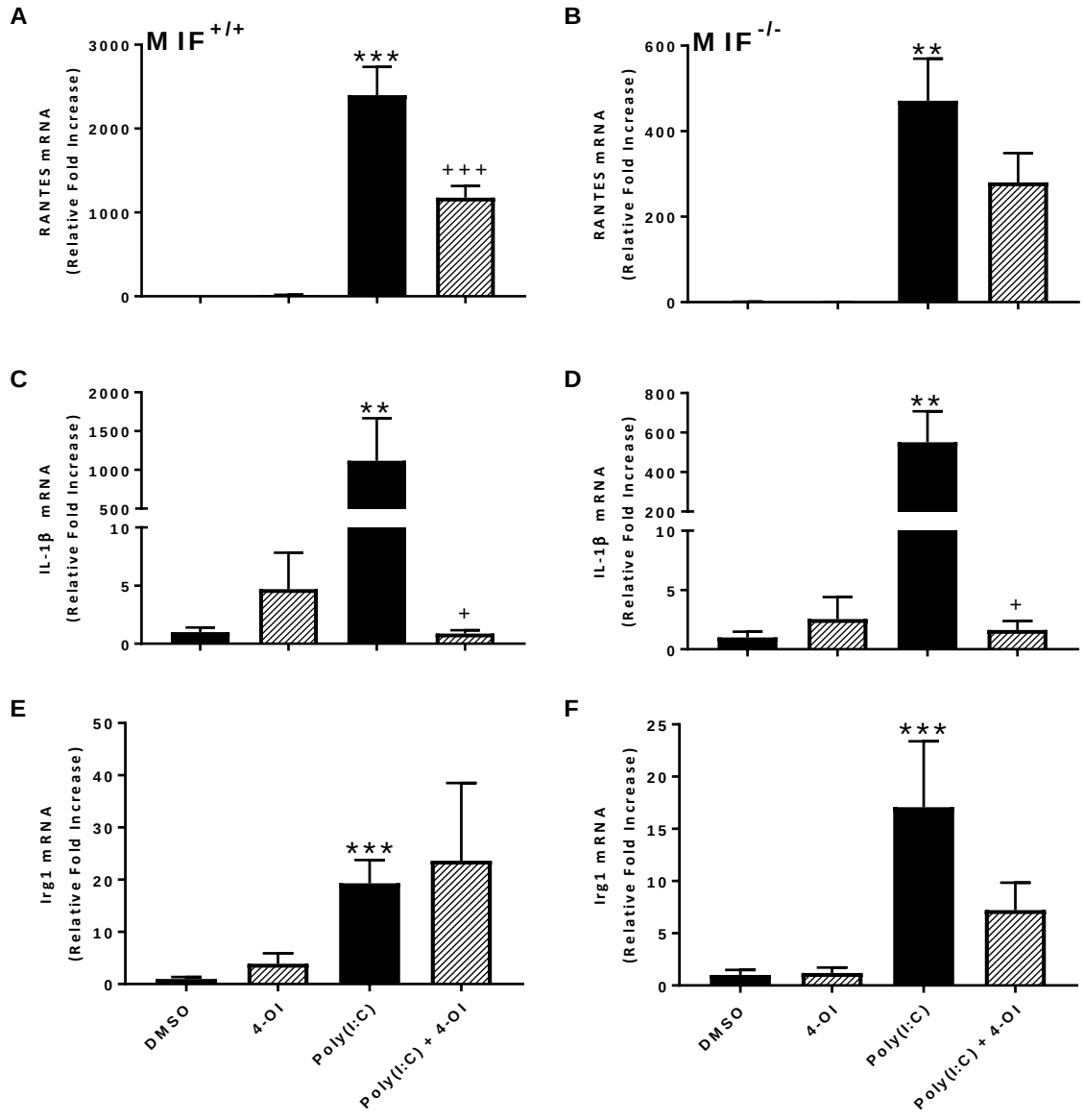

Figure 4.6. Effect of 4-OI on poly(I:C) induced RANTES, IL-1β and Irg1 mRNA expression in BMDMs from MIF$^{+/+}$ and MIF$^{-/-}$ mice.

BMDMs from MIF$^{+/+}$ and MIF$^{-/-}$ mice were stimulated with poly(I:C) (10 µg/ml) in the presence or absence of 4-OI (125 µM) for 24 hours. mRNA levels were quantified using qPCR analysis. RANTES mRNA levels were measured in (**A**) MIF$^{+/+}$ and (**B**) MIF$^{-/-}$ BMDMs. IL-1β mRNA was measured in (**C**) MIF$^{+/+}$ and (**D**) MIF$^{-/-}$ BMDMs. Irg1 mRNA was measured in (**E**) MIF$^{+/+}$ and (**F**) MIF$^{-/-}$ BMDMs mRNA levels were standardised per unit of β-actin. Results are expressed as a relative fold increase compared with DMSO. Data is presented as mean ± SEM of 3 independent experiments with 3 technical replicates. (**A**) A One-way ANOVA with a Tukey's multiple comparison post-hoc test was used to test for statistical differences. (**B-F**) A Kruskal-Wallis test with Dunn's multiple comparison post-hoc test was used to test for statistical differences. ** p< 0.01, *** p<0.001; respective treatment compared with DMSO. + p<0.05, +++ p<0.001; respective treatment compared with poly(I:C).

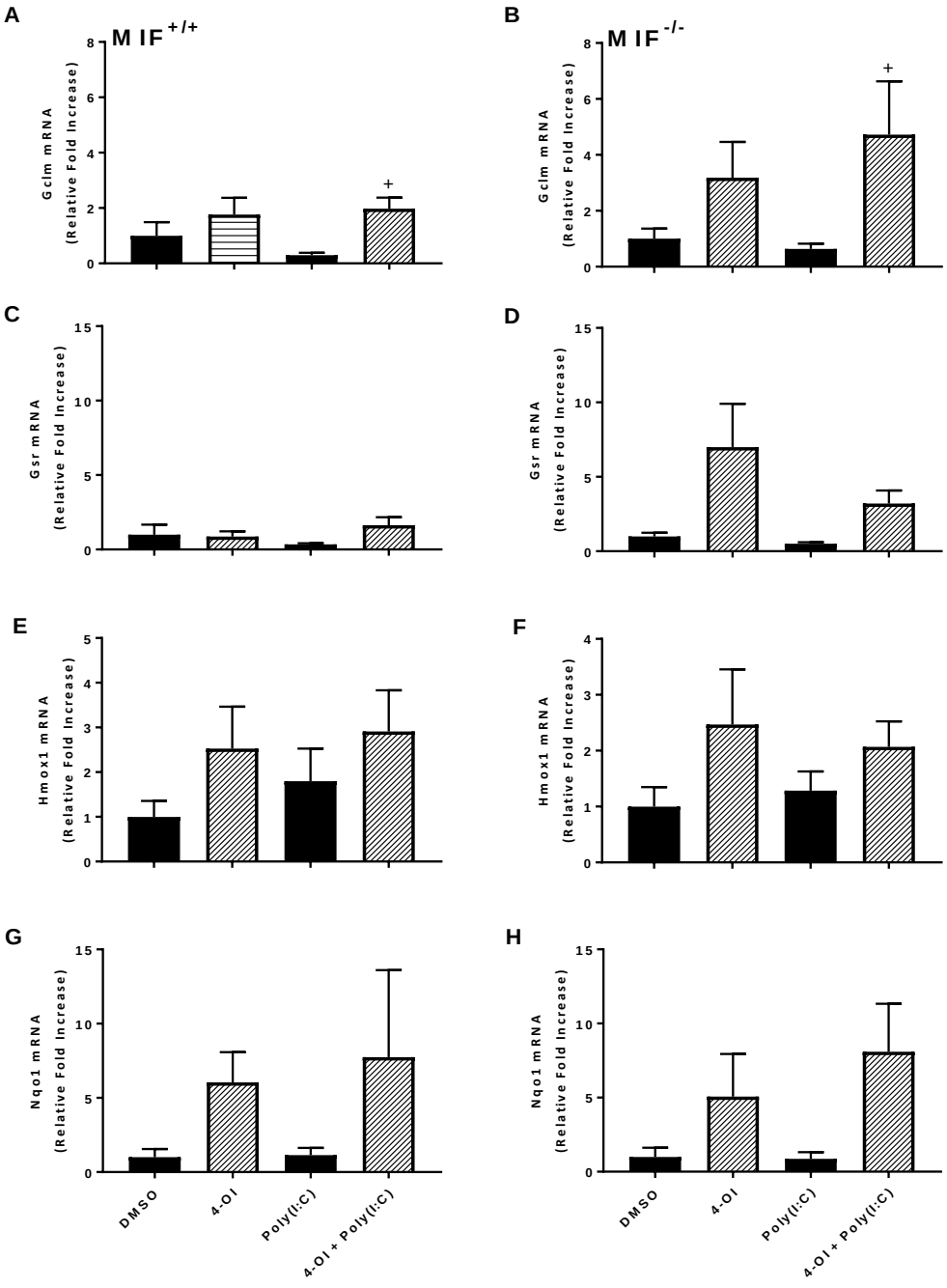

Figure 4.7. Effect of 4-OI on Gclm, Gsr, Hmox1 and Nqo1 mRNA expression in poly(I:C) stimulated BMDMs from MIF$^{+/+}$ and MIF$^{-/-}$ mice.

BMDMs from MIF$^{+/+}$ and MIF$^{-/-}$ mice were stimulated with poly(I:C) (10 µg/ml) in the presence or absence of 4-OI (125 µM) for 24 hours. mRNA levels were quantified using qPCR analysis. mRNA levels of (**A, B**) Gclm, (**C, D**) Gsr, (**E, F**) Hmox1 and (**G, H**) Nqo1 in MIF$^{+/+}$ and MIF$^{-/-}$ BMDMs. mRNA levels were standardised per unit of β-actin. Results are expressed as a relative fold increase compared with DMSO. Data is presented as mean ± SEM of 3 independent experiments with 3 technical replicates. (**A**) A Kruskal-Wallis test with Dunn's multiple comparison post-hoc test was used to test for statistical differences. (**B**) A One-way ANOVA with a Tukey's multiple comparison post-hoc test was used to test for statistical differences. + $p<0.05$; respective treatment compared with poly(I:C).

4.4 Time course to investigate the effects of 4-OI on the production of TNF-α and RANTES in HKPA stimulated RAW 264.7 cells.

As 4-OI has been shown by us and others to modulate the inflammatory response to LPS and poly(I:C) (**Figure 4.3 - Figure 4.7**), we were interested in examining the immunomodulatory effects of 4-OI in the context of HKPA stimulation. Here, we investigated the cytokine response of RAW 264.7 macrophages to HKPA stimulation, a TLR2 and TLR5 agonist, and the modulation of these cytokines by 4-OI. RAW 264.7 cells were used for preliminary experiments before progressing to BMDMs.

TNF-α is a pro-inflammatory cytokine that plays an important role in the immune response with effector functions including apoptosis, cell activation, induction of inflammatory cytokine production and recruitment of inflammatory cells to sites of infection (430). RANTES is a chemokine that recruits immune cells to sites of infection to promote pathogen clearance, but also inflammation (400, 401).

TNF-α and RANTES protein levels were analysed by ELISA at 6 and 24 hours following stimulation with HKPA (MOI 100) in the presence or absence of 4-OI (125 μM). Stimulation with HKPA induced TNF-α protein production at 6 and 24 hours, which was abrogated in cells stimulated with HKPA and 4-OI together at both 6 and 24 hours (**Figure 4.8A**). TNF-α protein production was significantly induced by HKPA compared with DMSO (*** $p<0.001$, **Figure 4.8A**), while 4-OI inhibited HKPA mediated TNF-α protein production (++ $p<0.01$, **Figure 4.8A**). Similarly, stimulation with HKPA induced RANTES protein production at 6 and 24 hours, with 4-OI inhibiting HKPA induced RANTES protein production at 24 hours in cells treated with both 4-OI and HKPA (**Figure 4.8B**). RANTES protein production was significantly induced by HKPA compared with DMSO treatment (*** $p<0.001$, **Figure 4.8B**), while 4-OI inhibited HKPA mediated RANTES protein production (+ $p<0.05$, **Figure 4.8B**).

These results demonstrate for the first time that 4-OI modulates the induction of pro-inflammatory cytokines by HKPA in RAW 264.7 cells.

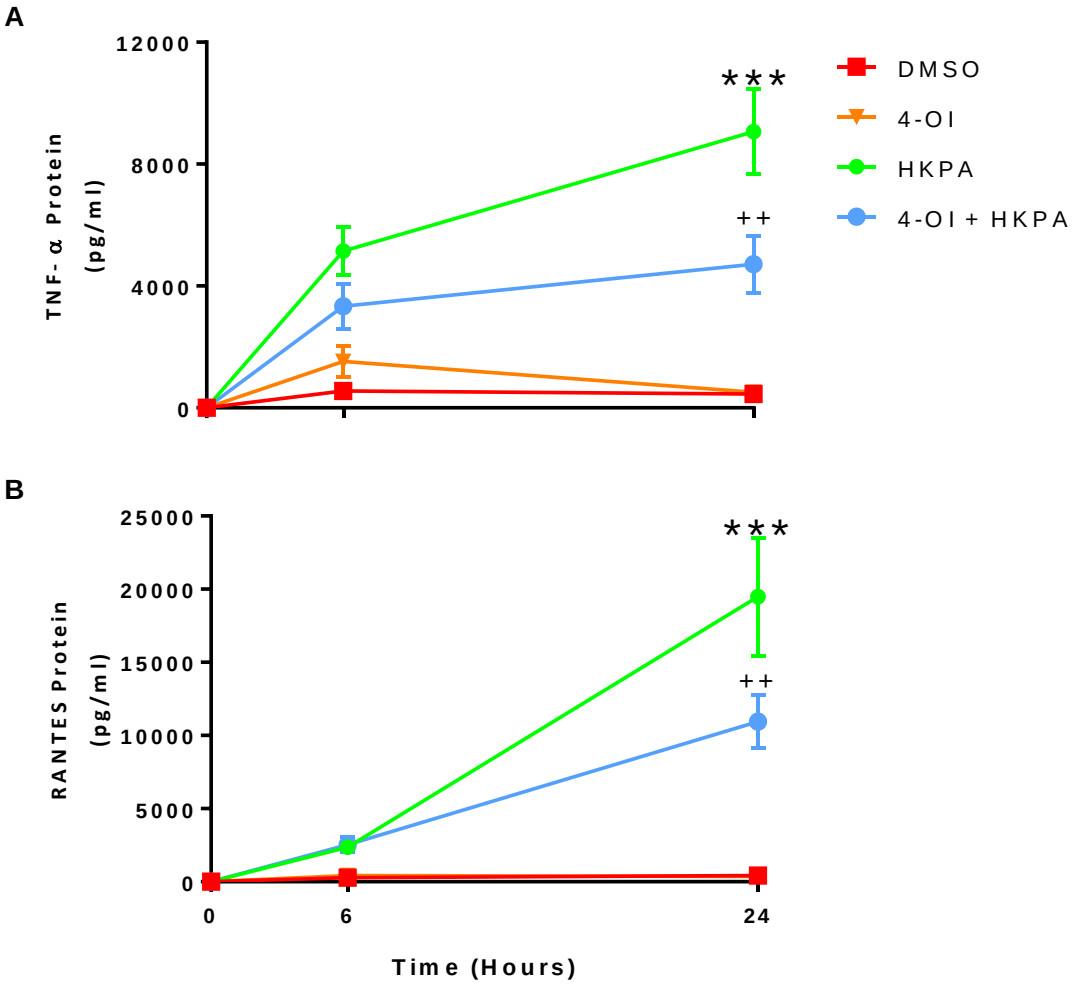

Figure 4.8. Time course of TNF-α and RANTES protein production by RAW 264.7 macrophages following HKPA and 4-OI treatment.

Secreted levels of (**A**) TNF-α and (**B**) RANTES from RAW 264.7 macrophages were assessed at 6 and 24 hours. Protein production was quantified by ELISA. Data is presented as mean ± SEM of 3 independent experiments with 3 technical replicates. [DMSO (red), 4-OI (orange), HKPA (green) and HKPA + 4-OI (blue); 4-OI, 125 µM; HKPA, MOI 100]. A One-way ANOVA with a Tukey's multiple comparison post-hoc test was used to test for statistical differences. *** $p<0.001$; HKPA compared with DMSO at 24 hours. + $p<0.05$, ++ $p<0.01$; HKPA compared with 4-OI + HKPA at 24 hours.

4.5 Regulation of the responses of BMDMs to HKPA stimulation by endogenous itaconate and 4-OI.

We have established that 4-OI can modulate the inflammatory response to HKPA stimulation in RAW 264.7 cells (**Figure 4.8**). Next, we examined the role of endogenous itaconate and 4-OI in the modulation of the inflammatory response to LPS and HKPA using BMDMs from $Irg1^{+/+}$ and $Irg1^{-/-}$ mice.

4.5.1 4-OI, but not endogenous itaconate, modulates LPS induced nitrite, TNF-α and KC protein production in BMDMs from $Irg1^{+/+}$ and $Irg1^{-/-}$ mice.

Here, we showed that LPS (100 ng/ml) stimulation induced significant TNF-α protein production in $Irg1^{+/+}$ (*** p<0.001, **Figure 4.9A**) and $Irg1^{-/-}$ (*** p<0.001, **Figure 4.9B**) BMDMs following 24 hours of stimulation, as expected. Treatment of cells with 4-OI (250 μM) significantly inhibited LPS induced TNF-α protein production in $Irg1^{+/+}$ (++ p<0.01, **Figure 4.9A**) and $Irg1^{-/-}$ BMDMs (++ p<0.01, **Figure 4.9B**) compared with LPS following 24 hours of stimulation. Levels of TNF-α induced by LPS were very similar in both genotypes.

LPS stimulation also induced significant KC protein production in $Irg1^{+/+}$ (*** p<0.001, **Figure 4.9C**) and $Irg1^{-/-}$ (*** p<0.001, **Figure 4.9D**) BMDMs following 24 hours of stimulation compared with DMSO treatment. Treatment of cells with 4-OI significantly enhanced LPS induced KC protein production in $Irg1^{+/+}$ (+++ p<0.001, **Figure 4.9C**) and $Irg1^{-/-}$ BMDMs (+++ p<0.001, **Figure 4.9D**) following 24 hours of stimulation, in line with our previous data (**Figure 4.3**). As with TNF-α, KC protein levels were similar across the two genotypes.

We next examined the induction of nitrite production following LPS stimulation. Nitrite quantification is used as a method of indirectly quantifying reactive nitrogen species as nitrite is formed from the oxidisation of nitric oxide (NO) (431). NO mediates cytotoxic and inflammatory effects trough the formation of peroxynitrite and

subsequent oxidative reactions with lipids, DNA and proteins (432). As expected, LPS significantly induced nitrite production in $Irg1^{+/+}$ BMDMs following 24 hours of stimulation compared with DMSO treatment (*** p<0.001, **Figure 4.9E**). 4-OI treatment significantly inhibited LPS induced nitrite production in $Irg1^{+/+}$ BMDMs after 24 hour stimulation compared with LPS (+++ p<0.001, **Figure 4.9E**). This data is in agreement with published data which demonstrated 4-OI-mediated inhibition of LPS-induced nitrite production (330). These authors hypothesised that 4-OI limited the production of nitrite, a reactive nitrogen species, due to upregulation of antioxidant genes as a result of Nrf2 induction (330). LPS stimulation also significantly induced nitrite production in $Irg1^{-/-}$ BMDMs following 24 hours of stimulation compared with DMSO treatment (*** p<0.001, **Figure 4.9F**), which was abrogated in cells simultaneously treated with LPS and 4-OI (+++ p<0.001, **Figure 4.9F**). Surprisingly, LPS induced notably higher levels of nitrite in $Irg1^{+/+}$ BMDMs compared with $Irg1^{-/-}$ BMDMs.

4.5.2 4-OI, but not endogenous itaconate, modulates HKPA induced nitrite, TNF-α and KC protein production in BMDMs from $Irg1^{+/+}$ and $Irg1^{-/-}$ mice.

We also examined the role endogenous itaconate in the modulation of the inflammatory response to HKPA. As we seen in RAW 264.7 cells (**Figure 4.8A**), HKPA (MOI 100) stimulation induced significant TNF-α protein production after 24 hours of stimulation in $Irg1^{+/+}$ BMDMs compared with DMSO (*** p<0.001, **Figure 4.10A**). Treatment of cells with 4-OI (250 μM) significantly inhibited HKPA induced TNF-α protein production in $Irg1^{+/+}$ BMDMs (+++ p<0.001, **Figure 4.10A**). Similarly, HKPA stimulation induced significant TNF-α protein production after 24 hours of stimulation in $Irg1^{-/-}$ BMDMs compared with DMSO (*** p<0.001, **Figure 4.10B**). Treatment of cells with 4-OI significantly inhibited HKPA induced TNF-α protein production in $Irg1^{-/-}$ BMDMs (+++ p<0.001, **Figure 4.10B**). In addition, protein production levels were notably similar within treatments between genotypes.

HKPA stimulation induced significant KC protein production in $Irg1^{+/+}$ (*** p<0.001, **Figure 4.10C**) and $Irg1^{-/-}$ (*** p<0.001, **Figure 4.10D**) BMDMs following 24

hours of stimulation compared with DMSO treatment. Treatment of cells with 4-OI significantly increased HKPA mediated KC protein production in $Irg1^{+/+}$ (+++ p<0.001, **Figure 4.10C**) and $Irg1^{-/-}$ BMDMs (+++ p<0.001, **Figure 4.10D**) following 24 hours of stimulation. As with TNF-α, KC protein levels were similar across the two genotypes.

HKPA stimulation significantly induced nitrite production in $Irg1^{+/+}$ BMDMs following 24 hours of stimulation compared with DMSO (*** p<0.001, **Figure 4.10E**). 4-OI treatment significantly inhibited HKPA induced nitrite production in $Irg1^{+/+}$ BMDMs after 24 hour stimulation (+++ p<0.001, **Figure 4.10E**). To our knowledge, this data is the first description of 4-OI inhibiting HKPA mediated nitrite production.

HKPA stimulation also significantly induced nitrite production in $Irg1^{-/-}$ BMDMs following 24 hours of stimulation compared with DMSO (** p<0.01, **Figure 4.10F**), which was abrogated in cells simultaneously treated with HKPA and 4-OI (250 μM) (++ p<0.01, **Figure 4.10F**). It is important to note that HKPA induced notably higher levels of nitrite in $Irg1^{+/+}$ BMDMs compared with $Irg1^{-/-}$ BMDMs, which was in agreement with our results observed in LPS stimulated cells.

4.5.3 4-OI induces Nrf2 protein expression and inhibits HKPA-induced pro-IL-1β protein expression in wild type BMDMs.

We next examined the effects of 4-OI on HKPA-induced Nrf2 and pro-IL-1β protein expression in wild type BMDMs. Here we demonstrated that 4-OI (250 μM) induced Nrf2 production after 24 hours of stimulation (**Figure 4.11A, B**). We also demonstrated for the first time that HKPA stimulation induced pro-IL-1β protein production, which was inhibited with 4-OI treatment after 24 hours (**Figure 4.11C, D**).

Overall, this data demonstrated that 4-OI modulated the production of both LPS and HKPA induced inflammatory mediators in both $Irg1^{+/+}$ and $Irg1^{-/-}$ BMDMs. However, our data suggested that endogenous itaconate does not play a major role in these responses.

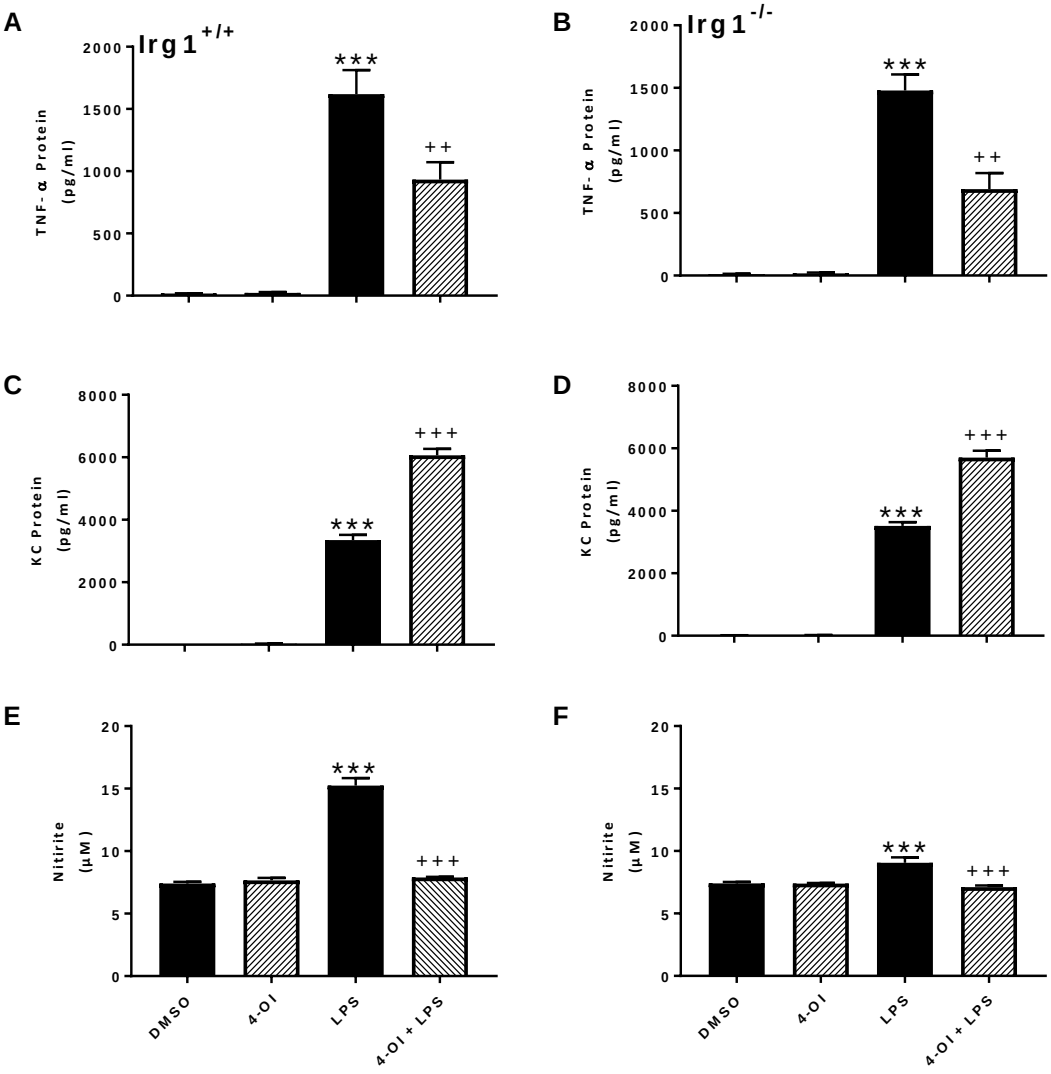

Figure 4.9. Effect of 4-OI on LPS induced nitrite, TNF-α and KC protein production in BMDMs from Irg1$^{+/+}$ and Irg1$^{-/-}$ mice.

BMDMs from Irg1$^{+/+}$ and Irg1$^{-/-}$ mice were stimulated with LPS (100 ng/ml) in the presence or absence of 4-OI (250 µM) for 24 hours. Protein expression was measured by ELISA. TNF-α protein production was measured in supernatant from (**A**) Irg1$^{+/+}$ and (**B**) Irg1$^{-/-}$ BMDMs. KC protein production was measured in supernatant from (**C**) Irg1$^{+/+}$ and (**D**) Irg1$^{-/-}$ BMDMs. Reactive nitrogen species were measured indirectly by quantifying nitrite production in supernatant using Griess reagent. Nitrite levels were measured in (**E**) Irg1$^{+/+}$ and (**F**) Irg1$^{-/-}$ BMDMs. Data is presented as mean ± SEM of 3 independent experiments with 3 technical replicates. A One-way ANOVA with a Tukey's multiple comparison post-hoc test was used to test for statistical differences. *** $p<0.001$; respective treatment compared with DMSO. ++ $p<0.01$, +++ $p<0.001$; respective treatment compared with LPS.

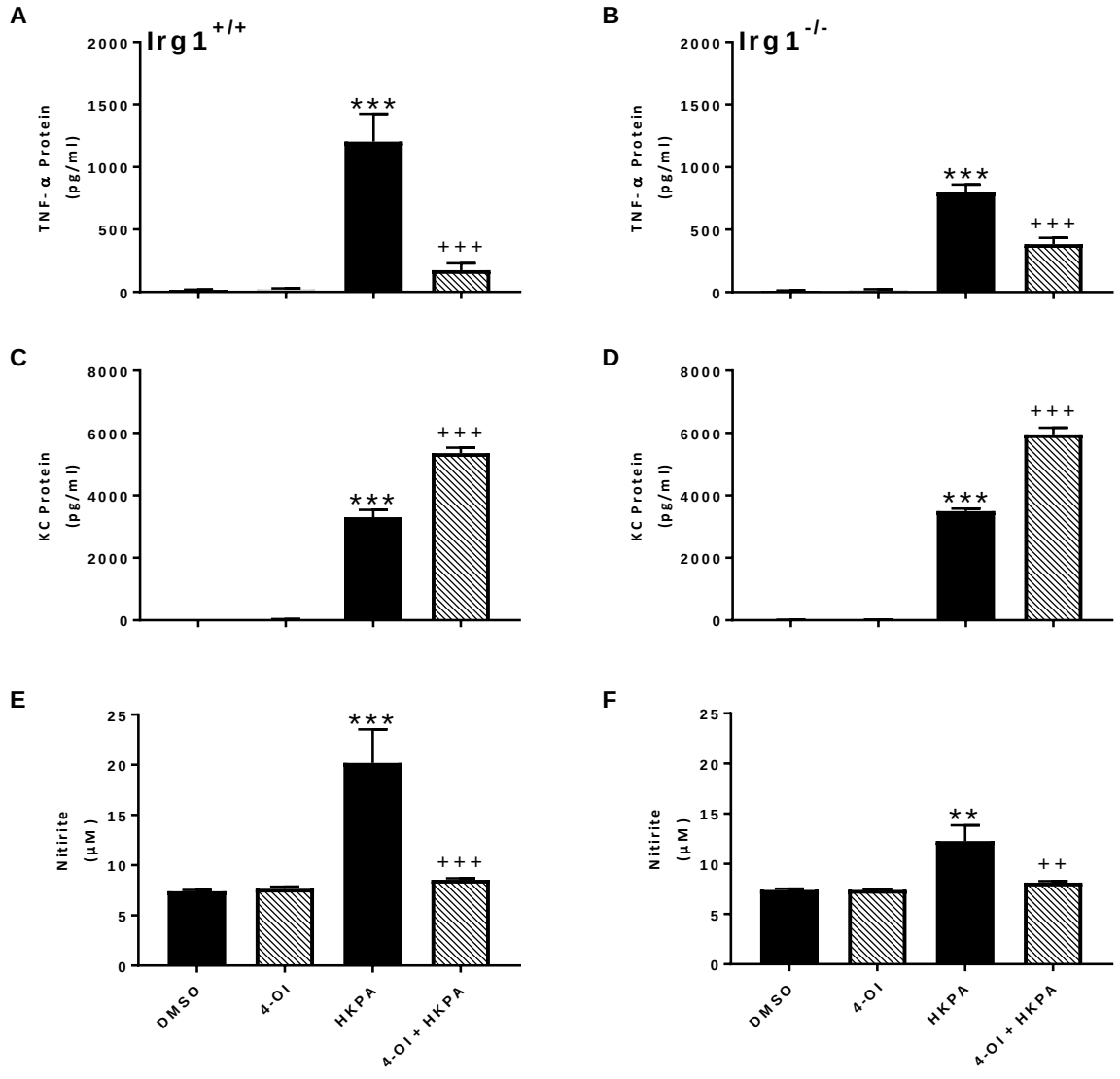

Figure 4.10. Effect of 4-OI on HKPA-induced nitrite, TNF-α and KC protein production in BMDMs from Irg1$^{+/+}$ and Irg1$^{-/-}$ mice.

BMDMs from Irg1$^{+/+}$ and Irg1$^{-/-}$ mice were stimulated with HKPA (MOI 100) in the presence or absence of 4-OI (250 µM) for 24 hours. Protein expression was measured by ELISA. TNF-α protein production was measured in supernatant from (**A**) Irg1$^{+/+}$ and (**B**) Irg1$^{-/-}$ BMDMs. KC protein production was measured in supernatant from (**C**) Irg1$^{+/+}$ and (**D**) Irg1$^{-/-}$ BMDMs. Reactive nitrogen species were measured indirectly by quantifying nitrite production in supernatant using Griess reagent. Nitrite levels were measured in (**E**) Irg1$^{+/+}$ and (**F**) Irg1$^{-/-}$ BMDMs. Data is presented as mean ± SEM of 3 independent experiments with 3 technical replicates. A One-way ANOVA with a Tukey's multiple comparison post-hoc test was used to test for statistical differences. ** p<0.01, *** p<0.001; respective treatment compared with DMSO. ++ p<0.01, +++ p<0.001; respective treatment compared with HKPA.

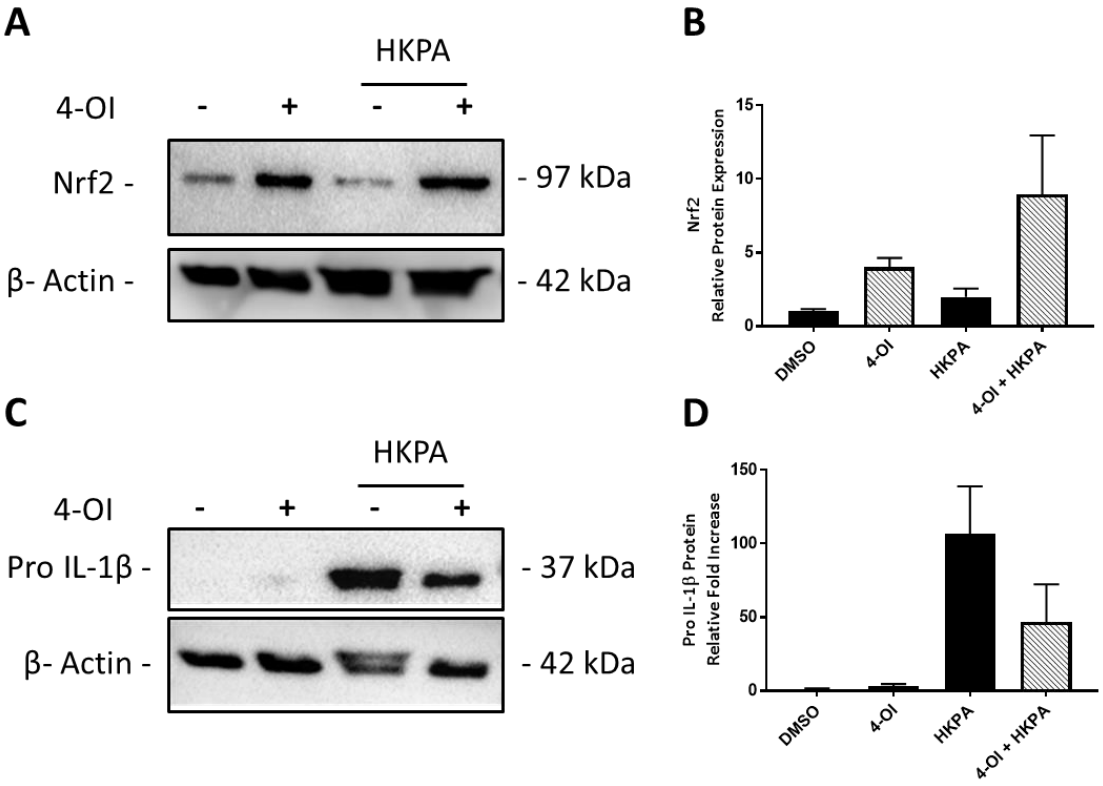

Figure 4.11. 4-OI induces Nrf2 protein expression and inhibits HKPA-induced pro-IL-1β protein expression in wild type BMDMs.

BMDMs from wild type mice were stimulated with HKPA (MOI 100) in the presence or absence of 4-OI (250 μM) for 24 hours. (**A, B**) Nrf2 and (**C, D**) pro-IL-1β protein levels were analysed by Western blot. Western blot image is representative of 3 independent experiments. ImageJ software was used to obtain densitometry data. For densitometry, protein levels were standardised per unit of β-actin. Results are expressed as a relative fold increase compared with DMSO. Data is presented as mean ± SEM of 3 independent replicates.

4.6 Investigation of the effects of a 4-OI concentration gradient on the responses of primary murine lung fibroblasts to LPS and HKPA stimulation

Lung fibroblasts function to produce and secrete the extracellular matrix (ECM) within the lung. The ECM is composed of a number of fibrous proteins, glycoproteins, and proteoglycans that form the non-cellular structure of the lung. The function of lung fibroblasts is to promote structural integrity and also wound healing and repair (433). The deposition of ECM results in the formation of stiff fibrotic scars which inhibit the efficiency of gaseous exchange (434). Chronic infection, inflammation and subsequent repair results in the development of scar tissue (433). In CF, chronic infection precedes the development of fibrosis impacting the gaseous exchange capabilities within the lung, resulting in the need for lung transplantation (435). Fibroblasts also play a role in promoting inflammation and can produce pro-inflammatory cytokines including TNF-α, IL-6, IL-8, RANTES and pro-IL-1β, contributing to inflammatory damage within the lung and subsequent fibrotic scar development (434, 436).

Here, we examined the inflammatory responses of primary lung fibroblasts from wild type mice to LPS and HKPA stimulation, and the respective effects of 4-OI on these responses.

4.6.1 4-OI regulates LPS-induced TNF-α and RANTES protein production in primary murine lung fibroblasts.

Here, we reported that LPS (100 ng/ml) induced significant TNF-α protein production in wild type primary lung fibroblasts after 24 hours of stimulation compared with DMSO (*** $p<0.001$, **Figure 4.12A**). We also report, for the first time, that 4-OI at all concentrations used (62.5, 125, 250 μM) significantly inhibited LPS induced TNF-α protein production compared with LPS alone (+++ $p<0.001$, **Figure 4.12A**). LPS stimulation also induced significant RANTES protein production in wild type primary lung fibroblasts after 24 hours of stimulation compared with DMSO (*** $p<0.001$, **Figure 4.12B**). In this instance, 4-OI did not modulate LPS induced RANTES protein production in wild type primary lung fibroblasts (**Figure 4.12B**).

4.6.2 4-OI regulates HKPA-induced TNF-α and RANTES protein production in induced in primary murine lung fibroblasts.

We also examined the induction of pro-inflammatory cytokines by HKPA in wild type primary lung fibroblasts. Here, we reported that HKPA (MOI 100) induced significant TNF-α protein production in primary lung fibroblasts after 24 hours of stimulation compared with DMSO (*** p<0.001, **Figure 4.13A**). Here we also reported, for the first time, that 4-OI (250 μM) inhibited HKPA mediated TNF-α protein production in wild type primary lung fibroblasts after 24 hours of stimulation compared with HKPA alone (+++ p<0.001, **Figure 4.13A**). HKPA stimulation also induced significant RANTES protein production in wild type primary lung fibroblasts after 24 hours of stimulation compared with DMSO (*** p<0.001, **Figure 4.13B**). HKPA mediated RANTES protein production was significantly inhibited upon treatment of cells with 62 μM, 125 μM and 250 μM 4-OI (+++ p<0.001, **Figure 4.13B**) respectively compared with HKPA alone.

4.6.3 4-OI regulates LPS-induced pro-IL-1β protein expression in primary murine lung fibroblasts.

LPS (100 ng/ml) stimulation significantly induced pro-IL-1β protein production in wild type primary lung fibroblasts after 24 hours of stimulation compared with DMSO (*** p<0.001, **Figure 4.14B**). We also report, for the first time, the significant inhibition of LPS mediated pro-IL-1β protein production by 125 μM (++ p<0.01, **Figure 4.14B**) and 250 μM (+++ p<0.001, **Figure 4.14B**) compared with LPS in primary lung fibroblasts. Stimulation with HKPA (MOI 100) for 24 hours did not induce any production of pro-IL-1β protein in wild type primary lung fibroblasts (**Figure 4.14B**).

4.6.4 4-OI induces Nrf2 protein expression in primary murine lung fibroblasts.

Finally, we examined Nrf2 protein production levels in wild type primary lung fibroblasts. Treatment of cells with 125 μM 4-OI significantly increased Nrf2 protein

production compared with DMSO (* p<0.05, **Figure 4.15A, B**), as did treatment with 250 µM (* p<0.05, **Figure 4.15A**, **B**). In LPS stimulated cells, 4-OI did not significantly increase Nrf2 protein expression (**Figure 4.15B**). In HKPA stimulated cells, treatment with 125 µM 4-OI significantly increased Nrf2 protein expression compared with HKPA alone (+ p<0.05, **Figure 4.15B**).

Overall, this data demonstrates that 4-OI can modulate the production of inflammatory cytokines and Nrf2 protein not only in innate immune cells, but also in structural cells of the lung.

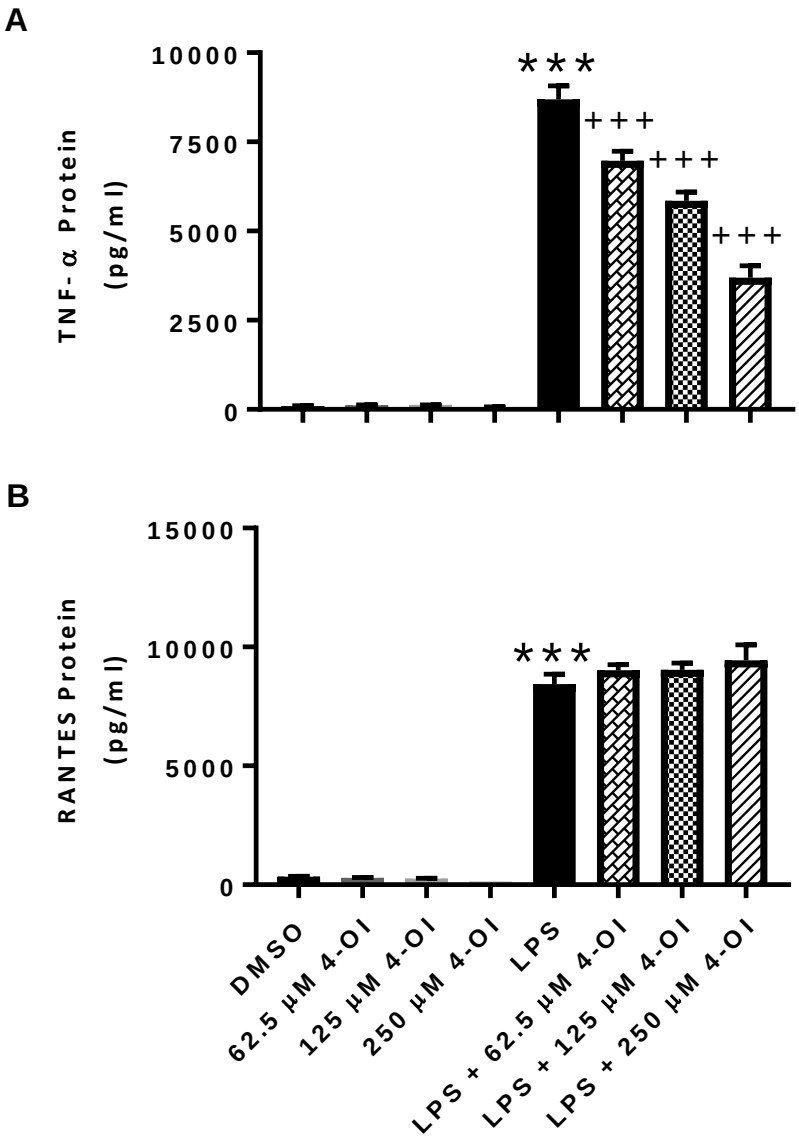

Figure 4.12. TNF-α and RANTES protein production is in induced in LPS stimulated primary murine lung fibroblasts, while 4-OI modulates LPS induced TNF-α expression.

Stimulation of primary murine lung fibroblasts with LPS (100 ng/ml) induces (**A**) TNF-α and (**B**) RANTES protein production respectively following 24 hours of stimulation. 4-OI (62.5, 125, 250 µM) treatment significantly inhibits (**A**) LPS induced TNF-α protein expression, but not (**B**) RANTES following 24 hours of treatment. Protein production was quantified by ELISA. Data is presented as mean ± SEM of 3 independent experiments with 3 technical replicates. A One-way ANOVA with a Tukey's multiple comparison post-hoc test was used to test for statistical differences. *** $p<0.001$: DMSO compared with LPS; +++ $p<0.001$: respective treatment compared with LPS.

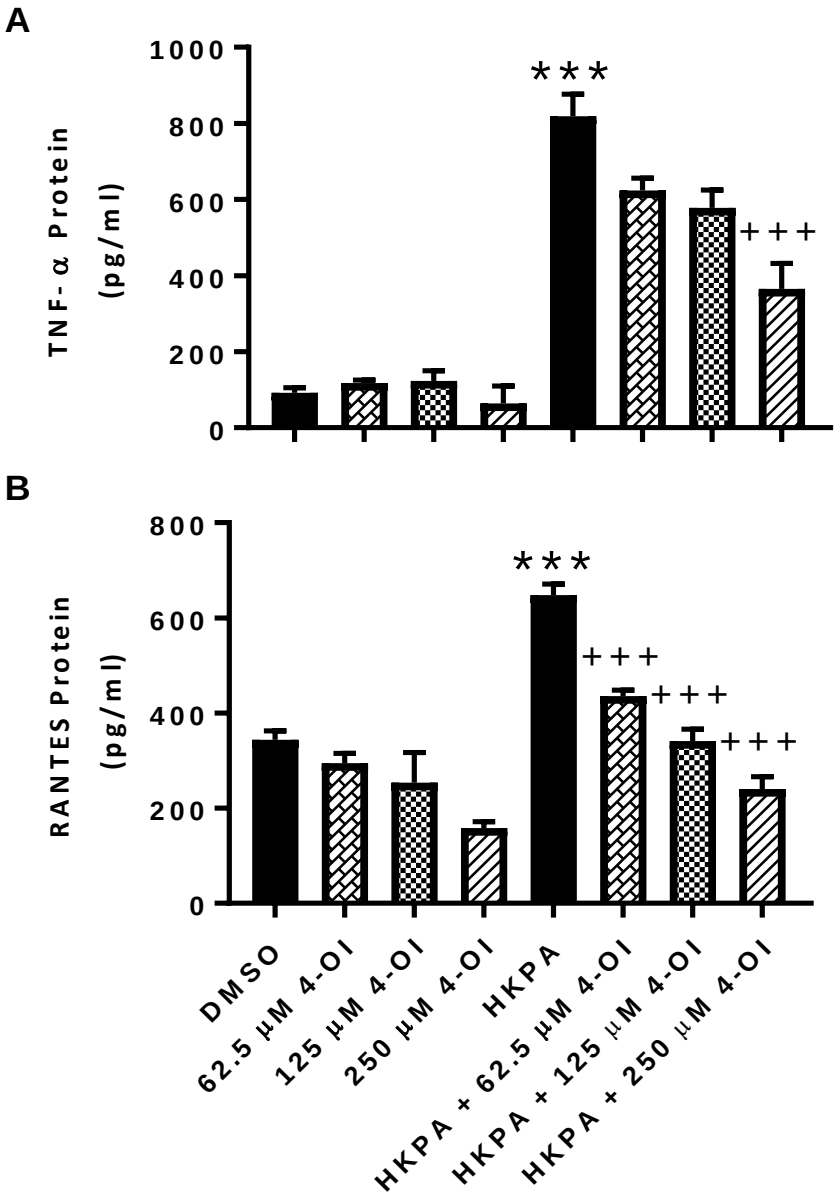

Figure 4.13. TNF-α and RANTES protein production is induced in primary murine lung fibroblasts by HKPA, with 4-OI capable of modulating both HKPA induced TNF-α and RANTES expression.

Stimulation of primary murine lung fibroblasts with TLR2/TLR5 agonist HKPA (MOI 100) induces (**A**) TNF-α and (**B**) RANTES protein production respectively following 24 hours of stimulation. 4-OI (62.5, 125, 250 μM) treatment significantly inhibits HKPA induced (**A**) TNF-α and (**B**) RANTES protein expression following 24 hours of stimulation. Protein expression was quantified by ELISA. Data is presented as mean ± SEM of 3 independent experiments with 3 technical replicates. (**A**) A One-way ANOVA with a Tukey's multiple comparison post-hoc test was used to test for statistical differences. A Kruskal-Wallis test with Dunn's multiple comparison post-hoc test was used to test for statistical differences. *** $p<0.001$; DMSO compared with HKPA. +++ $p<0.001$; HKPA compared with respective treatment.

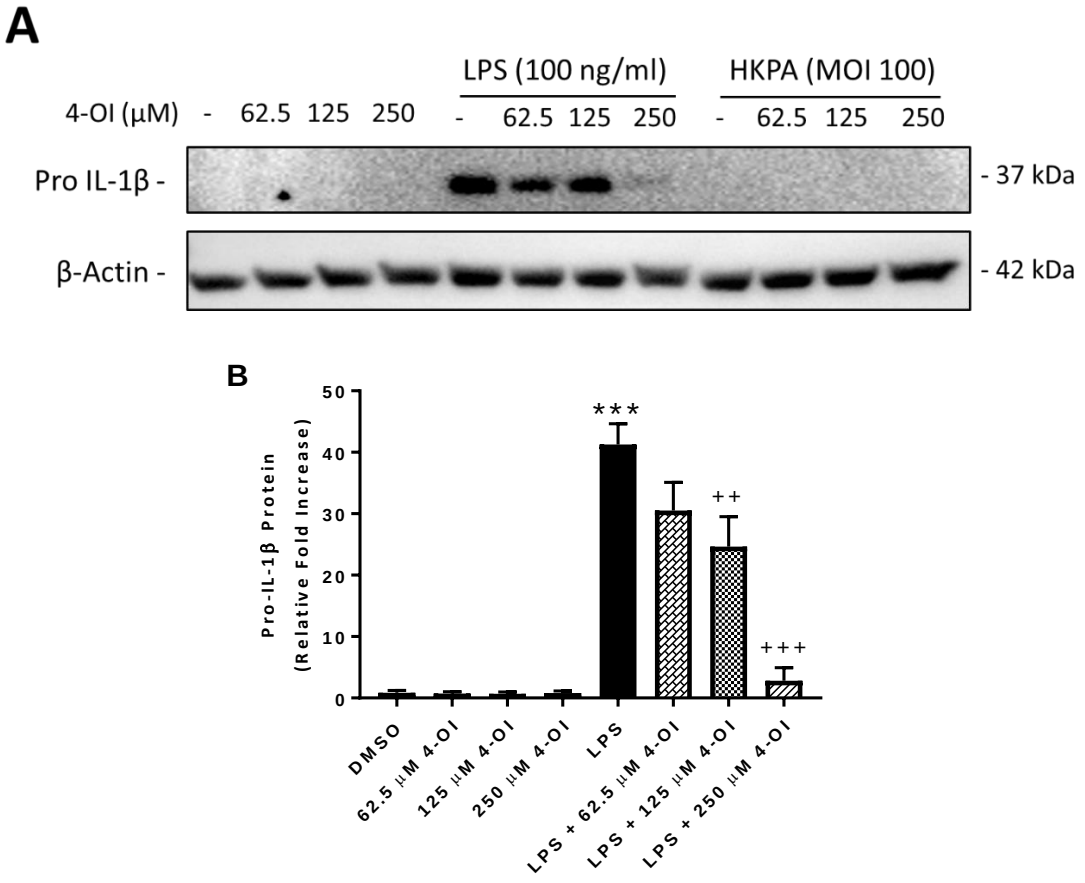

Figure 4.14. Effect of 4-OI on LPS and HKPA mediated pro-IL-1β protein expression in wild type primary lung fibroblasts.

Primary lung fibroblasts from wild type mice were stimulated with LPS (100 ng/ml) or HKPA (MOI 100) in the presence or absence of 4-OI (62.5, 125, 250 μM) for 24 hours. (**A**) Pro-IL-1β protein expression in both LPS and HKPA stimulated cells. (**B**) Densitometry for LPS and 4-OI treated cells. Pro-IL-1β protein levels were analysed by Western blot. Western blot image is representative of 3 independent experiments. ImageJ software was used to obtain densitometry data. For densitometry, protein levels were standardised per unit of β-actin. Results are expressed as a relative fold increase compared with DMSO. (**B**) Data is presented as mean ± SEM of 3 independent replicates. A One-way ANOVA with a Tukey's multiple comparison post-hoc test was used to test for statistical differences. *** $p<0.001$; respective treatment compared with DMSO. ++ $p<0.05$, +++ $p<0.001$; respective treatment compared with LPS.

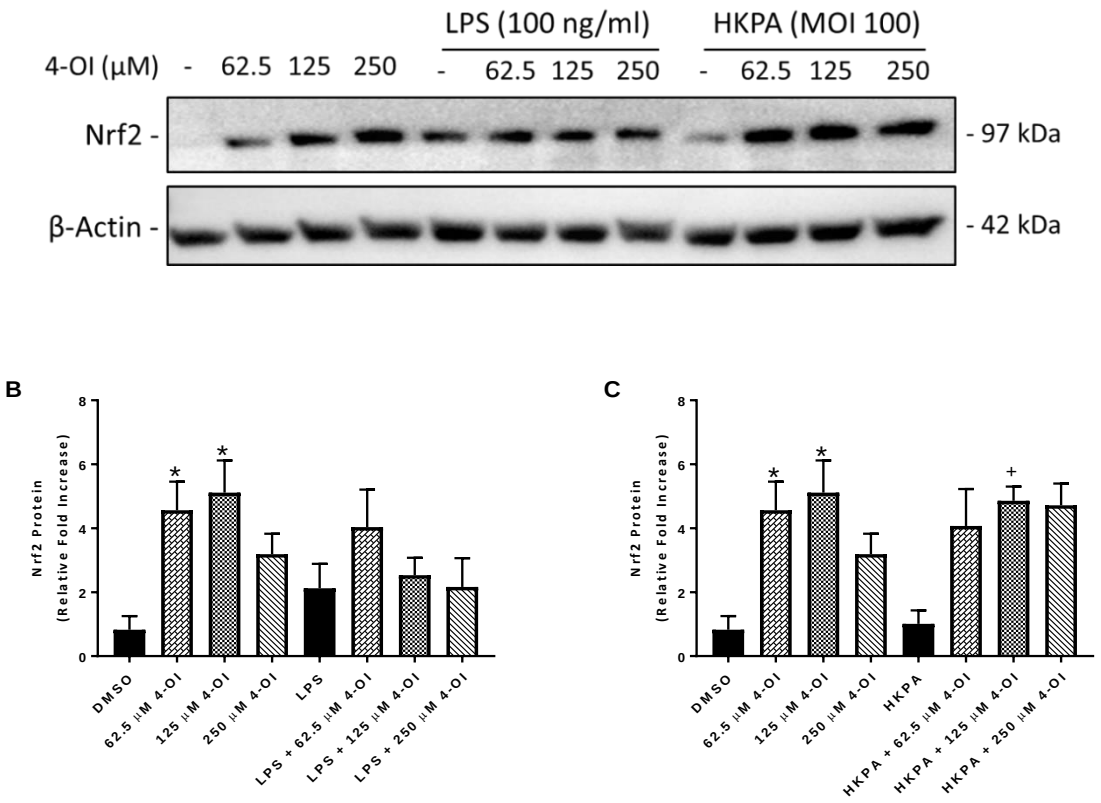

Figure 4.15. Effect of 4-OI on LPS and HKPA mediated Nrf2 protein expression in wild type primary lung fibroblasts.

Primary lung fibroblasts from wild type mice were stimulated with LPS (100 ng/ml) or HKPA (MOI 100) in the presence or absence of 4-OI (62.5, 125, 250 μM) for 24 hours. (**A**) Nrf2 protein expression in both LPS and HKPA stimulated cells. (**B**) Densitometry for LPS and 4-OI treated cells. (**C**) Densitometry for HKPA and 4-OI treated cells. Nrf2 protein levels were analysed by Western blot. Western blot image is representative of 3 independent experiments. ImageJ software was used to obtain densitometry data. For densitometry, protein levels were standardised per unit of β-actin. Results are expressed as a relative fold increase compared with DMSO. (**B, C**) Data is presented as mean ± SEM of 3 independent replicates. A One-way ANOVA with a Tukey's multiple comparison post-hoc test was used to test for statistical differences. * $p<0.05$; respective treatment compared with DMSO. + $p<0.05$; respective treatment compared with HKPA.

4.7 Discussion

In this chapter, we examined the immunomodulatory role of 4-OI and the endogenous itaconate in the context of: (i) LPS stimulation (ii) Poly (I:C) stimulation and (iii) HKPA stimulation. Itaconate has been described as a critical immunomodulatory metabolite, playing a pivotal role in the inflammatory response to synthetic stimuli and both viral and bacterial infections (330, 351, 361, 375, 383, 424). Upregulation of Irg1 mRNA and itaconate expression was first reported in the context of LPS stimulated macrophages (358, 359, 364). Itaconate limits inflammation through a variety of mechanisms. Inhibition of SDH by itaconate has been demonstrated, which limits the inflammation which occurs due to the generation of reactive species caused by succinate oxidation and the electron transport chain (295, 351, 374). Itaconate also promotes anti-inflammatory effects is through upregulation of Nrf2 which promotes the transcription of downstream antioxidant genes, while Irg1 deficient macrophages display impaired lack of activation of Nrf2 (375, 426). 4-OI also induces production of Nrf2 and initiates transcription of downstream antioxidant genes including Nqo1, Gclm, Gsr and Hmox1 (424, 427). Upregulation of these antioxidant effectors has been shown to reduce levels of ROS, which results in less HIF-1α stabilisation and decreased HIF-1α dependant inflammatory cytokine expression (424). The anti-inflammatory effects of itaconate have been demonstrated in LPS stimulated $Irg1^{-/-}$ BMDMs which produced significantly higher levels of IL-6, IL-1β and HIF-1α protein compared with $Irg1^{+/+}$ cells (327).

MIF is a key regulator of innate immunity and inflammation in numerous diseases including CF, rheumatoid arthritis and acute respiratory distress syndrome (110, 111, 114, 115, 124, 158, 177, 180, 393). MIF has been shown to promote inflammation through numerous mechanisms including activation of the MAPK pathway, NF-κB activation, increasing TLR4 expression and overriding the anti-inflammatory effects of glucocorticoids (161, 167, 170-172, 176, 177, 182). MIF has also been shown to be required for optimal HIF-1α stabilisation which drives pro-inflammatory cytokine production and cellular metabolism (183, 188, 189, 191-194).

As previously mentioned, the metabolism of LPS stimulated macrophages shifts towards aerobic glycolysis, also known as the Warburg effect (334-338). It has also been

demonstrated that HIF-1α promotes the expression of glycolytic processing enzymes, while HIF-1α$^{-/-}$ cells fail switch to this Warburg metabolism (343-345). LPS stimulated macrophages also display dysregulation of the TCA cycle whereby there is accumulation of succinate and citrate as a result of decreased activity of their respective processing enzymes (185, 328). Excess citrate is then processed for fatty acid synthesis and itaconate production (327, 328, 348, 349). The mechanism for this TCA cycle dysregulation remains unknown.

As mentioned, there are several overlaps between the effects of MIF and itaconate respectively. MIF has been shown to regulate TLR4 expression, a key receptor which promotes the induction of Irg1 expression when stimulated with LPS (182, 351). Furthermore, MIF is required for HIF-1α stabilisation which is essential for Warburg metabolism and mediates the anti-inflammatory effects of itaconate (193, 194, 318, 339). For these reasons, we hypothesised that MIF may play a mechanistic role in the immunomodulatory effects of itaconate and 4-OI. We hypothesised that MIF mediated increases in TLR4 expression would promote increased Irg1 expression and itaconate production following LPS stimulation (182). Furthermore, we believed that the effects of 4-OI would be limited in MIF deficient cells as one of the main mechanisms of 4-OI is inhibition of HIF-1α stabilisation, which has been shown to be reduced in MIF deficient cells (193). To date, there has been no reports of a link between MIF and itaconate mediated immunomodulation.

In this chapter, we have shown that MIF deficiency does not impact on *Irg1* gene expression or the immunomodulatory capabilities of 4-OI in the context of both LPS and poly(I:C) stimulation. Specifically, we observed that LPS and poly(I:C) significantly induced *Irg1* gene expression in both MIF$^{+/+}$ and MIF$^{-/-}$ BMDMs, however, there were no differences in the level of *Irg1* expression between the two genotypes. As such, any differences that were observed between the genotypes are not attributed to differential *Irg1* gene expression.

We also observed the ability of 4-OI to regulate the production of inflammatory cytokines and chemokines in activated BMDMs. In LPS stimulated BMDMs, we observed that 4-OI did not modulate LPS induced TNF-α in MIF$^{+/+}$ or MIF$^{-/-}$ BMDMs. This is agreement with previously published data, and indicates that the immunomodulatory

effects of 4-OI are not as a result of a shutdown of the inflammatory response (330). 4-OI also significantly increased the expression of LPS mediated KC protein in both $MIF^{+/+}$ and $MIF^{-/-}$ BMDMs. Interestingly, to our knowledge, there have been no published reports to date indicating that 4-OI enhances the expression of any pro-inflammatory factors. 4-OI also significantly inhibited the expression of LPS induced RANTES and IL-1β mRNA expression in both $MIF^{+/+}$ and $MIF^{-/-}$ BMDMs. Overall, there was no difference in the modulation of LPS induced TNF-α, KC, RANTES or IL-1β induction by 4-OI in $MIF^{+/+}$ or $MIF^{-/-}$ BMDMs. We also demonstrated that MIF deficiency did not impact the induction of antioxidant genes *Gclm*, *Gsr*, *Hmox1* or *Nqo1* by 4-OI in LPS stimulated cells as when the data were analysed relative to the vehicle control of $MIF^{+/+}$ cells, there was no difference in the induction of gene expression within treatments between genotypes.

Similarly, in poly(I:C) stimulated cells 4-OI inhibited the induction of RANTES and IL-1β mRNA in both $MIF^{+/+}$ and $MIF^{-/-}$ BMDMs. Similar to our data in LPS stimulated macrophages, MIF deficiency did not impact the induction of antioxidant genes *Gclm*, *Gsr*, *Hmox1* or *Nqo1* by 4-OI in poly(I:C) stimulated cells as when the data were analysed relative to the vehicle control of $MIF^{+/+}$ cells there was no difference in the induction of gene expression within treatments between genotypes. As a result of our data from $MIF^{+/+}$ and $MIF^{-/-}$ BMDMs, we concluded that MIF does not impact the induction of *Irg1* gene expression or the immunoregulatory activity of 4-OI in LPS or poly(I:C) stimulated macrophages.

The Donnelly Lab has a long standing interest in the regulation of the inflammatory response to *P. aeruginosa* infection in CF and the role of this inflammation in disease progression (110, 111, 113). In CF, disease progression occurs due to irreparable damage to the lungs as a result of chronic infection and consequent chronic inflammation (21, 233, 265). *P. aeruginosa* is the most commonly isolated pathogen from the CF lung (35). *P. aeruginosa* infection develops into bacterial biofilms which confer antibiotic resistance and tolerance to the host immune system, resulting in chronic infection and inflammation (113, 233, 437-439). As such, there is a major unmet clinic need for the development of anti-inflammatory therapies in CF (6, 219). We hypothesised that 4-OI would modulate cellular responses to HKPA, a synthetic ligand

of TLR2 and TLR5, which may be of benefit in the development of a novel anti-inflammatory therapy for the treatment of CF.

We conducted a preliminary study to examine the effects of 4-OI on the induction of TNF-α and RANTES by HKPA, two key pro-inflammatory mediators that are expressed during *P. aeruginosa* infection (150, 283, 284). HKPA is an agonist for TLR2 and TLR5, and we have demonstrated the induction of both TNF-α and RANTES protein production (*see* Chapter 3). Our data demonstrated for the first time the modulation of both TNF-α and RANTES protein production in HKPA stimulated macrophages by 4-OI. As previously mentioned, 4-OI employs numerous mechanisms to inhibit pro-inflammatory responses in activated macrophages (295, 330, 368, 379). In *P. aeruginosa* infection, the production of RANTES and TNF-α protein has been shown to be IRF3 dependant, with PA01 infected $IRF3^{-/-}$ mice having decreased RANTES and TNF-α levels in BAL fluid compared with $IRF3^{+/+}$. IRF3 is a key transcription factor that also induces the production of type I IFN genes (440, 441). 4-OI has been shown to reduce the transcription of type I IFN-dependant genes (330, 442). We believe that the 4-OI mediated decrease in HKPA mediated TNF-α and RANTES protein could be due activation of the negative feedback loop between 4-OI and type I interferons, however further work is necessary to confirm this. Furthermore, 4-OI also displays highly electrophilic characteristics with a significant induction of Nrf2 activation and downstream antioxidant genes, responses which have also been shown to limit pro-inflammatory cytokine production which may also play a role in it's regulation of the macrophage response to HKPA (330, 429, 442, 443).

In this chapter, following our demonstration that 4-OI modulated the response of LPS and HKPA stimulated macrophages, we subsequently examined the impact of endogenous itaconate on the response of macrophages to these stimuli. The *Irg1* gene is responsible for the production of cis-aconitate decarboxylase, which converts cis-aconitate to itaconate (359). Itaconate is an anti-bacterial and immunomodulatory metabolite that has been shown to be upregulated in LPS stimulated and *M. tb* infected cells (359, 365, 367). We hypothesised that itaconate deficiency would enhance the production of pro-inflammatory mediators in LPS and HKPA stimulated macrophages. We observed that LPS stimulation induced equivalent levels of TNF-α protein in $Irg1^{+/+}$

and Irg1$^{-/-}$ BMDMs. Levels of KC protein induced by LPS were also equivalent in Irg1$^{+/+}$ and Irg1$^{-/-}$ BMDMs. The induction of nitrite production by LPS was lower in Irg1$^{-/-}$ than Irg1$^{+/+}$ BMDMs. This was unexpected, as we hypothesised that expression of itaconate in Irg1$^{+/+}$ cells would inhibit the induction of nitrite production through the inhibition of ROS (330).

In HKPA stimulated cells, we observed the induction of equivalent levels of TNF-α and KC in Irg1$^{+/+}$ and Irg1$^{-/-}$ BMDMs. As detected in LPS stimulated cells, we were surprised that levels of nitrite production following HKPA stimulation was lower in Irg1$^{-/-}$ than Irg1$^{+/+}$. We also demonstrated, for the first time, the induction of Nrf2 protein in HKPA stimulated cells treated with 4-OI and subsequent inhibition of pro-IL-1β protein production in Irg1$^{+/+}$ BMDMs.

Interestingly, we also demonstrated that the effects of 4-OI on the modulation of BMDM responses to LPS and HKPA stimulation are not *Irg1* dependant, with no differences observed in the effects of 4-OI on the modulation of LPS and HKPA induced TNF-α, RANTES or nitrite between the two genotypes. This is similar to recently published data examining the effects of 4-OI and endogenous itaconate on particulate-matter induced inflammation (444). Overall, our data demonstrates differential effects between 4-OI and endogenously produced itaconate mediated by the Irg1 protein.

In this chapter, we also examined the effects of 4-OI on the induction of TNF-α, RANTES and pro-IL-1β protein by LPS and HKPA in primary murine lung fibroblasts. Typically, fibroblasts are associated with their role in the repair of damaged lung architecture through proliferation and subsequent secretion of the ECM (433). However, lung fibroblasts also play a role in airway inflammation through the recognition of pathogen-associated molecular patterns and damage-associated molecular patterns and subsequent generation of an inflammatory response (434, 445). Fibroblasts also play a role in promoting inflammation and can produce pro-inflammatory cytokines including TNF-α, RANTES and pro-IL-1β, contributing to inflammatory damage within the lung and subsequent fibrotic scar development (434, 436). As such, fibroblasts also mediate the inflammatory response to infection within the lung (446, 447).

In this chapter, we demonstrated a significant induction of TNF-α, RANTES and pro-IL-1β protein production in LPS stimulated fibroblasts. Furthermore, we observed significant inhibition of LPS mediated TNF-α and pro-IL-1β protein production with 4-OI treatment. We also observed the induction of Nrf2 protein production in these cells, demonstrating for the first time that 4-OI is also functional in primary murine lung fibroblasts, and not just myeloid derived lymphocytes.

In primary murine lung fibroblasts, HKPA stimulation induced the production of TNF-α and RANTES, but not pro-IL-1β. 4-OI treatment inhibited HKPA mediated TNF-α and RANTES production and also induced the production of Nrf2 protein, indicative of the activation of an antioxidant response (429). This was similar to the effects observed in LPS stimulated lung fibroblasts, although the level of induction of TNF-α and RANTES was not as high as in LPS stimulated cells, perhaps explaining why 4-OI was capable of inhibiting RANTES in HKPA but not LPS stimulated cells. These findings are important as it is the first description of the regulation of the inflammatory response of primary lung fibroblasts to LPS and HKPA by 4-OI. Potentially, by decreasing the inflammatory profile of tissue resident fibroblasts, 4-OI may in turn reduce the expression of pro-fibrotic markers including type I collagen and α-smooth muscle actin, although further work is necessary to examine this (448).

In CF, chronic inflammation withing the lung drives tissue damage and disease progression (21, 233, 265). As such, there is a major unmet clinic need for the development of anti-inflammatory therapies in CF (6, 219). Based on the immunomodulatory effects that we have observed, we believe that 4-OI may be of therapeutic benefit for the treatment of inflammation in CF (**Figure 4.16**). We have demonstrated that HKPA and LPS both induce TNF-α, pro-IL-1β, RANTES and nitrite production in macrophages and lung fibroblasts, all of which are inhibited by 4-OI treatment. Furthermore, 4-OI inhibits the production of these inflammatory factors and induces production of Nrf2 and transcription of antioxidant genes. These results are promising, although it is important to note that these synthetic ligands are not fully representative of a live *P. aeruginosa* infection. Further work is necessary to evaluate the effect of 4-OI on the responses of macrophages to *P. aeruginosa* infection.

In conclusion, we have demonstrated that MIF does not modulate the immunomodulatory effects of 4-OI in LPS and poly(I:C) stimulated BMDMs. We also demonstrated, for the first time, that 4-OI can modulate to response of BMDMs to HKPA. Our results also illustrated for the first time that 4-OI can modulate the inflammatory responses of primary murine lung fibroblasts to LPS and HKPA. Furthermore, we showed that endogenous itaconate has limited effect on the response of macrophages to HKPA stimulation, demonstrating differential effects between endogenous itaconate and 4-OI.

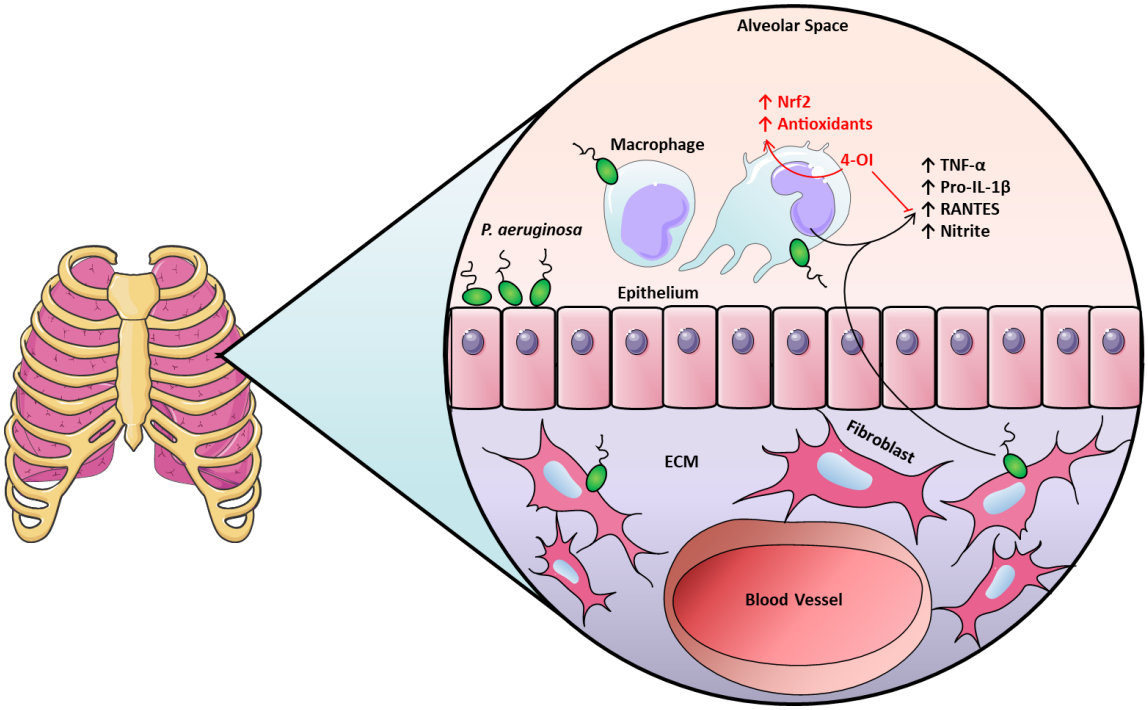

Figure 4.16. Model of 4-OI modulation of the immune response to HKPA and LPS.

HKPA and LPS both induce TNF-α, pro-IL-1β, RANTES and nitrite production in macrophages and lung fibroblasts. 4-OI inhibits the production of these inflammatory factors and induces production of Nrf2 and transcription of antioxidant genes.

Chapter 5 - Investigation of the effects of 4-OI and endogenous itaconate on live *P. aeruginosa* infection.

5.1 Introduction

In cystic fibrosis (CF), respiratory failure occurs as a result of chronic infection and inflammation (21, 233, 265). The most commonly isolated pathogen from the CF lung is *P. aeruginosa* (35). In 2017, the World Health Organisation deemed it of critical importance that new antibiotic regimes be developed against *P. aeruginosa* infection due to high levels of antibiotic resistance (449). As such, there is an unmet clinical need for the development of therapeutic agents that promote *P. aeruginosa* clearance and limit antibiotic resistance and pathogenic inflammation (6, 219).

In this chapter, we focused on the effects of itaconate and 4-OI on numerous aspects of live *P. aeruginosa* infection. As previously mentioned, itaconate is a by-product of the citric acid cycle that exerts both immunomodulatory and anti-bacterial effects (359). Itaconate production is mediated by the immunoresponsive gene 1 (Irg1) enzyme which is under the control of the *Irg1* gene (359). Irg1 has been shown to be rapidly upregulated in response to numerous bacterial infections including *Staphylococcus aureus (S. aureus)*, *Escherichia coli* and *Mycobacterium tuberculosis (M. tb)* (420, 421, 450).

As previously mentioned, itaconate has been shown to modulate a number of anti-inflammatory effects. While the exact mechanism of itaconate's anti-inflammatory effects remain to be investigated, one known mechanism of action is through the inhibition of succinate dehydrogenase (SDH) (327, 351, 374). SDH acts to oxidise succinate which results in the generation of reactive oxygen species (ROS), consequently inhibition of SDH has anti-inflammatory effects (295). Itaconate has also been shown to inhibit HIF-1α stabilisation in LPS stimulated $Irg1^{-/-}$ cells compared with $Irg1^{+/+}$ cells, providing a further mechanism for its anti-inflammatory activity (327).

The anti-inflammatory effects of endogenous itaconate have also been shown in an *in vivo* model of *M. tb* infection. $Irg1^{-/-}$ mice display increased mortality and inflammation within the lung compared with $Irg1^{+/+}$ mice in a model of *M. tb* infection (361). These authors demonstrated that this increased mortality was due to pathogenic inflammation as $Irg1^{-/-}$ mice which were treated with a neutrophil depleting antibody

displayed increased survival compared with Irg1$^{-/-}$ mice receiving control antibody in the same *M. tb* infection model (361).

Throughout this chapter we utilised 4-octyl itaconate (4-OI) as a cell permeable analogue of itaconate, as to date there has been no description of an itaconate receptor or transport channel. Furthermore, reports of itaconate gaining entry to the cytoplasm of cells remain limited (369, 370). 4-OI has previously been shown to inhibit LPS induced IL-1β mRNA expression and protein production in LPS stimulated macrophages (330, 360). 4-OI has also been shown to be active *in vivo*, inhibiting IL-1β and TNF-α protein production in a murine LPS lethality model (330, 360). 4-OI has been shown to exert its anti-inflammatory effects through the upregulation of nuclear factor erythroid 2-related factor 2 (Nrf2) protein expression and subsequent upregulation of anti-oxidant genes including NAD(P)H Quinone Dehydrogenase 1 (Nqo1), Glutamate-Cysteine Ligase Modifier (Gclm), Glutathione Reductase (Gsr) and Heme Oxygenase 1 (Hmox1) (330, 424, 427). This results in inhibition of ROS, decreased HIF-1α stabilisation and consequent reduction in HIF-1α dependant pro-inflammatory cytokine expression (424).

Itaconate has also been shown to have potent antibiotic properties (359). It has previously been demonstrated that *P. aeruginosa* expresses genes involved in the detoxification of itaconate (378, 381). These genes are *PA0878*, *PA0882* and *PA0883* which encode itaconyl-CoA hydratase (Ich), succinyl-CoA:itaconate CoA transferase (Ict), and (S)-citramalylCoA lyase (Ccl) respectively (378, 381).

In this chapter, we examined the ability of 4-OI to modulate macrophage responses to live *P. aeruginosa* infection. We also examined the role of endogenous itaconate in the response of macrophages to live *P. aeruginosa* infection using cells form Irg1$^{-/-}$ mice. We then investigated the effect of itaconate on *P. aeruginosa* growth and biofilm formation using lab strain PA01 and five *P. aeruginosa* strains isolated from CF patients. Furthermore, we examined the effects of itaconate on PA01 virulence factor expression and the susceptibility of PA01 to commonly used antibiotics against *P. aeruginosa*. Finally, we utilised the *Galleria mellonella* (*G. mellonella*) invertebrate model to examine the effects of itaconate and 4-OI on *P. aeruginosa* infection *in vivo*.

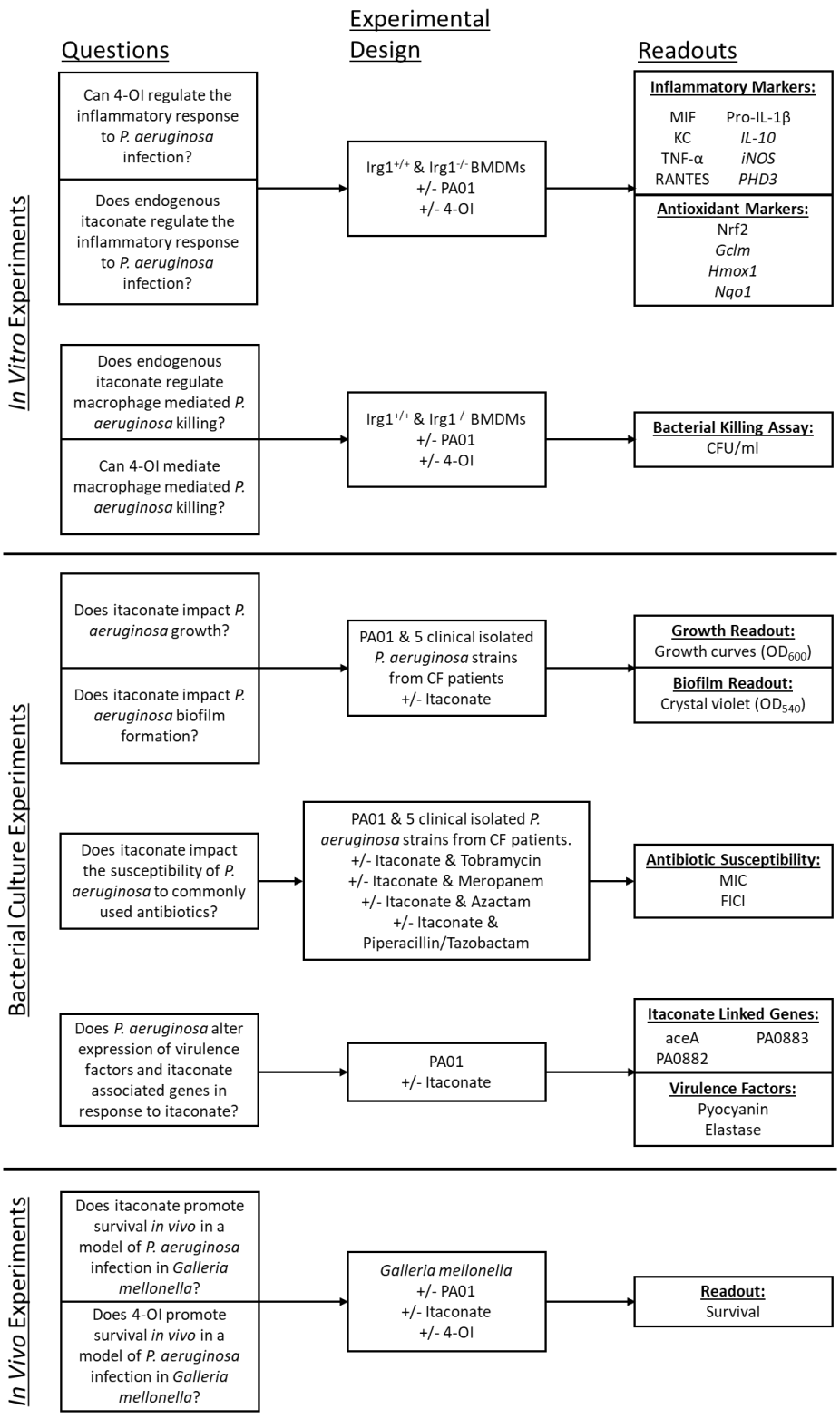

Figure 5.1. Overview of the experimental design for Chapter 5.

5.2 4-OI modulates the responses of RAW 264.7 cells to live *P. aeruginosa* infection

We have established that 4-OI can modulate the cytokine responses of RAW 264.7 cells following HKPA stimulation (**Figure 4.8**). Next, we examined the ability of 4-OI to modulate the response of RAW 264.7 cells to live *P. aeruginosa* infection. RAW 264.7 cells were used for preliminary experiments before repeating experiments in BMDMs.

P. aeruginosa is a gram-negative bacterium that expresses several PAMPs that result in the induction of a potent inflammatory response. These PAMPs include, but are not limited to, LPS, flagellin, bacterial DNA, peptidoglycan, diffusible signalling molecules and type III secretion system components (93, 230, 249, 281, 451, 452). PA01 is a commonly used laboratory-adapted strain of *P. aeruginosa* (453).

5.2.1 PA01 infection induces Irg1 mRNA expression in RAW 264.7 macrophages.

Previously, Irg1 mRNA has been shown to be upregulated in LPS stimulated human macrophages and also in the lungs of *M. tb* infected mice (364-367). Here, we described for the first time that PA01 infection (MOI 30) of RAW 264.7 cells significantly increased expression of Irg1 mRNA after 24 hours of infection compared with medium only (* $p<0.05$**, Figure 5.2**).

5.2.2 PA01 infection induces TNF-α and pro-IL-1β protein production and IL-1β mRNA expression, which is modulated by 4-OI treatment.

Next, we examined the ability of 4-OI (62.5-250 μM) to inhibit PA01 (MOI 30) induced cytokine production. Here, we demonstrated that PA01 infection (MOI 30) significantly induced TNF-α protein production after 8 hours of PA01 infection in RAW

264.7 cells compared with DMSO (*** p<0.001, **Figure 5.3**). 4-OI treatment dose dependently decreased PA01 mediated TNF-α protein production after 8 hours of PA01 infection in RAW 264.7 cells (+ p<0.05, +++ p<0.001, **Figure 5.3**).

Previous studies have shown that IL-1β inhibits macrophage mediated *P. aeruginosa* clearance (302). Inhibition of caspase-1, the enzyme which cleaves pro-IL-1β to mature IL-1β, results in bacterial burden in a model of *P. aeruginosa* induced ocular keratitis, while caspase-$1^{-/-}$ mice exhibit increased bacterial clearance compared with wild type mice (304, 305). As a result, we examined the effects of 4-OI on *P. aeruginosa* induced pro-IL-1β protein production.

PA01 (MOI 30) also significantly induced pro-IL-1β protein expression in RAW 264.7 cells after 8 hours of infection (*** p<0.001, **Figure 5.4B**). Treatment of cells with 4-OI (62.5-250 μM) significantly decreased the production of PA01 induced pro-IL-1β protein production in RAW 264.7 cells after 8 hours of infection (+++ p< 0.001, **Figure 5.4B**). IL-1β mRNA expression was also significantly induced by PA01 infection compared with DMSO (** p<0.01, **Figure 5.4C**), with treatment of 125 μM and 250 μM significantly inhibiting PA01 induced mRNA expression compared with PA01 (+ p<0.05, **Figure 5.4C**).

5.2.3 4-OI induces Nrf2 protein expression and downstream antioxidant genes Gclm, Gsr and Nqo1 mRNA; all of which are down regulated during PA01 infection in RAW 264.7 macrophages.

Next, we examined the effect of 4-OI on Nrf2 protein expression, as 4-OI has previously been shown to enhance Nrf2 protein levels (330). Here, we demonstrated that 4-OI (62.5-250 μM) induced Nrf2 protein expression in RAW 264.7 cells after 8 hours of stimulation (**Figure 5.5**). PA01 infection inhibits 4-OI mediated Nrf2 protein expression (**Figure 5.5**). We then examined the mRNA expression of antioxidant genes Gclm, Gsr and Nqo1, which are downstream of Nrf2 activation (330, 429). Treatment of RAW 264.7 cells with 250 μM 4-OI significantly increased the expression of Gclm and

Nqo1 mRNA after 8 hours (** p<0.01, **Figure 5.6A, C**). Interestingly, PA01 infection inhibited the ability of 4-OI to enhance Gclm, Gsr and Nqo1 mRNA expression. It is important to note that PA01 infected cells that were treated with 4-OI had higher levels of Gsr, Gclm and Nqo1 mRNA expression compared with those without 4-OI, although the difference was not significant (**Figure 5.6A-C**).

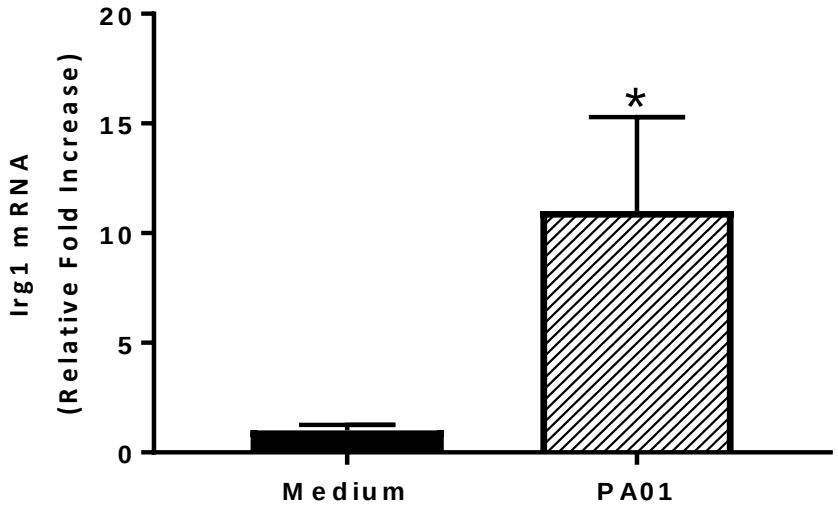

Figure 5.2. PA01 infection induces Irg1 mRNA expression in RAW 264.7 macrophages.

Infection of RAW 264.7 macrophages with PA01 (MOI 30) for 8 hours induces Irg1 mRNA expression, as quantified by qPCR analysis. mRNA levels were standardised per unit of β-actin. Results are expressed as a relative fold increase compared with medium. Data is presented as mean ± SEM of 3 independent experiments with 3 technical replicates. An unpaired T-test was used to test for statistical differences. * $p<0.05$; PA01 compared with medium.

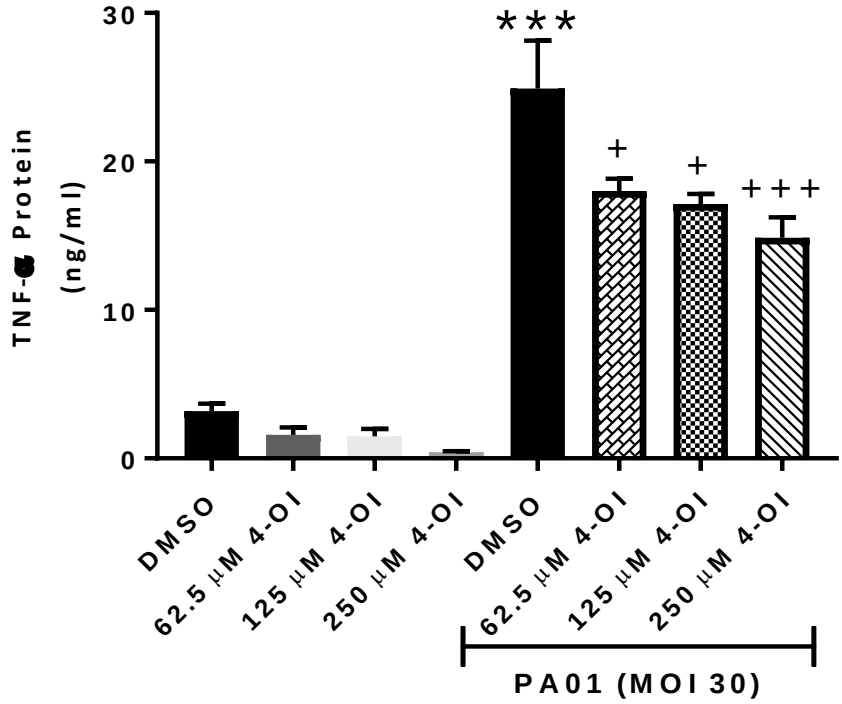

Figure 5.3. PA01 infection induces TNF-α protein production, which is modulated by 4-OI co-treatment.

PA01 infection induces TNF-α protein production following 8 hours of stimulation. 4-OI treatment significantly inhibits PA01 induced TNF-α protein production following 8 hours of treatment. Protein production was quantified by ELISA. Data is presented as mean ± SEM of 3 independent experiments with 3 technical replicates. A One-way ANOVA with a Tukey's multiple comparison post-hoc test was used to test for statistical differences. *** $p<0.001$; DMSO compared with PA01 + DMSO. + $p<0.05$, +++ $p<0.001$ respective 4-OI treatment compared with PA01 + DMSO.

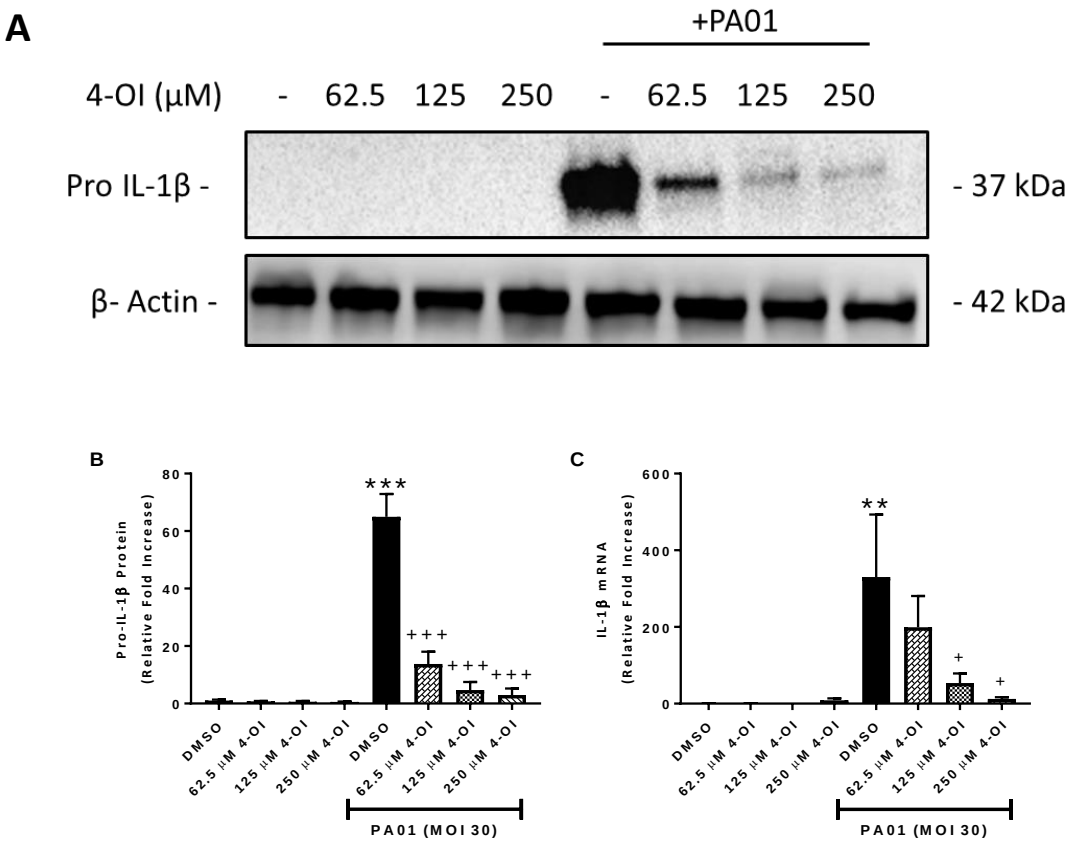

Figure 5.4. Pro-IL-1β protein and mRNA expression in RAW 264.7 macrophages following PA01 infection and 4-OI co-treatment.

RAW 264.7 macrophages expressed low levels of intracellular pro-IL-1β protein basally, with PA01 infection resulting in increased pro-IL-1β protein expression. Treatment with 4-OI leads to decreased pro-IL-1β expression. Protein levels were analysed by Western blot flowing 8 hours treatment with 4-OI ± PA01 (MOI 30). (**A**) Western blot image is representative of 3 independent experiments. ImageJ software was used to obtain densitometry data. For densitometry, protein levels were standardised per unit of β-actin. (**B**) Densitometry results are expressed as a relative fold increase compared with DMSO. (**C**) IL-1β mRNA as quantified by qPCR analysis. mRNA levels were standardised per unit of β-actin. Results are expressed as a relative fold increase compared with medium. Data is presented as mean ± SEM of 3 independent replicates. A One-way ANOVA with a Tukey's multiple comparison post-hoc test was used to test for statistical differences. (**B**) *** $p<0.001$; DMSO + PA01 compared with DMSO. +++ $p<0.001$; respective treatment compared with DMSO + PA01. (**C**) *** $p<0.001$; DMSO + PA01 compared with DMSO. + $p<0.05$; respective treatment compared with DMSO + PA01

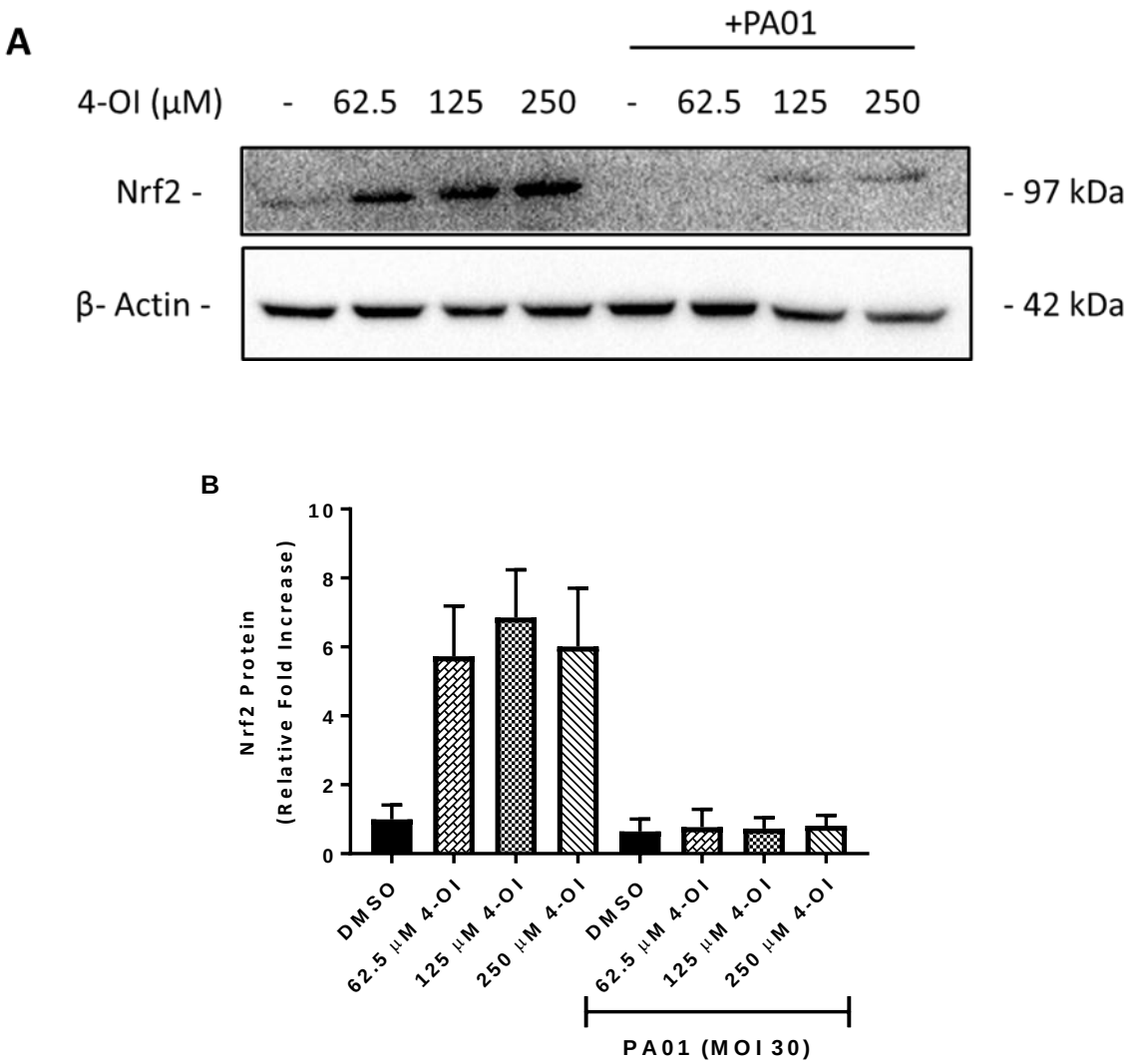

Figure 5.5. Nrf2 protein expression in RAW 264.7 macrophages following PA01 infection and 4-OI co-treatment.

RAW 264.7 macrophages expressed low levels of intracellular Nrf2 protein basally, with 4-OI increasing Nrf2 protein expression. Infection with PA01 inhibits 4-OI mediated Nrf2 expression. Protein levels were analysed by Western blot flowing 8 hours treatment with 4-OI ± PA01 (MOI 30). (**A**) Western blot image is representative of 3 independent experiments. ImageJ software was used to obtain densitometry data. For densitometry, protein levels were standardised per unit of β-actin. Results are expressed as a relative fold increase compared with DMSO. (**B**) Data is presented as mean ± SEM of 3 independent replicates.

.

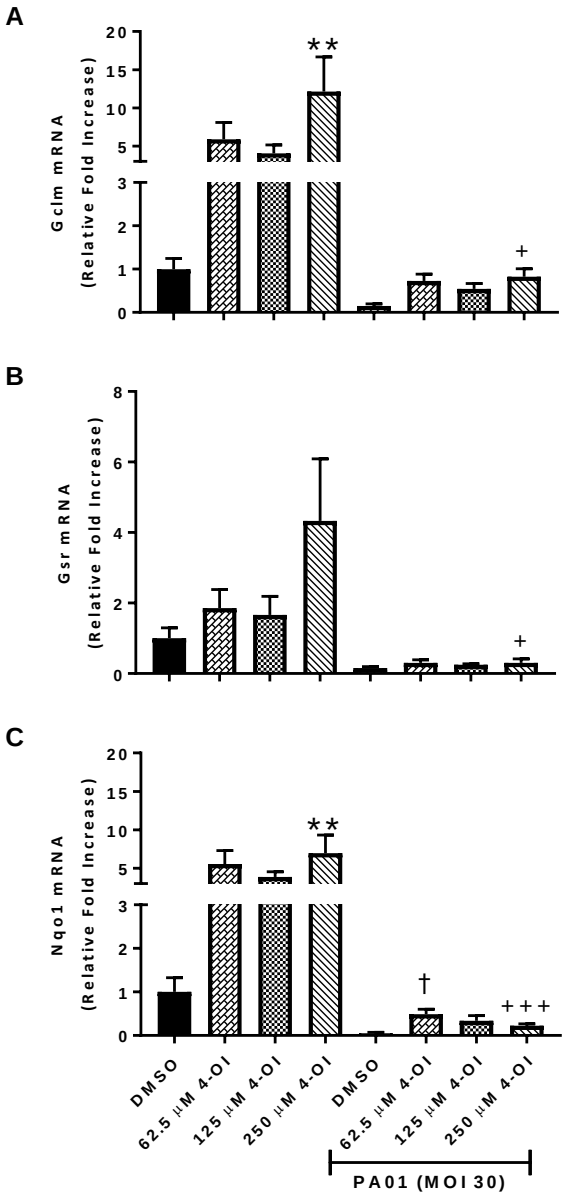

Figure 5.6. 4-OI induces expression of Gclm, Gsr and Nqo1 mRNA, which are down regulated during PA01 infection.

4-OI induced expression of (**A**) Gclm, (**B**) Gsr and (**C**) Nqo1 mRNA respectively following 8 hours of stimulation. Infection with PA01 inhibited 4-OI induced upregulation of Gclm, Gsr, and Nqo1 mRNA expression (**A-C**). Gene expression was quantified by qPCR analysis. mRNA levels were standardised per unit of β-actin. Results are expressed as a relative fold increase compared with DMSO. Data is presented as mean ± SEM of 3 independent experiments with 3 technical replicates. A One-way ANOVA with a Tukey's multiple comparison post-hoc test was used to test for statistical differences. (**A, C**) ** $p<0.01$; DMSO compared with 250 µM 4-OI. (**A-C**) + $p<0.05$, +++ $p<0.001$; 250 µM 4-OI compared with PA01 + 250 µM 4-OI. (**C**) † $p<0.05$; 62.5 µM 4-OI compared with PA01 + 62.5 µM 4-OI.

5.3 Investigation of the effects of 4-OI and endogenous itaconate on macrophage responses to *P. aeruginosa* infection

We have established during our preliminary experiments that 4-OI can modulate the inflammatory response to *P. aeruginosa* in RAW 264.7 cells, with 4-OI regulating cytokine production, Nrf2 protein expression and antioxidant gene expression (**Figure 5.3 - Figure 5.6**). Next, we utilised BMDMs wild type and itaconate deficient mice to examine the role of endogenous itaconate in the modulation of the inflammatory response to *P. aeruginosa*.

5.3.1 4-OI and PA01 are not cytotoxic to BMDMs.

Initially, we examined the levels of cytotoxicity associated with PA01 infection in wild type BMDMs. Following 8 hours of infection with PA01 (MOI 30) there was no induction of lactate dehydrogenase (LDH) release, an indirect marker of cytotoxicity, compared with DMSO treatment (**Figure 5.7**). Treatment of cells with 4-OI (250 µM) , and co-treatment with PA01 and 4-OI also failed to induce any LDH release compared with DMSO treatment (**Figure 5.7**). These results demonstrated that PA01 (MOI 30), 4-OI (250 µM) or PA01 and 4-OI co-treatment did not induce significant cell death in BMDMs in these experiments.

5.3.2 4-OI, but not endogenous itaconate, modulate PA01 induced TNF-α protein production in BMDMs from Irg1$^{+/+}$ and Irg1$^{-/-}$ mice.

We subsequently examined, for the first time, the effects of 4-OI and endogenous itaconate on the induction of pro-inflammatory cytokines by PA01 infection in BMDMs. Here, we demonstrated that PA01 (MOI 30) infection significantly induced MIF protein production in Irg1$^{+/+}$ BMDMs after 8 hours of infection compared with DMSO treatment (** $p<0.01$, **Figure 5.8A**). Treatment with 4-OI (250 µM) had no effect on PA01 induced MIF protein production compared with PA01 alone in Irg1$^{+/+}$

BMDMs (**Figure 5.8A**). In $Irg1^{-/-}$ BMDMs, PA01 infection did not induce MIF protein production compared with DMSO (**Figure 5.8B**), which could be due to higher constitutive levels of MIF in these cells. As with $Irg1^{+/+}$ cells, PA01 infection did not induce MIF protein production compared with DMSO in $Irg1^{-/-}$ BMDMs after 8 hours (**Figure 5.8B**).

PA01 infection induced significant KC protein production in $Irg1^{+/+}$ BMDMs compared with DMSO treatment (*** p<0.001, **Figure 5.8C**), while treatment with 4-OI had no effect on PA01 induced KC protein production compared with PA01 alone (**Figure 5.8C**). In $Irg1^{-/-}$ BMDMs, PA01 infection also significantly induced KC protein production compared with DMSO treatment (*** p<0.001, **Figure 5.8D**), with 4-OI treatment having no effect on PA01 induced KC protein production compared with PA01 alone (**Figure 5.8D**). Levels of KC protein were similar $Irg1^{+/+}$ BMDMs and $Irg1^{-/-}$ BMDMs that received the same treatments.

PA01 infection also induced significant TNF-α protein production in $Irg1^{+/+}$ BMDMs compared with DMSO treatment (*** p<0.001, **Figure 5.8E**), which was abrogated with 4-OI compared with PA01 alone (+++ p<0.001, **Figure 5.8E**). This data is consistent with our data from PA01 infected RAW 264.7 cells (**Figure 5.3**) In $Irg1^{-/-}$ BMDMs, PA01 infection induced significant TNF-α protein production compared with DMSO treatment (*** p<0.001, **Figure 5.8F**). The levels of TNF-α induced in $Irg1^{-/-}$ BMDMs upon PA01 infection was higher than that in $Irg1^{+/+}$ BMDMs. In $Irg1^{-/-}$ BMDMs, 4-OI treatment inhibited PA01 induced TNF-α compared with PA01 alone (+++ p<0.001, **Figure 5.8F**).

PA01 infection also induced significant RANTES protein production in $Irg1^{+/+}$ BMDMs compared with DMSO treatment (*** p<0.001, **Figure 5.8G**), which was unchanged with 4-OI treatment compared with PA01 alone (**Figure 5.8G**). In $Irg1^{-/-}$ BMDMs, PA01 infection also induced significant RANTES protein production compared with DMSO treatment (*** p<0.001, **Figure 5.8H**), which was significantly decreased with 4-OI treatment compared with PA01 alone (+++ p<0.001, **Figure 5.8H**).

5.3.3 Effect of 4-OI on IL-10, iNOS, TNF-α and PHD3 mRNA expression in PA01 infected BMDMs from Irg1$^{+/+}$ and Irg1$^{-/-}$ mice.

IL-10 is an anti-inflammatory cytokine that has been shown to limit inflammatory damage within the lungs of *P. aeruginosa* infected mice (454, 455). We demonstrated for the first time that in Irg1$^{+/+}$ BMDMs, 4-OI (250 μM) treatment significantly increased IL-10 mRNA in PA01 infected cells compared with PA01 after 8 hours (+ p<0.01, **Figure 5.9A**). In Irg1$^{-/-}$ BMDMs, PA01 infection induced significant IL-10 mRNA expression after 8 hours compared with DMSO treatment (* p<0.05, **Figure 5.9B**). Furthermore, 4-OI treatment enhanced this PA01 mediated increase in IL-10 mRNA compared with PA01 (+++ p<0.001, **Figure 5.9B**).

Inducible nitric oxide synthase II (iNOS) is the enzyme the is responsible for the production of NO (456). iNOS transcription is activated by numerous stimuli, including LPS, with activation of NF-κB and MAPK pathways converging to promote iNOS transcription (456). NO is a radical effector which exhibits anti-bacterial properties, but also has deleterious effects to the host cells (456, 457). 4-OI has previously been shown to modulate LPS induced iNOS expression in macrophages (330). Here, we demonstrated that PA01 infection significantly induced iNOS mRNA expression in Irg1$^{+/+}$ BMDMs after 8 hours compared with DMSO treatment(* p<0.05, **Figure 5.9C**). 4-OI had no effect of PA01 induced iNOS mRNA expression compared with PA01. In Irg1$^{-/-}$ BMDMs, PA01 infection also significantly induced iNOS mRNA expression after 8 hours compared with DMSO treatment (* p<0.05, **Figure 5.9D**), with 4-OI significantly decreasing PA01 mediated iNOS mRNA induction compared with PA01 (+ p<0.05, **Figure 5.9D**).

PA01 infection induced significant TNF-α mRNA in Irg1$^{+/+}$ BMDMs compared with DMSO treatment (*** p<0.001, **Figure 5.9E**), while 4-OI had no effect on PA01 induced TNF-α mRNA expression compared with PA01 (**Figure 5.9E**). Similar findings were observed in Irg1$^{-/-}$ cells, PA01 infection induced significant TNF-α mRNA in Irg1$^{-/-}$ BMDMs compared with DMSO treatment (** p<0.01, **Figure 5.9F**), while 4-OI had no effect on PA01 induced TNF-α mRNA expression compared with PA01 (**Figure 5.9F**).

HIF-1α is a transcription factor which regulates macrophage aggregation and invasion and also drives the expression of pro-inflammatory cytokines (458). HIF-1α levels are regulated by PHDs which target HIF-1α for degradation (184-186). For example, LPS stimulation decreases expression levels of PHDs, resulting in further HIF-1α stabilisation (190). PHD3 is a key regulation of HIF-1α protein levels (458). Here, we show that PA01 (MOI 30) infection significantly inhibited PHD3 mRNA expression in $Irg1^{+/+}$ BMDMS after 8 hours of infection compared with DMSO (* p<0.05, **Figure 5.9G**). 4-OI (250 μM) treatment did not impact PHD3 mRNA expression levels in $Irg1^{+/+}$ BMDMs compared with DMSO, nor in PA01 infected cells compared with PA01 (**Figure 5.9G**). In $Irg1^{-/-}$ BMDMs, PA01 infection inhibits PHD3 mRNA expression in $Irg1^{+/+}$ BMDMS after 8 hours of infection compared with DMSO, although this was not significant (**Figure 5.9H**). As with $Irg1^{+/+}$ BMDMs, 4-OI treatment did not impact PHD3 mRNA expression levels in $Irg1^{-/-}$ BMDMs compared with DMSO, nor in PA01 infected cells compared with PA01 (**Figure 5.9H**).

5.3.4 4-OI induces Nrf2 protein expression and inhibits P. aeruginosa induced pro-IL-1β protein expression in PA01 infected $Irg1^{+/+}$ and $Irg1^{-/-}$ BMDMs.

Next, we examined the induction of Nrf2 protein expression in $Irg1^{+/+}$ and $Irg1^{-/-}$ BMDMs following 4-OI treatment and *P. aeruginosa* infection. As previously mentioned, 4-OI has been shown to enhance Nrf2 protein levels (330). 4-OI (250 μM) treatment significantly increased Nrf2 protein after 8 hours of treatment compared with DMSO treatment (* p<0.05, **Figure 5.10A, C**) in $Irg1^{+/+}$ BMDMs. Nrf2 expression was also significantly increased in PA01 infected $Irg1^{+/+}$ BMDMs with 4-OI treatment compared with PA01 alone (+++ p<0.001, **Figure 5.10A, C**).

As previously mentioned, IL-1β has been associated with the inhibition of *P. aeruginosa* clearance both *in vitro* and *in vivo* (302, 304, 305). Here, we demonstrated that levels of pro-IL-1β protein were significantly increased upon PA01 infection in $Irg1^{+/+}$ BMDMS for 8 hours compared with DMSO treatment (*** p<0.001, **Figure 5.10A, E**). This data is consistent with our previous findings in PA01 infected RAW 264.7 cells

(**Figure 5.4**). 4-OI treatment significantly inhibited PA01 induced pro-IL-1β protein production compared with PA01 (+++ p<0.001, **Figure 5.10A, E**).

In Irg1$^{-/-}$ BMDMs, 4-OI (250 μM) treatment increased Nrf2 protein after 8 hours of treatment compared with DMSO alone, although this was not significant (**Figure 5.10B, D**). Pro-IL-1β protein production was significantly increased upon PA01 infection in Irg1$^{-/-}$ BMDMs following 8 hours of stimulation compared with DMSO (*** p<0.001, **Figure 5.10B, F**), which was significantly decreased upon 4-OI treatment compared with PA01 (+ p<0.05, **Figure 5.10D, F**).

5.3.5 4-OI, but not endogenous itaconate, regulates Gclm, Hmox1 and Nqo1 mRNA expression in PA01 infected BMDMs from Irg1$^{+/+}$ and Irg1$^{-/-}$ mice.

Once we observed significant upregulation of Nrf2 protein expression in 4-OI treated BMDMs, we subsequently examined the expression of antioxidant genes Gcml, Hmox1 and Nqo1 mRNA, which are downstream of Nrf2 (330, 429). As expected, 4-OI (250 μM) treatment significantly induced Gclm mRNA expression in Irg1$^{+/+}$ BMDMs after 8 hours compared with DMSO treatment (** p<0.01, **Figure 5.11A**). Upon PA01 infection (MOI 30) Gclm mRNA expression levels were decreased compared with DMSO treatment, while 4-OI enhanced Gclm expression in PA01 infected cells compared with PA01, although this is not significant (**Figure 5.11A**). Similarly, in Irg1$^{-/-}$ BMDMs 4-OI significantly increased Gclm mRNA expression after 8 hours compared with DMSO treatment (*** p<0.001, **Figure 5.11B**), with PA01 infection limiting this effect of 4-OI.

4-OI treatment significantly induced Hmox1 mRNA expression in Irg1$^{+/+}$ BMDMs after 8 hours compared with DMSO (******* p<0.001, **Figure 5.11C**). Upon PA01 infection Hmox1 mRNA expression levels are decreased compared with DMSO, while 4-OI increased Hmox1 mRNA expression in PA01 infected cells compared with PA01 although this is not significant (**Figure 5.11C**). In Irg1$^{-/-}$ BMDMs 4-OI increased Hmox1 mRNA expression after 8 hours compared with DMSO (**Figure 5.11D**), although this was not

significant. In PA01 infected Irg1$^{-/-}$ BMDMs, 4-OI did not significantly induce Hmox1 mRNA expression (**Figure 5.11D**).

Similarly, 4-OI treatment significantly induced Nqo1 mRNA expression in Irg1$^{+/+}$ BMDMs after 8 hours compared with DMSO (*** p<0.001, **Figure 5.11E**). PA01 infected Irg1$^{+/+}$ BMDMs express decreased levels of Nqo1 mRNA compared with DMSO, while 4-OI fails to induce Nqo1 mRNA expression in these infected cells (**Figure 5.11E**). In Irg1$^{-/-}$ BMDMs, 4-OI treatment significantly induced Nqo1 mRNA expression after 8 hours compared with DMSO (*** p<0.001, **Figure 5.11F**). PA01 infection decreased levels of Nqo1 mRNA in Irg1$^{-/-}$ BMDMs compared with DMSO, while 4-OI fails to induce Nqo1 mRNA expression in these infected cells (**Figure 5.11F**).

5.3.6 4-OI and endogenous itaconate regulate BMDM mediated P. aeruginosa killing.

Macrophages display potent anti-bacterial properties, playing an important role in the killing and removal of pathogens (72, 74). As previously mentioned, macrophages utilise numerous effector mechanisms to kill invading pathogens including ROS generation, phagocytic killing, and the release of anti-microbial peptides (200, 302, 403). Our aim was to investigate the effect of 4-OI and endogenous itaconate on BMDM mediated killing of *P. aeruginosa*.

Here, we demonstrated for the first time that 4-OI (250 μM) significantly promoted BMDM mediated killing of PA01 compared with DMSO (* p<0.05, **Figure 5.12A**) as a lower number of CFU/ml were recovered from cells treated with 4-OI compared with DMSO after 8 hours. We next examined the role of endogenous itaconate in BMDM mediated PA01 killing using itaconate expressing Irg1$^{+/+}$ BMDMs and itaconate deficient Irg1$^{-/-}$ cells. Here, we demonstrated for the first time that Irg1$^{+/+}$ BMDMs display significantly enhanced bactericidal capacity against PA01 compared with itaconate deficient Irg1$^{-/-}$ BMDMs (* p<0.05, **Figure 5.12B**) indicating that endogenous itaconate promotes the anti-bacterial activity of macrophages.

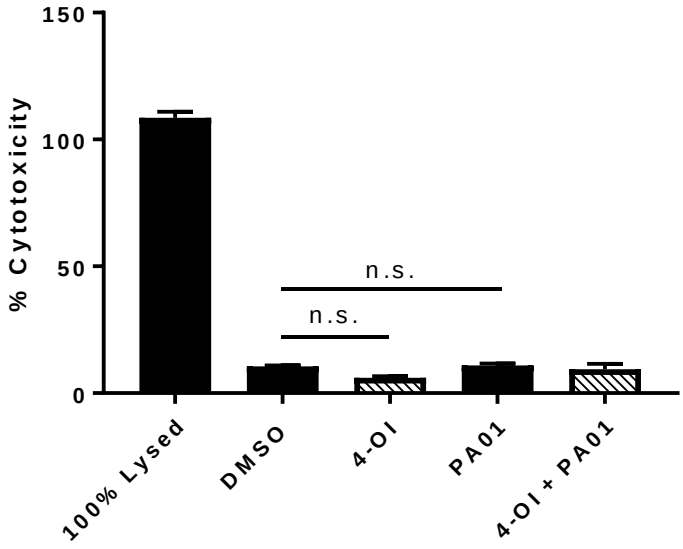

Figure 5.7. 4-OI and PA01 are not cytotoxic to BMDMs.

BMDMs from Irg1$^{+/+}$ mice were infected with PA01 (MOI 30) in the presence or absence of 4-OI (250 µM) for 8 hours. Cytotoxicity was measured by assessing lactate dehydrogenase release in cell supernatants. Results are expressed as a percentage of cytotoxicity of the 100% lysed positive control. Data is presented as mean ± SEM of 3 biological replicates with 3 technical replicates. A One-way ANOVA with a Tukey's multiple comparison post-hoc test was used to test for statistical differences. n.s; no significance.

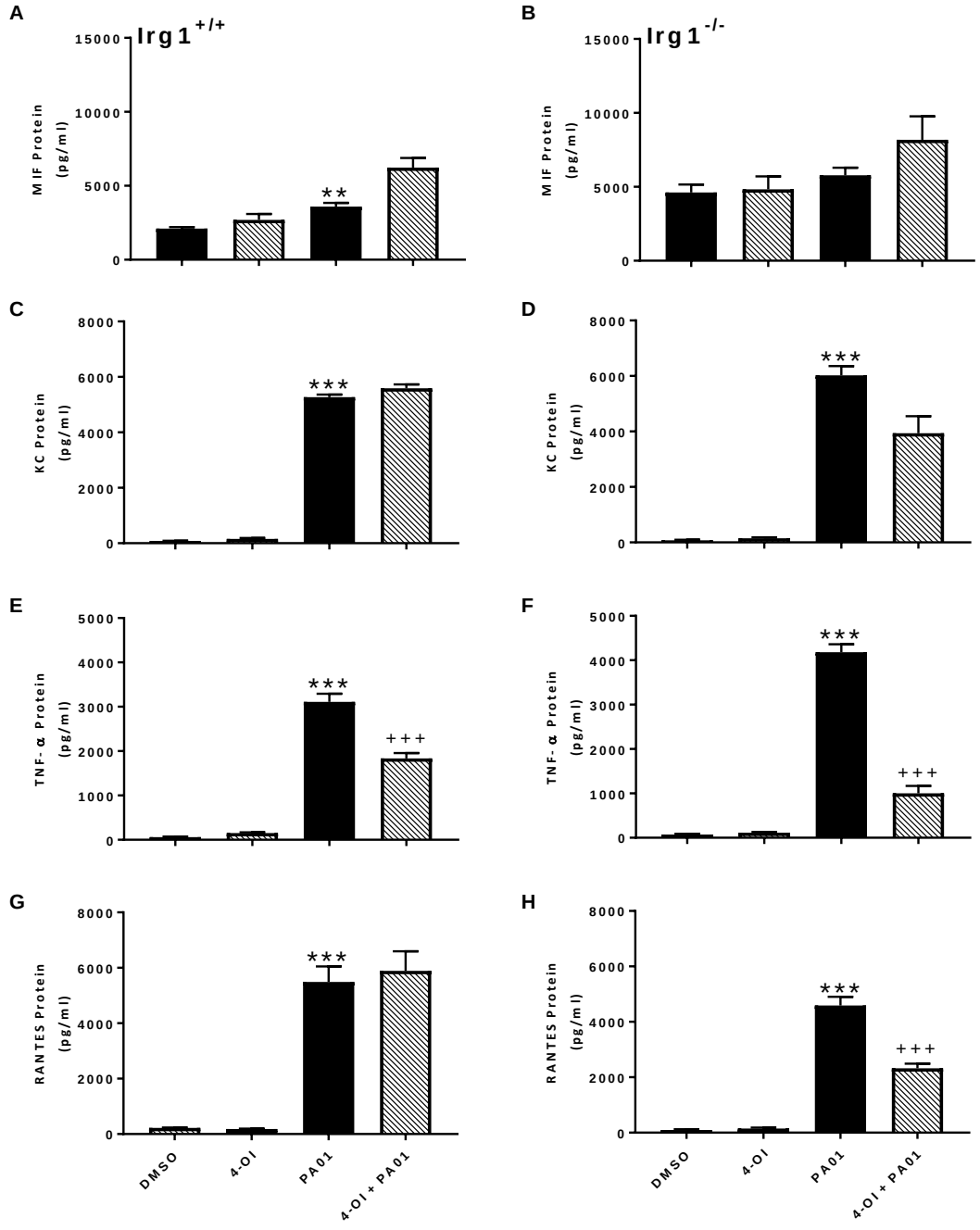

Figure 5.8. Effect of 4-OI on MIF, KC, TNF-α and RANTES protein production in PA01 infected BMDMs from Irg1$^{+/+}$ and Irg1$^{-/-}$ mice.

BMDMs from Irg1$^{+/+}$ and Irg1$^{-/-}$ mice were infected with PA01 (MOI 30) in the presence or absence of 4-OI (250 µM) for 8 hours. Protein levels of (**A, B**) MIF, (**C, D**) KC, (**E, F**) TNF- α and (**G, H**) RANTES were examined after 8 hours of infection. Protein production was quantified by ELISA. Data is presented as mean ± SEM of 3 independent experiments with 3 technical replicates. (**A, D, G**) A Kruskal-Wallis test with Dunn's multiple comparison post-hoc test was used to test for statistical differences. (**C, E, F, H**) A One-way ANOVA with a Tukey's multiple comparison post-hoc test was used to test for statistical differences. *** $p<0.001$; respective treatment compared with DMSO. +++ $p<0.001$; respective treatment compared with PA01.

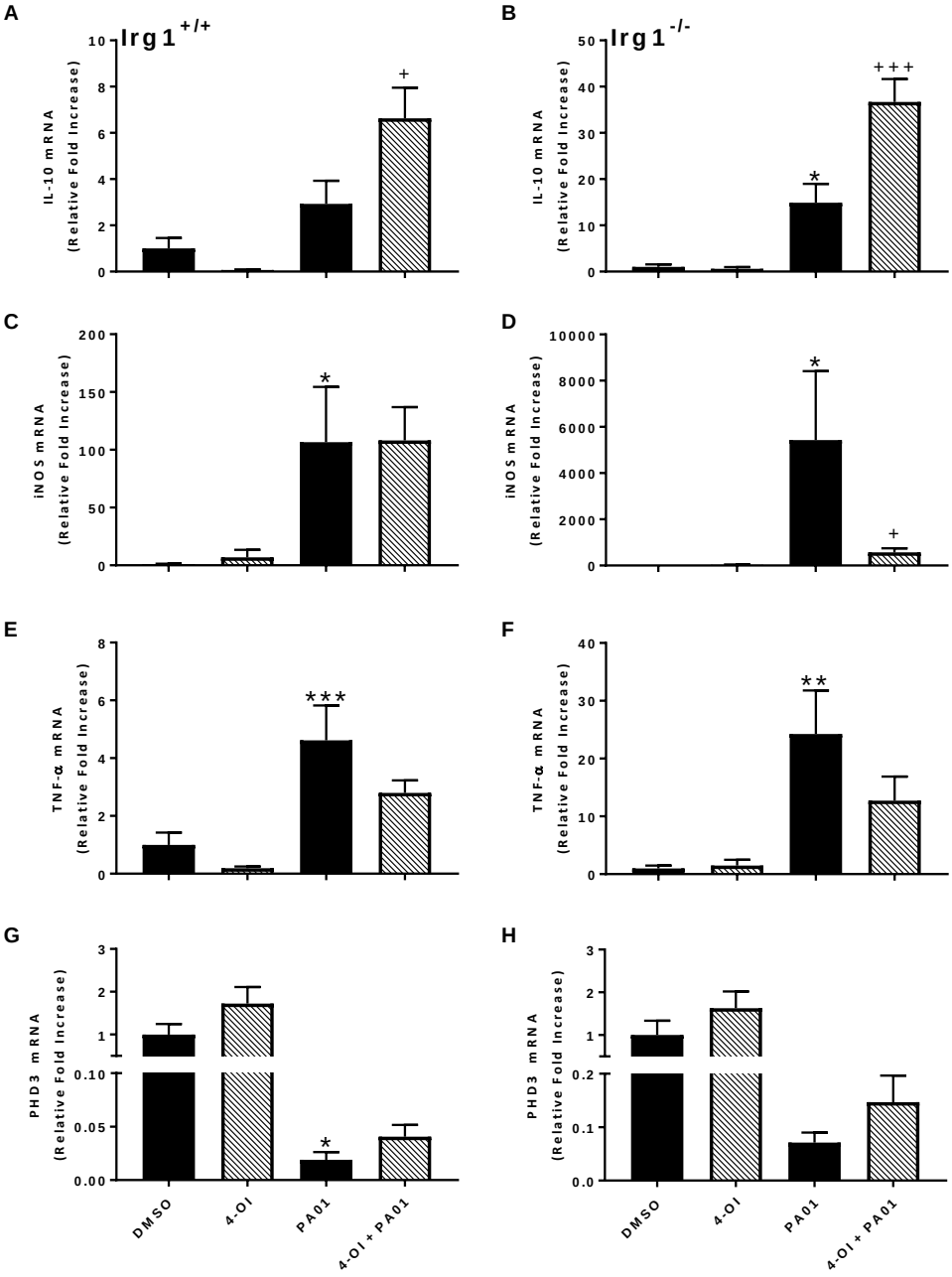

Figure 5.9. Effect of 4-OI on IL-10, iNOS, TNF-α and PHD3 mRNA expression in PA01 infected BMDMs from Irg1$^{+/+}$ and Irg1$^{-/-}$ mice.

BMDMs from Irg1$^{+/+}$ and Irg1$^{-/-}$ mice were infected with PA01 (MOI 30) in the presence or absence of 4-OI (250 µM) for 8 hours. mRNA levels of (**A, B**) IL-10, (**C, D)** iNOS, (**E, F**) TNF-α and (**G, H**) PHD3 were examined after 8 hours of infection. mRNA expression was assessed by qPCR. mRNA levels were standardised per unit of β-actin. Results are expressed as a relative fold increase compared with DMSO. Data is presented as mean ± SEM of 3 independent experiments with 3 technical replicates. A One-way ANOVA with a Tukey's multiple comparison post-hoc test was used to test for statistical differences. * p<0.05, ** p<0.01, *** p<0.001; respective treatment compared with DMSO.

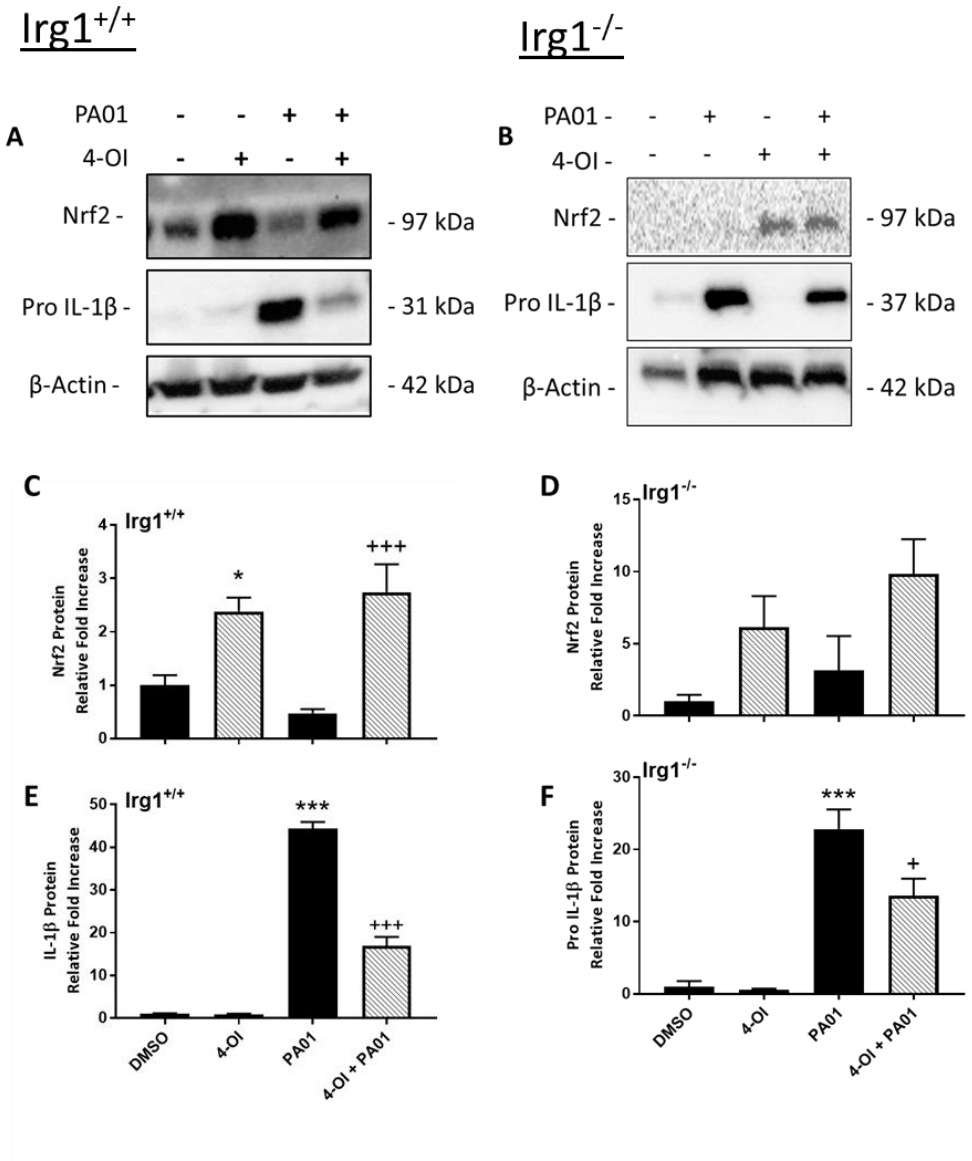

Figure 5.10. 4-OI induces Nrf2 protein expression and inhibits *P. aeruginosa* induced pro-IL-1β protein expression in PA01 infected Irg1$^{+/+}$ and Irg1$^{-/-}$ BMDMs.

Murine BMDMs were infected with PA01 (MOI 30) in the presence or absence of 4-OI (250 µM) for 8 hours. Levels of Nrf2 and pro-IL-1β were examined in Irg1$^{+/+}$ and Irg1$^{-/-}$ BMDMs respectively (**A, B**). Protein levels were analysed by Western blot. Western blot images are representative of 3 independent experiments. ImageJ software was used to obtain densitometry data. (**C**) Densitometry analysis of Nrf2 protein from Irg1$^{+/+}$ BMDMS. (**D**) Densitometry analysis of Nrf2 protein from Irg1$^{-/-}$ BMDMS (**E**) Densitometry analysis of pro-IL-1β protein from Irg1$^{+/+}$ BMDMS. (**F**) Densitometry analysis of pro-IL-1β protein from Irg1$^{-/-}$ BMDMS. For densitometry, protein levels were standardised per unit of β-actin. Results are expressed as a relative fold increase compared with DMSO. Data is presented as mean ± SEM of 3 independent replicates. A One-way ANOVA with a Tukey's multiple comparison post-hoc test was used to test for statistical differences. ***** p<0.05**,** *** p<0.001; respective treatment compared with DMSO. + P<0.05, +++ p< 0.001; respective treatment compared with PA01

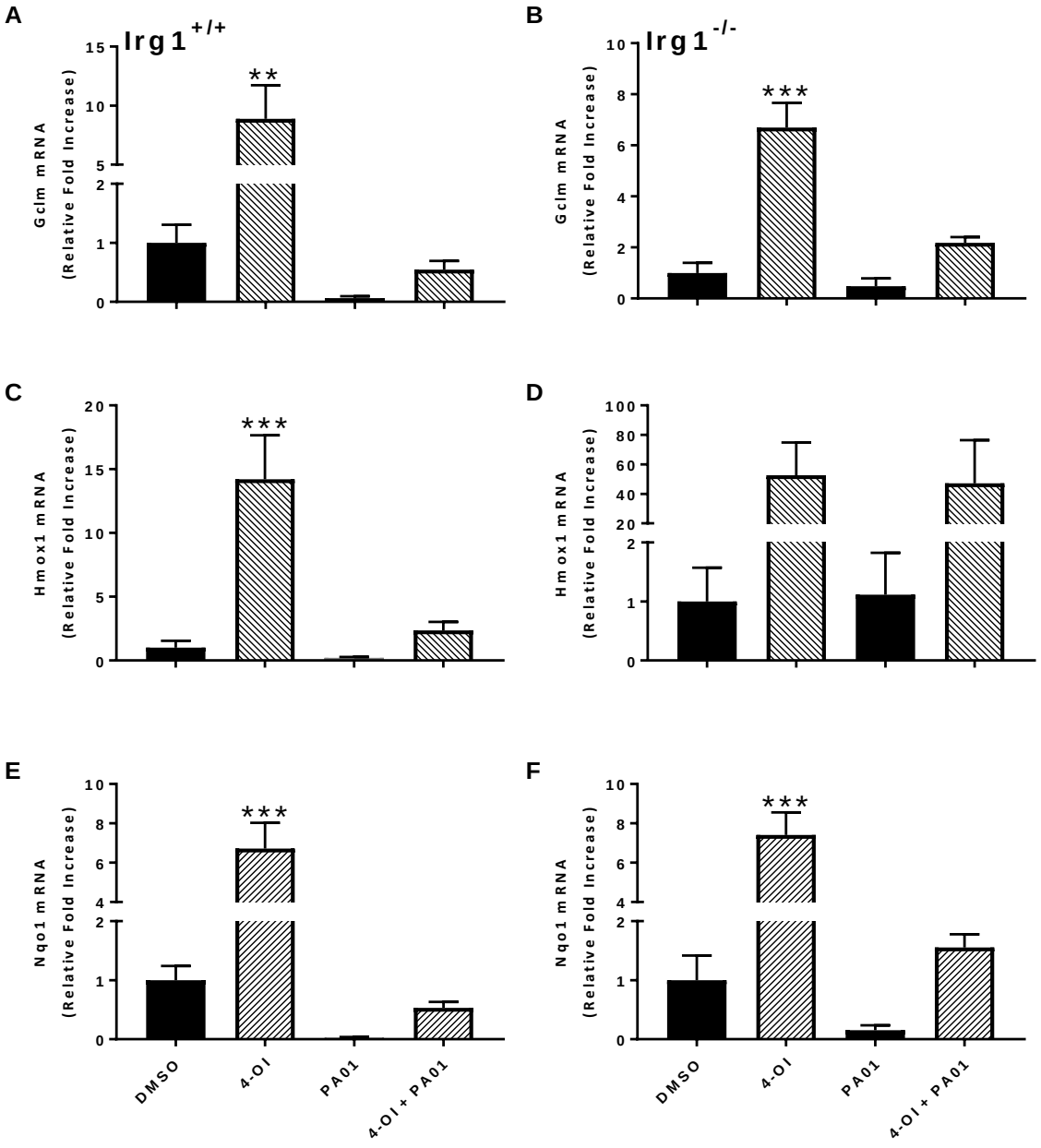

Figure 5.11. Effect of 4-OI on Gclm, Hmox1 and Nqo1 mRNA expression in PA01 infected BMDMs from Irg1$^{+/+}$ and Irg1$^{-/-}$ mice.

BMDMs from Irg1$^{+/+}$ and Irg1$^{-/-}$ mice were infected with PA01 (MOI 30) in the presence or absence of 4-OI (250 µM) for 8 hours. mRNA levels of (**A, B**) Gclm, (**C, D)** Hmox1 and (**E, F**) Nqo1 were examined after 8 hours of infection. mRNA expression was assessed by qPCR. mRNA levels were standardised per unit of β-actin. Results are expressed as a relative fold increase compared with DMSO. Data is presented as mean ± SEM of 3 independent experiments with 3 technical replicates. A One-way ANOVA with a Tukey's multiple comparison post-hoc test was used to test for statistical differences. ** p<0.01, *** p<0.001; respective treatment compared with DMSO.

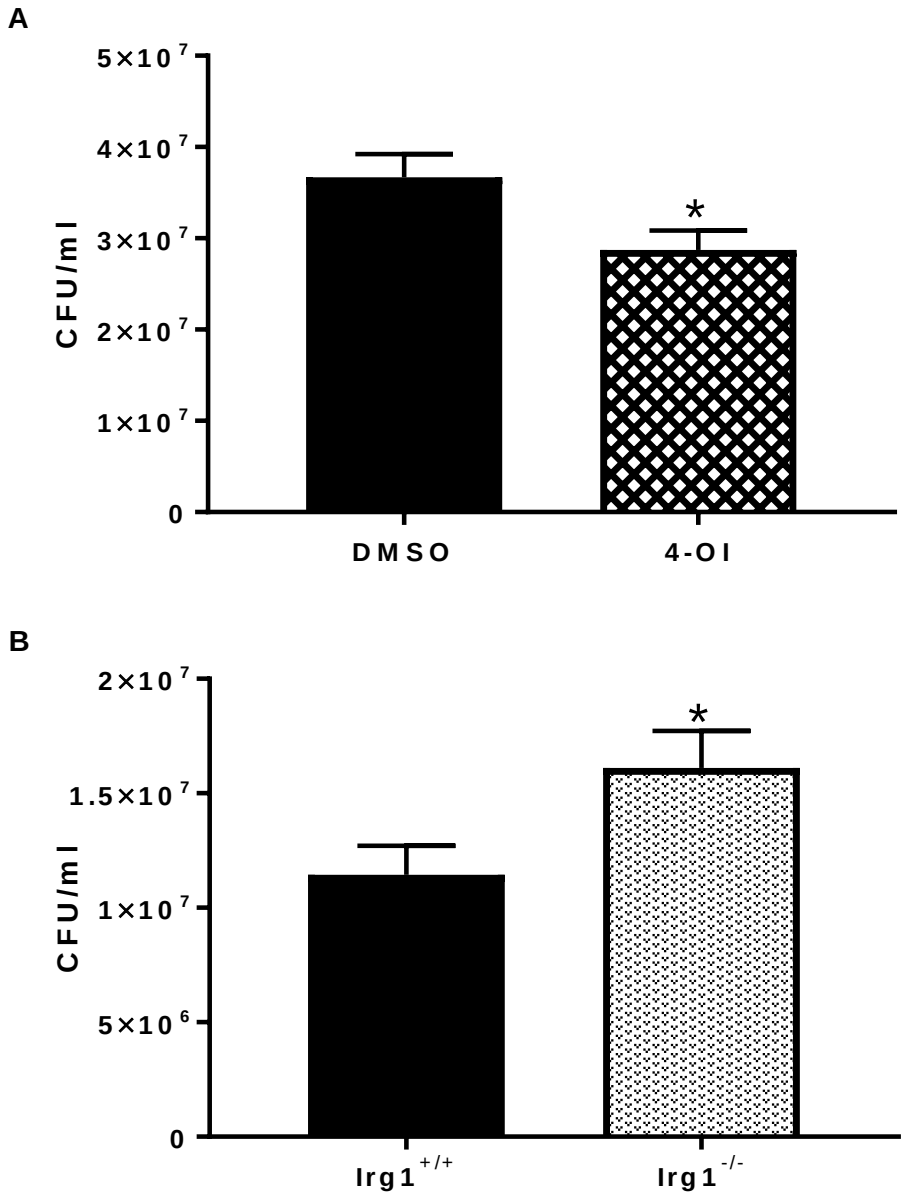

Figure 5.12. 4-OI and endogenous itaconate regulate BMDM mediated *P. aeruginosa* killing.

(**A**) 4-OI (250 µM) promotes macrophage mediated *P. aeruginosa* killing. (**B**) Itaconate deficiency inhibits macrophage mediated *P. aeruginosa* killing. BMDMs were infected with PA01 (MOI 10) for 4 hours. Macrophages were then lysed and combined with the respective supernatant before spot plating for CFU/ml analysis. Data is presented as mean ± SEM of 3 biological replicates with 3 technical replicates. A two-tailed unpaired t-test was used to test for statistical significance of differences. (**A**) * $p<0.05$; DMSO compared with 4-OI. (**B**) * $p<0.05$; $Irg1^{+/+}$ compared with $Irg1^{-/-}$.

5.4 Investigation of the effects of itaconate on *P. aeruginosa* growth, biofilm formation, virulence factor production and antibiotic resistance.

We have established that 4-OI and itaconate promote bacterial clearance by macrophages (**Figure 5.12**). Next, we examined the effects of itaconate on a number of key facets of *P. aeruginosa* infection.

5.4.1 Itaconate inhibits the growth of P. aeruginosa.

Firstly, we examined the effects of itaconate on *P. aeruginosa* growth. Here, we demonstrated that itaconate inhibits *P. aeruginosa* growth in LB broth. For PA01, bacterial growth was inhibited at a concentration of 780 μg/ml of itaconate (**Figure 5.13A**). For clinical isolates CI#5158, CI#5382, CI#5082 and CI#5194, bacterial growth was noticeably reduced at 780 μg/ml of itaconate compared with LB only and was completely inhibited at 1560 μg/ml of itaconate (**Figure 5.13B, C, D, F**). Similar to PA01, bacterial growth was inhibited at a concentration of 780 μg/ml of itaconate for clinical isolate CI#5436 (**Figure 5.13E**).

5.4.2 Itaconate inhibits P. aeruginosa biofilm formation.

P. aeruginosa is one of many types of bacterial pathogen that are capable of forming biofilms (459). Biofilm formation involves attachment to surrounding surfaces followed by division and growth of bacteria within a matrix consisting of extracellular polymeric substances such as mucus, lipids and extracellular DNA attachment (259, 260). By switching to a biofilm mode of growth *P. aeruginosa* displays increased antibiotic resistance which is of importance in diseases such as CF (233, 258, 278). As such, our aim was to examine the effects of itaconate on *P. aeruginosa* biofilm formation.

As we have established the impacts of itaconate on *P. aeruginosa* growth, we next investigated the effect of itaconate on biofilm formation. Here, we demonstrated

that itaconate dose dependently inhibited biofilm formation of PA01 after 24 hours of growth (**Figure 5.14A**). Furthermore, itaconate also inhibited biofilm formation in all five clinical isolated *P. aeruginosa* strains CI#5158, CI#5382, CI#5082, CI#5436 and CI#5194 respectively (**Figure 5.14B-F**). Complete inhibition of biofilm formation was observed at a concentration 1560 μg/ml of itaconate in five strains tested, while complete inhibition was observed at 3120 μg/ml of itaconate for CI#5158.

5.4.3 Itaconate antagonises the efficacy of commonly used antibiotics tobramycin, meropenem, azactam and piperacillin/tazobactam against P. aeruginosa.

We next examined the effects of itaconate on the tolerance of *P. aeruginosa* to four commonly used antibiotics against *P. aeruginosa*. To do this, we utilised the checkerboard assay which is routinely used to examine interactions between anti-microbial compounds (**Figure 5.15**). The checkerboard assay assesses the interaction between two compounds by examining a variety of concentrations of each compound in 2-fold dilutions (386). From this assay, the Fractional Inhibitory Concentration Index (FICI) is calculated. The FICI is calculated by comparing the Minimum Inhibitory Concentration (MIC), the lowest concentration of an agent required to inhibit bacterial growth, of each compound alone with the MIC of the compounds in combination (386). The FICI is calculated as per the following equation.

$$\text{FICI} = \frac{\text{Concentration of A in combination}}{\text{MIC of A alone}} + \frac{\text{Concentration of B in combination}}{\text{MIC of B}}$$

Compounds can act synergistically, whereby the presence of agent A lowers the concentration of agent B needed to inhibit bacterial growth to a concentration lower than that required when agent B is used alone. For example, agent A has an MIC of 32 μg/ml when used against *P. aeruginosa* alone, but in the presence of agent B the MIC of agent A becomes 8 μg/ml. Combinations of agents which result in a 4-fold decrease

(FICI ≤ 0.5) in the MIC compared with the MIC of agents alone are said to act synergistically (**Figure 5.15**) (386, 387).

Compounds can also act antagonistically whereby the presence of agent A increases the concentration of agent B needed to inhibit bacterial growth to a concentration higher than that required when agent B is used alone. For example, agent A has an MIC of 32 μg/ml when used against *P. aeruginosa* alone, but in the presence of agent B the MIC of agent A becomes 128 μg/ml. Combinations of agents which result in a 4-fold increase (FICI ≥ 4) in the MIC compared with the MIC of agents alone are said to act antagonistically (**Figure 5.15**) (386, 387). Alternatively, a FICI of between 0.5 and 4 indicates that the two compounds have no interactions.

In these experiments, we examined the effects of a concentration gradient of itaconate ranging from 48 μg/ml to 1560 μg/ml. These concentrations correspond to 0.375 mM to 12 mM itaconate.

Tobramycin is a broad spectrum antibiotic from the aminoglycoside family which is particularly effective against *P. aeruginosa* (49). Inhaled tobramycin is approved for the treatment of chronic *P. aeruginosa* infection in CF patients (48, 49). Here, we demonstrated for the first time that itaconate a concentration range of 195 – 390 μg/ml antagonises the anti-bacterial effects of tobramycin **(Table 5.1**). For PA01, the MIC of tobramycin was 4 μg/ml. When PA01 was cultured in LB broth containing 195 μg/ml of itaconate the MIC of tobramycin was 16 μg/ml. This corresponds to a FICI of 4.19 and as a result it is said that itaconate at a concentration of 195 μg/ml antagonises the effects of tobramycin on PA01. At a concentration of 390 μg/ml of itaconate, antagonistic effects on tobramycin were observed in PA01 and four of five clinical isolates where the FICI of ranged from 4.13 – 8.25.

Meropenem is a broad spectrum antibiotic from carbapenem family which is administered intravenously for the treatment of multi drug resistant gram negative bacterial infections, including *P. aeruginosa* (45, 46). Here, we demonstrated for the first time that itaconate a concentration of 390 μg/ml antagonises the anti-bacterial effects of meropenem (**Table 5.2**). For PA01, the MIC of meropenem was 1 μg/ml. When PA01 was cultured in LB broth containing 390 μg/ml of itaconate the MIC of meropenem

was 4 μg/ml. This corresponds to a FICI of 4.25 and as a result it is said that itaconate at a concentration of 390 μg/ml antagonises the effects of meropenem on PA01. At a concentration of 390 μg/ml of itaconate, antagonistic effects on meropenem were observed in PA01 and two of five clinical isolates where the FICI of ranged from 4.13 – 16.13.

Azactam is a member of the β-lactam antibiotic family and is primarily used to treat gram-negative bacterial infections (460). Azactam is delivered intravenously or as an inhaled agent and is approved for use in CF patients with *P. aeruginosa* infection (461). Here, we demonstrated for the first time that itaconate a concentration of 390 μg/ml antagonises the anti-bacterial effects of azactam (**Table 5.3**). For PA01, the MIC of azactam was 8 μg/ml. When PA01 was cultured in LB broth containing 390 μg/ml of itaconate the MIC of azactam was 32 μg/ml. This corresponds to a FICI of 4.25 and as a result it is said that itaconate at a concentration of 390 μg/ml antagonises the effects of azactam on PA01. At a concentration of 390 μg/ml of itaconate, antagonistic effects on azactam were observed in PA01 and five of five clinical isolates where the FICI of ranged from 4.13 – 16.13. Itaconate at a concentration of 195 μg/ml also antagonised the effects of azactam in CI#5382 and CI#5082, with a FICI of 4.09 observed in both strains. Itaconate at a lower concentration of 97.6 μg/ml also antagonised the effects of azactam on CI#5382 with a FIC of 4.06.

Piperacillin/tazobactam a combination antibiotic therapy comprised the β-lactam piperacillin and the β-lactamase inhibitor tazobactam. Is used intravenously to treat *P. aeruginosa* infection (462). Here, we demonstrated for the first time that itaconate a concentration of 390 μg/ml antagonises the anti-bacterial effects of piperacillin/tazobactam (**Table 5.4**). For PA01, the MIC of piperacillin/tazobactam was 4 μg/ml. When PA01 was cultured in LB broth containing 390 μg/ml of itaconate the MIC of piperacillin/tazobactam was 16 μg/ml. This corresponds to a FICI of 4.25 and as a result it is said that itaconate at a concentration of 390 μg/ml antagonises the effects of piperacillin/tazobactam on PA01. At a concentration of 390 μg/ml of itaconate, antagonistic effects on piperacillin/tazobactam were observed in PA01 and all five clinical isolates where the FICI of ranged from 4.13 – 8.13. In CI#5436, itaconate

antagonised the effects of piperacillin/tazobactam at the lowest concentration of itaconate tested (48.8 µg/ml) uo to 390 µg/ml.

5.4.4 Itaconate decreases PA01 pyocyanin production but not elastase activity, two key virulence factors.

As we have established that itaconate inhibits *P. aeruginosa* growth, we next examined the effects of itaconate on bacteria that were still viable and reproducing. Our aim was to examine the effects of itaconate on *P. aeruginosa* secreted virulence factors, pyocyanin and elastase.

Pyocyanin is a redox active phenazine that is secreted by *P. aeruginosa* which gives the liquid culture it's characteristic blue colour. Pyocyanin production has been shown to be essential virulence factor in *P. aeruginosa* pathogenesis. Murine models have demonstrated that pyocyanin drives lung inflammation and cellular damage, while infection with pyocyanin deficient isogenic mutants of PA01 results in less severe pneumonia in models of both acute and chronic lung infection in mice (463). Further models have shown pyocyanin to be necessary in the killing of plants, *Drosophila melanogaster* and *C. elegans* (464-466).

Here, we demonstrated for the first time that itaconate significantly inhibits the production of pyocyanin by PA01 after 18 hours of culture at concentrations of 97.5 µg/ml (** $p<0.01$, **Figure 5.16A**), 195 µg/ml (*** $p<0.001$, **Figure 5.16A**) and 390 µg/ml (*** $p<0.01$, **Figure 5.16A**), respectively.

Next, we examined the effect of itaconate on *P. aeruginosa* elastase production. Elastase is a virulence factor that is produced by *P. aeruginosa* and acts to degrade host elastin and compromise the barrier function of the epithelium through disruption of epithelial tight junction proteins (242, 243). Elastase has also been shown to degrade important host mucins and surfactant proteins which are necessary for effective bacterial clearance (467-469).

We utilised the elastin-Congo red assay whereby supernatant from bacterial cultures are incubated with elastin-Congo red which is insoluble in this medium.

Elastase acts to cleave the elastin, releasing the Congo red which is soluble in LB broth. Residual elastin-Congo red is removed by centrifugation and the absorbance of the sample recorded at 495 nm. Here, we demonstrated that itaconate did not impact the production of elastase by *P. aeruginosa* after 18 hours of culture, as quantified using the elastin-Congo red assay (**Figure 5.16B**).

5.4.5 Itaconate induces PA01 expression of PA0882 and PA0883 mRNA expression, but not aceA mRNA expression.

Previously, it has been demonstrated that itaconate inhibits isocitrate lyase in *Pseudomonas indigofera*, an enzyme that plays a role in the glyoxylate shunt (470). The isocitrate lyase enzyme, which is under the control of the *aceA* gene, is part of the glyoxylate shunt pathway in *P. aeruginosa* where it converts isocitrate to glyoxylate and succinate (471). They glyoxylate shunt enables bacteria to use alternative carbon sources such as acetate when simple sugars, such as glucose, are not readily available as a fuel source (470). The glyoxylate shunt is of importance as phagocytosed bacteria utilise this mechanism of energy generation within the phagosome of macrophages after phagocytosis where they experience nutrient starvation (472). As itaconate is known to inhibit the isocitrate lyase enzyme, we examined the effects of itaconate on aceA mRNA expression. Here, we demonstrated that itaconate has no effect on the expression of aceA mRNA in PA01 cultured in a LB broth for 18 hours (**Figure 5.17A**).

We next examined the effects of itaconate on the expression of PA0882 and PA0883 mRNA in PA01. *P. aeruginosa* has been shown to express genes involved in the detoxification of itaconate (378, 381). These genes are *PA0882* and *PA0883* which encode succinyl-CoA: itaconate CoA transferase and (S)-citramalyl-CoA lyase respectively, which act to process itaconate to Acetyl-CoA and pyruvate (378, 381). Here, we demonstrated that PA01 cultured in LB broth containing 97.5 μg/ml itaconate expressed significantly higher levels of PA0882 mRNA compared with medium only (** $p<0.01$, **Figure 5.17B**). Expression of PA0882 was also higher in PA01 cultured in LB broth containing 390 μg/ml itaconate compared with medium only, although this was not significant (**Figure 5.17B**). We also demonstrated an increase in PA0883 mRNA

expression in PA01 cultured in LB broth containing 97.5 and 195 μg/ml itaconate compared with medium (**Figure 5.17C**). PA0883 was significantly increased in PA01 cultured in LB broth containing 390 μg/ml itaconate compared with medium only (* $p<0.05$, **Figure 5.17C**).

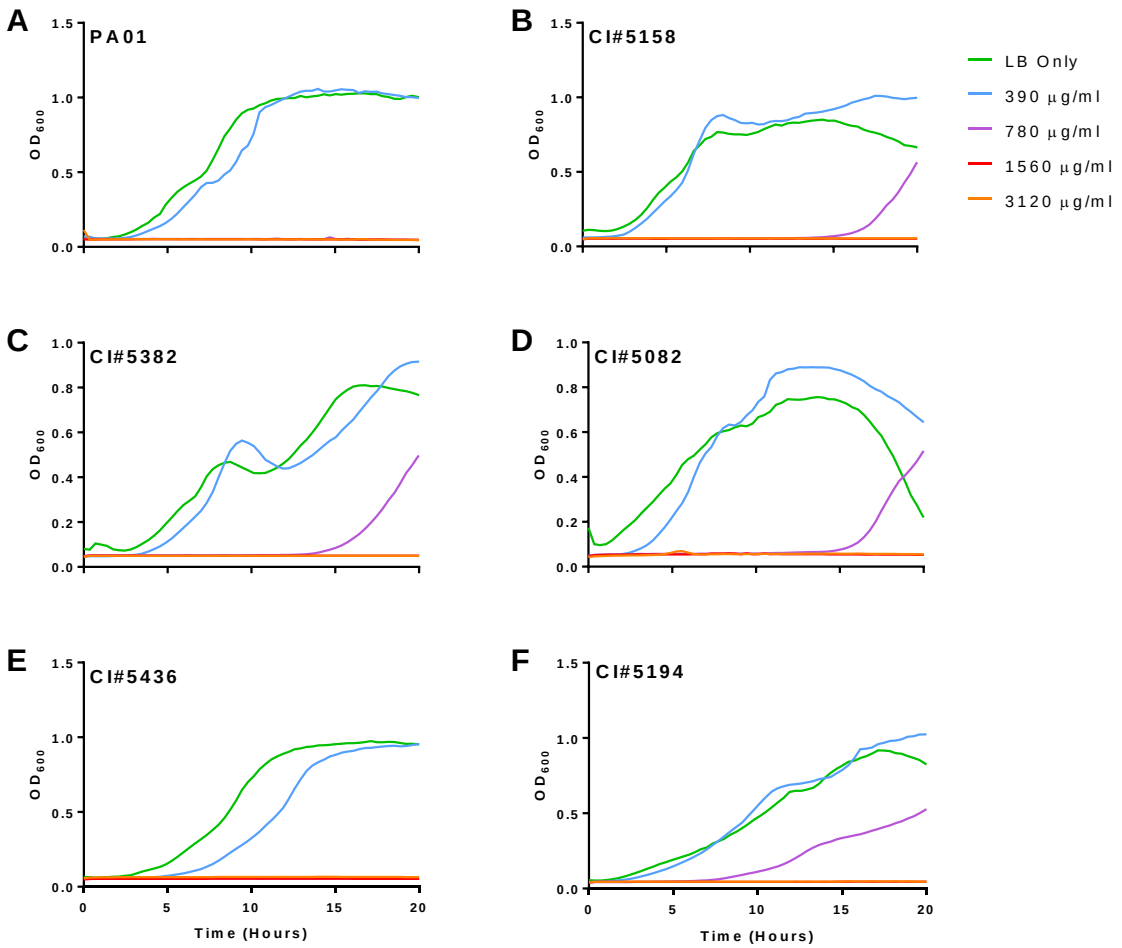

Figure 5.13. Itaconate inhibits the growth of *P. aeruginosa*.

Growth curves of (**A**) PA01 and clinical isolates from CF patients (**B**) CI#5158 (**C**) CI#5382 (**D**) CI#5082 (**E**) CI#5436 (**F**) CI#5194. Bacteria were cultured for 20 hours in LB broth containing itaconate (390, 780, 1560, 3120 µg/ml). Graphs are representative of 3 independent experiments with similar results.

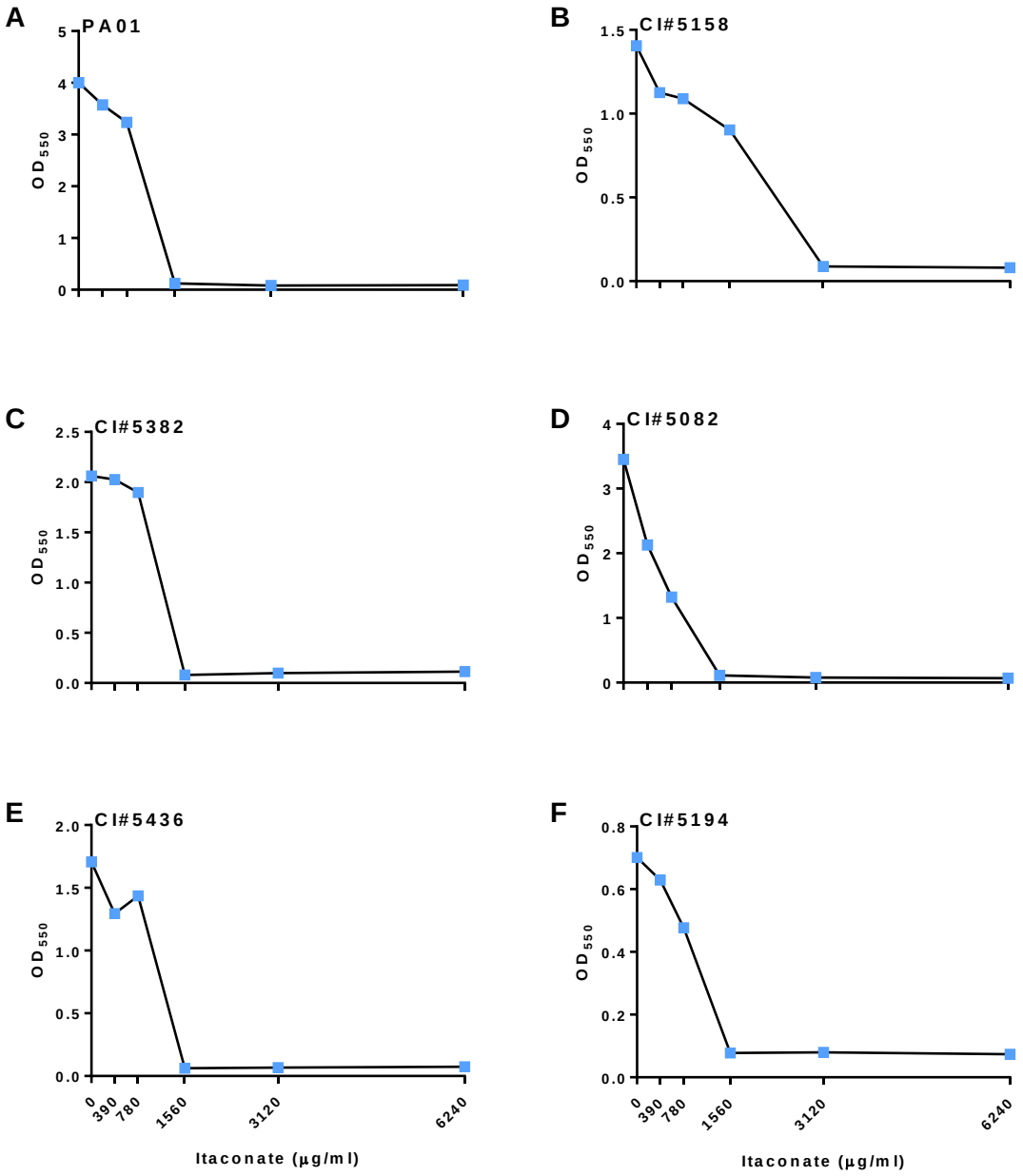

Figure 5.14. Itaconate inhibits the *P. aeruginosa* biofilm formation.

Biofilm formation of (**A**) PA01 and clinical isolates (**B**) CI#5158 (**C**) CI#5382 (**D**) CI#5082 (**E**) CI#5436 (**F**) CI#5194. Biofilms were cultured for 24 hours in LB broth containing itaconate (3, 6, 12, 24, 48 mM). Graphs are representative of 3 independent experiments with similar results.

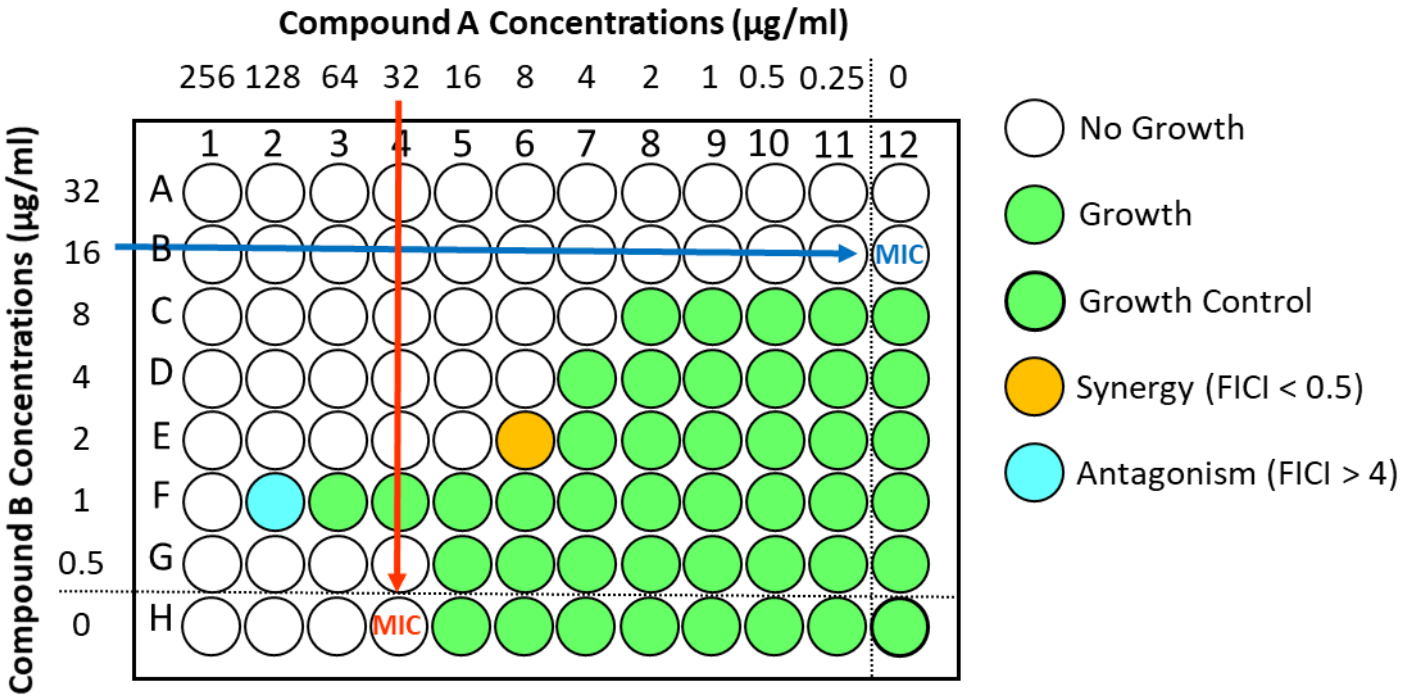

Figure 5.15. Illustrative example of the minimum inhibitory concentrations (MICs) (µg/ml) and corresponding fractional inhibitory concentration indices (FICI) of two compounds as calculated using the checkerboard assay.

The MIC of a compound is demonstrated by the lowest concentration of a single compound alone that is required to inhibit bacterial growth. Synergy is indicated by a FICI of < 0.5, as calculated by the FICI equation respectively. Antagonistic effects are indicated by a FICI > 4, as calculated by the FICI equation respectively.

Table 5.1. Tobramycin MICs (µg/ml) and corresponding FICI in the presence of increasing itaconate concentrations for PA01 and five *P. aeruginosa* clinical isolates as per checkerboard assay.

Strain	Itaconate MIC (µg/ml)	Tobramycin MIC (µg/ml)	Itaconate (µg/ml)									
			48.8		97.6		195		390		780	
			Tobramycin (µg/ml)	FICI	Tobramycin (µg/ml)	FICI	Tobramycin (µg/ml)	FICI	Tobramycin (µg/ml)	FICI	Tobramycin (µg/ml)	FICI
PA01	780	4	4	1.06	4	1.13	16	4.19	32	8.25	8	2.31
CI#5158	1560	4	8	2.03	8	2.06	8	2.09	16	4.13	8	2.16
CI#5382	1560	2	4	2.03	4	2.06	8	4.09	16	8.13	2	1.16
CI#5082	1560	4	4	1.03	8	2.06	8	2.09	16	4.13	4	1.16
CI#5436	780	16	16	1.06	16	1.13	16	1.19	16	1.25	-	-
CI#5194	1560	4	4	1.03	4	1.06	8	2.09	32	8.13	8	2.16

FICI values equating to antagonism are shown with blue shading.

Table 5.2. Meropenem MICs (µg/ml) and corresponding FICI in the presence of increasing itaconate concentrations for PA01 and five *P. aeruginosa* clinical isolates as per checkerboard assay.

Strain	Itaconate MIC (µg/ml)	Meropenem MIC (µg/ml)	Itaconate (µg/ml)									
			48.8		97.6		195		390		780	
			Meropenem (µg/ml)	FICI	Meropenem (µg/ml)	FICI	Meropenem (µg/ml)	FICI	Meropenem (µg/ml)	FICI	Meropenem (µg/ml)	FICI
PA01	780	1	1	1.06	1	1.13	2	2.19	4	4.25	2	2.31
CI#5158	1560	0.5	0.5	1.03	0.5	1.06	0.5	1.09	1	2.13	.25	0.66
CI#5382	1560	0.25	0.25	1.03	0.25	1.06	0.25	1.09	0.5	2.13	0.25	1.16
CI#5082	1560	0.5	0.5	1.03	0.5	1.06	1	2.09	4	16.13	0.5	1.16
CI#5436	780	16	16	1.06	16	1.13	16	1.19	16	1.25	-	-
CI#5194	1560	0.25	0.25	1.03	0.25	1.06	0.25	1.09	1	4.13	4	16.16

FICI values equating to antagonism are shown with blue shading.

Table 5.3. Azactam MICs (µg/ml) and corresponding FICI in the presence of increasing itaconate concentrations for PA01 and five *P. aeruginosa* clinical isolates as per checkerboard assay.

Strain	Itaconate MIC (µg/ml)	Azactam MIC (µg/ml)	Itaconate (µg/ml)									
			48.8		97.6		195		390		780	
			Azactam (µg/ml)	FICI	Azactam (µg/ml)	FICI	Azactam (µg/ml)	FICI	Azactam (µg/ml)	FICI	Azactam (µg/ml)	FICI
PA01	780	8	8	1.06	8	1.13	8	1.19	32	4.25	8	1.16
CI#5158	1560	8	8	1.03	8	1.06	16	2.09	64	8.13	8	1.16
CI#5382	1560	2	4	2.03	8	4.06	8	4.09	16	8.13	4	2.16
CI#5082	1560	4	4	1.03	8	2.06	16	4.09	64	16.13	2	0.66
CI#5436	780	8	8	1.06	8	1.13	16	2.19	32	4.25	-	-
CI#5194	1560	4	4	1.03	4	1.06	4	1.09	16	4.13	2	0.66

FICI values equating to antagonism are shown with blue shading.

Table 5.4. Piperacillin/Tazobactam MICs (µg/ml) and corresponding FICI in the presence of increasing itaconate concentrations for PA01 and five *P. aeruginosa* clinical isolates as per checkerboard assay.

Strain	Itaconate MIC (µg/ml)	Piperacillin/ Tazobactam MIC (µg/ml)	Itaconate (µg/ml)									
			48.8		97.6		195		390		780	
			Piperacillin/ Tazobactam (µg/ml)	FICI	Piperacillin/ Tazobactam (µg/ml)	FICI	Piperacillin/ Tazobactam (µg/ml)	FICI	Piperacillin/ Tazobactam (µg/ml)	FICI	Piperacillin/ Tazobactam (µg/ml)	FICI
PA01	780	4	4	1.06	4	1.13	4	1.19	16	4.25	4	1.16
CI#5158	1560	8	8	1.03	8	1.06	8	1.09	32	4.13	4	0.66
CI#5382	1560	2	4	2.03	4	2.06	4	2.09	16	8.13	1	0.66
CI#5082	1560	4	4	1.03	4	1.06	4	1.09	32	8.13	2	0.66
CI#5436	780	32	128	4.06	128	4.13	>256	>4	>256	>4	-	-
CI#5194	1560	2	2	2.03	2	2.06	4	2.09	8	4.13	2	1.16

FICI values equating to antagonism are shown with blue shading.

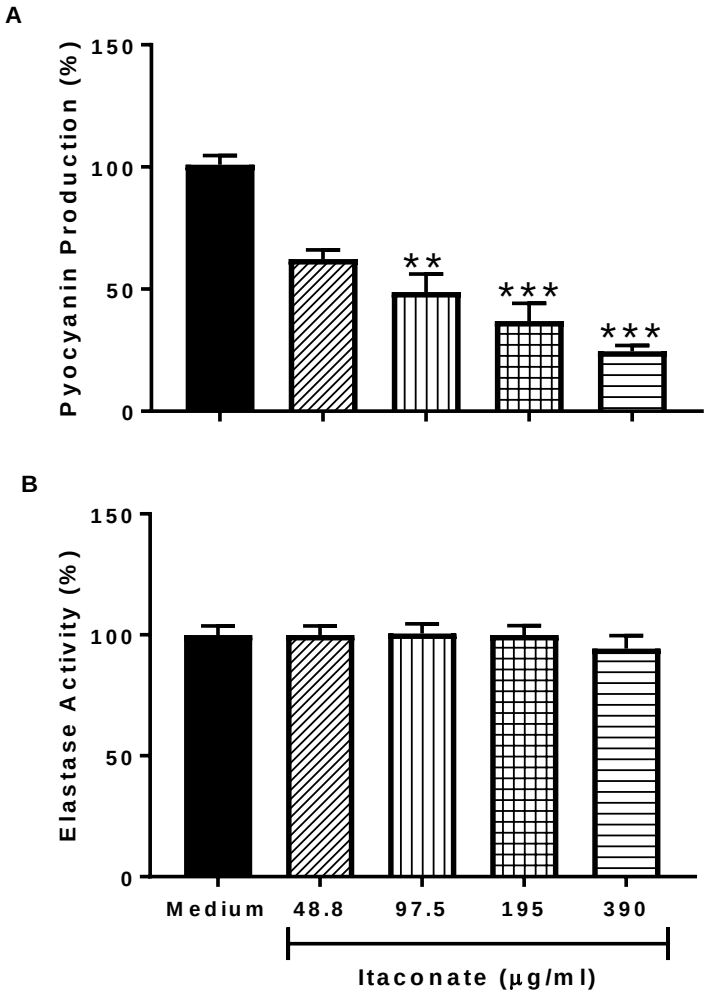

Figure 5.16. Effect of itaconate on PA01 pyocyanin production and elastase activity.

PA01 were cultured in LB broth containing itaconate (48.8 – 390 µg/ml) for 18 hours. (**A**) Pyocyanin was then extracted with chloroform and HCl, and absorbance readings were taken at 520 nm for pyocyanin quantification. (**B**) Elastase production in PA01 was measured by the elastin-Congo red assay. After 18 hours of culture, supernatants were then incubated with elastin-Congo red for 6 hours. The absorbance was recorded at 495 nm. Data is presented as mean ± SEM of 3 independent experiments with 3 technical replicates. A Kruskal-Wallis test with Dunn's multiple comparison post-hoc test was used to test for statistical differences. ** $p<0.01$, *** $p<0.001$; respective treatment compared with medium.

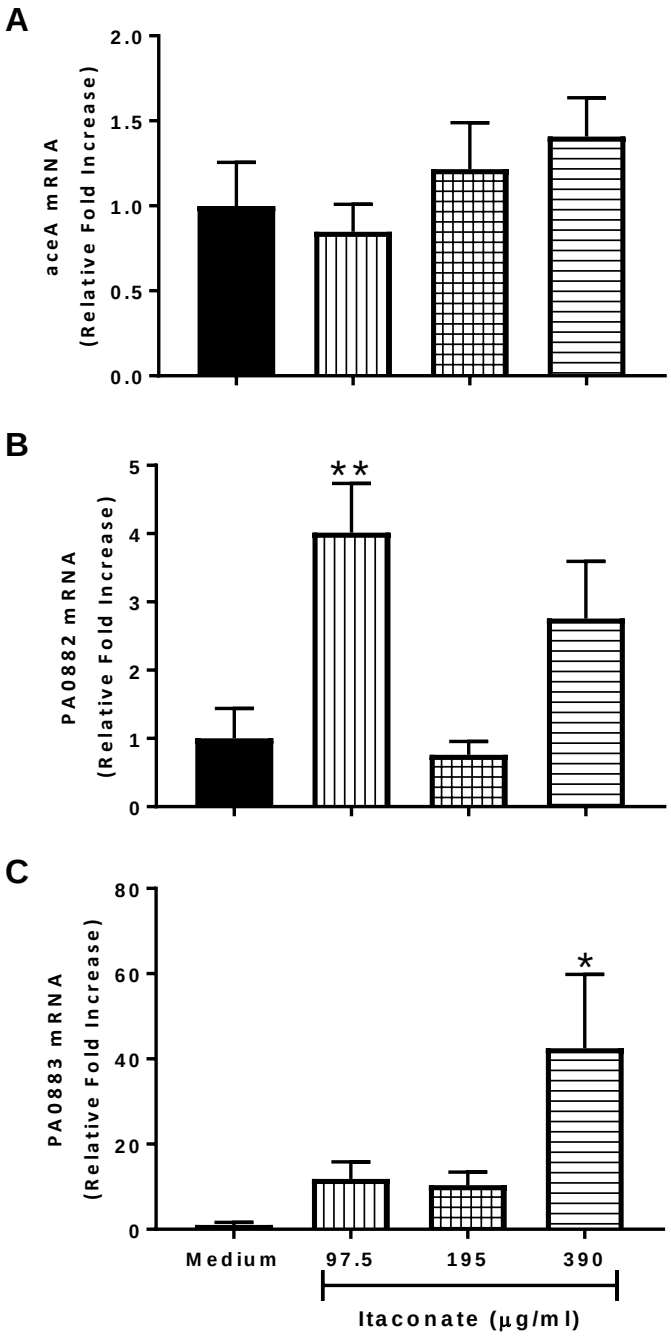

Figure 5.17. Effects of itaconate on aceA mRNA expression, from the glyoxylate shunt, and PA0882 and PA0883 mRNA expression, which are involved in itaconate detoxification.

PA01 was cultured for 24 hours in LB broth containing itaconate (97.5 – 390 µg/ml). mRNA levels of (**A**) aceA, (**B**) PA0882 and (**C**) PA0883 were quantified by qPCR analysis. mRNA levels were standardised per unit of rpoD. Results are expressed as a relative fold increase compared with medium. Data is presented as mean ± SEM of 3 independent experiments with 3 technical replicates. A One-way ANOVA with a Tukey's multiple comparison post-hoc test was used to test for statistical differences. * $p<0.05$, ** $p<0.01$; respective treatment compared with medium.

5.5 Investigation of the effects of itaconate and 4-OI on *P. aeruginosa* infection *in vivo* using the *G. mellonella* infection model.

In this chapter, we established that 4-OI limited *P. aeruginosa* induced inflammation in macrophages (**Figure 5.8 - Figure 5.11**). We also demonstrated that 4-OI and itaconate promote macrophage mediated *P. aeruginosa* clearance (**Figure 5.12**). Furthermore, we demonstrated that itaconate inhibits *P. aeruginosa* growth, biofilm formation any pyocyanin production (**Figure 5.14 - Figure 5.16**). However, we also observed increased antibiotic resistance in *P. aeruginosa* cultured in itaconate, most notably at a concentration of 390 µg/ml (**Table 5.1 - Table 5.4**). Following this, we examined the effects of itaconate and 4-OI on *P. aeruginosa* infection *in vivo*.

5.5.1 Itaconate is protective in vivo in a model of P. aeruginosa infection in G. mellonella.

We assessed the effects of itaconate and 4-OI *in vivo* using an invertebrate model of *P. aeruginosa* infection. *G. mellonella* larvae are becoming a popular tool as an *in vivo* model of bacterial infection (473). *G. mellonella* offer many benefits as they are inexpensive, are available in large numbers and do not require specialist laboratory equipment (473). Most importantly, although they lack an adaptive immune system, the innate immune system of *G. mellonella* is very similar to that of vertebrates (473). The humoral arm of the *G. mellonella* immune system is comprised of a variety of soluble factors which act to immobilise and kill pathogens (473-475). The cellular arm of the *G. mellonella* immune system is comprised of a variety of phagocytic cells knowns as haemocytes which act to phagocytose and kill invading pathogens (473, 476, 477).

G. mellonella are routinely utilised in studies examining the virulence of *P. aeruginosa* strains and efficacy of anti-microbial agents (473). Here, we demonstrated at inoculation of *G. mellonella* with 20 µl of PBS does not impact survival, while inoculation with 20 µl of PBS containing 2.5 x 10^3 CFU/ml of PA01, equating to 50 CFU, induces death at 24 hours, as indicated by melanisation (**Figure 5.18**).

Next, we examined the effect of itaconate alone on *G. mellonella* survival. *G. mellonella* use for this study had an average weight of 0.25 g, with every unit weighing between 0.2 and 0.3 g. Here, we demonstrated for the first time that itaconate alone was not toxic to *G. mellonella* when they are inoculated with 20 µl of PBS containing itaconate at a concentration of 3.9 mg of itaconate / kg of *G. mellonella* (0.975 µg of itaconate) (**Figure 5.19B**), 7.8 mg/kg (1.95 µg of itaconate) (**Figure 5.19C**), 15.6 mg/kg (3.9 µg of itaconate) (**Figure 5.19D**), 31.3 mg/kg (7.8 µg of itaconate) (**Figure 5.19E**), 62.5 mg/kg (15.6 µg of itaconate) (**Figure 5.19F**) or 125 mg/kg (31.2 µg of itaconate) (**Figure 5.19G**) respectively.

We also demonstrated for the first time that *G. mellonella* that were inoculated with *P. aeruginosa* and 62.5 mg/kg of itaconate had significantly increased survival compared to those inoculated with *P. aeruginosa* only (* $p<0.05$, **Figure 5.20**). Furthermore, *G. mellonella* that were inoculated with *P. aeruginosa* and 125 mg/kg of itaconate had significantly increased survival compared to those inoculated with *P. aeruginosa* only (*** $p<0.001$, **Figure 5.20**).

5.5.2 4-OI is protective in vivo in a model of P. aeruginosa infection in G. mellonella.

Having previously demonstrated that 4-OI inhibits macrophage mediated inflammatory responses (**Figure 5.8 - Figure 5.10**) and promotes macrophage mediated *P. aeruginosa* clearance (**Figure 5.12**), we subsequently examined the effects of 4-OI in the *G. mellonella* model of *P. aeruginosa* infection. 4-OI is non polar and must be dissolved in DMSO, although the concentration is low enough that it does not impact *G. mellonella* survival (**Figure 5.21A**). Here, we demonstrated for the first time that 4-OI alone was not toxic to *G. mellonella* when they are inoculated with 20 µl of PBS containing 4-OI at a concentration of 50 mg/kg (12.5 µg of 4-OI) (**Figure 5.21B**), 125 mg/kg (31.25 µg of 4-OI) (**Figure 5.21C**), or 250 mg/kg (62.5 µg of 4-OI) (**Figure 5.21D**) respectively. We also demonstrated for the first time that 4-OI promotes survival in *G. mellonella* challenged with *P. aeruginosa* (**Figure 5.22A-D**). *G. mellonella* that were inoculated with *P. aeruginosa* and 250 mg/kg of 4-OI had significantly increased survival

compared to those inoculated with *P. aeruginosa* and DMSO vehicle control (** $p<0.01$, **Figure 5.22E**).

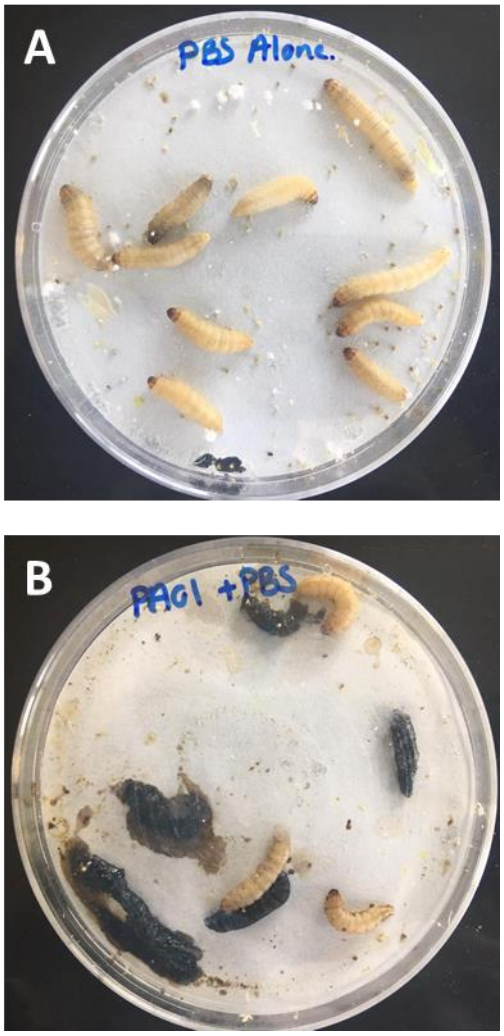

Figure 5.18. PA01 infection induces death of *G. mellonella* at 24 hours.

G. mellonella were inoculated with 20 µL of PBS or 2.5 x 10^3 CFU/ml of PA01 for 24 hours. (**A**) Inoculation with PBS only did not result in *G. mellonella* death. (**B**) Inoculation with PBS containing PA01 resulted in *G. mellonella* death, as indicated by decomposition and melanisation.

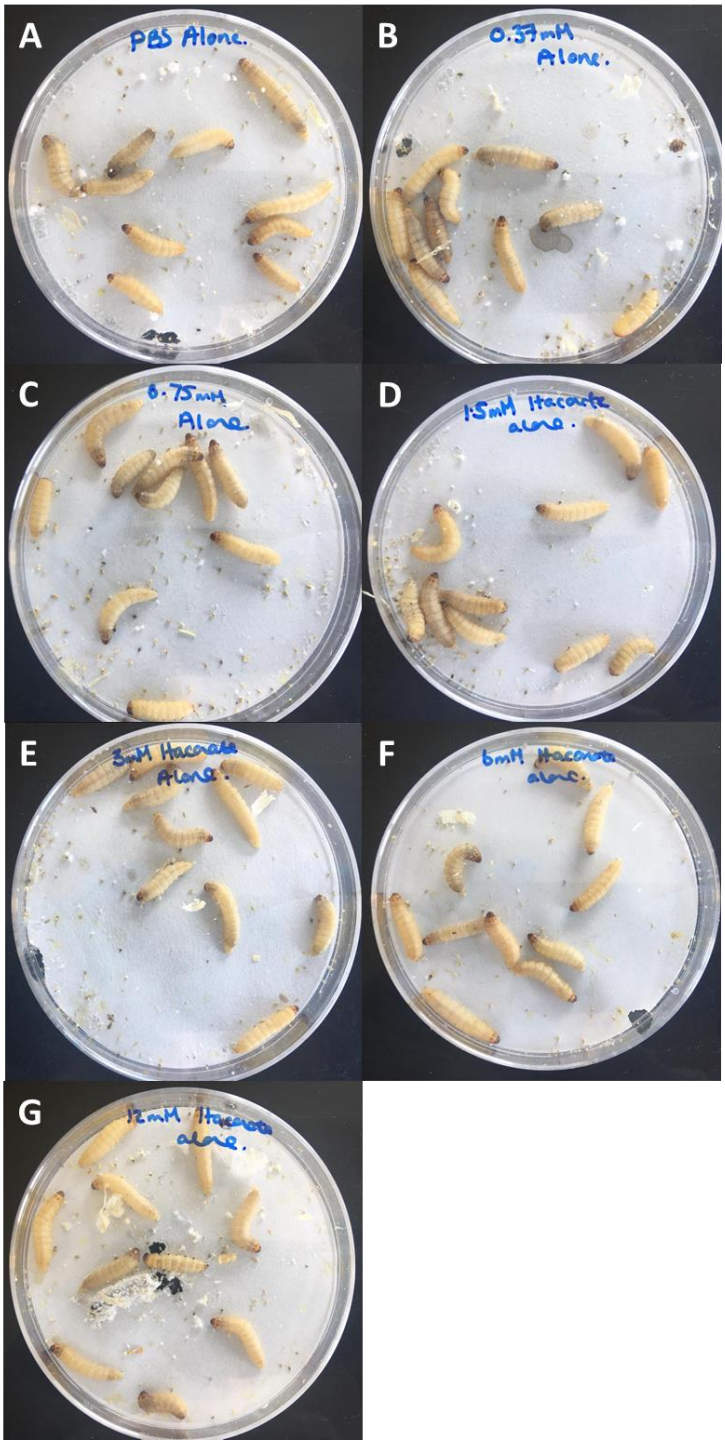

Figure 5.19. Itaconate is not toxic to *G. mellonella* at 24 hours.

G. mellonella were inoculated with 20 µLs of (**A**) PBS or itaconate at a concentration of (**B**) 3.9 mg/kg (0.37 mM) (**C**), 7.8 mg/kg (0.75 mM) (**D**), 15.6 mg/kg (1.5 mM) (**E**), 31.3 mg/kg (3 mM) (**F**), 62.5 mg/kg (6 mM) or (**G**) 125 mg/kg (12 mM) respectively. Treatment of *G. mellonella* with any of the concentrations of itaconate examined did not result in death. Figures are representative of 3 independent experiments.

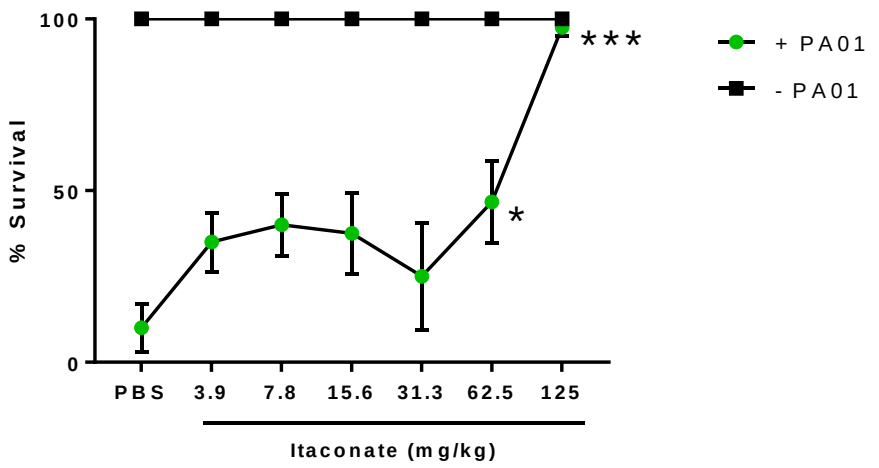

Figure 5.20. Itaconate co-treatment promotes survival of *G. mellonella* following challenge with PA01 at 24 hours.

Mean survival rates of *G. mellonella* 24 hours post inoculation of 20 µLs of 2.5 x 10^3 CFU/ml of PA01 and a concentration range of itaconate (3.9 – 125 mg/kg). Data is presented as mean ± SEM of 4 independent experiments. A two-way ANOVA with a Tukey's multiple comparison post-hoc test was used to test for statistical differences. * $p<0.05$; 62.5 mg/kg itaconate + PA01 compared with PBS + PA01. *** $p<0.001$; 125 mg/kg itaconate + PA01 compared with PBS + PA01.

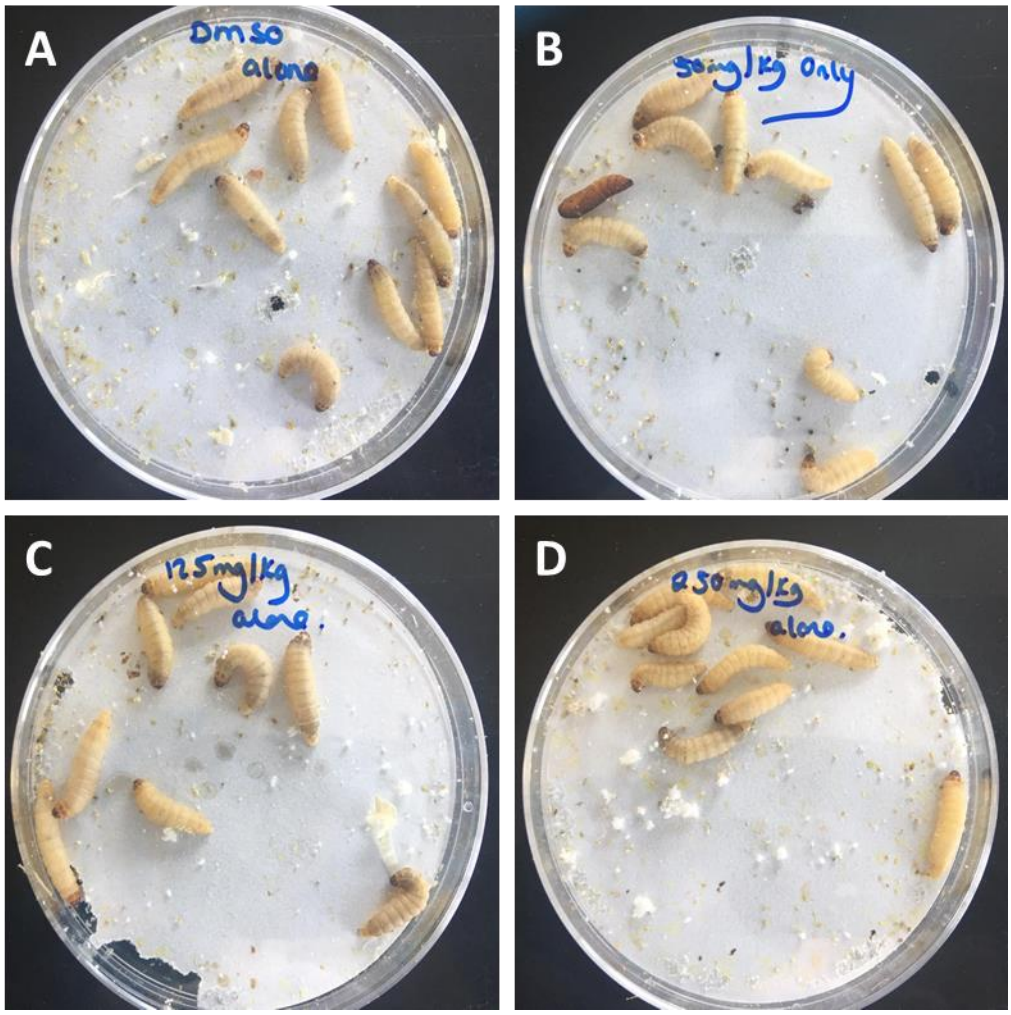

Figure 5.21. 4-OI is not toxic to *G. mellonella* at 24 hours.

G. mellonella were inoculated with 20 µLs of (**A**) DMSO or 4-OI at a concentration of (**B**) 50 mg/kg (**C**) 125 mg/kg (**D**) 250 mg/kg. Treatment of *G. mellonella* with any of the concentrations of 4-OI examined did not result in death. Figures are representative of 3 independent experiments.

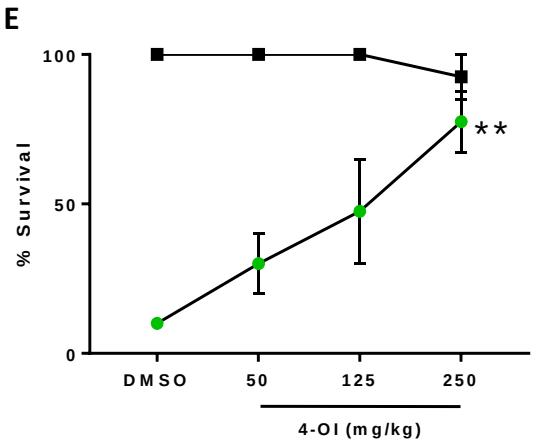

Figure 5.22. 4-OI co-treatment promotes survival of *G. mellonella* following challenge with PA01 at 24 hours.

G. mellonella were inoculated with 20 µLs of 2.5 x 10^3 CFU/ml of PA01 and (**A**) DMSO or 4-OI at a concentration of (**B**) 50 mg/kg (**C**) 125 mg/kg (**D**) 250 mg/kg respectively. Treatment of *G. mellonella* with 4-OI promotes survival in PA01 infected *G. mellonella*. Figures are representative of 4 independent experiments. (**E**) Mean survival rates of *G. mellonella* 24 hours post inoculation. Data is presented as mean ± SEM of 4 independent experiments. A two-way ANOVA with a Tukey's multiple comparison post-hoc test was used to test for statistical differences. ** $p<0.01$; 250 mg/kg 4-OI + PA01 compared with DMSO + PA01.

5.6 Discussion

In CF, there is an undeniable unmet clinical need for the development of novel anti-inflammatory and antimicrobial therapies as CF disease progresses due to respiratory damage from chronic inflammation and chronic infection (21, 233, 265). In order to address this, we have examined the effects of 4-OI and itaconate in this context. We conducted experiments examining the effects of 4-OI on the regulation of the inflammatory responses of macrophages to live *P. aeruginosa* infection. We also examined the effects of itaconate on *P. aeruginosa* growth, biofilm formation, virulence factor expression and antibiotic tolerance. Furthermore, we examined the effects of both 4-OI and itaconate on live *P. aeruginosa* infection *in vivo* using the *G. mellonella* infection model.

Anti-microbial resistance is undoubtedly one of the biggest challenges facing society, with estimations that up to 10,000,000 people a year will die due to antibiotic resistant infections (43). Although it is difficult to ascertain the exact number of individuals that will contract an antibiotic resistant infection, it remains undisputed that antibiotic resistance is a critical issue (478). As such, the development of new therapies that are antimicrobial or enhance the efficacy of current antibiotic regimes remains an unmet clinical need of crucial importance. Currently, antibiotic regimes classically target bacterial cells by a variety of mechanisms including inhibiting cell wall synthesis, nucleic acid synthesis and protein synthesis (479). Recently, host-directed therapies which target and manipulate the host immune response to infection in a manner that benefits the host and is detrimental to the pathogen have become an attractive new therapeutic prospect (480, 481).

Targeting metabolic products in activated immune cells has become an area of much research termed “immunometabolism” (186, 315, 318, 482, 483). In activated macrophages, metabolic rewiring occurs whereby there is a shift towards aerobic glycolysis, also known as the Warburg effect (334-338). Glycolysis is considered a hallmark of immune cells undergoing rapid activation and replication and serves to support phagocytosis and anti-bacterial functions (318, 339). Glycolysis has been shown to be required for production of nitric oxide, prostaglandins and ROS, while inhibition of glycolysis using 2-deoxyglucose (2-DG) has been shown to limit macrophage

activation and inflammation *in vivo* (185, 333, 340, 341). Furthermore, in classically activated macrophages there is dysregulation of the TCA cycle whereby there is accumulation of succinate and citrate as a result of decreased activity of their respective processing enzymes (185, 328). Excess citrate is then processed for fatty acid synthesis and itaconate production (327, 328, 348, 349).

Itaconate is a metabolic by-product that is being heralded as a valid therapeutic target for the development of anti-inflammatory therapies (327, 330, 351, 360, 375, 380, 382, 424, 426). Itaconate is a by-product of cellular metabolism that exerts strong anti-inflammatory effects. Itaconate is produced from *cis*-aconitate which is converted to itaconate by Irg1 protein (359). Upregulation of itaconate and Irg1 mRNA expression has been observed in a myriad of cells including LPS stimulated macrophages and in the lungs of *M. tb* infected mice (358, 365-367). One mechanism of itaconates anti-inflammatory activity is via inhibition of SDH, which was first demonstrated in 1949 (374). It has since been demonstrated that LPS stimulated $Irg1^{-/-}$ macrophages, which lack endogenous itaconate, have decreased succinate accumulation compared with wild type cells, indicative of SDH inhibition by itaconate (327, 351). Itaconate also modulates anti-inflammatory response through upregulation of the transcription factor Nrf2 (375). Nrf2 functions to upregulate antioxidant genes including *Hmox1*, *Gclm*, *Gsr* and *Nqo1* in response to cellular stress to limit inflammatory cytokine and ROS production (330, 377, 429). Irg1 deficient macrophages display impaired lack of activation of Nrf2 (426). Irg1 deficient mice have been used to demonstrate that itaconate modulates pro-inflammatory cytokine production following LPS stimulation (327). Furthermore, itaconate deficient mice are more susceptible to *M. tb* infection and display increased inflammation compared with wild type mice (361). As such, itaconate plays a role in the inflammation and the host response to infection.

In the previous chapter, we examined the effects of itaconate and 4-OI on the regulation of macrophage responses to synthetic stimuli LPS and HKPA. While these stimuli provide an insight into the regulatory effects of itaconate and 4-OI on TLR4 and TLR2/TLR5 activation respectively, and also limit cytotoxicity that may be introduced by live bacteria, it is not representative of a live bacterial infection (484-486). Although *P. aeruginosa* does express LPS, which induces itaconate production, it also possesses a

variety of other factors including quorum sensing molecules, secreted virulence factors and toxins all of which can impact on the response of macrophages (244, 249, 285-287, 487-491). Furthermore, different macrophage activating stimuli have been shown to induce differential metabolic profiles and consequently we must not assume that *P. aeruginosa* infection will induce itaconate production (332). As such, it important to use live *P. aeruginosa* in experiments in order to gain an accurate understanding of the immune response to infection.

Initially, we used RAW 264.7 murine macrophages for preliminary experiments of live *P. aeruginosa* infection as they are easier to source than primary murine cells. We demonstrated for the first time that infection of RAW 264.7 murine macrophages with PA01 significantly induced expression of Irg1 mRNA. Treatment of these cells with 4-OI inhibited the production of PA01 mediated TNF-α and pro-IL-1β protein, while 4-OI also enhanced Nrf2 protein expression and downstream antioxidant genes. Interestingly, infection with PA01 inhibited the induction of Nrf2 protein expression and subsequent induction of downstream genes *Gclm*, *Gsr* and *Nqo1*. This may be due to the inhibition of Nrf2 protein expression by 2-Heptyl-3-hydroxy-4(1H)-quinolone, a secreted quorum sensing molecule, which has previously been demonstrated to inhibit antioxidant gene expression, although further work is necessary to determine this mechanism (492). Nrf2 has previously been shown to be protective in *P. aeruginosa* infection (493). Nrf2 promotes phagocytic uptake of *P. aeruginosa* by murine alveolar macrophages and also decreases the recruitment of inflammatory cells to the lungs, as measured in BAL fluid, in a model of respiratory *P. aeruginosa* infection (493).

Following on from our finding that 4-OI can mediate the responses of PA01 infected macrophages, we next examined the role of endogenous itaconate in the macrophage response to *P. aeruginosa* infection. To do this, we used BMDMs from Irg1 deficient mice which lack the Irg1 protein necessary for itaconate production (359, 361, 425, 494). We hypothesised that itaconate deficiency would enhance the production of pro-inflammatory mediators in *P. aeruginosa* infected macrophages.

We observed that in $Irg1^{+/+}$ BMDMs, PA01 infection induced the production of MIF, KC, TNF-α and RANTES protein. Interestingly, the levels of these proteins that were produced were equivalent to those produced in $Irg1^{-/-}$ BMDMs. We also demonstrated

the induction of IL-10 and TNF-α mRNA in both $Irg1^{+/+}$ and $Irg1^{-/-}$ BMDMs following PA01 infection, with no differences in induction observed between the genotypes. PA01 infection also induced iNOS mRNA expression in both $Irg1^{+/+}$ and $Irg1^{-/-}$ BMDMs , with significantly higher induction in $Irg1^{-/-}$ BMDMs, which is consistent with data demonstrating itaconate mediated inhibition of LPS stimulated reactive nitrogen species production (330). PHD3 mRNA expression levels are used as a non-direct readout for HIF-1α activation levels, as PHD3 protein promotes HIF-1α destabilisation and subsequent degradation (295, 495, 496). PA01 infection resulted in reduced expression of PHD3, indicative of HIF-1α activation and subsequent pro-inflammatory cytokine expression. As 4-OI has been shown to inhibit LPS mediated HIF-1α stabilisation (330), we were surprised to observe that endogenous itaconate did not impact PHD3 expression levels.

We also examined the effects of 4-OI on the responses of macrophages to PA01 infection in both $Irg1^{+/+}$ and $Irg1^{-/-}$ BMDMs. In $Irg1^{+/+}$ BMDMs, 4-OI had no effect on PA01 induced MIF, KC or RANTES protein levels, but it did significantly inhibit PA01 induced TNF-α protein levels. 4-OI treatment also significantly enhanced the expression of IL-10 mRNA, an anti-inflammatory cytokine, in PA01 infected cells (454). Furthermore, pro-IL-1β protein levels were significantly inhibited by 4-OI in PA01 infected $Irg1^{+/+}$ cells. As was observed in $Irg1^{+/+}$ BMDMs, 4-OI treatment had no effect on PA01 induced MIF or KC protein in $Irg1^{-/-}$ BMDMs. 4-OI also inhibited PA01 induced TNF-α and pro-IL-1β protein production and enhanced IL-10 mRNA expression in PA01 infected $Irg1^{-/-}$ BMDMs. In PA01 infected $Irg1^{-/-}$ BMDMs, 4-OI inhibited RANTES protein production and iNOS mRNA expression, effects that were not observed in $Irg1^{+/+}$ BMDMs. This may be due, at least in part, to the lack of endogenous itaconate in $Irg1^{-/-}$ cells with 4-OI acting as an itaconate analogue, however further research is needed to investigate these differences.

In both genotypes, 4-OI enhanced the production of Nrf2 protein in both non-infected and PA01 infected cells. Downstream of Nrf2, 4-OI also enhanced the expression of Gclm, Hmox1 and Nqo1 mRNA in both non-infected and PA01 infected cells. There was higher levels of Gclm and Nqo1 mRNA expression in 4-OI stimulated

$Irg1^{+/+}$ cells compared with $Irg1^{-/-}$ cells, likely due in part to the presence of endogenous itaconate in the $Irg1^{+/+}$ cells.

Itaconate is a key immunoregulatory metabolite in cells stimulated with synthetic ligands including LPS and poly(I:C), and also cells infected with live pathogens, including *M. tb* and Zika virus (330, 358, 361, 383). *Irg1* gene expression is highly induced upon infection with numerous bacteria including *S. aureus*, *M. tb* and Listeria monocytogenes, viruses including Zika virus, West Nile virus and Respiratory syncytial virus and parasites including *Toxoplasma gondii* and *Leishmania donovani* (361, 383, 420-422, 450, 497, 498). As Itaconate production is mediated by a protein under the control of *Irg1* gene expression, one would expect to observe differences between *Irg1* expressing and *Irg1* deficient cells on effects including the modulation of the inflammatory response. In our experiments, we observed limited differences between these two genotypes. One potential reason that we observed subtle differences may be that $Irg1^{-/-}$ cells have developed a mechanism of compensation for the lack of itaconate, however this remains to be examined. As such, a more useful tool examining the effects of endogenous itaconate may be the development of a system that examines the effects of *Irg1*/itaconate overexpression, rather than deletion.

Overall, our results from $Irg1^{-/-}$ cells were surprising as the differences in the responses to live *P. aeruginosa* infection that we examined were somewhat limited compared with $Irg1^{+/+}$ BMDMs. For each protein we examined, the level of production induced by *P. aeruginosa* infection in both $Irg1^{+/+}$ and $Irg1^{-/-}$ cells were similar. Likewise, the levels of antioxidant gene expression in both non-infected and PA01 infected $Irg1^{+/+}$ and $Irg1^{-/-}$ cells were similar between the two genotypes. However, It is important to be cogniscent of the fact that the majority of experiments that focus on the effects of itaconate utilise synthetic ligands such as LPS and poly(I:C) (330, 351). As such, few experiments have been conducted to examine the role of itaconate during live bacterial or viral infection. Live *P. aeruginosa* infection has the potential to introduce a complex assortment of PAMPs into the experimental set up including, but not limited to LPS, alginate, quorum sensing molecules, pyocyanin, flagellin, diffusible signalling molecules, bacterial DNA and also complex T3SS's – all of which are capable of impacting on the macrophage response (78, 249, 252, 253, 285-287). Consequently, the

immunoregulatory effects of itaconate may be overshadowed by the other factors that are introduced using live bacteria.

Recently published data has also demonstrated limited differences between particulate-matter induced inflammation in $Irg1^{-/-}$ and $Irg1^{+/+}$ macrophages (444). Similar to our data, the authors also suggest differential effects between 4-OI and endogenous itaconate (444). Furthermore, it is also suggested that the effects of itaconate are stimulus dependant (444). Experiments examining macrophage mediated inflammation induced by particulate matter demonstrated limited differences in $Irg1^{+/+}$ macrophages compared with $Irg1^{-/-}$ (444). The authors also ran control experiments examining the regulation of macrophage responses to LPS by endogenous itaconate, and show that the effects of itaconate are stimulus dependant (444). Interestingly, these authors demonstrate that endogenous itaconate and 4-OI, an exogenous itaconate analogue, do in fact induce different effects (444). In $Irg1^{-/-}$ BMDMs stimulated with particulate matter, there was no difference in the mRNA expression levels of Gclm, Hmox1, Nqo1, TNF-α or IL-1β mRNA compared with $Irg1^{+/+}$ cells. However, in particulate matter stimulated $Irg1^{+/+}$ cells treated with 4-OI there was significantly higher expression levels of Gclm, Hmox1, Nqo1 mRNA and significantly reduced TNF-α or IL-1β mRNA expression levels compared with particulate matter stimulated cells that did not receive 4-OI (444). This data is in line with our own in which 4-OI treatment induced significant effects in *P. aeruginosa* infected cells, whereas there was limited differences observed between genotypes in experiments using $Irg1^{-/-}$ and $Irg1^{+/+}$ cells which highlights the fact that there are important differences between endogenous itaconate and 4-OI (444).

To date, the literature surrounding the use of itaconate and modified itaconate derivatives has yielded many results, however the variability in both the experimental conditions and the itaconate derivatives used has presented a challenge in the interpretation of key aspects of itaconates immunomodulatory activity (442). The two most commonly utilised itaconate derivatives are DI and 4-OI. DI is similar in structure to itaconate, although it has an esterified carboxyl group which acts to reduce the negative charge of itaconate and increase membrane permeability (424). However, further research demonstrated that this esterification increases the thiol-reactivity of

DI and as such increases the likelihood of itaconate-independent effects (330). Furthermore, DI is not metabolised into itaconate and as such should not be used to mimic endogenous itaconate (372, 442). 4-OI was developed as a more suitable itaconate surrogate, displaying similar thiol-reactivity to itaconate and hydrolysis to itaconate in LPS stimulates macrophages (330).

More recently, data which was published after we had conducted our experiments demonstrated that treatment of resting BMDMs with 4-OI does not enhance intracellular levels of itaconate, in line with Mills *et al* (330, 442). Furthermore, the authors demonstrated that unmodified itaconate does in fact accumulate within BMDMs at much shorter time points than previous publications (370, 442). Interestingly, 4-OI was shown to induce basal Nrf2 expression, transcription of *Nqo1* and *Hmox1* and inhibition of LPS mediated expression of IL-6 protein (442). Furthermore, none of these effects were observed in cells treated with unmodified itaconate. Considering that cells treated with unmodified itaconate had increased intracellular itaconate, but no induction of Nrf2 or downstream genes, this demonstrates that itaconate has a lower degree of electrophilicity compared with 4-OI (442).

Furthermore, the inhibition of IFN production by 4-OI was also observed, in line with previous research, however the authors also demonstrate that endogenous itaconate in fact increases IFN-β production and transcription of genes downstream of type I interferon signalling (330, 442). The use of $Irg1^{-/-}$ cells revealed significantly reduced expression of genes downstream of type I interferon signalling compared with $Irg1^{+/+}$ cells, which was rescued upon treatment with unmodified itaconate (442). This important study demonstrates drastic differences between the effects of 4-OI and itaconate and suggests that 4-OI is fact not a suitable itaconate surrogate, with unmodified itaconate being more physiologically relevant to *Irg1*-produced itaconate (442).

Based on the limited differences that we observed in experiments using $Irg1^{-/-}$ and $Irg1^{+/+}$, and the significant effects that we observed with 4-OI treatment in *P. aeruginosa* infected cells; it may be of value to consider the potential benefits of 4-OI in respiratory *P. aeruginosa* infection independent of itaconate. In our experiments, the

most striking effect of 4-OI was the inhibition of PA01 mediated pro-IL-1β expression. Previous studies have demonstrated a detrimental role for IL-1β in *P. aeruginosa* infection. Recombinant IL-1β has been shown to inhibit macrophage mediated *P. aeruginosa* clearance, while levels of IL-1β in CF BAL fluid have been shown to correlate with clinical outcome (302, 303). Caspase-1 is an enzyme which acts to proteolytically cleave pro-IL-1β to mature IL-1β. Treatment of mice with caspase-1 inhibitors has been shown to decrease inflammation and bacterial burden in a model of *P. aeruginosa* induced ocular keratitis, while caspase-$1^{-/-}$ mice exhibit enhanced bacterial clearance compared with wild type in the same model (304, 305). Recently, the use of an NLRP3 inhibitor, MCC950, has been shown to inhibit the production of IL-1β protein in the lungs of *P. aeruginosa* infected mice and also enhance bacterial clearance (303). Furthermore, 4-OI treatment boosted IL-10 transcription, an anti-inflammatory cytokine that has been shown to decrease inflammation and lessen disease severity in a model of *P. aeruginosa* infection (454). The induction of Nrf2 and subsequent induction of downstream anti-oxidant genes may also be on benefit in limiting excessive inflammation in CF, however further research is necessary to examine this. As such, the use of 4-OI may be of therapeutic interest in *P. aeruginosa* infection.

Itaconate has also been shown to display antibiotic properties against *methicillin resistant* S*taphylococcus aureus* (MRSA), *M. tb, Salmonella enterica* (*S. enterica*) and multidrug-resistant *Acinetobacter baumanni* (359, 361, 379). *In vivo*, endogenous itaconate promotes survival in a murine model of *M. tb* infection (361). Itaconate is known to inhibit isocitrate lyase - a key enzyme in the glyoxylate cycle, an anabolic process analogous to the TCA cycle in plants and microorganisms (378). However, itaconate also displays protective activities *in vivo* following infection with *M. tb l*acking a functional glyoxylate shunt , the mice still readily succumbed to infection suggesting an alternative mechanism of action for itaconates antimicrobial activity (361). As such, we hypothesised that itaconate would have antibacterial properties against *P. aeruginosa* infection.

We examined the effect of endogenous itaconate on macrophage mediated *P. aeruginosa* killing using macrophages from itaconate deficient and wild type macrophages. Our data demonstrated for the first time that endogenous itaconate

promotes the bactericidal capabilities of macrophages against *P. aeruginosa*. This finding may occur due to direct antibacterial activities of itaconate against *P. aeruginosa* or may be due to itaconate mediated regulation of the immune response to infection; further work is necessary to clarify this mechanism. We also demonstrated that 4-OI promoted macrophage mediated *P. aeruginosa* killing. This may occur as Nrf2, which is upregulated by 4-OI, promotes phagocytic uptake of *P. aeruginosa* by murine macrophages which may contribute to enhanced bacterial killing (493).

To investigate the effects of itaconate directly on *P. aeruginosa*, we cultured *P. aeruginosa* strains in LB broth containing itaconate. We demonstrated that PA01 upregulates the expression of *PA0882* and *PA0883* genes, which regulate the expression of itaconate processing genes, demonstrating that *P. aeruginosa* can detect the presence of itaconate (378, 381). We also demonstrated that itaconate inhibited growth of PA01 at a concentration of 780 μg/ml, which corresponds to 6mM. Furthermore, the growth of five clinical isolates was significantly stunted at a concentration of 780 μg/ml, and completely inhibited at 1560 μg/ml. We also demonstrated itaconate decreased biofilm formation in PA01 and all five clinical isolates that were examined. Biofilm formation was completely inhibited at concentrations from 780 to 1560 μg/ml, likely due to inhibition of bacterial growth, but also at lower concentrations examined. Biofilm formation confers antibiotic resistant properties to *P. aeruginosa* against commonly used antibiotics, with biofilm formation a major cause of chronic infections in CF (113, 437, 499, 500). As such, the antibacterial and anti-biofilm properties of itaconate may be of interest in CF patients.

We next examine the impacts of itaconate on the susceptibility of PA01 and five clinically isolated *P. aeruginosa* strains to commonly used antibiotics. To do this, we utilised the checkerboard assay which alloys the examination of the effects of a combination of two-fold dilutions of two independent treatments to be examined on bacterial growth. The MIC of itaconate against the strains examined ranged from 780 – 1560 μg/ml. Interestingly, at a concentration of 390 μg/ml itaconate had an antagonistic effect on the antibacterial effects of tobramycin in five of six strains that were examined. This means that itaconate induced at least a 4-fold increase in the concentration of tobramycin required to inhibit bacterial growth. Similarly, itaconate at

this concentration also antagonised the effects of meropenem in three of six strains examined. Antagonism by itaconate was observed in six of six strains against azactam and also against piperacillin/tazobactam.

Interestingly, it is common for sub-MIC concentrations of antibiotics to induce biofilm formation and antibiotic resistance in a variety of infections, including *S. aureus, S. enterica* and *P. aeruginosa* (501-506). The induction of biofilm formation is said to be a stress response to the antibacterial agents which results may also include changes in virulence factor expression and the development of persister cells (507). Sub-MIC concentrations of methicillin induces biofilm formation in *S. aureus* (504). Sodium hypochlorite, a common disinfectant agent, induces biofilm formation in *S. enterica*, common causative agent in acute gastroenteritis (505). In *P. aeruginosa*, sub-MIC concentrations of tobramycin, a commonly used antibiotic in CF, induces biofilm formation in a dose-dependent manner (501). Our findings demonstrate for the first time that sub-MIC concentrations of itaconate promote antibiotic resistance to commonly used antibiotics against *P. aeruginosa*, as determined by an FICI indicative of antagonism. Interestingly, this finding is in line with the induction of biofilm formation at sub-MIC ranges in the previous examples which occur at approximately ¼ to ½ of the MIC (501, 506). This may be of interest as if levels of itaconate were within this range, it may be of benefit to pharmacologically increase itaconate concentrations which would promote its antibacterial effects and overcome itaconate mediate antibiotic resistance.

We next examined the effect of itaconate on the expression of two common virulence factors expressed by PA01, elastase and pyocyanin. The concentrations of itaconate that we examined were below the MIC that were observed in the checkerboard assay experiments. *P. aeruginosa* elastase functions to degrade host elastin, compromising the barrier function of the lung epithelium and enabling bacterial invasion and inflammatory damage (242, 243). Elastase also degrades host factors, including mucins and surfactant proteins, which are required to bacterial clearance (467-469). We demonstrated that itaconate had no effect on elastase production by PA01 at any concentration examined.

Pyocyanin is an essential virulence factor in *P. aeruginosa* pathogenesis. Pyocyanin has been shown to promote lung inflammation and cellular damage *in vivo* in a murine model of *P. aeruginosa* infection (463). Furthermore, pyocyanin production by *P. aeruginosa* results in death in infection models of plants, *Drosophila melanogaster* and *C. elegans* (464-466). Pyocyanin causes cellular damage as it elevates through increasing levels of ROS including superoxide (O_2-) and hydrogen peroxide (H_2O_2) which cause cellular damage to DNA, mitochondria, cell membrane and cell cycle components (487, 488, 508, 509). We demonstrated that at sub-MIC concentrations that itaconate inhibits pyocyanin production in PA01 in a dose dependant manner. Infection of mice with pyocyanin deficient isogenic mutants of PA01 results in less severe pneumonia in models of both acute and chronic lung infection in mice (463). Inhibition of pyocyanin by itaconate may therefore be another beneficial effect of itaconate in the context of *P. aeruginosa* infection.

Finally, we examined the effects of itaconate and 4-OI *in vivo*. To do this, we utilised the larvae of the greater wax moth, *G. mellonella*, which offers a number of practical benefits over murine models. *G. mellonella* larvae are inexpensive and available in larger numbers which is ideal for our experiments. Furthermore, the do not require ethical approval or need to be housed in specialist equipment. When stored at 14 ^{o}C the larvae will remain viable, but it will slow down their development into pupae. They can also be housed at 37 ^{o}C for the duration of experiments, making it ideal for studying mammalian pathogens (473, 510). Most importantly, the immune system of *G. mellonella* is strikingly similar to that of the vertebrate innate immune system and is comprised of humoral and cellular arms (473-475). The humoral arm is a variety of soluble factors which act to immobilise and kill pathogens (473-475). The cellular arm is a variety of phagocytic cells knowns as haemocytes which act to phagocytose and kill invading pathogens (473, 476, 477).

In *G. mellonella*, melanisation, the production of melanin, is indicative of an active immune response. During infection, phagocytic cells secrete enzymes that are involved in the production of melanin which gives infected larvae a characteristic black colour. Melaninization is comparable to the compliment cascade in humans and results in pathogen encapsulation, followed by coagulation and opsonization and is analogous

to the formation of abscesses in mammalian infections (473, 511-513). *G. mellonella* are routinely utilised in studies examining the virulence of *P. aeruginosa* strains and efficacy of anti-microbial agents (473). *G. mellonella* are extremely susceptible to *P. aeruginosa* infection, with inoculum as low as 25 CFU of certain *P. aeruginosa* strains proving toxic (514). Previous studies have demonstrated strong correlations between antibiotic pharmacokinetics observed *in vitro* and the therapeutic effect in *P. aeruginosa* infected *G. mellonella* (514). Furthermore, the effects of antibiotics in *G. mellonella* are similar to those observed in murine models (515). As such, *G. mellonella* represent a valid tool in the initial study of anti-pseudomonal treatments.

Our data demonstrates for the first time that *G. mellonella* inoculated with PA01 and itaconate at concentrations corresponding to 780 and 1560 μg/ml respectively have significantly increased survival compared to those inoculated with PA01 alone. Increases in survival were also demonstrated at lower concentrations, although these were not significant, which may be due to decreased biofilm formation and pyocyanin production. In this case, the increase in survival is likely due to the antibiotic effects of itaconate on PA01 that we observed in the checkerboard assay experiments. Furthermore, *G. mellonella* inoculated with PA01 and 250 mg/kg of 4-OI have significantly increased survival compared with PA01 alone. This is a significant finding as it demonstrates for the first time that 4-OI promotes *P. aeruginosa* clearance *in vivo*.

Overall, we believe that 4-OI may represent a valid therapeutic agent in CF (**Figure 5.23**). CF pathophysiology is dominated by respiratory inflammation and chronic *P. aeruginosa* infection. As such, an unmet clinical need exists for the development of novel therapies that limit inflammation and promote *P. aeruginosa* clearance and antibacterial activity. We have demonstrated that 4-OI limits macrophage mediated inflammation in response to *P. aeruginosa*. Importantly, levels of IL-10 and Nrf2 were increased and levels of pro-IL-1β were reduced with 4-OI treatment, which has been shown to be beneficial in models of *P. aeruginosa* infection (454, 455) (493) (302). Furthermore, 4-OI has recently been shown to inhibit the NLRP3 inflammasome, a key protein complex involved in IL-1β processing (516). Previously, specific inhibition of NLRP3 has been shown to inhibit IL-1β and airway inflammation and promote *P. aeruginosa* clearance in the lungs of mice *in vivo* (303). 4-OI has been shown to increase

levels of itaconate production by macrophages, which may further promote antibacterial and downregulation of biofilm formation and pyocyanin production by *P. aeruginosa* (360, 516). Finally, both itaconate and 4-OI were protective *in vivo* in a model of *G. mellonella* infection with *P. aeruginosa*.

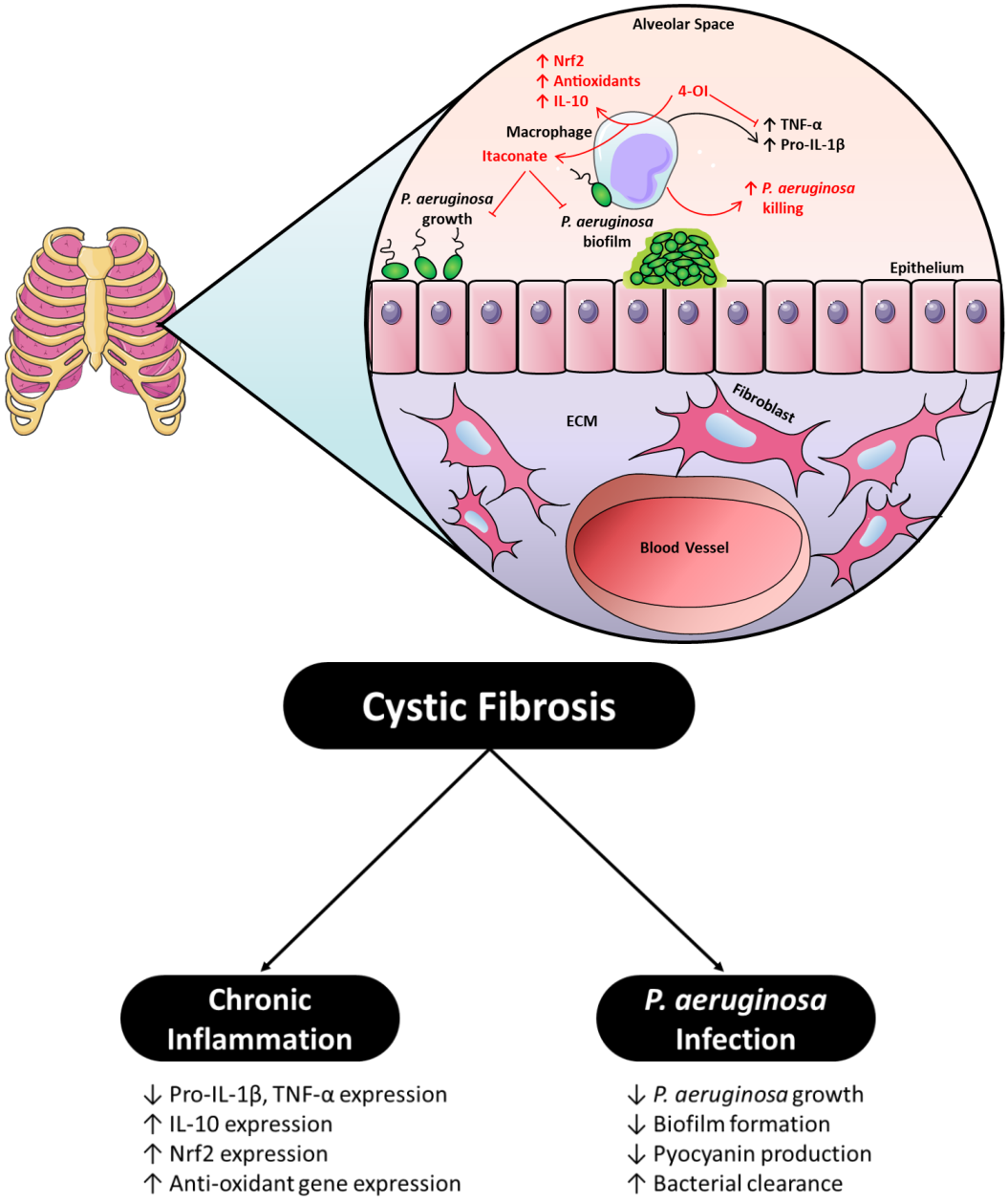

Figure 5.23. Proposed benefits of 4-OI/itaconate that may be of benefit in CF.

P. aeruginosa infection induces TNF-α and pro-IL-1β production in macrophages. Treatment with 4-OI inhibits production of TNF-α and pro-IL-1β, while increasing of itaconate, Nrf2, antioxidants and anti-inflammatory IL-10. Endogenous itaconate inhibits *P. aeruginosa* growth and biofilm formation. Furthermore, both endogenous itaconate and 4-OI promote *P. aeruginosa* killing by macrophages.

Chapter 6 - General Discussion

In this Ph.D. thesis, we have described the inhibition of *Pseudomonas aeruginosa* (*P. aeruginosa*) induced inflammation and also inhibition of key aspects of the pathogenesis of *P. aeruginosa* infection by two independent drug candidates, SCD and 4-octyl itaconate (4-OI). The primary focus of this work was to investigate the efficacy of two potential host-directed therapies for the treatment of *P. aeruginosa* infection in cystic fibrosis (CF). Initially, we focused on targeting macrophage migration inhibitory factor (MIF) using a novel, small molecular weight inhibitor, SCD-19. We hypothesised that SCD-19 could limit *P. aeruginosa* induced inflammatory responses of macrophages and also *P. aeruginosa* biofilm formation. We also focused on examining the effects of itaconate, an immunomodulatory metabolic by-product of the citric acid (TCA) cycle, on the growth, biofilm formation and virulence factor expression of *P. aeruginosa*. Furthermore, we examined the effects of 4-OI, a cell permeable itaconate derivative, on the responses of macrophages to *P. aeruginosa* infection. We hypothesised that itaconate could display antibacterial effects against *P. aeruginosa*, while 4-OI could limit the inflammatory responses of macrophages to *P. aeruginosa* infection.

CF is a life limiting genetic disease, the most common inherited disorder in the Caucasian population, with an estimated prevalence of 1 in 2000 births (1). CF arises from genetic mutations which cause defects in the Cystic Fibrosis Transmembrane Conductance Regulator (CFTR), resulting in impaired chloride ion transport across the surface of the lungs (2, 3). Consequently, patients suffer from thick, viscous secretions in the lungs, liver, pancreas and gallbladder (4, 5). Within the CF lung, a microenvironment develops which is conducive to bacterial colonisation and inflammation, mainly due to the build-up of thick mucus (4, 21). The effects of CF on the lungs are visible on CT scans in patients as young as 3 years old, with apparent mucus obstruction and bronchiectasis, and evidence of neutrophilic inflammation, neutrophil elastase activity and recurrent respiratory tract infections (26-29).

P. aeruginosa is the most commonly isolated pathogen from the CF lung (249). CF patients develop a series of recurrent, intermittent colonisations of *P. aeruginosa* before the acquisition of a chronic infection; as a result, *P. aeruginosa* is regarded as one of the most important bacteria in the pathogenesis of CF (2, 37). *P. aeruginosa*

switches from a planktonic mode of growth to a biofilm, whereby bacteria adhere to the epithelial cells of the lung and begin to secrete slimy extracellular polymeric substances (EPS) (259, 260). The EPS consists of extracellular DNA, proteins, lipids, pili and flagella which hold bacteria together, maintain structural integrity of the biofilm and enable surface attachment (259, 260). Biofilms confer protection against conventional antibiotic therapies and are said to be the cause of chronic infection in CF patients, ultimately driving chronic inflammation and irreversible lung damage (21, 113, 233, 265, 437-439, 517-519). As such, there is an unmet clinical need for the development of novel therapies that both limit inflammation and also promote antibacterial responses in CF patients.

MIF is a key regulator of innate immunity and has been implicated in the pathogenesis of many inflammatory diseases including rheumatoid arthritis, acute respiratory distress syndrome, various cancers and CF (110-112, 114, 115, 397, 520). MIF promotes inflammation through a variety of mechanisms including activation of the mitogen-activated protein kinase/extracellular signal-regulated kinases (MAPK/ERK) pathway, NF-κB mediated gene transcription, regulation of TLR4 expression and also the ability to override the anti-inflammatory effects of glucocorticoids (153, 161, 170, 176-179, 182). MIF expression levels have been shown to be regulated by a CATT microsatellite repeat in the promoter region of the MIF gene, with the number of CATT repeats corresponding to the expression levels of MIF (114). The Donnelly Lab has a longstanding interest in the role of MIF in the pathogenesis of CF. Previously, we have demonstrated that CF patients have higher levels of circulating MIF than healthy controls (111). Furthermore, we have also demonstrated that CF patients with 5-CATT repeats display decreased disease severity, decreased *P. aeruginosa* colonisation and a slower decline in lung function compared with those with more than 5-CATT repeats (110, 111). Bozza *et al* have previously demonstrated that MIF deficient mice were less susceptible to *P. aeruginosa* infection than wild type mice following intratracheal instillation of this bacteria (198). MIF also possesses enzymatic activity, although the physiological substrate for MIF remains unknown (109). The active site of MIF has proved useful in the generation of inhibitors of MIFs pro-inflammatory activity (111, 112, 141, 146, 150). The Donnelly Lab has demonstrated previously that the enzymatic

activity of MIF promotes inflammatory damage to the lung in a murine model of chronic *P. aeruginosa* infection (111). Most recently, we have demonstrated that MIF directly promotes *P. aeruginosa* biofilm formation and antibiotic resistance (113). Furthermore, inhibition of MIF using SCD-19, which targets the active site of MIF, promoted bacterial clearance in a murine model of chronic *P. aeruginosa* infection (113).

In this study, we hypothesised that SCD-19 could limit *P. aeruginosa* induced inflammatory responses of macrophages and also *P. aeruginosa* biofilm formation through the inhibition of MIF mediated effects. Ultimately, we predicted that SCD-19 would have both anti-inflammatory and anti-biofilm formation properties. To investigate this hypothesis, we examined the production of TNF-α and RANTES, two key inflammatory proteins regulated by MIF, in macrophages stimulated with heat killed *P. aeruginosa* (HKPA) and also planktonic *P. aeruginosa* filtrate (PPF), a cocktail of *P. aeruginosa* secreted products (198, 398, 399). We observed that our hypothesis was correct, and that SCD-19 did limit the production of these inflammatory proteins in our experiments.

We next examined the impacts of MIF on *P. aeruginosa* biofilm formation. As previously mentioned, The Donnelly Lab have demonstrated that MIF promotes *P. aeruginosa* biofilm formation on plastic surfaces, which occurs due to upregulation of genes involved in bacterial cell-to-cell communication, alginate production and mucoid converion (113). An *in vitro* cell culture model that is more representative of a lung infection in CF patients examines *P. aeruginosa* biofilm formation on monolayers of airway epithelial cells (206-209, 278). As such, we hypothesised that MIF would promote biofilm formation of *P. aeruginosa* on airway epithelial cells and that SCD-19 would inhibit such an effect. To examine this, we utilised a co-culture system whereby airway epithelial cell monolayers were infected with *P. aeruginosa* for a period before washing away non-adhered bacteria. The cells were then incubated for a further 3 hours and the number of adhered bacteria quantified. We observed that MIF promoted biofilm formation on these epithelial cells which was inhibited with SCD-19, which confirmed our hypothesis.

When one considers the therapeutic potential of SCD-19, a notable limitation is that it is poorly soluble in water. Solubility of therapeutic agents is a key factor which is

required to achieve desired concentrations of drug in systemic circulation necessary for optimal pharmacological response. Drugs which are poorly water-soluble require higher doses in order to reach therapeutic plasma concentrations after oral administration compared with water soluble compounds (408). To overcome this issue, The Donnelly Lab designed and characterised poly(lactic-co-glycolic acid) (PLGA) nanoparticles which were loaded with SCD-19. The design and characterisation of these nanoparticles was the focus of another Ph.D. thesis. These nanoparticles are soluble in water and saline, which enables them to be nebulised for use as an inhaled therapy. Furthermore, in collaboration with Aerogen®, a world leading biotechnology company specialising in the delivery of aerosolised therapies, these nanoparticles were shown to be capable of penetrating the deep lung. Inhalation therapy is associated with increased pulmonary drug delivery, while increasing the half-life of drugs within the lungs and limiting systemic toxicity (47, 402, 415).

In this study, we focused on the functionality of these nanoparticles in the context of the inhibition of *P. aeruginosa* induced inflammatory responses of macrophages and also *P. aeruginosa* biofilm formation on airway epithelial cells. As we have previously demonstrated that SCD-19 inhibited the production of TNF-α and RANTES in HKPA and planktonic *P. aeruginosa* filtrate (PPF) stimulated macrophages, we hypothesised that SCD-19 loaded nanoparticles should have similar effects. We observed that these nanoparticles also inhibited the production of TNF-α and RANTES. As drug-release from nanoparticles occurs over time, it was important to investigate the effects of the nanoparticles in this context, as it was not known if packaging SCD-19 within these nanoparticles would impact the efficacy of SCD-19. Similarly, it was necessary to investigate if the nanoparticles would inhibit biofilm formation of *P. aeruginosa* on airway epithelial cells. As we hypothesised, the nanoparticles inhibited the growth of both the PA01 lab strain and clinically isolated *P. aeruginosa* on healthy and CF bronchial epithelial cell monolayers.

These findings are promising in the context of CF, whereby two key issues in the pathophysiology of disease are over exuberant inflammation and chronic *P. aeruginosa* infection (21). Previously, we demonstrated that SCD-19 limits lung inflammation and promotes *P. aeruginosa* clearance *in vivo* (113). We have also demonstrated that these

SCD-19 nanoparticles are not cytotoxic and are capable of deep lung penetration (394). Our findings that SCD-19 nanoparticles inhibit inflammation and *P. aeruginosa* biofilm formation lead us to believe that nebulised SCD-19 nanoparticles represent a valid potential adjunctive therapy in CF.

It is important to note that there were several limitations to the experiments discussed previously. Firstly, while the use of HKPA and PPF limits cellulartoxicity *in vitro*, these stimuli are not fully representative of *P. aeruginosa* infection and as such may illicit differential responses from macrophages compared to live *P. aeruginosa* infection. As such, experiments utilising a more relevant *in vitro* cellular model examining the effects of SCD-19 and SCD-19 nanoparticles on macrophage responses to live *P. aeruginosa* infection should be conducted. A second limitation of our experiments is that the time point is relatively short in our model of *P. aeruginosa* biofilm formation on airway epithelial cells. Bacterial biofilm formation is a cyclical process that begins with initial bacterial attachment to surfaces and progresses through to the production of a mature biofilm (266). Our timepoint of 4 hours, chosen due to the induction of cell death, is therefore relatively short but does give us an insight into the very early stages of biofilm formation (266). Finally, the experiments outlined in this study only focus on *in vitro* experiments. In order to demonstrate the functionality of these nanoparticles and add weight to our hypothesis that they represent a valid therapy in CF, it is necessary to carry out an *in vivo* study. Ideally, this study would examine the effects of the nanoparticles on bacterial clearance, lung inflammation and systemic inflammation in a murine model of chronic *P. aeruginosa* infection.

In this study, we also described for the first time the characterisation of macrophages from novel, humanised mice which possess either a 5-CATT or 7-CATT repeat in the promoter region of their MIF gene. Characterisation of the responses of BMDMs from these mice to LPS and poly(I:C) is the first step in demonstrating the functionality of these mice. We believe that these mice may be an invaluable tool in studies examining the effects of the CATT repeat in MIF-mediated diseases. Although MIF knockout mice enable the effects of MIF to be examined *in vivo*, the CATT mice offer a more physiologically relevant model for examining the effects of the CATT microsatellite repeat in murine disease models.

As previously mentioned, CF patients with 5-CATT repeats display decreased disease severity, decreased *P. aeruginosa* colonisation and a slower decline in lung function compared with patients who possess more than 5-CATT repeats in their MIF promoter region (110, 111). As such, it may be of benefit from a personalised medicine perspective to stratify patients and tailor their treatments based on their MIF CATT genotype. For example, non-5-CATT patients may require higher antibiotic concentrations than their 5-CATT counterparts. We propose that these mice provide a platform for the investigation of the CATT microsatellite repeat in diseases and may inspire further translational research in the field of personalised medicine.

As previously mentioned, the focus of this Ph.D. project was to investigate the efficacy of two potential host-directed therapies for the treatment of *P. aeruginosa* infection in CF. The second potential therapy that we focused on was 4-OI, which is a cell permeable itaconate derivative. Itaconate is a metabolic by-product of TCA cycle that is becoming widely studied due to its potent immunoregulatory activity (318, 327, 424, 521). 4-OI was developed 2018 as, to date, there are very limited reports of cellular uptake of itaconate and no description of an extracellular receptor or transporter has been made. As such, 4-OI is used as a surrogate for itaconate in experiments using mammalian cells (369, 370). Itaconate is produced from *cis*-aconitate which is converted to itaconate by the immunoresponsive gene 1 (Irg1) protein (359). Itaconate levels and Irg1 mRNA expression are significantly upregulated in LPS and poly(I:C) stimulated macrophages and also in the lungs of mice infected with *Mycobacterium tuberculosis* (*M. tb*) (330, 359, 365-367). Itaconate exerts its anti-inflammatory effects through the inhibition of succinate dehydrogenase (SDH) and HIF-1α and also the upregulation of nuclear factor erythroid 2-related factor 2 (Nrf2) and downstream antioxidant genes including NAD(P)H quinone dehydrogenase 1 (Nqo1), glutamate-cysteine ligase modifier (Gclm), glutathione reductase (Gsr) and heme oxygenase 1 (Hmox1) (327, 330, 351, 375, 377, 429).

Initially, we hypothesised that MIF could play a role in the immunoregulatory effects of itaconate and 4-OI due to overlapping mechanisms of action relating to HIF-α stabilisation and the role of MIF in the promotion of glucose uptake and glycolytic processing (182, 193, 194, 318, 339, 351, 522). To investigate this, we utilised bone

marrow derived macrophages (BMDMs) from MIF-knockout and MIF wild type mice and examined their responses to LPS and poly(I:C) stimulation in the presence of 4-OI. In these experiments, we observed no significant difference in the responses of BMDMs from MIF-knockout and MIF wild type, and therefore, rejected our initial hypothesis. However, as itaconate's anti-inflammatory and antibacterial properties have been well described, we were interested in examining the effects of itaconate and 4-OI in the context of *P. aeruginosa* infection (359, 380, 470).

Initially, we examined the ability of 4-OI to inhibit TNF-α and RANTES protein production in HKPA stimulated RAW 264.7 macrophages. We hypothesised that 4-OI would inhibit the production of these proteins in a similar manner to our observations in LPS stimulated BMDMs. Our observation that 4-OI did inhibit HKPA-induced TNF-α and RANTES protein production in RAW 264.7 macrophages led us to examine this effect in primary murine BMDMs. In these cells we observed, for the first time, that 4-OI inhibited the HKPA-induced production of TNF-α protein, pro-IL-1β protein and nitrite production while increasing Nrf2 protein expression. Interestingly, we also conducted these experiments in Irg1-knockout BMDMs, which lack endogenous itaconate, and observed similar results to those observed in wild type macrophages (351).

Following on from these experiments, we subsequently examined the effects of 4-OI and endogenous itaconate on the responses of RAW 264.7 cells and primary BMDMs to live *P. aeruginosa* infection. As previously mentioned, while HKPA does provide an insight into the responses of macrophages to *P. aeruginosa*, the macrophage response is not fully representative of that which would be elicited during *P. aeruginosa* infection. HKPA lack of a variety of inflammatory stimuli produced by live bacteria including quorum sensing molecules, pyocyanin, diffusible signalling molecules, bacterial DNA and also complex type 3 secretion systems (78, 249, 252, 253, 285-287). We hypothesised that *P. aeruginosa* infection would induce Irg1 mRNA expression and inflammatory cytokines, while 4-OI would induce Nrf2 protein expression and limit pro-inflammatory cytokine production. Initially, we used RAW 264.7 cells in our preliminary experiments as they are easier to source than primary murine BMDMs. In our experiments, we demonstrated for the first time that *P. aeruginosa* infection induced

the expression of Irg1 mRNA in these cells. We also observed for the first time that 4-OI inhibited *P. aeruginosa* induced pro-IL-1β protein expression and TNF-α protein production from RAW 264.7 cells. As we had strong evidence in support of our hypothesis, we moved our experiments forward to live *P. aeruginosa* infection of both wild type and Irg1 deficient BMDMs. In these experiments, our aim was to investigate the effects of 4-OI on the responses of macrophages to live *P. aeruginosa* infection, but also the role of endogenous itaconate on these responses of macrophages. In wild type cells, we again observed inhibition of *P. aeruginosa* induced TNF-α and pro-IL-1β protein and the induction of Nrf2 protein in 4-OI treated cells. We also demonstrated the induction of anti-oxidant genes in *P. aeruginosa* infected cells in response to 4-OI treatment. Furthermore, we demonstrated for the first time that 4-OI promotes BMDM induced killing of *P. aeruginosa*. Taken together, this data suggests that 4-OI represents a potential therapeutic agent for the treatment of *P. aeruginosa* induced inflammation in CF.

As mentioned previously, we conducted experiments examining the responses of macrophages to live *P. aeruginosa* infection in wild type and Irg1 deficient BMDMs. We hypothesised that itaconate deficiency would enhance the production of pro-inflammatory mediators in *P. aeruginosa* infected macrophages. This hypothesis was based on previous research demonstrating a critical role for itaconate in limiting the inflammatory response to LPS stimulation and *M. tb* infection *in vivo* (330, 360, 361). In our experiments, we observed no significant differences between the responses of wild type and Irg1 deficient macrophages to *P. aeruginosa* infection. These observations were in agreement with our previous experiments utilising HKPA. This evidence suggested to us that our hypothesis was incorrect, and that the effects of endogenous itaconate are stimulus-dependant. Furthermore, it also provided evidence to us that the effects of 4-OI are not analogous to those of itaconate. During the completion of these experiments, there was no published data to suggest that 4-OI and itaconate may have divergent mechanisms of action. Recently, data has been published which demonstrates that there are limited differences between particulate-matter induced inflammation in Irg1-knockout and Irg1-wild type macrophages, demonstrating that the effects of itaconate are stimulus-dependent (444). Furthermore, these authors also

demonstrate the differential effects between 4-OI and endogenous itaconate (444). Specifically, 4-OI was demonstrated to promote the expression of Gclm, Hmox1, Nqo1 mRNA and significantly reduced TNF-α or IL-1β mRNA expression levels in wild type BMDMs stimulated with particulate matter (444). While Irg1 deficiency did not impact on these factors compared to particulate matter stimulated wild type cells (444). These findings are in agreement with our previous findings which demonstrated significant differences in macrophage responses in 4-OI treated cells compared with control, while Irg1 deficiency appeared to have limited effects. While it was surprising to demonstrate that the effects of 4-OI are not analogous to endogenous itaconate, we believe that 4-OI represents a valid therapeutic agent for the treatment of *P. aeruginosa* induced inflammation.

As previously mentioned, itaconate is a well established antibacterial agent that inhibits the growth of pathogens including *M. tb*, *Pseudomonas indigofera*, *methicillin resistant* S*taphylococcus aureus, Salmonella enterica* and multidrug-resistant *Acinetobacter baumanni* (359, 361, 379, 470). As a result, we hypothesised that itaconate may possess antibacterial properties during *P. aeruginosa* infection. To investigate this, we examined the effects of increasing dosed of itaconate treatment on the growth of the *P. aeruginosa* lab strain, PA01, and five clinically isolated strains from CF patients. In support of our hypothesis, itaconate inhibited the growth of each strain examined at a concentration range of between 780 – 1560 μg/ml. Furthermore, itaconate also inhibited biofilm formation in these strains and inhibited the production of a potent toxin, pyocyanin, by PA01 (463). This evidence suggested that itaconate may play a role in pathogen clearance by immune effector cells. To analyse this, we examined the effects of itaconate deficiency on the ability of macrophages to kill *P. aeruginosa*. We demonstrated that Irg1-knockout BMDMs display impaired *P. aeruginosa* killing compared with wild type macrophages, supporting our hypothesis that itaconate plays a role in the clearance of this pathogen.

Subsequently, we examined the effects of itaconate on antibiotic tolerance in the *P. aeruginosa* strains outlined above. As we had observed that itaconate displays antibacterial properties against *P. aeruginosa*, we hypothesised that itaconate may act synergistically with conventional antibiotics to reduce the concentration of antibiotic

necessary to inhibit bacterial growth. To investigate this, we carried out a checkerboard assay which examined the combinatory effects of two agents on bacterial growth at a variety of concentrations (386). We examined the effects of itaconate on the antibacterial properties of four conventional antibiotics used against *P. aeruginosa* infection; tobramycin, meropenem, azactam and piperacillin/tazobactam (45, 46, 48, 49, 460, 462). In these experiments, we observed that our hypothesis was incorrect, as itaconate antagonised the activity of these antibiotic meaning that higher concentrations were necessary in the presence of itaconate. This finding was unexpected, when considered in the context that itaconate inhibits *P. aeruginosa* growth. However, this finding is in agreement with current literature (501, 506). Previous experiments by other authors have demonstrated that sub-inhibitory concentrations of antibiotic agents can induce a stress response in bacteria whereby they induce biofilm formation and virulence factor expression as a protective mechanism (501, 506). For example, sub-inhibitory concentrations of tobramycin induce biofilm formation in a dose-dependent manner (501). Previously, this caused concern in clinicians that antibiotic treatment may be promoting bacterial biofilm formation within the deep lung, where sub-inhibitory concentrations were prevalent. However, tobramycin is still routinely used in CF (501). In this context, our experiments have increased the understanding of the effects of itaconate during *P. aeruginosa* infection. It may be interesting to consider these results in the context of the development of a treatment which boosts endogenous itaconate production, or the use of itaconate as an antipseudomonal therapy itself.

Our final experiments involved examining the effect of 4-OI and itaconate *in vivo*. We hypothesised that 4-OI and itaconate would exert protective effects *in vivo* in a model of *P. aeruginosa* infection. In order to test this hypothesis, we conducted these experiments in *Galleria mellonella* (*G. mellonella*) larvae which are routinely utilised in studies to examine the virulence of *P. aeruginosa* strains and efficacy of anti-microbial agents (473). The decision to employ the *G. mellonella* model was based on a number of benefits that this model offers over murine models. Firstly, *G. mellonella* larvae are inexpensive, do not require specialist equipment and are available in large numbers for experiments (473, 510). Furthermore, ethical approval is not required for experiments

which enabled these experiments to be carried out with little notice. Finally, the immune system of *G. mellonella* is strikingly similar to that of the vertebrate innate immune system and is comprised of humoral and cellular arms (473-475). The humoral arm is comprised of a variety of soluble factors which act to immobilise and kill pathogens (473-475). The cellular arm is comprised of a variety of phagocytic cells, knowns as haemocytes, which act to phagocytose and kill invading pathogens (473, 476, 477). In the context of *P. aeruginosa* infection, *G. mellonella* are extremely susceptible to infection, but previous studies have demonstrated strong correlations between antibiotic pharmacokinetics observed *in vitro* and the therapeutic effect in *P. aeruginosa* infected *G. mellonella* (514). Furthermore, the effects of antibiotics in *G. mellonella* are similar to those observed in murine models (515). For these reasons, we believed that *G. mellonella* was an ideal system to investigate our hypothesis.

Our findings demonstrated for the first time that itaconate is protective *in vivo* in an invertebrate model of *P. aeruginosa* infection. Furthermore, we also demonstrated for the first time that 4-OI is also protective in this model. These results are in agreement with our previous findings which demonstrated the antibacterial properties of both itaconate and 4-OI. This is the first description of the use of either 4-OI or itaconate as a therapeutic agent against *P. aeruginosa in vivo*. We propose that this adds further weight to the use of 4-OI as a therapeutic agent for the treatment of *P. aeruginosa* infection.

We believe that our data provides evidence for the use of 4-OI as a novel therapeutic agent for the treatment of *P. aeruginosa* infection in CF. As previously stated, inflammation and *P. aeruginosa* infection are major aspects of CF disease (21). In this study, we demonstrated that 4-OI limits the inflammatory responses of macrophages and promotes *P. aeruginosa* killing *in vitro* and also displays protective effects against *P. aeruginosa* infection *in vivo*. Further experimentation is necessary to ascertain the efficacy of 4-OI in this context. Ideally, further experiments would involve a murine model of chronic respiratory *P. aeruginosa* infection and subsequent administration of 4-OI to examine the effects within the lung on inflammation and also bacterial clearance. If these experiments were successful and demonstrated efficacy, 4-OI loaded nanoparticles could be prepared as previously carried out in The Donnelly Lab

using SCD-19. This would overcome the solubility issues associated with 4-OI and enable nebulised delivery for deep lung penetration.

It is important to recognise that our experiments examining 4-OI and itaconate are not without their limitations. As stated above, experiments using HKPA are not representative of live *P. aeruginosa* infection. However, we did endeavour to overcome this by examining he effects of 4-OI and endogenous itaconate on live *P. aeruginosa* infection. This subsequently introduced new difficulties, as it was necessary to change the time point for the experiment from 24 hours to 8 hours due to toxicity issues. As such, it is important to be cogniscent that we are examining a very early timepoint in the macrophage response. In the context of our *in vivo* study, *G. mellonella* were co-administered *P. aeruginosa* and itaconate or *P. aeruginosa* and 4-OI in a single injection. This was due to high levels of toxicity associated with *P. aeruginosa* infection in *G. mellonella*. Ideally, larvae would have been injected with *P. aeruginosa* and then at a later timepoint receive 4-OI or itaconate treatment, which would be more translational to a real-life infection.

In conclusion, in CF there is an unmet clinical need for the development of novel therapies that are both anti-inflammatory and antipseudomonal. In this thesis, we have characterised the effects of two potential host-directed therapies, SCD-19 and 4-OI respectively, in the context of *P. aeruginosa* infection. We have demonstrated that SCD-19 inhibits the inflammatory responses of macrophages to HKPA and secreted *P. aeruginosa* products. Furthermore, we have demonstrated that SCD-19 inhibits *P. aeruginosa* biofilm formation on airway epithelial cells. We have also successfully demonstrated these effects using SCD-19 loaded nanoparticles which have previously been shown to be capable of deep lung penetration. In the context of 4-OI, we have successfully demonstrated that 4-OI limits *P. aeruginosa* induced inflammatory responses in macrophages. Furthermore, we demonstrated that itaconate displays antipseudomonal properties. We have also demonstrated that both 4-OI and itaconate are protective *in vivo* in a model of *P. aeruginosa* infection. Overall, our findings suggest that SCD-19 and 4-OI, respectively, represent two novel potential treatments for CF patients. These findings warrant further investigation.

Chapter 7 - References

7.1 References

1. Gray RD, Hardisty G, Regan KH, Smith M, Robb CT, Duffin R, et al. Delayed neutrophil apoptosis enhances NET formation in cystic fibrosis. Thorax. 2018;73(2):134-44.
2. Folkesson A, Jelsbak L, Yang L, Johansen HK, Ciofu O, Høiby N, et al. Adaptation of Pseudomonas aeruginosa to the cystic fibrosis airway: an evolutionary perspective. Nature Reviews Microbiology. 2012;10:841.
3. Boucher RC. Relationship of airway epithelial ion transport to chronic bronchitis. Proc Am Thorac Soc. 2004;1(1):66-70.
4. Cutting GR. Cystic fibrosis genetics: from molecular understanding to clinical application. Nat Rev Genet. 2015;16(1):45-56.
5. Ooi CY, Durie PR. Cystic fibrosis from the gastroenterologist's perspective. Nat Rev Gastroenterol Hepatol. 2016;13(3):175-85.
6. Hisert KB, Heltshe SL, Pope C, Jorth P, Wu X, Edwards RM, et al. Restoring Cystic Fibrosis Transmembrane Conductance Regulator Function Reduces Airway Bacteria and Inflammation in People with Cystic Fibrosis and Chronic Lung Infections. Am J Respir Crit Care Med. 2017;195(12):1617-28.
7. Davis PB, Drumm M, Konstan MW. Cystic fibrosis. Am J Respir Crit Care Med. 1996;154(5):1229-56.
8. FitzSimmons SC. The changing epidemiology of cystic fibrosis. J Pediatr. 1993;122(1):1-9.
9. Cystic Fibrosis F. Cystic Fibrosis Foundation patient registry 2018 annual data report. Cystic Fibrosis Foundation; 2018.
10. Riordan JR, Rommens JM, Kerem B, Alon N, Rozmahel R, Grzelczak Z, et al. Identification of the cystic fibrosis gene: cloning and characterization of complementary DNA. Science. 1989;245(4922):1066-73.
11. Rommens JM, Iannuzzi MC, Kerem B, Drumm ML, Melmer G, Dean M, et al. Identification of the cystic fibrosis gene: chromosome walking and jumping. Science. 1989;245(4922):1059-65.
12. Consortium CFG-P. Correlation between genotype and phenotype in patients with cystic fibrosis. New England journal of medicine. 1993;329(18):1308-13.
13. Welsh MJ, Smith AE. Molecular mechanisms of CFTR chloride channel dysfunction in cystic fibrosis. Cell. 1993;73(7):1251-4.
14. Ponzano S, Nigrelli G, Fregonese L, Eichler I, Bertozzi F, Bandiera T, et al. A European regulatory perspective on cystic fibrosis: current treatments, trends in drug development and translational challenges for CFTR modulators. Eur Respir Rev. 2018;27(148).
15. Chang EH, Zabner J. Precision Genomic Medicine in Cystic Fibrosis. Clin Transl Sci. 2015;8(5):606-10.
16. McKone EF, Goss CH, Aitken ML. CFTR genotype as a predictor of prognosis in cystic fibrosis. Chest. 2006;130(5):1441-7.
17. Watson MS, Cutting GR, Desnick RJ, Driscoll DA, Klinger K, Mennuti M, et al. Cystic fibrosis population carrier screening: 2004 revision of American College of Medical Genetics mutation panel. Genet Med. 2004;6(5):387-91.
18. Ioannou L, McClaren BJ, Massie J, Lewis S, Metcalfe SA, Forrest L, et al. Population-based carrier screening for cystic fibrosis: a systematic review of 23 years of research. Genet Med. 2014;16(3):207-16.
19. Dalemans W, Barbry P, Champigny G, Jallat S, Dott K, Dreyer D, et al. Altered chloride ion channel kinetics associated with the delta F508 cystic fibrosis mutation. Nature. 1991;354(6354):526-8.
20. Lukacs GL, Chang XB, Bear C, Kartner N, Mohamed A, Riordan JR, et al. The delta F508 mutation decreases the stability of cystic fibrosis transmembrane conductance regulator in the

plasma membrane. Determination of functional half-lives on transfected cells. J Biol Chem. 1993;268(29):21592-8.
21. Rey MM, Bonk MP, Hadjiliadis D. Cystic Fibrosis: Emerging Understanding and Therapies. Annu Rev Med. 2019;70:197-210.
22. Wilschanski M, Durie PR. Pathology of pancreatic and intestinal disorders in cystic fibrosis. J R Soc Med. 1998;91 Suppl 34:40-9.
23. Ode KL, Moran A. New insights into cystic fibrosis-related diabetes in children. Lancet Diabetes Endocrinol. 2013;1(1):52-8.
24. Colombo C. Liver disease in cystic fibrosis. Curr Opin Pulm Med. 2007;13(6):529-36.
25. Popli K, Stewart J. Infertility and its management in men with cystic fibrosis: review of literature and clinical practices in the UK. Hum Fertil (Camb). 2007;10(4):217-21.
26. Elborn JS. Cystic fibrosis. Lancet. 2016;388(10059):2519-31.
27. Ramsey KA, Ranganathan S, Park J, Skoric B, Adams AM, Simpson SJ, et al. Early respiratory infection is associated with reduced spirometry in children with cystic fibrosis. Am J Respir Crit Care Med. 2014;190(10):1111-6.
28. Sly PD, Gangell CL, Chen L, Ware RS, Ranganathan S, Mott LS, et al. Risk factors for bronchiectasis in children with cystic fibrosis. The New England journal of medicine. 2013;368(21):1963-70.
29. Rosenow T, Oudraad MC, Murray CP, Turkovic L, Kuo W, de Bruijne M, et al. PRAGMA-CF. A Quantitative Structural Lung Disease Computed Tomography Outcome in Young Children with Cystic Fibrosis. Am J Respir Crit Care Med. 2015;191(10):1158-65.
30. Haq IJ, Gray MA, Garnett JP, Ward C, Brodlie M. Airway surface liquid homeostasis in cystic fibrosis: pathophysiology and therapeutic targets. Thorax. 2016;71(3):284-7.
31. Shah VS, Meyerholz DK, Tang XX, Reznikov L, Abou Alaiwa M, Ernst SE, et al. Airway acidification initiates host defense abnormalities in cystic fibrosis mice. Science. 2016;351(6272):503-7.
32. Hoegger MJ, Fischer AJ, McMenimen JD, Ostedgaard LS, Tucker AJ, Awadalla MA, et al. Impaired mucus detachment disrupts mucociliary transport in a piglet model of cystic fibrosis. Science. 2014;345(6198):818-22.
33. Keiser NW, Birket SE, Evans IA, Tyler SR, Crooke AK, Sun X, et al. Defective innate immunity and hyperinflammation in newborn cystic fibrosis transmembrane conductance regulator-knockout ferret lungs. Am J Respir Cell Mol Biol. 2015;52(6):683-94.
34. Parameswaran GI, Murphy TF. Infections in chronic lung diseases. Infect Dis Clin North Am. 2007;21(3):673-95, viii.
35. Paranjape SM, Mogayzel PJ, Jr. Cystic fibrosis. Pediatr Rev. 2014;35(5):194-205.
36. Filkins LM, O'Toole GA. Cystic Fibrosis Lung Infections: Polymicrobial, Complex, and Hard to Treat. PLoS pathogens. 2015;11(12):e1005258.
37. Burns JL, Gibson RL, McNamara S, Yim D, Emerson J, Rosenfeld M, et al. Longitudinal assessment of Pseudomonas aeruginosa in young children with cystic fibrosis. The Journal of infectious diseases. 2001;183(3):444-52.
38. Edmondson C, Davies JC. Current and future treatment options for cystic fibrosis lung disease: latest evidence and clinical implications. Ther Adv Chronic Dis. 2016;7(3):170-83.
39. Murray JF. The ketchup-bottle method. The New England journal of medicine. 1979;300(20):1155-7.
40. Konstan MW, Stern RC, Doershuk CF. Efficacy of the Flutter device for airway mucus clearance in patients with cystic fibrosis. J Pediatr. 1994;124(5 Pt 1):689-93.
41. Henke MO, Ratjen F. Mucolytics in cystic fibrosis. Paediatric respiratory reviews. 2007;8(1):24-9.
42. Doring G, Flume P, Heijerman H, Elborn JS. Treatment of lung infection in patients with cystic fibrosis: current and future strategies. J Cyst Fibros. 2012;11(6):461-79.

43. Neill O. Review on Antimicrobial Resistance Antimicrobial Resistance: Tackling a crisis for the health and wealth of nations. https://amr-review.org/sites/default/files/AMR%20Review%20Paper%20-%20Tackling%20a%20crisis%20for%20the%20health%20and%20wealth%20of%20nations_1.pdf2014.
44. Chmiel JF, Konstan MW, Elborn JS. Antibiotic and anti-inflammatory therapies for cystic fibrosis. Cold Spring Harb Perspect Med. 2013;3(10):a009779.
45. Trautmann M, Heinemann M, Zick R, Moricke A, Seidelmann M, Berger D. Antibacterial activity of meropenem against Pseudomonas aeruginosa, including antibiotic-induced morphological changes and endotoxin-liberating effects. Eur J Clin Microbiol Infect Dis. 1998;17(11):754-60.
46. Taccone FS, Cotton F, Roisin S, Vincent JL, Jacobs F. Optimal meropenem concentrations to treat multidrug-resistant Pseudomonas aeruginosa septic shock. Antimicrob Agents Chemother. 2012;56(4):2129-31.
47. Doroudian M, MacLoughlin R, Poynton F, Prina-Mello A, Donnelly SC. Nanotechnology based therapeutics for lung disease. Thorax. 2019;74(10):965-76.
48. Elborn JS, Vataire AL, Fukushima A, Aballea S, Khemiri A, Moore C, et al. Comparison of Inhaled Antibiotics for the Treatment of Chronic Pseudomonas aeruginosa Lung Infection in Patients With Cystic Fibrosis: Systematic Literature Review and Network Meta-analysis. Clin Ther. 2016;38(10):2204-26.
49. Hamed K, Debonnett L. Tobramycin inhalation powder for the treatment of pulmonary Pseudomonas aeruginosa infection in patients with cystic fibrosis: a review based on clinical evidence. Ther Adv Respir Dis. 2017;11(5):193-209.
50. Konstan MW, Geller DE, Minic P, Brockhaus F, Zhang J, Angyalosi G. Tobramycin inhalation powder for *P. aeruginosa* infection in cystic fibrosis: the EVOLVE trial. Pediatr Pulmonol. 2011;46(3):230-8.
51. Schuster A, Haliburn C, Doring G, Goldman MH. Safety, efficacy and convenience of colistimethate sodium dry powder for inhalation (Colobreathe DPI) in patients with cystic fibrosis: a randomised study. Thorax. 2013;68(4):344-50.
52. Flume PA, Liou TG, Borowitz DS, Li H, Yen K, Ordonez CL, et al. Ivacaftor in subjects with cystic fibrosis who are homozygous for the F508del-CFTR mutation. Chest. 2012;142(3):718-24.
53. Ramsey BW, Davies J, McElvaney NG, Tullis E, Bell SC, Drevinek P, et al. A CFTR potentiator in patients with cystic fibrosis and the G551D mutation. The New England journal of medicine. 2011;365(18):1663-72.
54. FDA expands approved use of Kalydeco to treat additional mutations of cystic fibrosis. [press release]. https://www.fda.gov/news-events/press-announcements/fda-expands-approved-use-kalydeco-treat-additional-mutations-cystic-fibrosis2017.
55. Bagdany M, Veit G, Fukuda R, Avramescu RG, Okiyoneda T, Baaklini I, et al. Chaperones rescue the energetic landscape of mutant CFTR at single molecule and in cell. Nature Communications. 2017;8(1):398.
56. Clancy JP, Rowe SM, Accurso FJ, Aitken ML, Amin RS, Ashlock MA, et al. Results of a phase IIa study of VX-809, an investigational CFTR corrector compound, in subjects with cystic fibrosis homozygous for the F508del-CFTR mutation. Thorax. 2012;67(1):12-8.
57. Wainwright CE, Elborn JS, Ramsey BW, Marigowda G, Huang X, Cipolli M, et al. Lumacaftor–Ivacaftor in Patients with Cystic Fibrosis Homozygous for Phe508del CFTR. New England Journal of Medicine. 2015;373(3):220-31.
58. Hubert D, Chiron R, Camara B, Grenet D, Prévotat A, Bassinet L, et al. Real-life initiation of lumacaftor/ivacaftor combination in adults with cystic fibrosis homozygous for the Phe508del CFTR mutation and severe lung disease. Journal of Cystic Fibrosis. 2017;16(3):388-91.

59. Taylor-Cousar JL, Munck A, McKone EF, van der Ent CK, Moeller A, Simard C, et al. Tezacaftor–Ivacaftor in Patients with Cystic Fibrosis Homozygous for Phe508del. New England Journal of Medicine. 2017;377(21):2013-23.
60. Middleton PG, Mall MA, Drevinek P, Lands LC, McKone EF, Polineni D, et al. Elexacaftor-Tezacaftor-Ivacaftor for Cystic Fibrosis with a Single Phe508del Allele. The New England journal of medicine. 2019;381(19):1809-19.
61. FDA approves new breakthrough therapy for cystic fibrosis [press release]. https://www.fda.gov/news-events/press-announcements/fda-approves-new-breakthrough-therapy-cystic-fibrosis2019.
62. Dasenbrook EC, Chmiel JF. Anti-inflammatory therapies for cystic fibrosis. Treatment of Cystic Fibrosis and Other Rare Lung Diseases: Springer; 2017. p. 139-51.
63. Kovesi TA, Swartz R, MacDonald N. Transient renal failure due to simultaneous ibuprofen and aminoglycoside therapy in children with cystic fibrosis. The New England journal of medicine. 1998;338(1):65-6.
64. Bell EA, Grothe R, Zivkovich V, Foote JM, Wellendorf J. Pyloric channel stricture secondary to high-dose ibuprofen therapy in a patient with cystic fibrosis. Ann Pharmacother. 1999;33(6):693-6.
65. Lai HC, FitzSimmons SC, Allen DB, Kosorok MR, Rosenstein BJ, Campbell PW, et al. Risk of persistent growth impairment after alternate-day prednisone treatment in children with cystic fibrosis. The New England journal of medicine. 2000;342(12):851-9.
66. Auerbach HS, Williams M, Kirkpatrick JA, Colten HR. Alternate-day prednisone reduces morbidity and improves pulmonary function in cystic fibrosis. Lancet. 1985;2(8457):686-8.
67. Tirouvanziam R, Conrad CK, Bottiglieri T, Herzenberg LA, Moss RB, Herzenberg LA. High-dose oral N-acetylcysteine, a glutathione prodrug, modulates inflammation in cystic fibrosis. Proc Natl Acad Sci U S A. 2006;103(12):4628-33.
68. Conrad C, Lymp J, Thompson V, Dunn C, Davies Z, Chatfield B, et al. Long-term treatment with oral N-acetylcysteine: affects lung function but not sputum inflammation in cystic fibrosis subjects. A phase II randomized placebo-controlled trial. J Cyst Fibros. 2015;14(2):219-27.
69. Iannitti RG, Napolioni V, Oikonomou V, De Luca A, Galosi C, Pariano M, et al. IL-1 receptor antagonist ameliorates inflammasome-dependent inflammation in murine and human cystic fibrosis. Nat Commun. 2016;7:10791.
70. Konstan MW, Doring G, Heltshe SL, Lands LC, Hilliard KA, Koker P, et al. A randomized double blind, placebo controlled phase 2 trial of BIIL 284 BS (an LTB4 receptor antagonist) for the treatment of lung disease in children and adults with cystic fibrosis. J Cyst Fibros. 2014;13(2):148-55.
71. Doring G, Bragonzi A, Paroni M, Akturk FF, Cigana C, Schmidt A, et al. BIIL 284 reduces neutrophil numbers but increases *P. aeruginosa* bacteremia and inflammation in mouse lungs. J Cyst Fibros. 2014;13(2):156-63.
72. Akira S. Pathogen recognition by innate immunity and its signaling. Proc Jpn Acad Ser B Phys Biol Sci. 2009;85(4):143-56.
73. Akira S, Takeda K. Toll-like receptor signalling. Nat Rev Immunol. 2004;4(7):499-511.
74. Akira S, Uematsu S, Takeuchi O. Pathogen recognition and innate immunity. Cell. 2006;124(4):783-801.
75. Beutler B. Innate immunity: an overview. Molecular Immunology. 2004;40(12):845-59.
76. Chaplin DD. Overview of the immune response. The Journal of allergy and clinical immunology. 2010;125(2 Suppl 2):S3-S23.
77. Bonilla FA, Oettgen HC. Adaptive immunity. Journal of Allergy and Clinical Immunology. 2010;125(2):S33-S40.
78. Kawai T, Akira S. The role of pattern-recognition receptors in innate immunity: update on Toll-like receptors. Nat Immunol. 2010;11(5):373-84.

79. Hashimoto C, Hudson KL, Anderson KV. The Toll gene of Drosophila, required for dorsal-ventral embryonic polarity, appears to encode a transmembrane protein. Cell. 1988;52(2):269-79.
80. Lemaitre B, Nicolas E, Michaut L, Reichhart JM, Hoffmann JA. The dorsoventral regulatory gene cassette spatzle/Toll/cactus controls the potent antifungal response in Drosophila adults. Cell. 1996;86(6):973-83.
81. West AP, Koblansky AA, Ghosh S. Recognition and signaling by toll-like receptors. Annu Rev Cell Dev Biol. 2006;22:409-37.
82. Jin MS, Lee JO. Structures of the toll-like receptor family and its ligand complexes. Immunity. 2008;29(2):182-91.
83. Bell JK, Mullen GE, Leifer CA, Mazzoni A, Davies DR, Segal DM. Leucine-rich repeats and pathogen recognition in Toll-like receptors. Trends in immunology. 2003;24(10):528-33.
84. Slack JL, Schooley K, Bonnert TP, Mitcham JL, Qwarnstrom EE, Sims JE, et al. Identification of two major sites in the type I interleukin-1 receptor cytoplasmic region responsible for coupling to pro-inflammatory signaling pathways. J Biol Chem. 2000;275(7):4670-8.
85. Pandey S, Kawai T, Akira S. Microbial sensing by Toll-like receptors and intracellular nucleic acid sensors. Cold Spring Harb Perspect Biol. 2014;7(1):a016246-a.
86. Collins B, Wilson IA. Crystal structure of the C-terminal domain of mouse TLR9. Proteins. 2014;82(10):2874-8.
87. Fitzgerald KA, Palsson-McDermott EM, Bowie AG, Jefferies CA, Mansell AS, Brady G, et al. Mal (MyD88-adapter-like) is required for Toll-like receptor-4 signal transduction. Nature. 2001;413(6851):78-83.
88. Sarkar SN, Elco CP, Peters KL, Chattopadhyay S, Sen GC. Two tyrosine residues of Toll-like receptor 3 trigger different steps of NF-kappa B activation. J Biol Chem. 2007;282(6):3423-7.
89. Griebel T, Maekawa T, Parker JE. NOD-like receptor cooperativity in effector-triggered immunity. Trends in immunology. 2014;35(11):562-70.
90. Kummer JA, Broekhuizen R, Everett H, Agostini L, Kuijk L, Martinon F, et al. Inflammasome components NALP 1 and 3 show distinct but separate expression profiles in human tissues suggesting a site-specific role in the inflammatory response. J Histochem Cytochem. 2007;55(5):443-52.
91. Meissner TB, Li A, Biswas A, Lee KH, Liu YJ, Bayir E, et al. NLR family member NLRC5 is a transcriptional regulator of MHC class I genes. Proc Natl Acad Sci U S A. 2010;107(31):13794-9.
92. Ting JPY, Lovering RC, Alnemri ES, Bertin J, Boss JM, Davis BK, et al. The NLR Gene Family: A Standard Nomenclature. Immunity. 2008;28(3):285-7.
93. Inohara, Chamaillard, McDonald C, Nunez G. NOD-LRR proteins: role in host-microbial interactions and inflammatory disease. Annu Rev Biochem. 2005;74:355-83.
94. Martinon F, Tschopp J. NLRs join TLRs as innate sensors of pathogens. Trends in immunology. 2005;26(8):447-54.
95. Alhazmi A. NOD-like receptor(s) and host immune responses with Pseudomonas aeruginosa infection. Inflamm Res. 2018;67(6):479-93.
96. Henao-Mejia J, Elinav E, Strowig T, Flavell RA. Inflammasomes: far beyond inflammation. Nat Immunol. 2012;13(4):321-4.
97. Rehwinkel J, Gack MU. RIG-I-like receptors: their regulation and roles in RNA sensing. Nature Reviews Immunology. 2020:1-15.
98. Loo Y-M, Gale Jr M. Immune signaling by RIG-I-like receptors. Immunity. 2011;34(5):680-92.
99. Yoneyama M, Fujita T. Function of RIG-I-like receptors in antiviral innate immunity. J Biol Chem. 2007;282(21):15315-8.

100. Yoneyama M, Kikuchi M, Natsukawa T, Shinobu N, Imaizumi T, Miyagishi M, et al. The RNA helicase RIG-I has an essential function in double-stranded RNA-induced innate antiviral responses. Nat Immunol. 2004;5(7):730-7.
101. Willment JA, Brown GD. C-type lectin receptors in antifungal immunity. Trends in microbiology. 2008;16(1):27-32.
102. Brown GD, Willment JA, Whitehead L. C-type lectins in immunity and homeostasis. Nature Reviews Immunology. 2018;18(6):374-89.
103. Drummond RA, Saijo S, Iwakura Y, Brown GD. The role of Syk/CARD9 coupled C-type lectins in antifungal immunity. Eur J Immunol. 2011;41(2):276-81.
104. Ishikawa H, Barber GN. STING is an endoplasmic reticulum adaptor that facilitates innate immune signalling. Nature. 2008;455(7213):674-8.
105. Ishikawa H, Ma Z, Barber GN. STING regulates intracellular DNA-mediated, type I interferon-dependent innate immunity. Nature. 2009;461(7265):788-92.
106. Burdette DL, Monroe KM, Sotelo-Troha K, Iwig JS, Eckert B, Hyodo M, et al. STING is a direct innate immune sensor of cyclic di-GMP. Nature. 2011;478(7370):515-8.
107. Motwani M, Pesiridis S, Fitzgerald KA. DNA sensing by the cGAS-STING pathway in health and disease. Nat Rev Genet. 2019;20(11):657-74.
108. Fang R, Wang C, Jiang Q, Lv M, Gao P, Yu X, et al. NEMO-IKKbeta Are Essential for IRF3 and NF-kappaB Activation in the cGAS-STING Pathway. Journal of immunology (Baltimore, Md : 1950). 2017;199(9):3222-33.
109. Lolis E, Bucala R. Macrophage migration inhibitory factor. Expert opinion on therapeutic targets. 2003;7(2):153-64.
110. Plant BJ, Gallagher CG, Bucala R, Baugh JA, Chappell S, Morgan L, et al. Cystic Fibrosis, Disease Severity, and a Macrophage Migration Inhibitory Factor Polymorphism. American Journal of Respiratory and Critical Care Medicine. 2005;172(11):1412-5.
111. Adamali H, Armstrong ME, McLaughlin AM, Cooke G, McKone E, Costello CM, et al. Macrophage migration inhibitory factor enzymatic activity, lung inflammation, and cystic fibrosis. Am J Respir Crit Care Med. 2012;186(2):162-9.
112. Mawhinney L, Armstrong ME, O'Reilly C, Bucala R, Leng L, Fingerle-Rowson G, et al. Macrophage Migration Inhibitory Factor (MIF) Enzymatic Activity and Lung Cancer. Molecular Medicine. 2014;20(1):729.
113. Tynan A, Mawhinney L, Armstrong ME, O'Reilly C, Kennedy S, Caraher E, et al. Macrophage migration inhibitory factor enhances Pseudomonas aeruginosa biofilm formation, potentially contributing to cystic fibrosis pathogenesis. The FASEB Journal. 2017;31(11):5102-10.
114. Baugh J, Chitnis S, Donnelly S, Monteiro J, Lin X, Plant B, et al. A functional promoter polymorphism in the macrophage migration inhibitory factor (MIF) gene associated with disease severity in rheumatoid arthritis. Genes and immunity. 2002;3(3):170-6.
115. Donnelly SC, Haslett C, Reid PT, Grant IS, Wallace WA, Metz CN, et al. Regulatory role for macrophage migration inhibitory factor in acute respiratory distress syndrome. Nature medicine. 1997;3(3):320-3.
116. Bloom BR, Bennett B. Mechanism of a reaction in vitro associated with delayed-type hypersensitivity. Science. 1966;153(3731):80-2.
117. David JR. Delayed hypersensitivity in vitro: its mediation by cell-free substances formed by lymphoid cell-antigen interaction. Proc Natl Acad Sci U S A. 1966;56(1):72.
118. Weiser WY, Temple PA, Witek-Giannotti JS, Remold HG, Clark SC, David JR. Molecular cloning of a cDNA encoding a human macrophage migration inhibitory factor. Proc Natl Acad Sci U S A. 1989;86(19):7522-6.
119. Bernhagen J, Calandra T, Mitchell RA, Martin SB, Tracey KJ, Voelter W, et al. MIF is a pituitary-derived cytokine that potentiates lethal endotoxaemia. Nature. 1993;365(6448):756-9.

120. Bernhagen J, Mitchell RA, Calandra T, Voelter W, Cerami A, Bucala R. Purification, Bioactivity, and Secondary Structure Analysis of Mouse and Human Macrophage Migration Inhibitory Factor (MIF). Biochemistry. 1994;33(47):14144-55.
121. Calandra T, Bernhagen J, Mitchell RA, Bucala R. The macrophage is an important and previously unrecognized source of macrophage migration inhibitory factor. J Exp Med. 1994;179(6):1895-902.
122. Daryadel A, Grifone RF, Simon HU, Yousefi S. Apoptotic neutrophils release macrophage migration inhibitory factor upon stimulation with tumor necrosis factor-alpha. J Biol Chem. 2006;281(37):27653-61.
123. Imamura K, Nishihira J, Suzuki M, Yasuda K, Sasaki S, Kusunoki Y, et al. Identification and immunohistochemical localization of macrophage migration inhibitory factor in human kidney. Biochem Mol Biol Int. 1996;40(6):1233-42.
124. Calandra T, Roger T. Macrophage migration inhibitory factor: a regulator of innate immunity. Nature reviews immunology. 2003;3(10):791-800.
125. Rossi AG, Haslett C, Hirani N, Greening AP, Rahman I, Metz CN, et al. Human circulating eosinophils secrete macrophage migration inhibitory factor (MIF). Potential role in asthma. J Clin Invest. 1998;101(12):2869-74.
126. Bacher M, Metz CN, Calandra T, Mayer K, Chesney J, Lohoff M, et al. An essential regulatory role for macrophage migration inhibitory factor in T-cell activation. Proc Natl Acad Sci U S A. 1996;93(15):7849-54.
127. Paralkar V, Wistow G. Cloning the Human Gene for Macrophage Migration Inhibitory Factor (MIF). Genomics. 1994;19(1):48-51.
128. Bozza M, Kolakowski LF, Jr., Jenkins NA, Gilbert DJ, Copeland NG, David JR, et al. Structural characterization and chromosomal location of the mouse macrophage migration inhibitory factor gene and pseudogenes. Genomics. 1995;27(3):412-9.
129. Kozak CA, Adamson MC, Buckler CE, Segovia L, Paralkar V, Wistow G. Genomic cloning of mouse MIF (macrophage inhibitory factor) and genetic mapping of the human and mouse expressed gene and nine mouse pseudogenes. Genomics. 1995;27(3):405-11.
130. Sun HW, Bernhagen J, Bucala R, Lolis E. Crystal structure at 2.6-A resolution of human macrophage migration inhibitory factor. Proc Natl Acad Sci U S A. 1996;93(11):5191-6.
131. Sugimoto H, Suzuki M, Nakagawa A, Tanaka I, Nishihira J. Crystal structure of macrophage migration inhibitory factor from human lymphocyte at 2.1 A resolution. FEBS Lett. 1996;389(2):145-8.
132. Kato Y, Muto T, Tomura T, Tsumura H, Watarai H, Mikayama T, et al. The crystal structure of human glycosylation-inhibiting factor is a trimeric barrel with three 6-stranded beta-sheets. Proc Natl Acad Sci U S A. 1996;93(7):3007-10.
133. Sun HW, Swope M, Cinquina C, Bedarkar S, Bernhagen J, Bucala R, et al. The subunit structure of human macrophage migration inhibitory factor: evidence for a trimer. Protein Eng. 1996;9(8):631-5.
134. Suzuki M, Sugimoto H, Nakagawa A, Tanaka I, Nishihira J, Sakai M. Crystal structure of the macrophage migration inhibitory factor from rat liver. Nat Struct Biol. 1996;3(3):259-66.
135. Rosengren E, Bucala R, Aman P, Jacobsson L, Odh G, Metz CN, et al. The immunoregulatory mediator macrophage migration inhibitory factor (MIF) catalyzes a tautomerization reaction. Mol Med. 1996;2(1):143-9.
136. Rosengren E, Aman P, Thelin S, Hansson C, Ahlfors S, Bjork P, et al. The macrophage migration inhibitory factor MIF is a phenylpyruvate tautomerase. FEBS Lett. 1997;417(1):85-8.
137. Subramanya HS, Roper DI, Dauter Z, Dodson EJ, Davies GJ, Wilson KS, et al. Enzymatic ketonization of 2-hydroxymuconate: specificity and mechanism investigated by the crystal structures of two isomerases. Biochemistry. 1996;35(3):792-802.
138. Chook YM, Gray JV, Ke H, Lipscomb WN. The monofunctional chorismate mutase from Bacillus subtilis. Structure determination of chorismate mutase and its complexes with a

transition state analog and prephenate, and implications for the mechanism of the enzymatic reaction. J Mol Biol. 1994;240(5):476-500.
139. Lubetsky JB, Swope M, Dealwis C, Blake P, Lolis E. Pro-1 of macrophage migration inhibitory factor functions as a catalytic base in the phenylpyruvate tautomerase activity. Biochemistry. 1999;38(22):7346-54.
140. Fingerle-Rowson G, Kaleswarapu DR, Schlander C, Kabgani N, Brocks T, Reinart N, et al. A Tautomerase-Null Macrophage Migration-Inhibitory Factor (MIF) Gene Knock-In Mouse Model Reveals That Protein Interactions and Not Enzymatic Activity Mediate MIF-Dependent Growth Regulation. Molecular and Cellular Biology. 2009;29(7):1922-32.
141. Al-Abed Y, Dabideen D, Aljabari B, Valster A, Messmer D, Ochani M, et al. ISO-1 binding to the tautomerase active site of MIF inhibits its pro-inflammatory activity and increases survival in severe sepsis. J Biol Chem. 2005;280(44):36541-4.
142. Al-Abed Y, VanPatten S. MIF as a disease target: ISO-1 as a proof-of-concept therapeutic. Future Med Chem. 2011;3(1):45-63.
143. Lubetsky JB, Dios A, Han J, Aljabari B, Ruzsicska B, Mitchell R, et al. The tautomerase active site of macrophage migration inhibitory factor is a potential target for discovery of novel anti-inflammatory agents. J Biol Chem. 2002;277(28):24976-82.
144. Dios A, Mitchell RA, Aljabari B, Lubetsky J, O'Connor K, Liao H, et al. Inhibition of MIF bioactivity by rational design of pharmacological inhibitors of MIF tautomerase activity. J Med Chem. 2002;45(12):2410-6.
145. Russell KE, Chung KF, Clarke CJ, Durham AL, Mallia P, Footitt J, et al. The MIF Antagonist ISO-1 Attenuates Corticosteroid-Insensitive Inflammation and Airways Hyperresponsiveness in an Ozone-Induced Model of COPD. PloS one [Internet]. 2016 2016; 11(1):[e0146102 p.]. Available from: http://europepmc.org/abstract/MED/26752192

https://doi.org/10.1371/journal.pone.0146102

https://europepmc.org/articles/PMC4709227

https://europepmc.org/articles/PMC4709227?pdf=render.
146. Chen PF, Luo YL, Wang W, Wang JX, Lai WY, Hu SM, et al. ISO-1, a macrophage migration inhibitory factor antagonist, inhibits airway remodeling in a murine model of chronic asthma. Mol Med. 2010;16(9-10):400-8.
147. He XX, Chen K, Yang J, Li XY, Gan HY, Liu CY, et al. Macrophage migration inhibitory factor promotes colorectal cancer. Mol Med. 2009;15(1-2):1-10.
148. Meyer-Siegler KL, Iczkowski KA, Leng L, Bucala R, Vera PL. Inhibition of macrophage migration inhibitory factor or its receptor (CD74) attenuates growth and invasion of DU-145 prostate cancer cells. Journal of immunology (Baltimore, Md : 1950). 2006;177(12):8730-9.
149. Winner M, Meier J, Zierow S, Rendon BE, Crichlow GV, Riggs R, et al. A novel, macrophage migration inhibitory factor suicide substrate inhibits motility and growth of lung cancer cells. Cancer Res. 2008;68(18):7253-7.
150. Gadjeva M, Nagashima J, Zaidi T, Mitchell RA, Pier GB. Inhibition of Macrophage Migration Inhibitory Factor Ameliorates Ocular Pseudomonas aeruginosa-Induced Keratitis. PLoS pathogens. 2010;6(3):e1000826.
151. Radstake TR, Sweep FC, Welsing P, Franke B, Vermeulen SH, Geurts-Moespot A, et al. Correlation of rheumatoid arthritis severity with the genetic functional variants and circulating levels of macrophage migration inhibitory factor. Arthritis Rheum. 2005;52(10):3020-9.
152. Bucala R. MIF, MIF alleles, and prospects for therapeutic intervention in autoimmunity. J Clin Immunol. 2013;33 Suppl 1:S72-8.
153. Kang I, Bucala R. The immunobiology of MIF: function, genetics and prospects for precision medicine. Nat Rev Rheumatol. 2019;15(7):427-37.

154. Llamas-Covarrubias MA, Valle Y, Bucala R, Navarro-Hernandez RE, Palafox-Sanchez CA, Padilla-Gutierrez JR, et al. Macrophage migration inhibitory factor (MIF): genetic evidence for participation in early onset and early stage rheumatoid arthritis. Cytokine. 2013;61(3):759-65.
155. Donn RP, Plant D, Jury F, Richards HL, Worthington J, Ray DW, et al. Macrophage migration inhibitory factor gene polymorphism is associated with psoriasis. The Journal of investigative dermatology. 2004;123(3):484-7.
156. Morales-Zambrano R, Bautista-Herrera LA, De la Cruz-Mosso U, Villanueva-Quintero GD, Padilla-Gutierrez JR, Valle Y, et al. Macrophage migration inhibitory factor (MIF) promoter polymorphisms (-794 CATT5-8 and -173 G>C): association with MIF and TNFalpha in psoriatic arthritis. Int J Clin Exp Med. 2014;7(9):2605-14.
157. Amoli MM, Donn RP, Thomson W, Hajeer AH, Garcia-Porrua C, Lueiro M, et al. Macrophage migration inhibitory factor gene polymorphism is associated with sarcoidosis in biopsy proven erythema nodosum. J Rheumatol. 2002;29(8):1671-3.
158. Leng L, Metz CN, Fang Y, Xu J, Donnelly S, Baugh J, et al. MIF Signal Transduction Initiated by Binding to CD74. The Journal of Experimental Medicine. 2003;197(11):1467-76.
159. Shi X, Leng L, Wang T, Wang W, Du X, Li J, et al. CD44 is the signaling component of the macrophage migration inhibitory factor-CD74 receptor complex. Immunity. 2006;25(4):595-606.
160. Yoo SA, Leng L, Kim BJ, Du X, Tilstam PV, Kim KH, et al. MIF allele-dependent regulation of the MIF coreceptor CD44 and role in rheumatoid arthritis. Proc Natl Acad Sci U S A. 2016;113(49):E7917-E26.
161. Mitchell RA, Metz CN, Peng T, Bucala R. Sustained mitogen-activated protein kinase (MAPK) and cytoplasmic phospholipase A2 activation by macrophage migration inhibitory factor (MIF) Regulatory role in cell proliferation and glucocorticoid action. Journal of Biological Chemistry. 1999;274(25):18100-6.
162. Gore Y, Starlets D, Maharshak N, Becker-Herman S, Kaneyuki U, Leng L, et al. Macrophage migration inhibitory factor induces B cell survival by activation of a CD74-CD44 receptor complex. J Biol Chem. 2008;283(5):2784-92.
163. Chatterjee M, Borst O, Walker B, Fotinos A, Vogel S, Seizer P, et al. Macrophage migration inhibitory factor limits activation-induced apoptosis of platelets via CXCR7-dependent Akt signaling. Circ Res. 2014;115(11):939-49.
164. Nakanishi M, Rosenberg DW. Multifaceted roles of PGE2 in inflammation and cancer. Semin Immunopathol. 2013;35(2):123-37.
165. Guo P, Wang J, Liu J, Xia M, Li W, He M. Macrophage immigration inhibitory factor promotes cell proliferation and inhibits apoptosis of cervical adenocarcinoma. Tumour Biol. 2015;36(7):5095-102.
166. Han JA, Kim JI, Ongusaha PP, Hwang DH, Ballou LR, Mahale A, et al. P53-mediated induction of Cox-2 counteracts p53- or genotoxic stress-induced apoptosis. EMBO J. 2002;21(21):5635-44.
167. Mitchell RA, Liao H, Chesney J, Fingerle-Rowson G, Baugh J, David J, et al. Macrophage migration inhibitory factor (MIF) sustains macrophage proinflammatory function by inhibiting p53: Regulatory role in the innate immune response. Proceedings of the National Academy of Sciences. 2002;99(1):345-50.
168. Bucala R, Shachar I. The integral role of CD74 in antigen presentation, MIF signal transduction, and B cell survival and homeostasis. Mini Rev Med Chem. 2014;14(14):1132-8.
169. Schneppenheim J, Dressel R, Huttl S, Lullmann-Rauch R, Engelke M, Dittmann K, et al. The intramembrane protease SPPL2a promotes B cell development and controls endosomal traffic by cleavage of the invariant chain. J Exp Med. 2013;210(1):41-58.
170. Lantner F, Starlets D, Gore Y, Flaishon L, Yamit-Hezi A, Dikstein R, et al. CD74 induces TAp63 expression leading to B-cell survival. Blood. 2007;110(13):4303-11.

171. Bernhagen J, Krohn R, Lue H, Gregory JL, Zernecke A, Koenen RR, et al. MIF is a noncognate ligand of CXC chemokine receptors in inflammatory and atherogenic cell recruitment. Nat Med. 2007;13(5):587-96.
172. Schwartz V, Lue H, Kraemer S, Korbiel J, Krohn R, Ohl K, et al. A functional heteromeric MIF receptor formed by CD74 and CXCR4. FEBS Lett. 2009;583(17):2749-57.
173. Kleemann R, Hausser A, Geiger G, Mischke R, Burger-Kentischer A, Flieger O, et al. Intracellular action of the cytokine MIF to modulate AP-1 activity and the cell cycle through Jab1. Nature. 2000;408(6809):211-6.
174. Wang A, Al-Kuhlani M, Johnston SC, Ojcius DM, Chou J, Dean D. Transcription factor complex AP-1 mediates inflammation initiated by Chlamydia pneumoniae infection. Cellular microbiology. 2013;15(5):779-94.
175. Claret FX, Hibi M, Dhut S, Toda T, Karin M. A new group of conserved coactivators that increase the specificity of AP-1 transcription factors. Nature. 1996;383(6599):453-7.
176. Bucala R. MIF rediscovered: cytokine, pituitary hormone, and glucocorticoid-induced regulator of the immune response. FASEB J. 1996;10(14):1607-13.
177. Calandra T, Bernhagen J, Metz CN, Spiegel LA, Bacher M, Donnelly T, et al. MIF as a glucocorticoid-induced modulator of cytokine production. Nature. 1995;377(6544):68-71.
178. Daun JM, Cannon JG. Macrophage migration inhibitory factor antagonizes hydrocortisone-induced increases in cytosolic IkappaBalpha. Am J Physiol Regul Integr Comp Physiol. 2000;279(3):R1043-9.
179. Wang FF, Zhu LA, Zou YQ, Zheng H, Wilson A, Yang CD, et al. New insights into the role and mechanism of macrophage migration inhibitory factor in steroid-resistant patients with systemic lupus erythematosus. Arthritis Res Ther. 2012;14(3):R103.
180. Roger T, Chanson AL, Knaup-Reymond M, Calandra T. Macrophage migration inhibitory factor promotes innate immune responses by suppressing glucocorticoid-induced expression of mitogen-activated protein kinase phosphatase-1. Eur J Immunol. 2005;35(12):3405-13.
181. Swantek JL, Cobb MH, Geppert TD. Jun N-terminal kinase/stress-activated protein kinase (JNK/SAPK) is required for lipopolysaccharide stimulation of tumor necrosis factor alpha (TNF-alpha) translation: glucocorticoids inhibit TNF-alpha translation by blocking JNK/SAPK. Mol Cell Biol. 1997;17(11):6274-82.
182. Roger T, Froidevaux C, Martin C, Calandra T. Macrophage migration inhibitory factor (MIF) regulates host responses to endotoxin through modulation of Toll-like receptor 4 (TLR4). Journal of endotoxin research. 2003;9(2):119-23.
183. Halligan DN, Murphy SJ, Taylor CT. The hypoxia-inducible factor (HIF) couples immunity with metabolism. Semin Immunol. 2016;28(5):469-77.
184. Masoud GN, Li W. HIF-1alpha pathway: role, regulation and intervention for cancer therapy. Acta Pharm Sin B. 2015;5(5):378-89.
185. Tannahill GM, Curtis AM, Adamik J, Palsson-McDermott EM, McGettrick AF, Goel G, et al. Succinate is an inflammatory signal that induces IL-1β through HIF-1α. Nature. 2013;496:238.
186. Palsson-McDermott EM, O'Neill LAJ. Targeting immunometabolism as an anti-inflammatory strategy. Cell Res. 2020;30(4):300-14.
187. D'Ignazio L, Bandarra D, Rocha S. NF-kappaB and HIF crosstalk in immune responses. FEBS J. 2016;283(3):413-24.
188. van Uden P, Kenneth NS, Rocha S. Regulation of hypoxia-inducible factor-1alpha by NF-kappaB. Biochem J. 2008;412(3):477-84.
189. van Uden P, Kenneth NS, Webster R, Müller HA, Mudie S, Rocha S. Evolutionary Conserved Regulation of HIF-1β by NF-κB. PLOS Genetics. 2011;7(1):e1001285.
190. Peyssonnaux C, Cejudo-Martin P, Doedens A, Zinkernagel AS, Johnson RS, Nizet V. Cutting edge: Essential role of hypoxia inducible factor-1alpha in development of lipopolysaccharide-induced sepsis. Journal of immunology (Baltimore, Md : 1950). 2007;178(12):7516-9.

191. Semenza GL, Roth PH, Fang HM, Wang GL. Transcriptional regulation of genes encoding glycolytic enzymes by hypoxia-inducible factor 1. J Biol Chem. 1994;269(38):23757-63.
192. Carmeliet P, Dor Y, Herbert JM, Fukumura D, Brusselmans K, Dewerchin M, et al. Role of HIF-1alpha in hypoxia-mediated apoptosis, cell proliferation and tumour angiogenesis. Nature. 1998;394(6692):485-90.
193. Winner M, Koong AC, Rendon BE, Zundel W, Mitchell RA. Amplification of tumor hypoxic responses by macrophage migration inhibitory factor-dependent hypoxia-inducible factor stabilization. Cancer Res. 2007;67(1):186-93.
194. Baugh JA, Gantier M, Li L, Byrne A, Buckley A, Donnelly SC. Dual regulation of macrophage migration inhibitory factor (MIF) expression in hypoxia by CREB and HIF-1. Biochemical and biophysical research communications. 2006;347(4):895-903.
195. Li J, Zhang J, Xie F, Peng J, Wu X. Macrophage migration inhibitory factor promotes Warburg effect via activation of the NFkappaB/HIF1alpha pathway in lung cancer. Int J Mol Med. 2018;41(2):1062-8.
196. Fu H, Luo F, Yang L, Wu W, Liu X. Hypoxia stimulates the expression of macrophage migration inhibitory factor in human vascular smooth muscle cells via HIF-1α dependent pathway. BMC Cell Biology. 2010;11(1):66.
197. Gaber T, Schellmann S, Erekul KB, Fangradt M, Tykwinska K, Hahne M, et al. Macrophage Migration Inhibitory Factor Counterregulates Dexamethasone-Mediated Suppression of Hypoxia-Inducible Factor-1α Function and Differentially Influences Human CD4⁺ T Cell Proliferation under Hypoxia. The Journal of Immunology. 2011;186(2):764-74.
198. Bozza M, Satoskar AR, Lin G, Lu B, Humbles AA, Gerard C, et al. Targeted disruption of migration inhibitory factor gene reveals its critical role in sepsis. J Exp Med. 1999;189(2):341-6.
199. Savva A, Brouwer MC, Roger T, Valls Serón M, Le Roy D, Ferwerda B, et al. Functional polymorphisms of macrophage migration inhibitory factor as predictors of morbidity and mortality of pneumococcal meningitis. Proc Natl Acad Sci U S A. 2016;113(13):3597-602.
200. Das R, Koo M-S, Kim BH, Jacob ST, Subbian S, Yao J, et al. Macrophage migration inhibitory factor (MIF) is a critical mediator of the innate immune response to Mycobacterium tuberculosis. Proceedings of the National Academy of Sciences. 2013;110(32):E2997-E3006.
201. Koebernick H, Grode L, David JR, Rohde W, Rolph MS, Mittrücker H-W, et al. Macrophage migration inhibitory factor (MIF) plays a pivotal role in immunity against Salmonella typhimurium. Proceedings of the National Academy of Sciences. 2002;99(21):13681-6.
202. Koebernick H, Grode L, David JR, Rohde W, Rolph MS, Mittrucker HW, et al. Macrophage migration inhibitory factor (MIF) plays a pivotal role in immunity against Salmonella typhimurium. Proc Natl Acad Sci U S A. 2002;99(21):13681-6.
203. Satoskar AR, Bozza M, Rodriguez Sosa M, Lin G, David JR. Migration-inhibitory factor gene-deficient mice are susceptible to cutaneous Leishmania major infection. Infect Immun. 2001;69(2):906-11.
204. Rodriguez-Sosa M, Rosas LE, David JR, Bojalil R, Satoskar AR, Terrazas LI. Macrophage migration inhibitory factor plays a critical role in mediating protection against the helminth parasite Taenia crassiceps. Infect Immun. 2003;71(3):1247-54.
205. Sauler M, Bucala R, Lee PJ. Role of macrophage migration inhibitory factor in age-related lung disease. American Journal of Physiology - Lung Cellular and Molecular Physiology. 2015;309(1):L1-L10.
206. Anderson GG, Kenney TF, Macleod DL, Henig NR, O'Toole GA. Eradication of Pseudomonas aeruginosa biofilms on cultured airway cells by a fosfomycin/tobramycin antibiotic combination. Pathog Dis. 2013;67(1):39-45.

207. Anderson GG, Moreau-Marquis S, Stanton BA, O'Toole GA. In Vitro Analysis of Tobramycin-Treated Pseudomonas aeruginosa Biofilms on Cystic Fibrosis-Derived Airway Epithelial Cells. Infection and Immunity. 2008;76(4):1423-33.
208. Au - O'Toole GA. Microtiter Dish Biofilm Formation Assay. JoVE. 2011(47):e2437.
209. Moreau-Marquis S, Stanton BA, O'Toole GA. Pseudomonas aeruginosa biofilm formation in the cystic fibrosis airway. Pulmonary pharmacology & therapeutics. 2008;21(4):595-9.
210. Nathwani D, Raman G, Sulham K, Gavaghan M, Menon V. Clinical and economic consequences of hospital-acquired resistant and multidrug-resistant Pseudomonas aeruginosa infections: a systematic review and meta-analysis. Antimicrob Resist Infect Control. 2014;3(1):32.
211. Weiner LM, Webb AK, Limbago B, Dudeck MA, Patel J, Kallen AJ, et al. Antimicrobial-Resistant Pathogens Associated With Healthcare-Associated Infections: Summary of Data Reported to the National Healthcare Safety Network at the Centers for Disease Control and Prevention, 2011-2014. Infect Control Hosp Epidemiol. 2016;37(11):1288-301.
212. Fridkin SK, Gaynes RP. Antimicrobial resistance in intensive care units. Clin Chest Med. 1999;20(2):303-16, viii.
213. McManus AT, Mason AD, Jr., McManus WF, Pruitt BA, Jr. Twenty-five year review of Pseudomonas aeruginosa bacteremia in a burn center. Eur J Clin Microbiol. 1985;4(2):219-23.
214. Koch C. Early infection and progression of cystic fibrosis lung disease. Pediatr Pulmonol. 2002;34(3):232-6.
215. Hoiby N, Johansen HK. Isolation measures for prevention of infection with respiratory pathogens in cystic fibrosis: a systematic review? J Hosp Infect. 2007;65(4):374-5; author reply 5-6.
216. Gessard C. On the Blue and Green Coloration that Appears on Bandages. Reviews of Infectious Diseases. 1984;6(Supplement_3):S775-S6.
217. Schmidt KD, Tummler B, Romling U. Comparative genome mapping of Pseudomonas aeruginosa PAO with *P. aeruginosa* C, which belongs to a major clone in cystic fibrosis patients and aquatic habitats. J Bacteriol. 1996;178(1):85-93.
218. Lee DG, Urbach JM, Wu G, Liberati NT, Feinbaum RL, Miyata S, et al. Genomic analysis reveals that Pseudomonas aeruginosa virulence is combinatorial. Genome biology. 2006;7(10):R90.
219. Malhotra S, Hayes D, Jr., Wozniak DJ. Cystic Fibrosis and Pseudomonas aeruginosa: the Host-Microbe Interface. Clin Microbiol Rev. 2019;32(3).
220. Gellatly SL, Hancock RE. Pseudomonas aeruginosa: new insights into pathogenesis and host defenses. Pathog Dis. 2013;67(3):159-73.
221. World Health O. Guidelines for the prevention and control of carbapenem-resistant Enterobacteriaceae, Acinetobacter baumannii and Pseudomonas aeruginosa in health care facilities. Geneva: World Health Organization; 2017 2017.
222. Boulant T, Jousset AB, Bonnin RA, Barrail-Tran A, Borgel A, Oueslati S, et al. A 2.5-years within-patient evolution of a Pseudomonas aeruginosa with *in vivo* acquisition of ceftolozane-tazobactam and ceftazidime-avibactam resistance upon treatment. Antimicrob Agents Chemother. 2019.
223. Fazeli H, Akbari R, Moghim S, Narimani T, Arabestani MR, Ghoddousi AR. Pseudomonas aeruginosa infections in patients, hospital means, and personnel's specimens. J Res Med Sci. 2012;17(4):332-7.
224. Harris AD, Smith D, Johnson JA, Bradham DD, Roghmann MC. Risk factors for imipenem-resistant Pseudomonas aeruginosa among hospitalized patients. Clin Infect Dis. 2002;34(3):340-5.

225. Trautmann M, Lepper PM, Haller M. Ecology of Pseudomonas aeruginosa in the intensive care unit and the evolving role of water outlets as a reservoir of the organism. Am J Infect Control. 2005;33(5 Suppl 1):S41-9.
226. Nseir S, Ader F, Lubret R, Marquette CH. Pathophysiology of airway colonization in critically ill COPD patient. Curr Drug Targets. 2011;12(4):514-20.
227. Sadikot RT, Blackwell TS, Christman JW, Prince AS. Pathogen-host interactions in Pseudomonas aeruginosa pneumonia. Am J Respir Crit Care Med. 2005;171(11):1209-23.
228. Cook D, Walter S, Freitag A, Guyatt G, Devitt H, Meade M, et al. Adjudicating ventilator-associated pneumonia in a randomized trial of critically ill patients. J Crit Care. 1998;13(4):159-63.
229. Hospital-acquired pneumonia in adults: diagnosis, assessment of severity, initial antimicrobial therapy, and preventive strategies. A consensus statement, American Thoracic Society, November 1995. Am J Respir Crit Care Med. 1996;153(5):1711-25.
230. Williams BJ, Dehnbostel J, Blackwell TS. Pseudomonas aeruginosa: host defence in lung diseases. Respirology. 2010;15(7):1037-56.
231. Kaireit TF, Sorrentino SA, Renne J, Schoenfeld C, Voskrebenzev A, Gutberlet M, et al. Functional lung MRI for regional monitoring of patients with cystic fibrosis. PLoS One. 2017;12(12):e0187483.
232. Bhagirath AY, Li Y, Somayajula D, Dadashi M, Badr S, Duan K. Cystic fibrosis lung environment and Pseudomonas aeruginosa infection. BMC Pulm Med. 2016;16(1):174.
233. Costerton JW, Stewart PS, Greenberg EP. Bacterial biofilms: a common cause of persistent infections. Science. 1999;284(5418):1318-22.
234. Wolfgang MC, Jyot J, Goodman AL, Ramphal R, Lory S. Pseudomonas aeruginosa regulates flagellin expression as part of a global response to airway fluid from cystic fibrosis patients. Proc Natl Acad Sci U S A. 2004;101(17):6664-8.
235. Casilag F, Lorenz A, Krueger J, Klawonn F, Weiss S, Haussler S. The LasB Elastase of Pseudomonas aeruginosa Acts in Concert with Alkaline Protease AprA To Prevent Flagellin-Mediated Immune Recognition. Infect Immun. 2016;84(1):162-71.
236. Luzar MA, Thomassen MJ, Montie TC. Flagella and motility alterations in Pseudomonas aeruginosa strains from patients with cystic fibrosis: relationship to patient clinical condition. Infect Immun. 1985;50(2):577-82.
237. Pier GB, Coleman F, Grout M, Franklin M, Ohman DE. Role of alginate O acetylation in resistance of mucoid Pseudomonas aeruginosa to opsonic phagocytosis. Infect Immun. 2001;69(3):1895-901.
238. Leid JG, Willson CJ, Shirtliff ME, Hassett DJ, Parsek MR, Jeffers AK. The exopolysaccharide alginate protects Pseudomonas aeruginosa biofilm bacteria from IFN-gamma-mediated macrophage killing. Journal of immunology (Baltimore, Md : 1950). 2005;175(11):7512-8.
239. Wood LF, Ohman DE. Identification of genes in the sigma(2)(2) regulon of Pseudomonas aeruginosa required for cell envelope homeostasis in either the planktonic or the sessile mode of growth. mBio. 2012;3(3).
240. Mathee K, Ciofu O, Sternberg C, Lindum PW, Campbell JIA, Jensen P, et al. Mucoid conversion of Pseudomonas aeruginosa by hydrogen peroxide: a mechanism for virulence activation in the cystic fibrosis lung. Microbiology. 1999;145 (Pt 6):1349-57.
241. Faure E, Kwong K, Nguyen D. Pseudomonas aeruginosa in Chronic Lung Infections: How to Adapt Within the Host? Frontiers in immunology. 2018;9:2416.
242. Yang J, Zhao HL, Ran LY, Li CY, Zhang XY, Su HN, et al. Mechanistic insights into elastin degradation by pseudolysin, the major virulence factor of the opportunistic pathogen Pseudomonas aeruginosa. Sci Rep. 2015;5:9936.

243. Nomura K, Obata K, Keira T, Miyata R, Hirakawa S, Takano K, et al. Pseudomonas aeruginosa elastase causes transient disruption of tight junctions and downregulation of PAR-2 in human nasal epithelial cells. Respir Res. 2014;15:21.
244. Leidal KG, Munson KL, Johnson MC, Denning GM. Metalloproteases from Pseudomonas aeruginosa degrade human RANTES, MCP-1, and ENA-78. J Interferon Cytokine Res. 2003;23(6):307-18.
245. Matheson NR, Potempa J, Travis J. Interaction of a novel form of Pseudomonas aeruginosa alkaline protease (aeruginolysin) with interleukin-6 and interleukin-8. Biol Chem. 2006;387(7):911-5.
246. Schmidtchen A, Frick IM, Andersson E, Tapper H, Bjorck L. Proteinases of common pathogenic bacteria degrade and inactivate the antibacterial peptide LL-37. Molecular microbiology. 2002;46(1):157-68.
247. Yang J, Lee K-M, Park S, Cho Y, Lee E, Park J-H, et al. Bacterial Secretant from Pseudomonas aeruginosa Dampens Inflammasome Activation in a Quorum Sensing-Dependent Manner. Frontiers in immunology. 2017;8(333).
248. Le Berre R, Nguyen S, Nowak E, Kipnis E, Pierre M, Ader F, et al. Quorum-sensing activity and related virulence factor expression in clinically pathogenic isolates of Pseudomonas aeruginosa. Clin Microbiol Infect. 2008;14(4):337-43.
249. Hauser AR. The type III secretion system of Pseudomonas aeruginosa: infection by injection. Nat Rev Microbiol. 2009;7(9):654-65.
250. Dacheux D, Attree I, Schneider C, Toussaint B. Cell death of human polymorphonuclear neutrophils induced by a Pseudomonas aeruginosa cystic fibrosis isolate requires a functional type III secretion system. Infect Immun. 1999;67(11):6164-7.
251. Garrity-Ryan L, Kazmierczak B, Kowal R, Comolli J, Hauser A, Engel JN. The arginine finger domain of ExoT contributes to actin cytoskeleton disruption and inhibition of internalization of Pseudomonas aeruginosa by epithelial cells and macrophages. Infect Immun. 2000;68(12):7100-13.
252. Mustafi S, Rivero N, Olson JC, Stahl PD, Barbieri MA. Regulation of Rab5 function during phagocytosis of live Pseudomonas aeruginosa in macrophages. Infect Immun. 2013;81(7):2426-36.
253. Miao EA, Mao DP, Yudkovsky N, Bonneau R, Lorang CG, Warren SE, et al. Innate immune detection of the type III secretion apparatus through the NLRC4 inflammasome. Proc Natl Acad Sci U S A. 2010;107(7):3076-80.
254. Huus KE, Joseph J, Zhang L, Wong A, Aaron SD, Mah TF, et al. Clinical Isolates of Pseudomonas aeruginosa from Chronically Infected Cystic Fibrosis Patients Fail To Activate the Inflammasome during Both Stable Infection and Pulmonary Exacerbation. Journal of immunology (Baltimore, Md : 1950). 2016;196(7):3097-108.
255. Jain M, Ramirez D, Seshadri R, Cullina JF, Powers CA, Schulert GS, et al. Type III secretion phenotypes of Pseudomonas aeruginosa strains change during infection of individuals with cystic fibrosis. J Clin Microbiol. 2004;42(11):5229-37.
256. Jain M, Bar-Meir M, McColley S, Cullina J, Potter E, Powers C, et al. Evolution of Pseudomonas aeruginosa type III secretion in cystic fibrosis: a paradigm of chronic infection. Transl Res. 2008;152(6):257-64.
257. Valentini M, Filloux A. Biofilms and Cyclic di-GMP (c-di-GMP) Signaling: Lessons from Pseudomonas aeruginosa and Other Bacteria. J Biol Chem. 2016;291(24):12547-55.
258. Hoiby N, Krogh Johansen H, Moser C, Song Z, Ciofu O, Kharazmi A. Pseudomonas aeruginosa and the in vitro and *in vivo* biofilm mode of growth. Microbes and infection. 2001;3(1):23-35.
259. Donlan RM. Biofilms: microbial life on surfaces. Emerg Infect Dis. 2002;8(9):881-90.
260. Karatan E, Watnick P. Signals, regulatory networks, and materials that build and break bacterial biofilms. Microbiol Mol Biol Rev. 2009;73(2):310-47.

261. Bjarnsholt T, Ciofu O, Molin S, Givskov M, Hoiby N. Applying insights from biofilm biology to drug development - can a new approach be developed? Nat Rev Drug Discov. 2013;12(10):791-808.
262. Shirtliff M, Leid JG, Shirtliff M. The role of biofilms in device-related infections: Springer; 2009.
263. Percival SL, McCarty SM, Lipsky B. Biofilms and Wounds: An Overview of the Evidence. Adv Wound Care (New Rochelle). 2015;4(7):373-81.
264. Singh PK, Schaefer AL, Parsek MR, Moninger TO, Welsh MJ, Greenberg EP. Quorum-sensing signals indicate that cystic fibrosis lungs are infected with bacterial biofilms. Nature. 2000;407(6805):762-4.
265. Costerton JW. Cystic fibrosis pathogenesis and the role of biofilms in persistent infection. Trends in microbiology. 2001;9(2):50-2.
266. Rasamiravaka T, Labtani Q, Duez P, El Jaziri M. The formation of biofilms by Pseudomonas aeruginosa: a review of the natural and synthetic compounds interfering with control mechanisms. Biomed Res Int. 2015;2015:759348.
267. O'Toole GA, Kolter R. Flagellar and twitching motility are necessary for Pseudomonas aeruginosa biofilm development. Molecular microbiology. 1998;30(2):295-304.
268. Wagner VE, Iglewski BH. *P. aeruginosa* Biofilms in CF Infection. Clinical Reviews in Allergy & Immunology. 2008;35(3):124-34.
269. Costerton JW, Cheng KJ, Geesey GG, Ladd TI, Nickel JC, Dasgupta M, et al. Bacterial biofilms in nature and disease. Annu Rev Microbiol. 1987;41:435-64.
270. Nickel JC, Ruseska I, Wright JB, Costerton JW. Tobramycin resistance of Pseudomonas aeruginosa cells growing as a biofilm on urinary catheter material. Antimicrob Agents Chemother. 1985;27(4):619-24.
271. Stewart PS, Costerton JW. Antibiotic resistance of bacteria in biofilms. Lancet. 2001;358(9276):135-8.
272. Stewart PS. Theoretical aspects of antibiotic diffusion into microbial biofilms. Antimicrob Agents Chemother. 1996;40(11):2517-22.
273. Zaidi T, Reidy T, D'Ortona S, Fichorova R, Pier G, Gadjeva M. CD74 deficiency ameliorates Pseudomonas aeruginosa-induced ocular infection. Scientific Reports. 2011;1:58.
274. Knight DA, Holgate ST. The airway epithelium: structural and functional properties in health and disease. Respirology. 2003;8(4):432-46.
275. Whitsett JA, Alenghat T. Respiratory epithelial cells orchestrate pulmonary innate immunity. Nat Immunol. 2015;16(1):27-35.
276. Knowles MR, Boucher RC. Mucus clearance as a primary innate defense mechanism for mammalian airways. J Clin Invest. 2002;109(5):571-7.
277. Tecle T, Tripathi S, Hartshorn KL. Review: Defensins and cathelicidins in lung immunity. Innate Immun. 2010;16(3):151-9.
278. Moreau-Marquis S, Bomberger JM, Anderson GG, Swiatecka-Urban A, Ye S, O'Toole GA, et al. The DeltaF508-CFTR mutation results in increased biofilm formation by Pseudomonas aeruginosa by increasing iron availability. Am J Physiol Lung Cell Mol Physiol. 2008;295(1):L25-37.
279. Jennings R, Premanandan C, CIANCIOLO R, WILKIE D, WONG A, KENDZIORSKI J. Veterinary Histology: Ohio State University Libraries; 2017.
280. Iwasaki A, Foxman EF, Molony RD. Early local immune defences in the respiratory tract. Nature Reviews Immunology. 2016;17:7.
281. Chuang TH, Lee J, Kline L, Mathison JC, Ulevitch RJ. Toll-like receptor 9 mediates CpG-DNA signaling. J Leukoc Biol. 2002;71(3):538-44.
282. Uehara A, Fujimoto Y, Fukase K, Takada H. Various human epithelial cells express functional Toll-like receptors, NOD1 and NOD2 to produce anti-microbial peptides, but not proinflammatory cytokines. Mol Immunol. 2007;44(12):3100-11.

283. Power MR, Li B, Yamamoto M, Akira S, Lin TJ. A role of Toll-IL-1 receptor domain-containing adaptor-inducing IFN-beta in the host response to Pseudomonas aeruginosa lung infection in mice. Journal of immunology (Baltimore, Md : 1950). 2007;178(5):3170-6.
284. Carrigan SO, Junkins R, Yang YJ, Macneil A, Richardson C, Johnston B, et al. IFN regulatory factor 3 contributes to the host response during Pseudomonas aeruginosa lung infection in mice. Journal of immunology (Baltimore, Md : 1950). 2010;185(6):3602-9.
285. Smith RS, Fedyk ER, Springer TA, Mukaida N, Iglewski BH, Phipps RP. IL-8 production in human lung fibroblasts and epithelial cells activated by the Pseudomonas autoinducer N-3-oxododecanoyl homoserine lactone is transcriptionally regulated by NF-kappa B and activator protein-2. Journal of immunology (Baltimore, Md : 1950). 2001;167(1):366-74.
286. Leidal KG, Munson KL, Denning GM. Small molecular weight secretory factors from Pseudomonas aeruginosa have opposite effects on IL-8 and RANTES expression by human airway epithelial cells. Am J Respir Cell Mol Biol. 2001;25(2):186-95.
287. Denning GM, Wollenweber LA, Railsback MA, Cox CD, Stoll LL, Britigan BE. Pseudomonas pyocyanin increases interleukin-8 expression by human airway epithelial cells. Infect Immun. 1998;66(12):5777-84.
288. Mijares LA, Wangdi T, Sokol C, Homer R, Medzhitov R, Kazmierczak BI. Airway epithelial MyD88 restores control of Pseudomonas aeruginosa murine infection via an interleukin-1 dependent pathway. Journal of immunology (Baltimore, Md : 1950). 2011;186(12):7080-8.
289. Carevic M, Oz H, Fuchs K, Laval J, Schroth C, Frey N, et al. CXCR1 Regulates Pulmonary Anti-Pseudomonas Host Defense. J Innate Immun. 2016;8(4):362-73.
290. Raoust E, Balloy V, Garcia-Verdugo I, Touqui L, Ramphal R, Chignard M. Pseudomonas aeruginosa LPS or flagellin are sufficient to activate TLR-dependent signaling in murine alveolar macrophages and airway epithelial cells. PLoS One. 2009;4(10):e7259.
291. Sadikot RT, Zeng H, Joo M, Everhart MB, Sherrill TP, Li B, et al. Targeted immunomodulation of the NF-kappaB pathway in airway epithelium impacts host defense against Pseudomonas aeruginosa. Journal of immunology (Baltimore, Md : 1950). 2006;176(8):4923-30.
292. Maus UA, Waelsch K, Kuziel WA, Delbeck T, Mack M, Blackwell TS, et al. Monocytes are potent facilitators of alveolar neutrophil emigration during lung inflammation: role of the CCL2-CCR2 axis. Journal of immunology (Baltimore, Md : 1950). 2003;170(6):3273-8.
293. Espinosa V, Jhingran A, Dutta O, Kasahara S, Donnelly R, Du P, et al. Inflammatory monocytes orchestrate innate antifungal immunity in the lung. PLoS pathogens. 2014;10(2):e1003940.
294. Pålsson-McDermott EM, O'Neill LAJ. Signal transduction by the lipopolysaccharide receptor, Toll-like receptor-4. Immunology. 2004;113(2):153-62.
295. Mills EL, Kelly B, Logan A, Costa ASH, Varma M, Bryant CE, et al. Succinate Dehydrogenase Supports Metabolic Repurposing of Mitochondria to Drive Inflammatory Macrophages. Cell. 2016;167(2):457-70 e13.
296. Bauernfeind FG, Horvath G, Stutz A, Alnemri ES, MacDonald K, Speert D, et al. Cutting edge: NF-kappaB activating pattern recognition and cytokine receptors license NLRP3 inflammasome activation by regulating NLRP3 expression. Journal of immunology (Baltimore, Md : 1950). 2009;183(2):787-91.
297. Tenthorey JL, Kofoed EM, Daugherty MD, Malik HS, Vance RE. Molecular basis for specific recognition of bacterial ligands by NAIP/NLRC4 inflammasomes. Mol Cell. 2014;54(1):17-29.
298. Rauch I, Tenthorey JL, Nichols RD, Al Moussawi K, Kang JJ, Kang C, et al. NAIP proteins are required for cytosolic detection of specific bacterial ligands *in vivo*. J Exp Med. 2016;213(5):657-65.
299. Zhao Y, Yang J, Shi J, Gong YN, Lu Q, Xu H, et al. The NLRC4 inflammasome receptors for bacterial flagellin and type III secretion apparatus. Nature. 2011;477(7366):596-600.

300. Lin CK, Kazmierczak BI. Inflammation: A Double-Edged Sword in the Response to Pseudomonas aeruginosa Infection. J Innate Immun. 2017;9(3):250-61.
301. Evavold CL, Ruan J, Tan Y, Xia S, Wu H, Kagan JC. The Pore-Forming Protein Gasdermin D Regulates Interleukin-1 Secretion from Living Macrophages. Immunity. 2018;48(1):35-44 e6.
302. Deng Q, Wang Y, Zhang Y, Li M, Li D, Huang X, et al. Pseudomonas aeruginosa Triggers Macrophage Autophagy To Escape Intracellular Killing by Activation of the NLRP3 Inflammasome. Infect Immun. 2016;84(1):56-66.
303. McElvaney OJ, Zaslona Z, Becker-Flegler K, Palsson-McDermott EM, Boland F, Gunaratnam C, et al. Specific Inhibition of the NLRP3 Inflammasome as an Anti-Inflammatory Strategy in Cystic Fibrosis. Am J Respir Crit Care Med. 2019.
304. Thakur A, Barrett RP, Hobden JA, Hazlett LD. Caspase-1 inhibitor reduces severity of pseudomonas aeruginosa keratitis in mice. Invest Ophthalmol Vis Sci. 2004;45(9):3177-84.
305. Thakur A, Barrett R, McClellan S, Hazlett L. Regulation of Pseudomonas aeruginosa corneal infection in IL-1ß converting enzyme (ICE, caspase-1) deficient mice. Current Eye Research. 2004;29(4-5):225-33.
306. Schultz MJ, Rijneveld AW, Florquin S, Edwards CK, Dinarello CA, Poll Tvd. Role of interleukin-1 in the pulmonary immune response duringPseudomonas aeruginosa pneumonia. American Journal of Physiology-Lung Cellular and Molecular Physiology. 2002;282(2):L285-L90.
307. Riquelme SA, Lozano C, Moustafa AM, Liimatta K, Tomlinson KL, Britto C, et al. CFTR-PTEN-dependent mitochondrial metabolic dysfunction promotes Pseudomonas aeruginosa airway infection. Sci Transl Med. 2019;11(499).
308. Valentini M, Lapouge K. Catabolite repression in Pseudomonas aeruginosa PAO1 regulates the uptake of C4 -dicarboxylates depending on succinate concentration. Environmental microbiology. 2013;15(6):1707-16.
309. Kharazmi A. Mechanisms involved in the evasion of the host defence by Pseudomonas aeruginosa. Immunol Lett. 1991;30(2):201-5.
310. Mittal R, Sharma S, Chhibber S, Harjai K. Effect of macrophage secretory products on elaboration of virulence factors by planktonic and biofilm cells of Pseudomonas aeruginosa. Comparative Immunology, Microbiology and Infectious Diseases. 2006;29(1):12-26.
311. Lewenza S. Extracellular DNA-induced antimicrobial peptide resistance mechanisms in Pseudomonas aeruginosa. Frontiers in microbiology. 2013;4:21.
312. Yamada KJ, Kielian T. Biofilm-Leukocyte Cross-Talk: Impact on Immune Polarization and Immunometabolism. J Innate Immun. 2019;11(3):280-8.
313. van Gennip M, Christensen LD, Alhede M, Qvortrup K, Jensen PO, Hoiby N, et al. Interactions between polymorphonuclear leukocytes and Pseudomonas aeruginosa biofilms on silicone implants *in vivo*. Infect Immun. 2012;80(8):2601-7.
314. Wang A, Luan HH, Medzhitov R. An evolutionary perspective on immunometabolism. Science. 2019;363(6423).
315. Ryan DG, O'Neill LAJ. Krebs Cycle Reborn in Macrophage Immunometabolism. Annual review of immunology. 2020;38:289-313.
316. Lunt SY, Vander Heiden MG. Aerobic glycolysis: meeting the metabolic requirements of cell proliferation. Annu Rev Cell Dev Biol. 2011;27:441-64.
317. Li XB, Gu JD, Zhou QH. Review of aerobic glycolysis and its key enzymes - new targets for lung cancer therapy. Thorac Cancer. 2015;6(1):17-24.
318. O'Neill LA, Kishton RJ, Rathmell J. A guide to immunometabolism for immunologists. Nat Rev Immunol. 2016;16(9):553-65.
319. Martinez-Reyes I, Chandel NS. Mitochondrial TCA cycle metabolites control physiology and disease. Nat Commun. 2020;11(1):102.
320. Remington SJ. Structure and mechanism of citrate synthase. Curr Top Cell Regul. 1992;33:209-29.

321. Lloyd SJ, Lauble H, Prasad GS, Stout CD. The mechanism of aconitase: 1.8 A resolution crystal structure of the S642a:citrate complex. Protein Sci. 1999;8(12):2655-62.
322. Ma T, Peng Y, Huang W, Liu Y, Ding J. The beta and gamma subunits play distinct functional roles in the alpha2betagamma heterotetramer of human NAD-dependent isocitrate dehydrogenase. Sci Rep. 2017;7:41882.
323. Sheu KF, Blass JP. The alpha-ketoglutarate dehydrogenase complex. Ann N Y Acad Sci. 1999;893:61-78.
324. Johnson JD, Muhonen WW, Lambeth DO. Characterization of the ATP- and GTP-specific succinyl-CoA synthetases in pigeon. The enzymes incorporate the same alpha-subunit. J Biol Chem. 1998;273(42):27573-9.
325. Rose IA. How fumarase recycles after the malate --> fumarate reaction. Insights into the reaction mechanism. Biochemistry. 1998;37(51):17651-8.
326. Chapman AD, Cortes A, Dafforn TR, Clarke AR, Brady RL. Structural basis of substrate specificity in malate dehydrogenases: crystal structure of a ternary complex of porcine cytoplasmic malate dehydrogenase, alpha-ketomalonate and tetrahydoNAD. J Mol Biol. 1999;285(2):703-12.
327. Lampropoulou V, Sergushichev A, Bambouskova M, Nair S, Vincent EE, Loginicheva E, et al. Itaconate Links Inhibition of Succinate Dehydrogenase with Macrophage Metabolic Remodeling and Regulation of Inflammation. Cell Metab. 2016;24(1):158-66.
328. Jha AK, Huang SC, Sergushichev A, Lampropoulou V, Ivanova Y, Loginicheva E, et al. Network integration of parallel metabolic and transcriptional data reveals metabolic modules that regulate macrophage polarization. Immunity. 2015;42(3):419-30.
329. Everts B, Amiel E, Huang SC, Smith AM, Chang CH, Lam WY, et al. TLR-driven early glycolytic reprogramming via the kinases TBK1-IKKvarepsilon supports the anabolic demands of dendritic cell activation. Nat Immunol. 2014;15(4):323-32.
330. Mills EL, Ryan DG, Prag HA, Dikovskaya D, Menon D, Zaslona Z, et al. Itaconate is an anti-inflammatory metabolite that activates Nrf2 via alkylation of KEAP1. Nature. 2018;556:113.
331. Galvan-Pena S, O'Neill LA. Metabolic reprograming in macrophage polarization. Frontiers in immunology. 2014;5:420.
332. Lachmandas E, Boutens L, Ratter JM, Hijmans A, Hooiveld GJ, Joosten LA, et al. Microbial stimulation of different Toll-like receptor signalling pathways induces diverse metabolic programmes in human monocytes. Nat Microbiol. 2016;2:16246.
333. Russell DG, Huang L, VanderVen BC. Immunometabolism at the interface between macrophages and pathogens. Nat Rev Immunol. 2019;19(5):291-304.
334. Rodríguez-Prados J-C, Través PG, Cuenca J, Rico D, Aragonés J, Martín-Sanz P, et al. Substrate Fate in Activated Macrophages: A Comparison between Innate, Classic, and Alternative Activation. The Journal of Immunology. 2010;185(1):605-14.
335. Krawczyk CM, Holowka T, Sun J, Blagih J, Amiel E, DeBerardinis RJ, et al. Toll-like receptor–induced changes in glycolytic metabolism regulate dendritic cell activation. Blood. 2010;115(23):4742-9.
336. Donnelly RP, Loftus RM, Keating SE, Liou KT, Biron CA, Gardiner CM, et al. mTORC1-Dependent Metabolic Reprogramming Is a Prerequisite for NK Cell Effector Function. The Journal of Immunology. 2014;193(9):4477-84.
337. Michalek RD, Gerriets VA, Jacobs SR, Macintyre AN, MacIver NJ, Mason EF, et al. Cutting edge: distinct glycolytic and lipid oxidative metabolic programs are essential for effector and regulatory CD4+ T cell subsets. Journal of immunology (Baltimore, Md : 1950). 2011;186(6):3299-303.
338. Warburg O, Wind F, Negelein E. The Metabolism of Tumors in the Body. J Gen Physiol. 1927;8(6):519-30.

339. Nagy C, Haschemi A. Time and Demand are Two Critical Dimensions of Immunometabolism: The Process of Macrophage Activation and the Pentose Phosphate Pathway. Frontiers in immunology. 2015;6:164.
340. Hamilton JA, Vairo G, Lingelbach SR. CSF-1 stimulates glucose uptake in murine bone marrow-derived macrophages. Biochemical and biophysical research communications. 1986;138(1):445-54.
341. Michl J, Ohlbaum DJ, Silverstein SC. 2-Deoxyglucose selectively inhibits Fc and complement receptor-mediated phagocytosis in mouse peritoneal macrophages. I. Description of the inhibitory effect. J Exp Med. 1976;144(6):1465-83.
342. Selak MA, Armour SM, MacKenzie ED, Boulahbel H, Watson DG, Mansfield KD, et al. Succinate links TCA cycle dysfunction to oncogenesis by inhibiting HIF-alpha prolyl hydroxylase. Cancer Cell. 2005;7(1):77-85.
343. Blouin CC, Page EL, Soucy GM, Richard DE. Hypoxic gene activation by lipopolysaccharide in macrophages: implication of hypoxia-inducible factor 1alpha. Blood. 2004;103(3):1124-30.
344. Nishi K, Oda T, Takabuchi S, Oda S, Fukuda K, Adachi T, et al. LPS induces hypoxia-inducible factor 1 activation in macrophage-differentiated cells in a reactive oxygen species-dependent manner. Antioxid Redox Signal. 2008;10(5):983-95.
345. Cramer T, Yamanishi Y, Clausen BE, Forster I, Pawlinski R, Mackman N, et al. HIF-1alpha is essential for myeloid cell-mediated inflammation. Cell. 2003;112(5):645-57.
346. Peyssonnaux C, Datta V, Cramer T, Doedens A, Theodorakis EA, Gallo RL, et al. HIF-1alpha expression regulates the bactericidal capacity of phagocytes. J Clin Invest. 2005;115(7):1806-15.
347. Kim JW, Tchernyshyov I, Semenza GL, Dang CV. HIF-1-mediated expression of pyruvate dehydrogenase kinase: a metabolic switch required for cellular adaptation to hypoxia. Cell Metab. 2006;3(3):177-85.
348. Owen OE, Kalhan SC, Hanson RW. The key role of anaplerosis and cataplerosis for citric acid cycle function. J Biol Chem. 2002;277(34):30409-12.
349. O'Neill LA. A broken krebs cycle in macrophages. Immunity. 2015;42(3):393-4.
350. Infantino V, Convertini P, Cucci L, Panaro MA, Di Noia MA, Calvello R, et al. The mitochondrial citrate carrier: a new player in inflammation. Biochem J. 2011;438(3):433-6.
351. Cordes T, Wallace M, Michelucci A, Divakaruni AS, Sapcariu SC, Sousa C, et al. Immunoresponsive Gene 1 and Itaconate Inhibit Succinate Dehydrogenase to Modulate Intracellular Succinate Levels. J Biol Chem. 2016;291(27):14274-84.
352. Chen C, Pore N, Behrooz A, Ismail-Beigi F, Maity A. Regulation of glut1 mRNA by hypoxia-inducible factor-1. Interaction between H-ras and hypoxia. J Biol Chem. 2001;276(12):9519-25.
353. Semenza GL, Jiang BH, Leung SW, Passantino R, Concordet JP, Maire P, et al. Hypoxia response elements in the aldolase A, enolase 1, and lactate dehydrogenase A gene promoters contain essential binding sites for hypoxia-inducible factor 1. J Biol Chem. 1996;271(51):32529-37.
354. Riddle SR, Ahmad A, Ahmad S, Deeb SS, Malkki M, Schneider BK, et al. Hypoxia induces hexokinase II gene expression in human lung cell line A549. Am J Physiol Lung Cell Mol Physiol. 2000;278(2):L407-16.
355. Obach M, Navarro-Sabate A, Caro J, Kong X, Duran J, Gomez M, et al. 6-Phosphofructo-2-kinase (pfkfb3) gene promoter contains hypoxia-inducible factor-1 binding sites necessary for transactivation in response to hypoxia. J Biol Chem. 2004;279(51):53562-70.
356. Gao L, Mejias R, Echevarria M, Lopez-Barneo J. Induction of the glucose-6-phosphate dehydrogenase gene expression by chronic hypoxia in PC12 cells. FEBS Lett. 2004;569(1-3):256-60.

357. Moser C, Kjaergaard S, Pressler T, Kharazmi A, Koch C, Hoiby N. The immune response to chronic Pseudomonas aeruginosa lung infection in cystic fibrosis patients is predominantly of the Th2 type. APMIS. 2000;108(5):329-35.
358. Lee CG, Jenkins NA, Gilbert DJ, Copeland NG, O'Brien WE. Cloning and analysis of gene regulation of a novel LPS-inducible cDNA. Immunogenetics. 1995;41(5):263-70.
359. Michelucci A, Cordes T, Ghelfi J, Pailot A, Reiling N, Goldmann O, et al. Immune-responsive gene 1 protein links metabolism to immunity by catalyzing itaconic acid production. Proc Natl Acad Sci U S A. 2013;110(19):7820-5.
360. Liao ST, Han C, Xu DQ, Fu XW, Wang JS, Kong LY. 4-Octyl itaconate inhibits aerobic glycolysis by targeting GAPDH to exert anti-inflammatory effects. Nat Commun. 2019;10(1):5091.
361. Nair S, Huynh JP, Lampropoulou V, Loginicheva E, Esaulova E, Gounder AP, et al. Irg1 expression in myeloid cells prevents immunopathology during M. tuberculosis infection. J Exp Med. 2018;215(4):1035-45.
362. Weiss JM, Davies LC, Karwan M, Ileva L, Ozaki MK, Cheng RY, et al. Itaconic acid mediates crosstalk between macrophage metabolism and peritoneal tumors. J Clin Invest. 2018;128(9):3794-805.
363. Baup S. Ueber eine neue Pyrogen-Citronensäure, und über Benennung der Pyrogen-Säuren überhaupt. Annalen der Pharmacie. 1836;19(1):29-38.
364. Kawai T, Takeuchi O, Fujita T, Inoue J, Muhlradt PF, Sato S, et al. Lipopolysaccharide stimulates the MyD88-independent pathway and results in activation of IFN-regulatory factor 3 and the expression of a subset of lipopolysaccharide-inducible genes. Journal of immunology (Baltimore, Md : 1950). 2001;167(10):5887-94.
365. Shin JH, Yang JY, Jeon BY, Yoon YJ, Cho SN, Kang YH, et al. (1)H NMR-based metabolomic profiling in mice infected with Mycobacterium tuberculosis. J Proteome Res. 2011;10(5):2238-47.
366. Sugimoto M, Sakagami H, Yokote Y, Onuma H, Kaneko M, Mori M, et al. Non-targeted metabolite profiling in activated macrophage secretion. Metabolomics. 2012;8(4):624-33.
367. Strelko CL, Lu W, Dufort FJ, Seyfried TN, Chiles TC, Rabinowitz JD, et al. Itaconic acid is a mammalian metabolite induced during macrophage activation. Journal of the American Chemical Society. 2011;133(41):16386-9.
368. Li Y, Zhang P, Wang C, Han C, Meng J, Liu X, et al. Immune Responsive Gene 1 (IRG1) Promotes Endotoxin Tolerance by Increasing A20 Expression in Macrophages through Reactive Oxygen Species. Journal of Biological Chemistry. 2013;288(23):16225-34.
369. Shen H, Campanello GC, Flicker D, Grabarek Z, Hu J, Luo C, et al. The Human Knockout Gene CLYBL Connects Itaconate to Vitamin B(12). Cell. 2017;171(4):771-82.e11.
370. Puchalska P, Huang X, Martin SE, Han X, Patti GJ, Crawford PA. Isotope Tracing Untargeted Metabolomics Reveals Macrophage Polarization-State-Specific Metabolic Coordination across Intracellular Compartments. iScience. 2018;9:298-313.
371. Meiser J, Kraemer L, Jaeger C, Madry H, Link A, Lepper PM, et al. Itaconic acid indicates cellular but not systemic immune system activation. Oncotarget. 2018;9(63):32098-107.
372. ElAzzouny M, Tom CTMB, Evans CR, Olson LL, Tanga MJ, Gallagher KA, et al. Dimethyl Itaconate Is Not Metabolized into Itaconate Intracellularly. The Journal of biological chemistry. 2017;292(12):4766-9.
373. Jamal Uddin M, Joe Y, Kim SK, Oh Jeong S, Ryter SW, Pae HO, et al. IRG1 induced by heme oxygenase-1/carbon monoxide inhibits LPS-mediated sepsis and pro-inflammatory cytokine production. Cell Mol Immunol. 2016;13(2):170-9.
374. Ackermann WW, Potter VR. Enzyme inhibition in relation to chemotherapy. Proc Soc Exp Biol Med. 1949;72(1):1-9.

375. Bambouskova M, Gorvel L, Lampropoulou V, Sergushichev A, Loginicheva E, Johnson K, et al. Electrophilic properties of itaconate and derivatives regulate the IkappaBzeta-ATF3 inflammatory axis. Nature. 2018;556(7702):501-4.
376. Ahmed SM, Luo L, Namani A, Wang XJ, Tang X. Nrf2 signaling pathway: Pivotal roles in inflammation. Biochim Biophys Acta Mol Basis Dis. 2017;1863(2):585-97.
377. Hayes JD, Dinkova-Kostova AT. The Nrf2 regulatory network provides an interface between redox and intermediary metabolism. Trends Biochem Sci. 2014;39(4):199-218.
378. Williams JO, Roche TE, McFadden BA. Mechanism of action of isocitrate lyase from Pseudomonas indigofera. Biochemistry. 1971;10(8):1384-90.
379. Naujoks J, Tabeling C, Dill BD, Hoffmann C, Brown AS, Kunze M, et al. IFNs Modify the Proteome of Legionella-Containing Vacuoles and Restrict Infection Via IRG1-Derived Itaconic Acid. PLoS pathogens. 2016;12(2):e1005408.
380. Luan HH, Medzhitov R. Food Fight: Role of Itaconate and Other Metabolites in Antimicrobial Defense. Cell Metab. 2016;24(3):379-87.
381. Sasikaran J, Ziemski M, Zadora PK, Fleig A, Berg IA. Bacterial itaconate degradation promotes pathogenicity. Nature Chemical Biology. 2014;10:371.
382. O'Neill LAJ, Artyomov MN. Itaconate: the poster child of metabolic reprogramming in macrophage function. Nature Reviews Immunology. 2019;19(5):273-81.
383. Daniels BP, Kofman SB, Smith JR, Norris GT, Snyder AG, Kolb JP, et al. The Nucleotide Sensor ZBP1 and Kinase RIPK3 Induce the Enzyme IRG1 to Promote an Antiviral Metabolic State in Neurons. Immunity. 2019;50(1):64-76 e4.
384. Cho H, Proll SC, Szretter KJ, Katze MG, Gale M, Jr., Diamond MS. Differential innate immune response programs in neuronal subtypes determine susceptibility to infection in the brain by positive-stranded RNA viruses. Nat Med. 2013;19(4):458-64.
385. Liu Y, You Y, Lu Z, Yang J, Li P, Liu L, et al. N (6)-methyladenosine RNA modification-mediated cellular metabolism rewiring inhibits viral replication. Science. 2019;365(6458):1171-6.
386. Doern CD. When does 2 plus 2 equal 5? A review of antimicrobial synergy testing. J Clin Microbiol. 2014;52(12):4124-8.
387. Saiman L. Clinical utility of synergy testing for multidrug-resistant Pseudomonas aeruginosa isolated from patients with cystic fibrosis: 'the motion for'. Paediatric respiratory reviews. 2007;8(3):249-55.
388. Chekabab SM, Silverman RJ, Lafayette SL, Luo Y, Rousseau S, Nguyen D. Staphylococcus aureus Inhibits IL-8 Responses Induced by Pseudomonas aeruginosa in Airway Epithelial Cells. PLoS One. 2015;10(9):e0137753.
389. Descamps D, Le Gars M, Balloy V, Barbier D, Maschalidi S, Tohme M, et al. Toll-like receptor 5 (TLR5), IL-1β secretion, and asparagine endopeptidase are critical factors for alveolar macrophage phagocytosis and bacterial killing. Proc Natl Acad Sci U S A. 2012;109(5):1619-24.
390. Mizue Y, Ghani S, Leng L, McDonald C, Kong P, Baugh J, et al. Role for macrophage migration inhibitory factor in asthma. Proc Natl Acad Sci U S A. 2005;102(40):14410-5.
391. Chen LC, Lei HY, Liu CC, Shiesh SC, Chen SH, Liu HS, et al. Correlation of serum levels of macrophage migration inhibitory factor with disease severity and clinical outcome in dengue patients. Am J Trop Med Hyg. 2006;74(1):142-7.
392. Calandra T, Echtenacher B, Roy DL, Pugin J, Metz CN, Hultner L, et al. Protection from septic shock by neutralization of macrophage migration inhibitory factor. Nat Med. 2000;6(2):164-70.
393. Roger T, David J, Glauser MP, Calandra T. MIF regulates innate immune responses through modulation of Toll-like receptor 4. Nature. 2001;414(6866):920-4.
394. Doroudian M, O'Neill A, O'Reilly C, Tynan A, Mawhinney L, McElroy A, et al. Aerosolized drug-loaded nanoparticles targeting migration inhibitory factors inhibit Pseudomonas

aeruginosa-induced inflammation and biofilm formation. Nanomedicine (London, England). 2020.
395. Lam J, Chan R, Lam K, Costerton JW. Production of mucoid microcolonies by Pseudomonas aeruginosa within infected lungs in cystic fibrosis. Infection and Immunity. 1980;28(2):546-56.
396. Moreau-Marquis S, Redelman CV, Stanton BA, Anderson GG. Co-culture Models of Pseudomonas aeruginosa Biofilms Grown on Live Human Airway Cells. Journal of Visualized Experiments : JoVE. 2010(44):2186.
397. Armstrong ME, Gantier M, Li L, Chung WY, McCann A, Baugh JA, et al. Small interfering RNAs induce macrophage migration inhibitory factor production and proliferation in breast cancer cells via a double-stranded RNA-dependent protein kinase-dependent mechanism. Journal of immunology (Baltimore, Md : 1950). 2008;180(11):7125-33.
398. Liu T, Zhang L, Joo D, Sun S-C. NF-κB signaling in inflammation. Signal transduction and targeted therapy. 2017;2:17023.
399. Zhou Y, Guo W, Zhu Z, Hu Y, Wang Y, Zhang X, et al. Macrophage migration inhibitory factor facilitates production of CCL5 in astrocytes following rat spinal cord injury. J Neuroinflammation. 2018;15(1):253.
400. Genin P, Algarte M, Roof P, Lin R, Hiscott J. Regulation of RANTES chemokine gene expression requires cooperativity between NF-kappa B and IFN-regulatory factor transcription factors. Journal of immunology (Baltimore, Md : 1950). 2000;164(10):5352-61.
401. Appay V, Rowland-Jones SL. RANTES: a versatile and controversial chemokine. Trends in immunology. 2001;22(2):83-7.
402. Bhavna, Ahmad FJ, Mittal G, Jain GK, Malhotra G, Khar RK, et al. Nano-salbutamol dry powder inhalation: a new approach for treating broncho-constrictive conditions. Eur J Pharm Biopharm. 2009;71(2):282-91.
403. Hiemstra PS, Eisenhauer PB, Harwig SS, van den Barselaar MT, van Furth R, Lehrer RI. Antimicrobial proteins of murine macrophages. Infect Immun. 1993;61(7):3038-46.
404. Santos LL, Fan H, Hall P, Ngo D, Mackay CR, Fingerle-Rowson G, et al. Macrophage migration inhibitory factor regulates neutrophil chemotactic responses in inflammatory arthritis in mice. Arthritis Rheum. 2011;63(4):960-70.
405. Oghumu S, Knobloch TJ, Terrazas C, Varikuti S, Ahn-Jarvis J, Bollinger CE, et al. Deletion of macrophage migration inhibitory factor inhibits murine oral carcinogenesis: Potential role for chronic pro-inflammatory immune mediators. Int J Cancer. 2016;139(6):1379-90.
406. Patra JK, Das G, Fraceto LF, Campos EVR, Rodriguez-Torres MdP, Acosta-Torres LS, et al. Nano based drug delivery systems: recent developments and future prospects. Journal of Nanobiotechnology. 2018;16(1):71.
407. Loftsson T, Brewster ME. Pharmaceutical applications of cyclodextrins: basic science and product development. Journal of Pharmacy and Pharmacology. 2010;62(11):1607-21.
408. Savjani KT, Gajjar AK, Savjani JK. Drug solubility: importance and enhancement techniques. ISRN Pharm. 2012;2012:195727-.
409. Danhier F, Ansorena E, Silva JM, Coco R, Le Breton A, Preat V. PLGA-based nanoparticles: an overview of biomedical applications. J Control Release. 2012;161(2):505-22.
410. Aerogen. Aerogen Solo: Aerogen; 2016 [Available from: https://www.aerogen.com/aerogen-solo-3/.
411. Ali T, Kaitha S, Mahmood S, Ftesi A, Stone J, Bronze MS. Clinical use of anti-TNF therapy and increased risk of infections. Drug Healthc Patient Saf. 2013;5:79-99.
412. Haussler S, Ziegler I, Lottel A, Gotz FV, Rohde M, Wehmhohner D, et al. Highly adherent small-colony variants of Pseudomonas aeruginosa in cystic fibrosis lung infection. J Med Microbiol. 2003;52(Pt 4):295-301.
413. Koo H, Allan RN, Howlin RP, Stoodley P, Hall-Stoodley L. Targeting microbial biofilms: current and prospective therapeutic strategies. Nat Rev Microbiol. 2017;15(12):740-55.

414. Günday Türeli N, Torge A, Juntke J, Schwarz BC, Schneider-Daum N, Türeli AE, et al. Ciprofloxacin-loaded PLGA nanoparticles against cystic fibrosis *P. aeruginosa* lung infections. European Journal of Pharmaceutics and Biopharmaceutics. 2017;117:363-71.
415. Clancy JP, Dupont L, Konstan MW, Billings J, Fustik S, Goss CH, et al. Phase II studies of nebulised Arikace in CF patients with Pseudomonas aeruginosa infection. Thorax. 2013;68(9):818-25.
416. Meyer-Siegler KL, Vera PL, Iczkowski KA, Bifulco C, Lee A, Gregersen PK, et al. Macrophage migration inhibitory factor (MIF) gene polymorphisms are associated with increased prostate cancer incidence. Genes Immun. 2007;8(8):646-52.
417. Takahashi N, Yamada T, Narita N, Fujieda S. Double-stranded RNA induces production of RANTES and IL-8 by human nasal fibroblasts. Clin Immunol. 2006;118(1):51-8.
418. Lu Y-C, Yeh W-C, Ohashi PS. LPS/TLR4 signal transduction pathway. Cytokine. 2008;42(2):145-51.
419. Kumar A, Zhang J, Yu F-SX. Toll-like receptor 3 agonist poly(I:C)-induced antiviral response in human corneal epithelial cells. Immunology. 2006;117(1):11-21.
420. Dix A, Hunniger K, Weber M, Guthke R, Kurzai O, Linde J. Biomarker-based classification of bacterial and fungal whole-blood infections in a genome-wide expression study. Frontiers in microbiology. 2015;6:171.
421. Wu R, Chen F, Wang N, Tang D, Kang R. ACOD1 in immunometabolism and disease. Cell Mol Immunol. 2020.
422. Degrandi D, Hoffmann R, Beuter-Gunia C, Pfeffer K. The proinflammatory cytokine-induced IRG1 protein associates with mitochondria. J Interferon Cytokine Res. 2009;29(1):55-67.
423. Tallam A, Perumal TM, Antony PM, Jager C, Fritz JV, Vallar L, et al. Gene Regulatory Network Inference of Immunoresponsive Gene 1 (IRG1) Identifies Interferon Regulatory Factor 1 (IRF1) as Its Transcriptional Regulator in Mammalian Macrophages. PLoS One. 2016;11(2):e0149050.
424. Hooftman A, O'Neill LAJ. The Immunomodulatory Potential of the Metabolite Itaconate. Trends in immunology. 2019;40(8):687-98.
425. Chen B, Zhang D, Pollard JW. Progesterone regulation of the mammalian ortholog of methylcitrate dehydratase (immune response gene 1) in the uterine epithelium during implantation through the protein kinase C pathway. Molecular endocrinology (Baltimore, Md). 2003;17(11):2340-54.
426. Yi Z, Deng M, Scott MJ, Fu G, Loughran PA, Lei Z, et al. IRG1/Itaconate Activates Nrf2 in Hepatocytes to Protect Against Liver Ischemia-Reperfusion Injury. Hepatology. 2020.
427. Zhang DD, Hannink M. Distinct cysteine residues in Keap1 are required for Keap1-dependent ubiquitination of Nrf2 and for stabilization of Nrf2 by chemopreventive agents and oxidative stress. Mol Cell Biol. 2003;23(22):8137-51.
428. Jantsch J, Chakravortty D, Turza N, Prechtel AT, Buchholz B, Gerlach RG, et al. Hypoxia and hypoxia-inducible factor-1 alpha modulate lipopolysaccharide-induced dendritic cell activation and function. Journal of immunology (Baltimore, Md : 1950). 2008;180(7):4697-705.
429. Lee JM, Calkins MJ, Chan K, Kan YW, Johnson JA. Identification of the NF-E2-related factor-2-dependent genes conferring protection against oxidative stress in primary cortical astrocytes using oligonucleotide microarray analysis. J Biol Chem. 2003;278(14):12029-38.
430. Rychly DJ, DiPiro JT. Infections associated with tumor necrosis factor-alpha antagonists. Pharmacotherapy. 2005;25(9):1181-92.
431. Di Meo S, Reed TT, Venditti P, Victor VM. Role of ROS and RNS Sources in Physiological and Pathological Conditions. Oxidative medicine and cellular longevity. 2016;2016:1245049-.
432. Pacher P, Beckman JS, Liaudet L. Nitric oxide and peroxynitrite in health and disease. Physiol Rev. 2007;87(1):315-424.

433. White ES. Lung extracellular matrix and fibroblast function. Annals of the American Thoracic Society. 2015;12 Suppl 1(Suppl 1):S30-S3.
434. O'Dwyer DN, Armstrong ME, Trujillo G, Cooke G, Keane MP, Fallon PG, et al. The Toll-like receptor 3 L412F polymorphism and disease progression in idiopathic pulmonary fibrosis. Am J Respir Crit Care Med. 2013;188(12):1442-50.
435. Friedman PJ, Harwood I, Ellenbogen P. Pulmonary cystic fibrosis in the adult: early and late radiologic findings with pathologic correlations. American Journal of Roentgenology. 1981;136(6):1131-44.
436. Huaux F, Noel S, Dhooghe B, Panin N, Lo Re S, Lison D, et al. Dysregulated proinflammatory and fibrogenic phenotype of fibroblasts in cystic fibrosis. PLoS One. 2013;8(5):e64341.
437. Bjarnsholt T. The role of bacterial biofilms in chronic infections. APMIS Suppl. 2013(136):1-51.
438. Bjarnsholt T, Jensen PO, Fiandaca MJ, Pedersen J, Hansen CR, Andersen CB, et al. Pseudomonas aeruginosa biofilms in the respiratory tract of cystic fibrosis patients. Pediatr Pulmonol. 2009;44(6):547-58.
439. Ciofu O, Tolker-Nielsen T, Jensen PO, Wang H, Hoiby N. Antimicrobial resistance, respiratory tract infections and role of biofilms in lung infections in cystic fibrosis patients. Adv Drug Deliv Rev. 2015;85:7-23.
440. Sato M, Suemori H, Hata N, Asagiri M, Ogasawara K, Nakao K, et al. Distinct and essential roles of transcription factors IRF-3 and IRF-7 in response to viruses for IFN-alpha/beta gene induction. Immunity. 2000;13(4):539-48.
441. Tamura T, Yanai H, Savitsky D, Taniguchi T. The IRF family transcription factors in immunity and oncogenesis. Annual review of immunology. 2008;26:535-84.
442. Swain A, Bambouskova M, Kim H, Andhey PS, Duncan D, Auclair K, et al. Comparative evaluation of itaconate and its derivatives reveals divergent inflammasome and type I interferon regulation in macrophages. Nature Metabolism. 2020:1-9.
443. Piantadosi CA, Withers CM, Bartz RR, MacGarvey NC, Fu P, Sweeney TE, et al. Heme oxygenase-1 couples activation of mitochondrial biogenesis to anti-inflammatory cytokine expression. J Biol Chem. 2011;286(18):16374-85.
444. Sun KA, Li Y, Meliton AY, Woods PS, Kimmig LM, Cetin-Atalay R, et al. Endogenous itaconate is not required for particulate matter-induced NRF2 expression or inflammatory response. Elife. 2020;9.
445. Krausgruber T, Fortelny N, Fife-Gernedl V, Senekowitsch M, Schuster LC, Lercher A, et al. Structural cells are key regulators of organ-specific immune responses. Nature. 2020;583(7815):296-302.
446. Coward WR, Forrester D, Knox AJ, Bolton CE, Williams P, Pang L. Pseudomonas AerugINOSa Infected Human Lung Fibroblasts And Epithelial Cells Enhance The Migration Of Neutrophils To Promote Bacterial Survival. C59 NEW INSIGHTS INTO THE IMMUNOLOGY OF BACTERIAL PNEUMONIA: American Thoracic Society; 2013. p. A4548-A.
447. Azghani AO, Neal K, Idell S, Amaro R, Baker JW, Omri A, et al. Mechanism of fibroblast inflammatory responses to Pseudomonas aeruginosa elastase. Microbiology. 2014;160(Pt 3):547-55.
448. Sivakumar P, Ntolios P, Jenkins G, Laurent G. Into the matrix: targeting fibroblasts in pulmonary fibrosis. Curr Opin Pulm Med. 2012;18(5):462-9.
449. WHO publishes list of bacteria for which new antibiotics are urgently needed. [press release]. 2017.
450. Shi S, Blumenthal A, Hickey CM, Gandotra S, Levy D, Ehrt S. Expression of many immunologically important genes in Mycobacterium tuberculosis-infected macrophages is independent of both TLR2 and TLR4 but dependent on IFN-alphabeta receptor and STAT1. Journal of immunology (Baltimore, Md : 1950). 2005;175(5):3318-28.

451. Torrens G, Escobar-Salom M, Pol-Pol E, Camps-Munar C, Cabot G, Lopez-Causape C, et al. Comparative Analysis of Peptidoglycans From Pseudomonas aeruginosa Isolates Recovered From Chronic and Acute Infections. Frontiers in microbiology. 2019;10:1868.
452. Maurice NM, Bedi B, Yuan Z, Goldberg JB, Koval M, Hart CM, et al. Pseudomonas aeruginosa Induced Host Epithelial Cell Mitochondrial Dysfunction. Sci Rep. 2019;9(1):11929.
453. Chandler CE, Horspool AM, Hill PJ, Wozniak DJ, Schertzer JW, Rasko DA, et al. Genomic and Phenotypic Diversity among Ten Laboratory Isolates of Pseudomonas aeruginosa PAO1. J Bacteriol. 2019;201(5).
454. Chmiel JF, Konstan MW, Knesebeck JE, Hilliard JB, Bonfield TL, Dawson DV, et al. IL-10 attenuates excessive inflammation in chronic Pseudomonas infection in mice. Am J Respir Crit Care Med. 1999;160(6):2040-7.
455. Chmiel JF, Konstan MW, Saadane A, Krenicky JE, Lester Kirchner H, Berger M. Prolonged inflammatory response to acute Pseudomonas challenge in interleukin-10 knockout mice. American journal of respiratory and critical care medicine. 2002;165(8):1176-81.
456. Lowenstein CJ, Padalko E. iNOS (NOS2) at a glance. Journal of Cell Science. 2004;117(14):2865-7.
457. Burney S, Caulfield JL, Niles JC, Wishnok JS, Tannenbaum SR. The chemistry of DNA damage from nitric oxide and peroxynitrite. Mutat Res. 1999;424(1-2):37-49.
458. Palazon A, Goldrath AW, Nizet V, Johnson RS. HIF transcription factors, inflammation, and immunity. Immunity. 2014;41(4):518-28.
459. López D, Vlamakis H, Kolter R. Biofilms. Cold Spring Harb Perspect Biol. 2010;2(7):a000398-a.
460. James CW, Gurk-Turner C. Cross-reactivity of beta-lactam antibiotics. Proc (Bayl Univ Med Cent). 2001;14(1):106-7.
461. Elson EC, Mermis J, Polineni D, Oermann CM. Aztreonam Lysine Inhalation Solution in Cystic Fibrosis. Clin Med Insights Circ Respir Pulm Med. 2019;13:1179548419842822.
462. Lodise TP, Jr., Lomaestro B, Drusano GL. Piperacillin-tazobactam for Pseudomonas aeruginosa infection: clinical implications of an extended-infusion dosing strategy. Clin Infect Dis. 2007;44(3):357-63.
463. Lau GW, Ran H, Kong F, Hassett DJ, Mavrodi D. Pseudomonas aeruginosa pyocyanin is critical for lung infection in mice. Infect Immun. 2004;72(7):4275-8.
464. Lau GW, Goumnerov BC, Walendziewicz CL, Hewitson J, Xiao W, Mahajan-Miklos S, et al. The Drosophila melanogaster toll pathway participates in resistance to infection by the gram-negative human pathogen Pseudomonas aeruginosa. Infect Immun. 2003;71(7):4059-66.
465. Mahajan-Miklos S, Tan M-W, Rahme LG, Ausubel FM. Molecular Mechanisms of Bacterial Virulence Elucidated Using a Pseudomonas aeruginosa–Caenorhabditis elegans Pathogenesis Model. Cell. 1999;96(1):47-56.
466. Rahme LG, Ausubel FM, Cao H, Drenkard E, Goumnerov BC, Lau GW, et al. Plants and animals share functionally common bacterial virulence factors. Proc Natl Acad Sci U S A. 2000;97(16):8815-21.
467. Kuang Z, Hao Y, Walling BE, Jeffries JL, Ohman DE, Lau GW. Pseudomonas aeruginosa Elastase Provides an Escape from Phagocytosis by Degrading the Pulmonary Surfactant Protein-A. PLOS ONE. 2011;6(11):e27091.
468. Mun JJ, Tam C, Kowbel D, Hawgood S, Barnett MJ, Evans DJ, et al. Clearance of Pseudomonas aeruginosa from a healthy ocular surface involves surfactant protein D and is compromised by bacterial elastase in a murine null-infection model. Infection and immunity. 2009;77(6):2392-8.
469. Alcorn JF, Wright JR. Degradation of pulmonary surfactant protein D by Pseudomonas aeruginosa elastase abrogates innate immune function. Journal of Biological Chemistry. 2004;279(29):30871-9.

470. McFadden BA, Purohit S. Itaconate, an isocitrate lyase-directed inhibitor in Pseudomonas indigofera. Journal of Bacteriology. 1977;131(1):136-44.
471. Ahn S, Jung J, Jang IA, Madsen EL, Park W. Role of Glyoxylate Shunt in Oxidative Stress Response. J Biol Chem. 2016;291(22):11928-38.
472. Lorenz MC, Fink GR. Life and death in a macrophage: role of the glyoxylate cycle in virulence. Eukaryot Cell. 2002;1(5):657-62.
473. Tsai CJ, Loh JM, Proft T. Galleria mellonella infection models for the study of bacterial diseases and for antimicrobial drug testing. Virulence. 2016;7(3):214-29.
474. Brown SE, Howard A, Kasprzak AB, Gordon KH, East PD. A peptidomics study reveals the impressive antimicrobial peptide arsenal of the wax moth Galleria mellonella. Insect Biochem Mol Biol. 2009;39(11):792-800.
475. Mukherjee K, Altincicek B, Hain T, Domann E, Vilcinskas A, Chakraborty T. Galleria mellonella as a model system for studying Listeria pathogenesis. Appl Environ Microbiol. 2010;76(1):310-7.
476. Browne N, Heelan M, Kavanagh K. An analysis of the structural and functional similarities of insect hemocytes and mammalian phagocytes. Virulence. 2013;4(7):597-603.
477. Bergin D, Reeves EP, Renwick J, Wientjes FB, Kavanagh K. Superoxide production in Galleria mellonella hemocytes: identification of proteins homologous to the NADPH oxidase complex of human neutrophils. Infect Immun. 2005;73(7):4161-70.
478. de Kraker ME, Stewardson AJ, Harbarth S. Will 10 Million People Die a Year due to Antimicrobial Resistance by 2050? PLoS Med. 2016;13(11):e1002184.
479. Kapoor G, Saigal S, Elongavan A. Action and resistance mechanisms of antibiotics: A guide for clinicians. J Anaesthesiol Clin Pharmacol. 2017;33(3):300-5.
480. Baillie JK. Translational genomics. Targeting the host immune response to fight infection. Science. 2014;344(6186):807-8.
481. Kelly AM, McLoughlin RM. Target the Host, Kill the Bug; Targeting Host Respiratory Immunosuppressive Responses as a Novel Strategy to Improve Bacterial Clearance During Lung Infection. Frontiers in immunology. 2020;11(767).
482. O'Neill L. Immunometabolism and the land of milk and honey. Nat Rev Immunol. 2017;17(4):217.
483. O'Neill LA, Pearce EJ. Immunometabolism governs dendritic cell and macrophage function. J Exp Med. 2016;213(1):15-23.
484. An LL, Gorman JV, Stephens G, Swerdlow B, Warrener P, Bonnell J, et al. Complement C5a induces PD-L1 expression and acts in synergy with LPS through Erk1/2 and JNK signaling pathways. Sci Rep. 2016;6:33346.
485. Takeda K, Akira S, editors. TLR signaling pathways. Seminars in immunology; 2004: Elsevier.
486. Lavoie EG, Wangdi T, Kazmierczak BI. Innate immune responses to Pseudomonas aeruginosa infection. Microbes and infection. 2011;13(14-15):1133-45.
487. Hall S, McDermott C, Anoopkumar-Dukie S, McFarland AJ, Forbes A, Perkins AV, et al. Cellular Effects of Pyocyanin, a Secreted Virulence Factor of Pseudomonas aeruginosa. Toxins (Basel). 2016;8(8):236.
488. Lau GW, Hassett DJ, Ran H, Kong F. The role of pyocyanin in Pseudomonas aeruginosa infection. Trends Mol Med. 2004;10(12):599-606.
489. Lee VT, Smith RS, Tummler B, Lory S. Activities of Pseudomonas aeruginosa effectors secreted by the Type III secretion system in vitro and during infection. Infect Immun. 2005;73(3):1695-705.
490. Passador L, Cook JM, Gambello MJ, Rust L, Iglewski BH. Expression of Pseudomonas aeruginosa virulence genes requires cell-to-cell communication. Science. 1993;260(5111):1127-30.

491. Toder DS, Gambello MJ, Iglewski BH. Pseudomonas aeruginosa LasA: a second elastase under the transcriptional control of lasR. Molecular microbiology. 1991;5(8):2003-10.
492. Abdalla MY, Hoke T, Seravalli J, Switzer BL, Bavitz M, Fliege JD, et al. Pseudomonas Quinolone Signal Induces Oxidative Stress and Inhibits Heme Oxygenase-1 Expression in Lung Epithelial Cells. Infect Immun. 2017;85(9).
493. Harvey CJ, Thimmulappa RK, Sethi S, Kong X, Yarmus L, Brown RH, et al. Targeting Nrf2 Signaling Improves Bacterial Clearance by Alveolar Macrophages in Patients with COPD and in a Mouse Model. Science Translational Medicine. 2011;3(78):78ra32-78ra32.
494. Cheon Y-P, Xu X, Bagchi MK, Bagchi IC. Immune-responsive gene 1 is a novel target of progesterone receptor and plays a critical role during implantation in the mouse. Endocrinology. 2003;144(12):5623-30.
495. Ryan DG, O'Neill LAJ. Krebs cycle rewired for macrophage and dendritic cell effector functions. FEBS Lett. 2017;591(19):2992-3006.
496. Epstein ACR, Gleadle JM, McNeill LA, Hewitson KS, O'Rourke J, Mole DR, et al. C. elegans EGL-9 and Mammalian Homologs Define a Family of Dioxygenases that Regulate HIF by Prolyl Hydroxylation. Cell. 2001;107(1):43-54.
497. Ren K, Lv Y, Zhuo Y, Chen C, Shi H, Guo L, et al. Suppression of IRG-1 Reduces Inflammatory Cell Infiltration and Lung Injury in Respiratory Syncytial Virus Infection by Reducing Production of Reactive Oxygen Species. J Virol. 2016;90(16):7313-22.
498. Kong F, Saldarriaga OA, Spratt H, Osorio EY, Travi BL, Luxon BA, et al. Transcriptional Profiling in Experimental Visceral Leishmaniasis Reveals a Broad Splenic Inflammatory Environment that Conditions Macrophages toward a Disease-Promoting Phenotype. PLoS pathogens. 2017;13(1):e1006165.
499. Abdulhaq N, Nawaz Z, Zahoor MA, Siddique AB. Association of biofilm formation with multi drug resistance in clinical isolates of Pseudomonas aeruginosa. EXCLI J. 2020;19:201-8.
500. Cao B, Christophersen L, Thomsen K, Sonderholm M, Bjarnsholt T, Jensen PO, et al. Antibiotic penetration and bacterial killing in a Pseudomonas aeruginosa biofilm model. J Antimicrob Chemother. 2015;70(7):2057-63.
501. Hoffman LR, D'Argenio DA, MacCoss MJ, Zhang Z, Jones RA, Miller SI. Aminoglycoside antibiotics induce bacterial biofilm formation. Nature. 2005;436(7054):1171-5.
502. Wright EA, Fothergill JL, Paterson S, Brockhurst MA, Winstanley C. Sub-inhibitory concentrations of some antibiotics can drive diversification of Pseudomonas aeruginosa populations in artificial sputum medium. BMC Microbiol. 2013;13:170.
503. Kaplan JB. Antibiotic-induced biofilm formation. Int J Artif Organs. 2011;34(9):737-51.
504. Kaplan JB, Izano EA, Gopal P, Karwacki MT, Kim S, Bose JL, et al. Low levels of beta-lactam antibiotics induce extracellular DNA release and biofilm formation in Staphylococcus aureus. mBio. 2012;3(4):e00198-12.
505. Capita R, Buzon-Duran L, Riesco-Pelaez F, Alonso-Calleja C. Effect of Sub-Lethal Concentrations of Biocides on the Structural Parameters and Viability of the Biofilms Formed by Salmonella Typhimurium. Foodborne Pathog Dis. 2017;14(6):350-6.
506. Ranieri MRM, Whitchurch CB, Burrows LL. Mechanisms of biofilm stimulation by subinhibitory concentrations of antimicrobials. Current Opinion in Microbiology. 2018;45:164-9.
507. Aka ST, Haji SH. Sub-MIC of antibiotics induced biofilm formation of Pseudomonas aeruginosa in the presence of chlorhexidine. Braz J Microbiol. 2015;46(1):149-54.
508. Gardner PR. Superoxide production by the mycobacterial and pseudomonad quinoid pigments phthiocol and pyocyanine in human lung cells. Arch Biochem Biophys. 1996;333(1):267-74.
509. Ran H, Hassett DJ, Lau GW. Human targets of Pseudomonas aeruginosa pyocyanin. Proc Natl Acad Sci U S A. 2003;100(24):14315-20.

510. Pereira MF, Rossi CC, Vieira de Queiroz M, Martins GF, Isaac C, Bossé JT, et al. Galleria mellonella is an effective model to study Actinobacillus pleuropneumoniae infection. Microbiology. 2015;161(Pt 2):387-400.
511. Pereira TC, de Barros PP, Fugisaki LRO, Rossoni RD, Ribeiro FC, de Menezes RT, et al. Recent Advances in the Use of Galleria mellonella Model to Study Immune Responses against Human Pathogens. Journal of fungi (Basel, Switzerland). 2018;4(4).
512. Wojda I. Immunity of the greater wax moth Galleria mellonella. Insect Sci. 2017;24(3):342-57.
513. Jiravanichpaisal P, Lee BL, Soderhall K. Cell-mediated immunity in arthropods: hematopoiesis, coagulation, melanization and opsonization. Immunobiology. 2006;211(4):213-36.
514. Hill L, Veli N, Coote PJ. Evaluation of Galleria mellonella larvae for measuring the efficacy and pharmacokinetics of antibiotic therapies against Pseudomonas aeruginosa infection. Int J Antimicrob Agents. 2014;43(3):254-61.
515. Ignasiak K, Maxwell A. Galleria mellonella (greater wax moth) larvae as a model for antibiotic susceptibility testing and acute toxicity trials. BMC Res Notes. 2017;10(1):428.
516. Hooftman A, Angiari S, Hester S, Corcoran SE, Runtsch MC, Ling C, et al. The Immunomodulatory Metabolite Itaconate Modifies NLRP3 and Inhibits Inflammasome Activation. Cell Metabolism. 2020.
517. Calo L, Passali GC, Galli J, Fadda G, Paludetti G. Role of biofilms in chronic inflammatory diseases of the upper airways. Adv Otorhinolaryngol. 2011;72:93-6.
518. Hoiby N, Bjarnsholt T, Moser C, Jensen PO, Kolpen M, Qvist T, et al. Diagnosis of biofilm infections in cystic fibrosis patients. APMIS. 2017;125(4):339-43.
519. Hoiby N, Ciofu O, Johansen HK, Song ZJ, Moser C, Jensen PO, et al. The clinical impact of bacterial biofilms. Int J Oral Sci. 2011;3(2):55-65.
520. Wilson JM, Coletta PL, Cuthbert RJ, Scott N, MacLennan K, Hawcroft G, et al. Macrophage migration inhibitory factor promotes intestinal tumorigenesis. Gastroenterology. 2005;129(5):1485-503.
521. O'Neill LAJ, Artyomov MN. Itaconate: the poster child of metabolic reprogramming in macrophage function. Nat Rev Immunol. 2019;19(5):273-81.
522. Benigni F, Atsumi T, Calandra T, Metz C, Echtenacher B, Peng T, et al. The proinflammatory mediator macrophage migration inhibitory factor induces glucose catabolism in muscle. J Clin Invest. 2000;106(10):1291-300.